Interaction of Platinum(II) Anticancer Drugs with RNA

DISSERTATION

zur

Erlangung der naturwissenschaftlichen Doktorwürde

(Dr. sc. nat.)

vorgelegt der

Mathematisch-naturwissenschaftlichen Fakultät

der

Universität Zürich

von

Marianthi Zampakou

aus

Griechenland

Promotionskomitee

Prof. Dr. Roland K. O. Sigel (Vorsitz)

Dr. Daniela Donghi (Leitung der Dissertation)

PD Dr. Eva Freisinger

Prof. Dr. Sofi K. C. Elmroth

Zürich, 2017

For my family

Acknowledgments

My very special thanks go to my PhD supervisor Dr. Daniela Donghi for providing me with this very interesting and challenging project, for all the scientific advices, her continuous support and everything that she taught me over the last four years. I would also like to thank Prof. Dr. Roland K. O. Sigel for accepting me in his lab and giving me the opportunity to work in such nice and inspiring environment.

Many thanks to Dr. Eva Freisinger and Prof. Dr. Sofi K. C. Elmroth for being part of my PhD committee and for all helpful discussions.

I would like to thank also Prof. Dr. Sofi K. C. Elmroth for our research collaboration and for welcoming me in Lund for a short scientific stay. A big thank you goes also to Dr. Alak Alshiekh for her great help during my stay in Lund.

A great thank you is also for the Prof. James Hoeschele for all the nice discussions we had and the donation of kiteplatin for my studies.

I am obliged also to other people that contributed to this thesis, both in scientific and other ways:

The whole SF-Lab (current and former members), for the good daily working atmosphere.

The NMR subgroup members: Dr. Silke Johannsen, Dr. Magdalena Rowinska-Zyrek, Dr. Alicia Dominguez-Martin, Dr. Maria Pechlaner, Dr. Miriam Skilandant, Dr. Bhaumik Dave, Elena Alberti, Simona Bartova, Kenneth Adea and Irina Markova for all the helpful discussion, the advices, the support and the very nice time spent together.

Dr. Silke Johnansen, Dr. Alicia Dominguez-Martin, Susann Zelger-Paulus and Elena Alberti for reading parts of my thesis and giving me very useful advices and feedbacks.

Tobias Weber for his help with the german translation and Dr. Sofia Gallo and Dr. Silke Johannsen for its revision.

Dr. Pallavi Choudhary for her scientific advices during my first days and all the nice time we spent together in the lab.

Dr. Igor Oleinich for always being ready to answer all my questions about HPLC; Dr. Anastasia Musiari, Dr. Sofia Gallo and Dr. Anita Schmitz for the introduction and all the help with HPLC.

Dr. Anastasia Musiari and Dr. Erica Fiorini for the advices, help and nice time in the radiolab.

Dr. Sofia Gallo, Dr. Michelle Schaffer and Susann Zelger-Paulus for the tips and tricks to improve my gels.

Jovana Jakovleska, Jelena Habjanic and Alma Salim for their help with the AAS measurements but mostly for their very positive attitude and cheerful discussions.

Dr. Bhaumik Dave and Dr. Richard Boerner for help with the troubleshooting of the UV spectrometers.

Melodie Hadzik for always being available to solve PC problems and to give me advices on Origin matters and Fabio Stefan for his support with the Citavi.

The University of Zurich and the Graduate School CMSZH for financial support.

Dr. Sabine Stockhause, Beatrice Spichtig, Nathalie Melunsky-Fichter and Ramona Erni for the administrative support.

Special thanks go also to Dr. Sabine Stockhause and Beatrice Spichtig for their help during the retreat organization.

Some people but for being amazing colleagues, are also very good friends! Since my very first day in Zurich, my Nachbar Bhaumik Dave is always around to help me with everything, to remind me of the passwords that I keep on forgetting, and to be a very patient and good friend. Helping, advising, supporting, cheering, motivating and encouraging me are only few of the things for which I thank Magda Rowinska-Zyrek and Alicia Dominguez-Martin. The list of the things for which I thank Elena Alberti is actually quite long. She was a great lab mate with who I could share all my thoughts and problems concerning work and from who I received a lot of help for many things. However, apart from being my "other half" at work she is also a great friend. Awesome summer vacations, trips to Italy and being my shopping partner are only few of the nice things we shared the last years. Together with Bhaumik Dave, Magda Rowinska-Zyrek, Alicia Dominguez-Martin and Elena Alberti I would also like to thank Meng Zhao, Fabio Amadei, and Kenneth Adea for all the dinners, BBQs and good times we spent together!

A very special period during these last four years was the Seebacherstrasse era. During that time, countless dinners with nice people and funny moments took place! For these times a great thank you goes to Jovana Jakovleska for being an amazing Nachbarin and to Magda Rowinska-Zyrek (Elizabeth) for making this big house, home!

For the last four years, I own many thanks to Tobias Weber for listening to me in the good and bad days and for his constant support and encouragement.

Finally, a huge thank you to my family for always supporting, encouraging and helping me.

Table of Contents

Abbreviations List

A	Adenine
Acryl-Bisacryl	Acrylamide / bis-acrylamide solution
AMP	Adenosine monophosphate
ATP	Adenosine triphosphate
bb	Bromophenol blue
C	Cytidine
CD	Circular dichroism
CIAP	Calf intestinal alkaline phosphatase
cisPt	Cisplatin
CMP	Cytidine monophosphate
CTP	Cytidine triphosphate
1D	Mono-dimensional
2D	Two-dimensional
DACH	1,2-Diaminecyclohexane
ddH_2O	Double-distilled water
Deph-	Dephosphorylated
DNA	Deoxy-ribonucleic acid
ds	Double-stranded
E. coli	Escherichia coli
Eq	Equivalent(s)
FDA	Food and drug administration
G	Guanine
GMP	Guanosine monophosphate
GTP	Guanosine triphosphate
HPLC	High performance liquid chromatography
ESI-MS	Electrospray ionisation mass spectrometry
KitePt	Kiteplatin

MALDI-MS	Matrix-assisted laser desorption mass spectrometry
miRNA	micro RNA
mRNA	Messenger RNA
NaOAc	Sodium acetate
NH_4OAc	Ammonium acetate
NMR	Nuclear magnetic resonance spectroscopy
nt	Nucleotide
NTP	Nucleoside 5'-triphosphate
OxaliPt	Oxaliplatin
PAGE	Polyacrylamide gel electrophoresis
RNA	Ribonucleic acid
RNase	Ribonuclease
rRNA	Ribosomal RNA
siRNA	small interfering RNA
Tm	Melting temperature
Triph	Triphosphate group
tRNA	transfer RNA
TSIAP	Thermosensitive alkaline phosphatase
U	Uracil
UMP	Uridine monophosphate
UTP	Uridine triphosphate
Uv/Vis	Ultraviolet/Visible spectrometry
xc	Xylene Cyanol

1 Introduction

1.1 RNA importance and functions

1.1.1 Comparison of DNA and RNA

RNA and DNA are large biomolecules, which together with proteins, lipids and carbohydrates are essential for all known forms of life. Nucleic acids are polymers and consist of four different monomers, which are called nucleotides. Each nucleotide is composed of a phosphate group, a sugar ring and one of the four nucleobases: guanine (G), adenine (A), cytosine (C) and uracil (U) (RNA) or thymine (T) (DNA). The bases have either purine based structures (A and G) or pyrimidine based structures (U, C and T). The sugar ring is a 2'-deoxyribose for DNA and a ribose for RNA (Figure 1.1, left panel). The presence of the 2'-hydroxyl group differentiates RNA from DNA and makes the first more prone to self-cleavage through in-line nucleophilic attack on the neighbouring 3′-phosphate group. Additionally, it is also responsible for their structural difference, as it will be discussed below (Figure 1.2) and enables RNA to have catalytic activity (e.g. Group II introns). Neighbouring nucleotides are covalently linked with each other through phosphate groups linking the 5′-end of one sugar to the 3′-end of the next resulting in the formation of a highly negatively charged backbone (strand) with a well-defined directionality (5′- to 3′-direction). Both DNA and RNA strands have a hydroxyl group on the sugar moiety at the 3′-end and a terminal phosphate group at the 5′-end. This strand constitutes the primary structure of nucleic acids. The secondary structure of nucleic acids is the double-stranded arrangement, which is the result of hybridization of their complementary strands in an antiparallel way. The bases are forming hydrogen bonds with each other by the establishment of Watson-Crick base-pairs (canonical base-pairing) where guanine pairs with cytosine through three hydrogen bonds and thymine/uracil pairs with adenine through two hydrogen bonds. Besides the Watson-Crick base-pairs other base-pairing schemes are also encountered in RNA like the Hoogsteen base-pairing and G-U wobbles[1,2] (Figure 1.1, right panel). Apart from the formation of hydrogen bonds the π-π interactions between the stacked aromatic rings of neighbouring nucleobases play the most important role in the duplex stability[3].

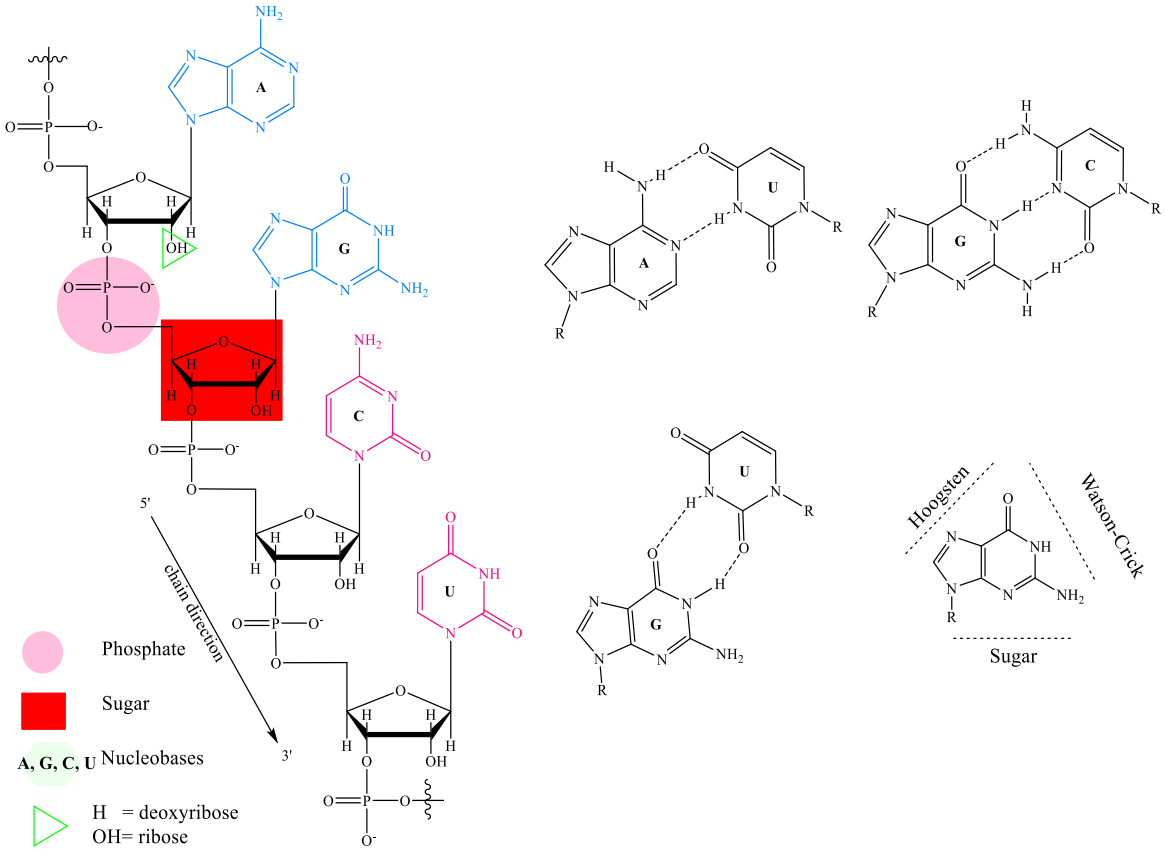

Figure 1.1: *Left panel: An illustration of an RNA strand. The purines (A, G) are coloured in blue and the pyrimidines (C, U) in magenta. The phosphate backbone and the ribose are marked with a purple oval and a red square respectively. Right panel: Watson-Crick base pairs of A-U and G-C (top), a G-U wobble base pair and a guanine base with indicated the Hoogsten and Watson-Crick sites (bottom).*

Duplex nucleic acids can adopt various conformations (e.g. A-, B- and Z-form) with DNA being usually found in B-form and RNA in A-form (Figure 1.3, left panel)[4–6]. A comparison of some parameters for A- and B-helical forms are summarized in Table 1.1. Both helices are right-handed and the choice between the two conformations depends mostly on the sugar pucker conformation. More specifically the 2′-OH group of ribose is forcing the RNA sugar into a C3′ *endo* conformation while in B-form DNA the sugar is found a C2′ *endo* arrangement (Figure 1.2). The A-form RNA has a deep and narrow major groove and wide and shallow minor groove while DNA grooves are of a similar depth. Despite their similarities on a chemical base, the two nucleic acids have important differences concerning their secondary structures. DNA is found usually in a double-stranded helical B-form. RNA is transcribed as a single strand but it folds in a complex three-dimensional structure in order to minimize its overall energy. Because of this it can adopt different

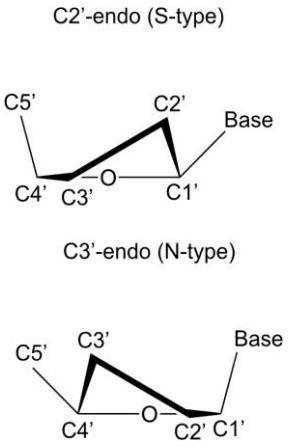

Figure 1.2: *The sugar pucker conformations of deoxyribose (C2'-endo) and ribose sugars (C3'-endo).*

secondary structures including hairpins, internal/terminal loops, bulges, and junctions[7] (Figure 1.3, right panel). These non-helical regions are stabilized by stacking interactions and hydrogen bonds and provide potential binding sites for proteins or other molecules. Additionally, they contribute to the formation of tertiary interactions which are crucial for RNA folding[8].

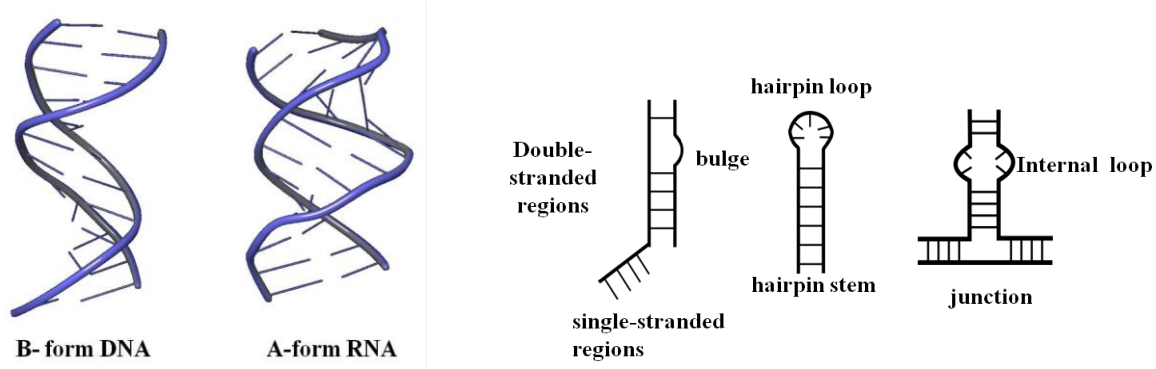

Figure 1.3: *Left panel: Illustration of B-form DNA helix and A-form RNA helix. The figures were prepared using Maestro Schrödinger Version 10.5.014 based on the PDB files 1BNA9 and 1RNA10 respectively. Right panel: Schematic representation of RNA secondary structural elements.*

Table 1.1: *Some parameters for the A-helical and the B-helical form of nucleic acids*[3,11]

	A-helical form	**B-helical form**
Helix Sense	Right handed	Right handed
Average base pairs / turn	10.7	10
Rotation / base pair	33.6°	35.9°
Pitch / turn of helix	24.6 Å	33.2 Å
Rise / base pair along axis	2.3 Å	3.32 Å
Propeller twist	+18°	+16°
Glycosyl angle	Anti	Anti
Sugar pucker	C3′-endo	C2′-endo
Diameter	26 Å	20 Å

1.1.2 The importance of RNA structure

According to the central dogma of molecular biology, DNA contains all the information necessary to build up an organism. The three main types of RNA namely messenger RNA (mRNA), transfer RNA (tRNA) and ribosomal RNA (rRNA) convert this information into a protein sequence. During the last decades, it was found that RNA is more than an intermediate between DNA and proteins, having many more essential functions. More specifically, a great variety of non-coding RNAs have been discovered and were found to be involved in very important biological functions[12]. For example, ribozymes are

catalytically active RNAs, which are able to perform catalysis without the presence of a protein[12] (e.g. group II introns which can undergo self-splicing[13–15]) and riboswitches were found to be important for gene regulation[16]. Critical to its functions are the specific three-dimensional structures that RNA can adopt[7]. While DNA is typically helical, RNA folds into complicated structures, which resemble the ones from proteins. For instance, in eukaryotes, RNA based processes like splicing and mRNA maturation are performed from a complex RNA-protein molecular machine with complex tertiary structures called spliceosome[17]. Targeting and disturbing these structures is a way to interfere with RNA function.

1.1.3 RNA and metal ion interactions

The structural complexity of RNA cannot be achieved in the absence of metal ions. Monovalent and divalent cations are needed for the stabilization of secondary and tertiary RNA structures. Metal ions have been found to be important for both RNA folding and function[18]. They primarily serve as charge screeners of the negatively charged phosphate backbone. Upon RNA folding the phosphate groups of the backbone are coming closer further intensifying the negative charge and creating unspecific or specific binding pockets for metal ions[19–21]. The monovalent ions are usually bound to RNA for charge neutralization and enable the formation of the secondary structures while the divalent ones stabilize the tertiary structure[22]. Two very important metal ions are K(I) and Mg(II). The first is the most abundant intracellular monovalent ion (140 mM)[23] and is bound to RNA for charge neutralization and pre-organization of the RNA structure. However, it has been reported that ribosomal RNA unfolds upon reduction of K(I) suggesting that its role it is not limited only to charge screening[24]. Mg(II) is the most important divalent metal ion in RNA folding and catalysis. It is crucial for folding the RNA into its complex and functional tertiary structures[25]. Mg(II) is also considered an RNA cofactor for catalytically active RNAs (e.g. group II introns)[14,26]. For example in the two-metal-ion mechanism, which has been proposed for the prosphoryl transfer reactions catalysed by the group I and group II introns, Mg(II) ions both activate the attacking nucleophile and stabilize the leaving group[19].

Various methods have been used for the investigation of the interactions between metal ions and RNAs[27,28], including biochemical (e.g. hydrolytic cleavage experiments, nucleotide analogue interference mapping etc.) and spectroscopic techniques (NMR, EPR, X-ray crystallography etc.). Moreover, transition metal ions and lanthanides[29] have been used for mapping RNA structures and identifying metal ion binding sites. In contrast to metal ion-RNA interactions, the data on metal complexes-RNA interactions are still very scarce[30].

1.1.4 Our model RNA: D1-27

To gain insights into the binding of metal complexes to RNA, we decided to investigate the interaction of an important class of metal complexes, namely platinum(II) anticancer drugs, with RNA. For the current study, a model RNA system was needed and for this purpose a 27nt long RNA was employed.

This RNA is derived from the mitochondrial group II intron *Sc*.ai5γ from Saccharomyces cerevisiae (S. cerevisiae), baker's yeast[31] (Figure 1.4, left panel), and corresponds to the central part of domain 1, from which the name D1-27 comes (Figure 1.4, right panel).

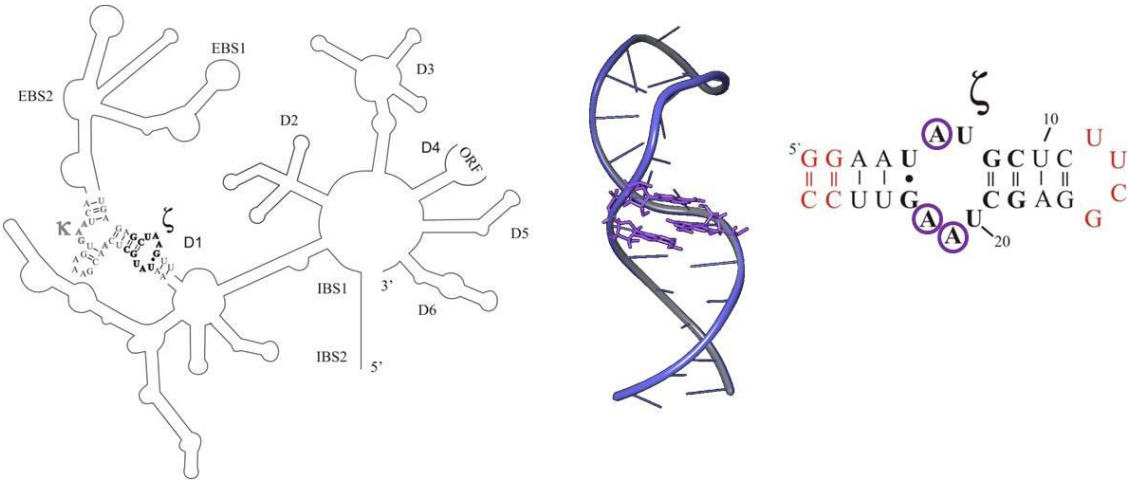

Figure 1.4: *Left panel: Schematic representation of the secondary structure of the group II intron Sc.ai5γ from S. cerevisiae[14] from which our model RNA (D1-27) derives. Right panel: The 3D structure of D1-27 and its secondary structure[32]. The internal loop is depicted in bold and the stacked adenines are highlighted in purple. The 3D figure was prepared using Maestro Schrödinger, Version 10.5.014.*

D1-27 has structural features which are common in many RNAs. More specifically, it contains an artificially inserted -UUCG- tetraloop and an 11nt asymmetric internal loop. The asymmetric 11nt internal loop of D1-27 (Figure 1.4, right panel, bold) contains a G-U wobble base-pair, three stacked adenines and a U-U mismatch[33,34]. The -UUCG- tetraloop was added to stabilize the whole construct[33] and the 5′-end guanosines were added in order to increase the transcription yield[35]. In the context of the whole group II intron, the internal loop acts as a tetraloop receptor for the -GAAA- tetraloop[36,37]. In general the interactions between GNRA tetraloops (N = any nucleotide, R = purine) and their receptors represent an important RNA folding motif[38]. It is well known that the interactions of -GAAA- tetraloops with their receptors are necessary for the correct folding and function of various RNAs like the Group I and II introns and RNase P[39]. Upon tetraloop binding a conformational rearrangement of the receptor is observed[34,40,41]. This tetraloop receptor system represents a good model to study metal ion-RNA interactions[38]. Interestingly, it was shown that upon Mg(II) titration no structural changes were induced on the isolated tetraloop receptor[34]. The structure of the receptor docked to a -GAAA- tetraloop showed no difference in the presence of various cations and in this docked form the AA platform in the internal loop acts as binding site for monovalent metal ions [K(I)][39,42]. Recently, NMR studies on metal ion binding to the undocked tetraloop receptor of D1-27

have revealed a general electrostatic interaction at the internal loop region upon addition of Cd(II), Mg(II) and cobalt(III)hexammine with all three metal ions exhibiting only slightly different behaviour[43].

In conclusion, the chosen RNA contains structural features widespread in many RNAs, thus representing a good model system to investigate structural preferences of drug interaction. Moreover, its NMR characterization in solution is available, making the NMR investigation of platinum(II)-RNA species easier[32]. Finally, knowing already the Mg(II) binding sites on this RNA construct, which based on a recent study are closely related to the platination sites[44], we wanted to further investigate the platinum(II) binding using platinum(II) anticancer drugs.

In addition to D1-27, three more RNA constructs were also used for this study (Figure 1.5). More specifically an analogue of D1-27 without the internal loop was used in order to study the influence of the internal loop on the platination sites and was named RNA 26 (Chapter 2, Paragraph 2.6 and Chapter 3, Paragraph 3.3.3). To investigate preferential binding sites of platinum(II) complexes over different terminal loops, the -UUCG- terminal loop was replaced for the -GAAA- (Chapter 3, Paragraph 3.3.2), and this RNA was named D1-27$_{GAAA}$. Finally, an analogue of D1-27 containing two terminal U-A base-pairs instead of the two G-C base pairs was used to study the effect of platination at the 5'-end GG. The latter construct was named RNAUU (Chapter 4, Paragraph 4.10).

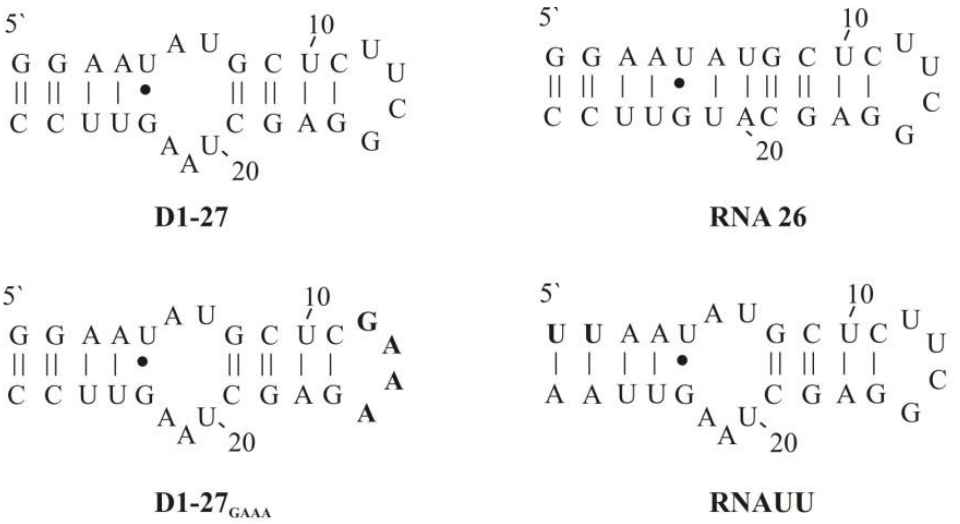

Figure 1.5: *The secondary structures of all the RNA constructs used for this study. Starting from the original construct D1-27 other three D1-27 analogues were used. RNA 26 does not contain the internal loop, D1-27$_{GAAA}$ has a -GAAA- tetraloop instead of the -UUCG- and RNAUU has two U-A terminal base-pairs instead of two G-C base pairs.*

1.2 Platinum(II) anticancer drugs

1.2.1 The anticancer drug cisplatin

In 1965 Rosenberg and co-workers reported the inhibition of cell division in *Escherichia coli* (*E. coli*) by electrolysis products from a platinum electrode[45]. The therapeutic potentials of whatever was causing this behaviour were enormous and follow-up studies revealed that the *cis*-$[Pt(NH_3)_2Cl_2]$ complex (cisplatin) could inhibit cell division of *E. coli*[46]. Upon the discovery of the biological activity of cisplatin, the medicinal inorganic chemistry as a discipline came to exist and vigorous research on how platinum(II) complexes are functional as anticancer drugs started[47]. Cisplatin was approved for clinical use from FDA in 1978. It is best known for the treatment of testicular cancer but it is also used for curing other cancers like lung, bladder, cervical and ovarian cancer[48]. It is believed that the anticancer activity is due to the covalent binding of cisplatin to nuclear DNA preferably at the N7 sites of two adjacent guanines. Despite its success, cisplatin has several limitations, like severe side-effects (nausea, vomiting, kidney and nervous system toxicity) and tumours can develop drug resistance[49]. Additionally, cisplatin was not effective in the treatment of two very common types of cancer, the colorectal and breast tumours[50]. Over forty years of research have been invested to develop cisplatin analogues with similar or improved clinical activity and reduced side-effects. From all the platinum-based drugs entered clinical trials only two gained international clinical approval and these are the second generation platinum anticancer drug carboplatin and the third-generation platinum anticancer drug oxaliplatin[48] (Figure 1.6). The term second and third generation refers to the development of the new platinum(II) complexes. For example in the second generation the ammine or chloride ligands were replaced by more stable chelating ligands (see carboplatin) and in the third generation both leaving and non-leaving groups were replaced (see oxaliplatin)[51].

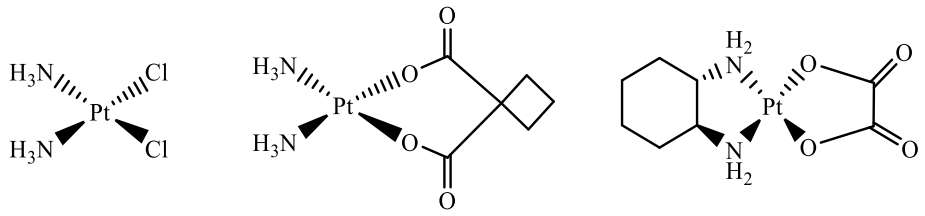

Figure 1.6: *Platinum(II) drugs which are in clinical use worldwide: Left: cisplatin; middle: carboplatin: right: oxaliplatin.*

1.2.2 Chemistry and development of platinum(II) complexes

Cisplatin is a square-planar platinum(II) complex. It has two relatively exchange-inert ammine ligands and opposite to them two kinetically-labile chloride ligands in a *cis* geometry around the platinum(II) metal centre. This scaffold is characteristic for all platinum(II) anticancer drugs (Figure 1.6, left). Their biological activity depends on how fast their leaving groups can be substituted from water molecules

leading to the active form of the complex. Upon formation of the aquated platinum(II) complex they have the tendency to form kinetically-inert complexes with soft ligands. This class of ligands includes cyanato, thiocyanato, sulfido, thiolate, thiol, phosphine, ammines and imines groups[52]. For the development of new improved platinum(II) anticancer complexes structure-activity relationship rules were established upon screening of many platinum compounds[53,54]. These rules are summarized in the following:

1. The compound should be neutral
2. Two *cis* monodentate leaving groups with intermediate binding strength to platinum(II) are required
3. The presence of amine ligands with *cis* configuration lead to active species
4. The less the alkyl substituent on the amine ligands the better the activity

Beside these structural requirements, platinum drugs, which will be considered for clinical approval, should further bring along:

1. Activity in cisplatin resistant tumours or improved activity towards tumours responding to cisplatin
2. Reduced toxicity and side-effects
3. Improved physical properties like better water solubility

Carboplatin belongs to the second generation platinum(II) anticancer drugs (Figure 1.6, middle); it has similar activity like cisplatin but reduced side effects. Its lower toxicity was connected to the slower hydrolysis of its cyclobutanedicarboxylate ligand. Additionally, its side effects are different compared to the ones of cisplatin[48]. Upon aquation it forms the same active species and the same DNA adducts as cisplatin and therefore is only clinically different to its parent compound.

Oxaliplatin belongs to the third generation platinum(II) anticancer drugs (Figure 1.6, right). Compared to cisplatin it has a single bidendate ligand (1R,2R-cyclohexane-1,2-diamine) instead of the two ammine groups and the two chlorides are replaced by an oxalate group. It was approved for clinical use due its capability to treat cisplatin resistant tumours. The presence of the oxalate was found to be responsible for its reduced side effect compared to cisplatin[55]. Oxaliplatin is the platination agent that will be used in the current study and more details about its function, including comparison with cisplatin, will be discussed in chapter 2 (Paragraph 2.4).

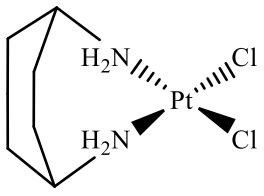

Figure 1.7: Kiteplatin.

Another platinum(II) complex was also used in this thesis, namely kiteplatin (kitePt). Its chemical structure is shown in Figure 1.7. The *in vivo* and *in vitro* activity of kitePt was reported for the first time more than 20 years ago[56] but in the last years its potency as possible anticancer drug has been revisited[57]. The interest in this compound resulted from its activity against cisplatin- and oxaliplatin-resistant

tumors[57,58] as well as from its potential application against colorectal cancer[56,57]. Structurally it contains an isomeric form of the diammino DACH ligand of oxaliPt (cis-1,4-DACH) as non-leaving group, while its leaving groups are two chlorides similarly to cisPt. A special feature of the cis-1,4-DACH is the formation of a seven-membered chelate ring which results in a larger bite angle (97 °) compared to cisPt and oxaliPt, which might affect the mobility of the cis ligands[59,60]. Preliminary studies were performed in order to compare its behaviour with oxaliplatin and cisplatin and these will be discussed in chapter 3 (Paragraphs 3.6 - 3.10).

1.2.3 Platinum(II) binding targets in cell: The example of cisplatin

The suggested mechanism of action of cisplatin is shown in Figure 1.8. Cisplatin is administered intravenously into the bloodstream where the high chloride concentration (~100 mM) is preventing the displacement of its chloride ligands. Once in the bloodstream, studies have shown that after one day 65 - 98 % platinum is bound to proteins found in the plasma. This might be connected to its deactivations and/or its side effects. Cisplatin can enter the cell either by passive diffusion[61] or by active uptake through copper transporter proteins[62] (Figure 1.8). Upon its entrance the lower intracellular chloride concentration (~ 4 mM) promotes the exchange of chloride ligands giving rise to the formation of positively charged monoaquated platinum complexes[63] (Figure 1.8). Possible targets of this cationic platinum(II) complex are biomolecules which contain soft nucleophiles found in proteins and on RNA and DNA nucleobases. In proteins cysteine, methionine and histidine residues represent good platinum(II) targets while in DNA and RNA bases N7 position of both guanine and adenine, but also N1 of adenine and N3 of cytidine, can behave as platinum binding sites[64]. Cisplatin is considered to exert its anticancer activity upon covalent binding to nuclear DNA. *In vitro* studies have shown that the monoaquated complex is responsible for at least 98 % of the nuclear DNA platinum binding. At first, it usually reacts with a guanine base at the N7 position forming monofunctional adducts. Further aquation of the second chloride leads to rapid ring closure and formation of bifunctional Pt(II)-DNA adducts. These bifunctional adducts are usually bound to the N7 atoms of adjacent purine nucleotides with the 1,2-Pt-GG adducts representing the 65 % and the 1,2-Pt-AG adducts the 25 % of the platinated species formed. The platinated DNA adducts are significantly distorted and can be recognised by DNA damage repair proteins. These proteins will either repair the platinated DNA or they will initiate apoptosis[49].

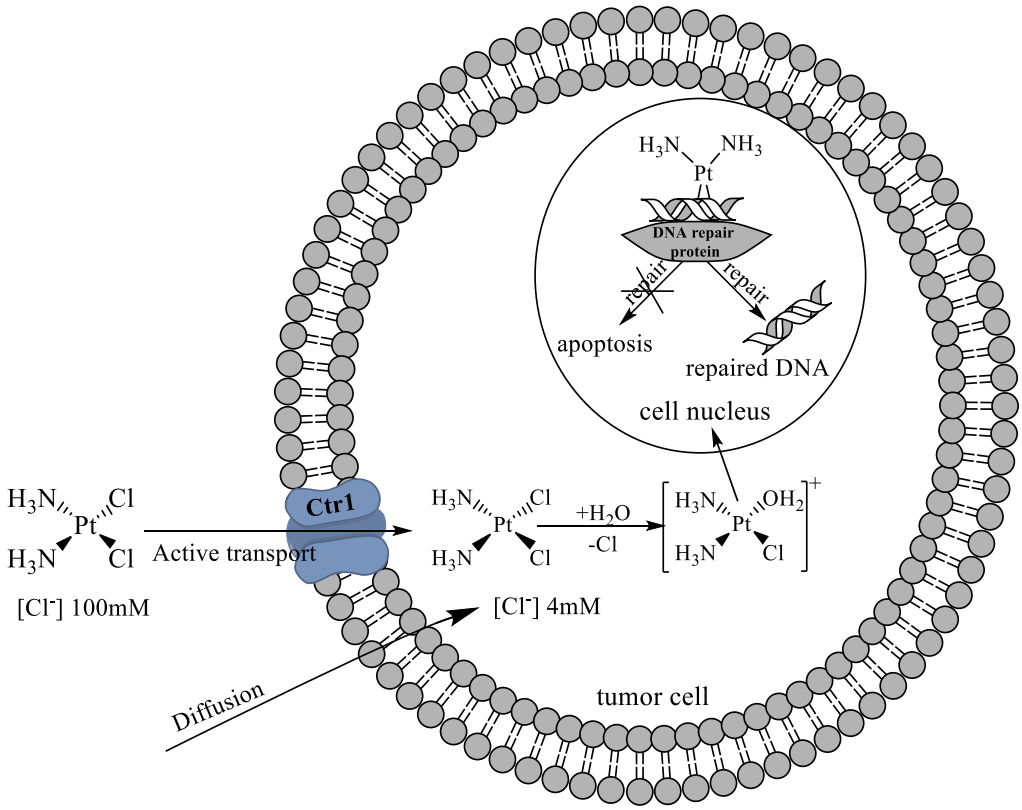

Figure 1.8: *Schematic representation of the suggested mechanism of action for cisplatin[49]. Upon entering the intracellular environment, cisplatin undergoes hydrolysis and the aquated species can bind to the nuclear DNA. Inability of repairing the platinated DNA could lead to apoptosis.*

1.2.4 Platinum(II)-DNA interactions

In general, platinum(II)-DNA interactions are linked with the anticancer activity of cisplatin and platinum(II) drugs[49]. Cisplatin can bind to DNA only after hydrolysis of the first chloride which is the rate-limiting step for platinum binding[65]. The positively charged monoaquated cisplatin is probably first associated electrostatically with the negatively charged phosphate backbone of the DNA before forming a covalent bond with the nucleobases[66]. The preference for binding first at the N7 site of guanines was attributed to the fact that guanine is the most nucleophilic base. However, the basicity of the coordination site is not the main factor affecting the platinum(II) binding. Studies revealed that the preference for this site could be either due to the hydrogen bond formation of the ammine group of cisplatin with the O6 keto oxygen of the guanosine or the hydrogen bonding between the water molecule of the aquated cisplatin with the O6 keto oxygen of the guanosine. It has been reported that the first plays only a minor role while the latter is the main reason for the preference of cisplatin to guanine over adenine[67]. After the monofunctional adduct is formed closure of the ring (chelation) to form the bifunctional species can take place either directly from the monofunctional or it might involve aquation of the second chloride ligand[49]. Due to the very slow ligand exchange of the platinum(II) complexes their adduct formation is under kinetic rather than thermodynamic control. This hypothesis seems to be

accepted for the first platination step that leads to mono-adduct formation while the chelation step that leads to bi-adduct formation is suggested to be partially under thermodynamic rather than under kinetic control[68]. The major intrastrand bifunctional adducts formed can be either GG (65 %) or AG (25 %) (Figure 1.9, left). Other minor species formed include: 1) 1,3-GNG intrastrand adducts, with N being any of the nucleobases, 2) GG interstrand species, 3) G monofunctional adducts (X = water molecule or chloride) and 4) G-protein cross-linked species (Figure 1.9)[64].

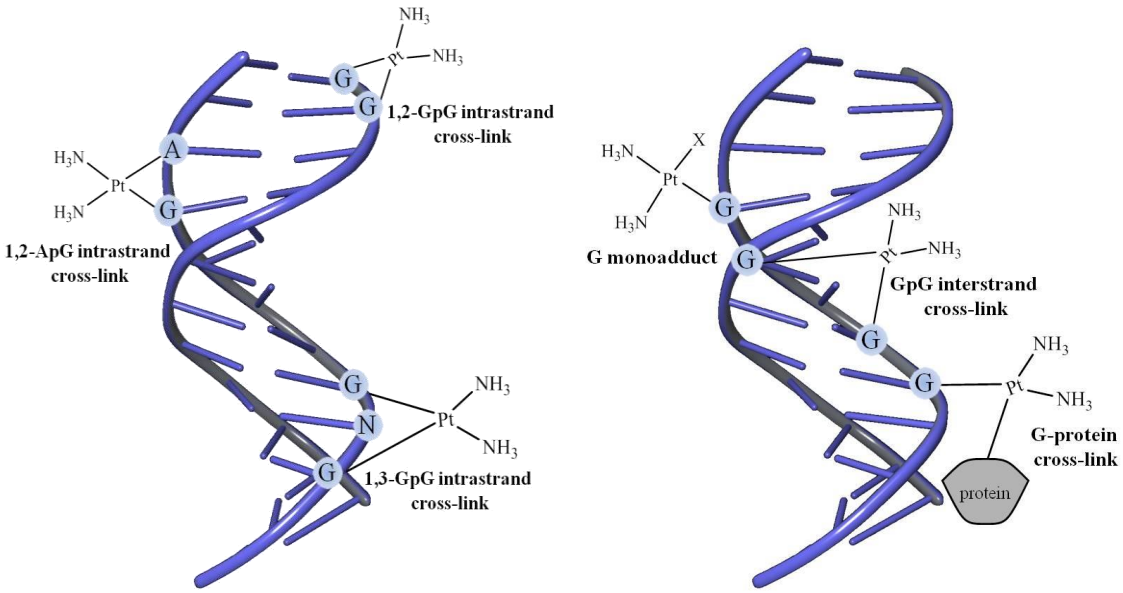

Figure 1.9: *Illustration of the possible cisplatin-DNA adducts.*

Crystal structures as well as NMR solution structures of platinated DNAs have been reported[69–71]. Upon binding of cisplatin to DNA the double helix is bended (32 ° - 35 °) towards the major groove, widening and flattening of the minor groove opposite the platinated adducts occur and a generalized distortion over 4-5 bases from the platination site was reported[72]. This distortion makes the phosphate groups of the backbone moving closer to the platinum site resulting in the formation of hydrogen bonding between a phosphate oxygen atom and the ammine ligand, which however does not play a role in the activity of cisplatin. Depending on the type of adducts formed (1,2-GG, 1,2-GA or 1,3-GNG) the DNA helix unwinds to a different degree (21 °, 13 ° and 23 ° in the case of 1,2-GG, 1,2-GA and 1,3-GNG adducts, respectively) but they all have the ability to bend DNA helix to the same extent. High-mobility group (HMG) domain proteins can recognise the DNA helix bending and unwinding. Their binding to the platinated nuclear DNA is believed to interfere with the removal and repair of the platinated site from the normal DNA repair proteins thus initiating apoptosis (cell death)[73]. The 1,2-GG intrastrand adduct is considered to play the major role in toxicity of cisplatin and it is specifically recognised by several proteins (HMGB1 and TATA-binding proteins)[72]. However, the importance of the minor adducts

should not be underestimated when describing the overall profile of cisplatin toxicity. Towards this direction it should be noted that cisplatin forms adducts also with the mitochondrial DNA, and this could contribute to its toxicity[74]. Moreover, cisplatin can interact with cellular targets other than DNA. In this regard, the interaction between proteins and platinum(II) drugs[75] is also investigated, in an attempt to understand better their mechanism of action, which could lead to optimized drug development. Surprisingly, much less studied are the interactions of platinum(II) complexes with RNA, despite its biological importance[30,76].

The potency of RNA as possible drug target and more specifically as potential target for platinum(II) anticancer drugs will be discussed in the following paragraphs.

1.3 RNA as possible target for platinum(II) drugs

1.3.1 Targeting RNA with small molecules

Apart from the early discovered mRNA, tRNA and rRNA which are the intermediate between DNA and proteins a large variety of new classes of non-coding RNAs exhibiting multiple functional roles in regulating cellular processes have been discovered in the last few decades[12,77] (Paragraph 1.1.2). These findings greatly expanded the functions in which RNA is involved including regulation of transcription and translation, catalysis of protein synthesis and control of gene expression. RNA is very rich in non-canonical structural elements (Paragraph 1.1.1) which are essential for the tertiary interactions leading to the correct RNA folding. RNA functions are very closely related with its structure and a promising, even if challenging, way to interfere with its functions is by targeting these structural elements. Indeed, the involvement of RNA in crucial cellular functions, together with the large variety of non-canonical structural features which could serve as specific binding sites, makes RNA a very interesting drug target[78,79]. Towards this direction the use of oligonucleotides as well as small organic molecules were employed for targeting RNAs[79]. Approaches which are used to modulate RNAs function are 1) antisense oligonucleotides which is an oligonucleotide-based approach where an RNA sequence is bound selectively[80,81] and 2) small organic molecules which are employed for targeting specific structural elements[78].

In the last few years, a few small organic molecules have been developed which are able to target RNA and alter its functions. Some examples of these molecules are the following[78,79]: 1) a few classes of antibiotics (e.g. aminoglycosides and tetracyclines) known to exert their activity by targeting bacterial RNA[82], 2) cyclic peptides which are able to target HIV-1 RNA[83], 3) small molecules with the ability to modulate miRNAs functions[84] and 4) small molecules which can target nucleotide repeats known to cause neuromuscular diseases[85]. Small molecules can bind in many sites within RNA, but in order to have an impact the binding to these sites should have a biological consequence (functional sites)[84]. Additionally, RNAs are expressed at low levels (except for rRNA) making the targeting of functional

RNA sites very challenging[79]. Despite the challenges of this approach, there are significant advantages of using small molecules for RNA targeting. Small molecules are often orally available and in case of toxicity synthesis of their derivatives could be enough to overcome this problem. Their most important benefit though is that they can recognise different RNA structures and not only sequences[79].

Among small molecules with biological importance are the platinum(II) anticancer drugs which are known to interact with DNA. Investigating their interactions with other biological targets, like RNA, is crucial for a more complete understanding of their biological activity. In this regard the following paragraphs are dedicated to the description of RNA as platinum(II) target including the influence of Pt(II)-RNA adducts on RNA based processes, as well as to a few examples of platinum(II) binding to RNA.

1.3.2 RNA as target for platinum(II) drugs

DNA is the target that is considered to be responsible for the biological activity of cisplatin[49]. However, as discussed above, cisplatin can also interact with other biological targets like RNA and proteins. Studying the interactions of platinum(II) drugs with molecules other than DNA is necessary in order to obtain a better picture of its biological activity[76]. RNA is chemically very similar to DNA, therefore cisplatin and its derivatives are expected to bind to RNA as well. Being already available in the cytosol it is very probable that platinum(II) drugs could easily bind to RNA. Indeed, recent studies using inductively coupled plasma mass spectrometry (ICP-MS) reported that after treatment of *S. cerevisiae* with cisplatin, platinum accumulates in total 4- to 20-fold more in total cellular RNA than in genomic DNA[86]. Additionally, *in vitro* studies suggested that RNA platination kinetically competes or is even preferred over DNA platination[66,87]. Consequently, Pt(II)-RNA interactions might play a role in cisplatin or platinum(II) drugs activity, in cell resistance and/or toxicity, and investigation of such interactions might be helpful towards better understanding of their activity[76].

1.3.3 Influence of platinum(II) compounds on RNA-based processes

Early findings supported the hypothesis of RNA being a good platinum(II) drug target by showing that biologically important RNA processes are inhibited upon platinum(II) administration. An important step in RNAs lifecycle is the splicing, where the mature RNA is formed. Inhibition of splicing upon platination has been reported in the presence of cisplatin[88]. Similar behaviour was also found upon cisplatin treatment of the protein independent self-splicing *Tetrahymena* rRNA group I intron and it was related with the formation of interstrand cisplatin-RNA crosslinking[89]. For the efficient and correct translation of RNA into proteins, fully functional RNA molecules such as mRNA, tRNA and rRNA are important. Studies have suggested that the platination of precursor mRNAs (pre-mRNA) or rRNAs could interfere with translation. Indeed, *in vitro* studies have shown that upon cisplatin administration the synthesis of peptides was inhibited suggesting that is related with cisplatin interaction with mRNA[90]. The inhibition of translation was connected with the blockage of the initiation of translation[91]. More

recent findings on the level of translation revealed that cisplatin influences mRNA function and its effects on mRNA are more pronounced compared to oxaliplatin and carboplatin[92]. Several studies were devoted also to the investigation of the ribosomal RNA platination suggesting a potential ribotoxic role for platinum which could contribute to its general cytotoxicity[86,93]. Lastly, *in vitro* studies revealed that platinated RNA adducts can inhibit the function of important RNA processing enzymes such as endonucleases and exonucleases[94].

1.3.4 Examples of platinum(II) binding to RNA

In the last few years, several examples of platinum(II)-RNA interactions have been reported[30,76], some of which are summarized below. More specifically the examples are divided into two main categories. The first category includes platination of short RNA duplexes, and the second includes platination of structured RNAs such as tRNA, rRNA and spliceosomal RNA. In addition, the effect of platination on RNA silencing is briefly described.

Upon platinum(II) binding to DNA and RNA duplexes their melting profiles are strongly influenced. To gain more information into this topic, Elmroth and co-workers measured the destabilization induced by cisplatin and oxaliplatin in two small RNA and DNA duplexes *via* UV/Vis. These duplexes contained as central platination site either -GG- or -GNG- (N = T or U). They showed that both platinum complexes cause destabilization (reduced melting temperatures) with the larger changes observed for the -GNG- containing duplexes, especially for the RNA species[95]. After these findings, small RNA duplexes were also used in studying the kinetics of monoaquated cisplatin binding using UV/Vis, and the influence of various parameters was examined. From this investigation it was concluded that 1) the monoaquated cisplatin, under physiological conditions, is able to discriminate between different RNA targets, 2) local structure variations (such as, the length of the duplex, the nature of the bases around a GG site and the presence of mismatches) can influence the duplex reactivity, and 3) the platination of short RNA duplexes with monoaquated cisplatin is favoured in the intracellular [presence of K(I)] rather than in the extracellular [presence of Na(I)] environment and that increased hydrophobicity of the environment can reduce reactivity[96–98].

Understanding how platinum(II) anticancer drugs can bind to structured RNAs is important in order to understand how platinum binding can affect biologically important RNA processes (Paragraph 1.3.3). Towards this direction Elmroth and co-workers studied the platination of a full length $tRNA^{Ala}$ and of hairpin models of the anticodon loop and the acceptor stem with cisplatin [Figure 1.10, $tRNA^{Ala}$, Mh^{Ala} (blue frame), $acMh^{Ala}$ (green frame)], using biochemical assays in order to get information about sequence and structure specificity of platinum(II) binding. They reported that the replacement of a native G-U wobble with a G-C base pair (Figure 1.10, Mh^{Ala}, blue frame, G-U wobble in red) inhibited the platination at this site and that the replacement of a natural -UGC- sequence in the terminal loop by -GGC- (Figure 1.10, $acMh^{Ala}$, green frame, -XGC- in red) increased the platination at this site. In addition to these findings, they found that the attachment of a 5′-terminal phosphate group changes the

distribution of the observed platinated products (Figure 1.10, Mh^{Ala}, phosphate group in red)[99,100]. Combined these results showed that platination takes place at GG sites when RNA is used as target, similarly to what was found with DNA, and suggest that small sequence variations and local structure could significantly influence the platinum binding.

Another example of platinum binding to highly structured RNAs is the platination of a model system of the spliceosome. The spliceosome is a complex RNA-protein molecular machine, which removes introns from a transcribed pre-mRNA in the eukaryotes. Its catalytic core consists of the U2-U6 snRNA complex. A model system of this core was platinated with monoaquated cisplatin and formation of an intramolecular crosslink was observed in the internal loop (Figure 1.10, BBD RNA). The formation of this crosslink may influence RNA dynamics and function[101].

Platination of ribosomal RNA (rRNA) have also been reported and addition of cisplatin to *S. cerevisiae in cellulo* has shown significantly larger amounts of platinum in rRNA compared to mRNA[86]. Cisplatin has been utilized as chemical probe for identifying solvent exposed purine nucleotides in helix 24 of *E. coli* rRNA[102]. For this purpose, primer extension in order to detect platinum dependent stops of reverse transcription was employed. Two consecutive guanines located in a non-Watson-Crick base paired region were platinated even if a competing GG sequence close-by was present (Figure 1.10, helix 24). Specific GG binding and changes in loops upon platination was also reported when two highly conserved *E. coli* hairpins from rRNA were platinated with cisplatin[103]. Platination of rRNA was also performed using amino acid-linked cisplatin derivatives. The size and the charge of the platinum complexes used resulted in different RNA platination profiles[104]. Moreover, recent *in vivo* studies have revealed that cisplatin accumulates in the sarcin-rich loop and at the peptidyl transferase centre of rRNA[93] and that tRNA is also a possible cisplatin substrate.

Finally, the effect of platination on siRNA silencing was also investigated. RNA silencing refers to gene silencing in which the gene expression is regulated by non-coding RNAs like miRNA and siRNA[105]. Elmroth and co-workers platinated siRNA with cisplatin and oxaliplatin and observed that even if the RNAs were still active upon platination, an overall decrease of silencing activity was found with this effect to be more pronounced with oxaliplatin[87,106].

A common characteristic of all the Pt(II)-RNA adducts mentioned in these examples is the binding of platinum(II) in non-Watson-Crick base paired regions and its high selectivity towards the GG sites.

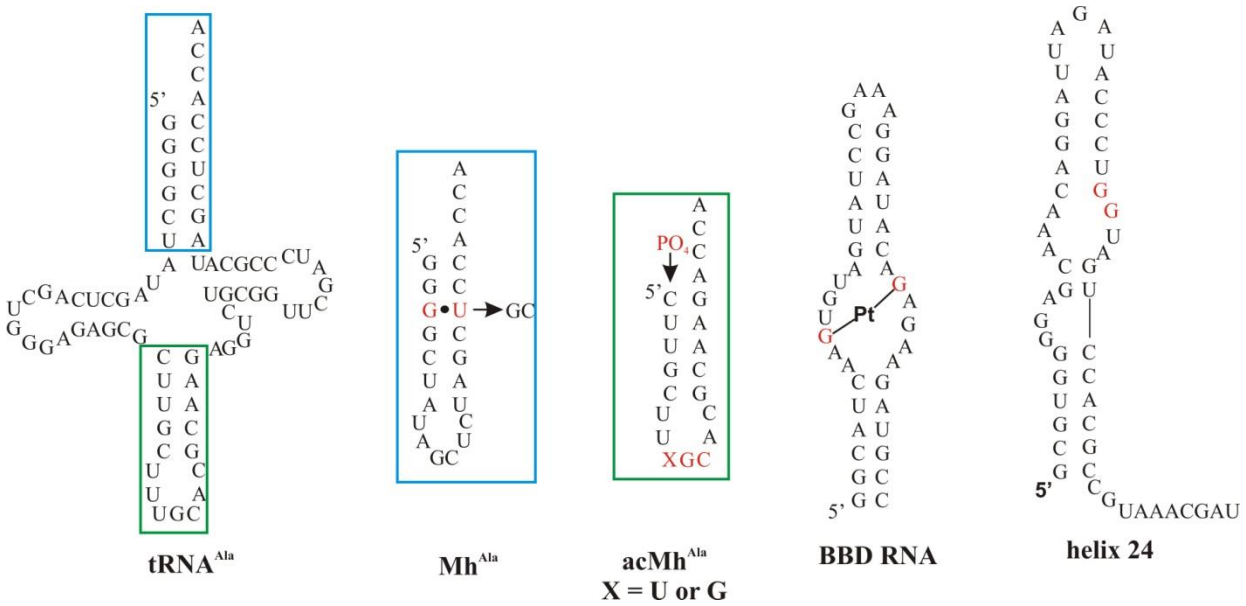

Figure 1.10: *Examples of platination of structured RNAs such as RNA hairpins derived from the tRNA$^{Ala\ 99,100}$ [(Mh^{Ala} (blue frame) and acMh^{Ala} (green frame)], a purine-rich internal loop derived from the spliceosome[101] (BBD RNA) and a region of the 16S rRNA[102] (helix 24). The modifications inserted (G-U to G-C, in Mh^{Ala}; the phosphate group and the -XGC- in acMh^{Ala}) as well as the guanines involved in platination are shown in red.*

1.3.5 Structural determination of platinum(II)-RNA adducts

Shortly after the antitumor activity of cisplatin was discovered, few preliminary X-ray studies were performed aiming at identifying the possible platination sites in tRNA$^{Phe107–109}$. However, the crystal structure resolution was rather low preventing a detailed analysis. Only very recently the first 2.6 Å resolution crystal structure of a platinated ribosome was reported[44]. Cisplatin was used as platination agent. Surprisingly out of the two thousand two hundred possible binding sites, only nine cisplatin-modified sites were found. Three of the cisplatin units were observed at the N7 atoms of adenines (A790 of the 16S rRNA and A1848, A2531 of the 23S the rRNA), five were located at the N7 atoms of guanines (G1300 of the 16S rRNA and G27, G425, G2220, G2221 of the 23S rRNA), and one platinum moiety was found bound at the N-terminus of the ribosomal protein L9. Out of all the affected nucleobases only G425 is found in a canonical G-C base pair while all the rest are located in non-canonical regions (bulges, junctions, internal and hairpin loops), which are quite common in RNAs. The preference of platinum(II) binding to irregular RNA structures confirms what was also observed from previous studies on Pt(II)-RNA adducts, suggesting that the presence of not-regular RNA geometries may be used as a criterion for the prediction of possible platination sites. At the guanine platinated sites it was found that, the interaction was not limited to the N7 position but contacts were formed also between neighbouring phosphate groups and the amino groups of cisplatin. Highly folded RNAs result in having in close proximity the N7 atoms of guanines to the phosphates, which could

explain why cisplatin binding occurs in non-Watson-Crick geometries. Another criterion for predicting platinum reactivity towards a guanine could be its ability to coordinate Mg(II). Indeed, all five guanines coordinated to cisplatin did coordinate Mg(II) in the untreated ribosome. On the other hand, all platinated adenines are positioned immediately before a guanine in an AG-motif. In this motif, cisplatin is covalently bound to N7 of adenine while its amine group interacts with the O6 atom of the neighbouring guanine. All the AG platinated motifs showed a slight structural distortion in the untreated ribosome, and this is believed to be the cause for their platination. Moreover, they are located at the RNA-RNA and RNA-protein interfaces. Out of an overall of three hundred and forty three AG-sites only twelve could accommodate cisplatin and only three were actually platinated. This suggests that the surroundings, and not only the structure and accessibility of the N7 atoms, are important for platinum(II) reactivity. These findings offer a third criterion for predicting cisplatin reactivity, i.e. adenine could be a possible platination site if found within an AG-motif. Finally, during rapid soaking experiments it was found that only adenines were platinated suggesting that they react faster compared to guanines. In paragraph 1.3.3 it was mentioned that the presence of platinum(II) could inhibit protein synthesis. In the crystal structure of the platinated ribosome cisplatin moieties were bound in many functional centres of the ribosome such as the mRNA channel, the peptide exit channel, the GTPase activating centre and the bridge B7a between the two ribosomal subunits, which could justify the ability of cisplatin to inhibit protein synthesis[44].

1.3.6 Comparison of platinum(II)-DNA and platinum(II)-RNA adducts

Since DNA is considered the main responsible for cisplatin anticancer activity, its interaction with platinum(II) drugs has been extensively studied. Platinum(II) drugs bind to the major groove of B-form DNA with simultaneous widening of the minor groove. These perturbations lead to a combination of A- and B-form around the platination site. More specifically the N7 sites of neighbouring purines are closer, the major groove becomes narrower, the minor groove wider and shallower, and the nucleotide at the 5′ to the platination site shows a C3′-end conformation which is found in A-form helices. Additionally, a hydrogen bond between the O6 of a guanine and the ammine group of cisplatin is observed. These observations were done on B-form DNA, whereas crystal structures of Z-form DNA with cisplatin showed very little distortion of the helix while the O6-ammine hydrogen bond was still present[110].

The equivalent positions of cisplatin binding in DNA are significantly buried in the deep and narrow major groove of A-form RNA probably excluding the formation of the same type of platinum adducts. From the only one high-resolution crystal structure of the platinated ribosome available together with biochemical and spectroscopic studies on structured RNAs is concluded that platination is favoured in non-helical regions of RNA, and that cisplatin binds with high affinity at GG sites. Internal and terminal loops, bulged regions and mismatches are preferred over helical regions suggesting that the presence of distorted geometries is probably the cause and not the consequence of RNA platination[44].

Interestingly, only few information are available on possible RNA platinum binding sites and even less on RNA structural distortions caused by platinum(II) binding. Towards a better understanding of Pt(II)-RNA interactions, the current study is dedicated to the isolation of a homogeneously platinated RNA aiming at investigating the structural preferences of platinum(II) binding as well as the effect of platinum(II) binding on RNA structure.

1.4 Thesis outline and aims

Platinum(II)-DNA interactions have been extensively studied since the anticancer activity of cisplatin was discovered (Paragraph 1.2.3 - 1.2.4). However, very little is known on the interaction of platinum(II) drugs with RNA. Understanding the interactions of platinum(II) anticancer drugs with other biologically relevant targets is important for a better understanding of their mechanism of actions as well as for the development of less toxic and more effective antitumor drugs (Paragraph 1.3.2 - 1.3.3). RNA is an important potential drug target considering the variety of biologically crucial RNA-dependent processes and its crucial structure-function relationship (Paragraph 1.3).

Towards this direction, the topic of this thesis was the investigation of the interaction between platinum(II) drugs and RNA. In particular, a homogeneously platinated RNA was prepared and characterized in detail using various biochemical and spectroscopic techniques, in order to study the effect of platinum(II) binding on RNA structure. For this study, a model RNA construct (D1-27) was employed and cisplatin and oxaliplatin were used as platination agents. The RNA construct chosen contains several structural features common in many RNAs, which allowed us investigating possible structural preferences of platinum binding (Paragraph 1.1.4).

The first part of **Chapter 2** is dedicated to the investigation of the platination reaction conditions which lead to a homogeneously platinated RNA (monoplatinated) using both cisplatin and oxaliplatin. For this investigation gel mobility shift assays and MALDI-MS analysis were utilized. The data collected showed that the use of oxaliplatin led to the formation of a homogeneous platinated species in higher yield than cisplatin. For this reason, oxaliplatin was used as platination agent in all the following investigation, and the isolated oxaliplatin-modified RNA adduct was carefully characterized. The latter migrates slowly in gels performed on platination mixtures, and gives rise to a well-defined upper band. In the second part of the chapter, the methods used for the isolation of the monoplatinated oxaliplatin-RNA adduct as well as the use of dephosphorylated RNA as starting material for the platination reactions are described.

In **Chapter 3** the use of ^{1}H-NMR time evolution experiments to study platination reactions is described. Indeed, changes in imino proton resonances upon platinum binding can give a quick indication of platinum binding sites. The experiments were used to 1) study the influence of the internal loop, the 5′-end phosphate group and the terminal tetraloop on the platination profile of D1-27 in the presence of

oxaliplatin, 2) screen the platination behaviour of oxaliplatin, cisplatin and kiteplatin towards D1-27 and 3) investigate the role of Cl^- in the platination reaction in the presence of cisplatin. Denaturing gels were also employed to compare the platination reactions of D1-27 with various platinum(II) complexes, and to evaluate the platination profiles using different salt conditions. Finally, the behaviour of oxaliplatin, cisplatin and kiteplatin towards plasmid DNA was also compared, using plasmid binding assays.

Having optimized the reaction conditions for the platination of D1-27 with oxaliplatin (Chapter 2) and established that dephosphorylated RNA will be used in order to have a homogeneous starting RNA sample, time evolution NMR experiments were performed, which provided us with a first information on which nucleobases were mostly affected upon platination (Chapter 3). Therefore, the characterization of the homogeneously platinated dephosphorylated RNA sample, isolated from the upper band on gels performed on platination mixtures, was the next step, and it is described in **Chapter 4**. Thermal melting studies were used to assess the stability of the RNA sample before and after platination, circular dichroism was used to probe the influence of platinum(II) on RNA structure, and enzymatic digestions of ^{32}P-end labelled samples and HPLC analysis showed which nucleobases were affected upon platination. In the end 1D and 2D-NMR experiments were performed to further confirm the platinum(II) binding sites. In the very last part of the chapter a short characterization of the additional minor platinated RNA species formed using dephosphorylated RNA is also described.

Finally, in **Chapter 5** the experimental details for all the studies performed throughout this thesis are given.

1.5 References

1. Hou, Y.-M. in *Encyclopedia of Life Sciences* (John Wiley & Sons, Ltd, Chichester, UK, 2001).
2. Nikolova, E. N., Zhou, H., Gottardo, F. L., Alvey, H. S., Kimsey, I. J. & Al-Hashimi, H. M. A historical account of Hoogsteen base-pairs in duplex DNA. *Biopolymers* **99,** 955–968 (2013).
3. Egli, M. & Saengen, W. *Principles of Nucleic Acid Structure* (Springer New York, New York, NY, 1984).
4. Watson, J. D. & Crick, F. H. C. Molecular structure of nucleic acids. A structure for deoxyribose nucleic acid (Reprinted from Nature, April 25, 1953). *Nature* **224,** 470–471 (1969).
5. Watson, J. D. & Crick, F. H. C. Molecular structure of nucleic acids. A structure for deoxyribose nucleic acid. *Nature* **171,** 737–738 (1953).
6. Pauling, L. & Corey, R. B. A proposed structure for the nucleic acids. *Proc. Natl. Acad. Sci. U. S. A.* **39,** 84–97 (1953).
7. Butcher, S. E. & Pyle, A. M. The molecular interactions that stabilize RNA tertiary structure: RNA motifs, patterns, and networks. *Acc. Chem. Res.* **44,** 1302–1311 (2011).
8. Batey, R. T., Rambo, R. P. & Doudna, J. A. Tertiary motifs in RNA structure and folding. *Angew. Chem. Int. Ed.* **38,** 2326–2343 (1999).
9. Drew, H. R., Wing, R. M., Takano, T., Broka, C., Tanaka, S., Itakura, K. & Dickerson, R. E. Structure of a B-DNA dodecamer: conformation and dynamics. *Proc. Natl. Acad. Sci. U. S. A.* **78,** 2179–2183 (1981).
10. Dock-Bregeon, A. C., Chevrier, B., Podjarny, A., Johnson, J., Bear, J. S. de, Gough, G. R., Gilham, P. T. & Moras, D. Crystallographic structure of an RNA helix: $[U(UA)_6A]_2$. *J. Mol. Biol.* **209,** 459–474 (1989).
11. Ghosh, A. & Bansal, M. A glossary of DNA structures from A to Z. *Acta Crystallogr. D Biol. Crystallogr.* **59,** 620–626 (2003).
12. Cech, T. R. & Steitz, J. A. The noncoding RNA revolution—Trashing old rules to forge new ones. *Cell* **157,** 77–94 (2014).
13. Donghi, D. & Schnabl, J. Multiple roles of metal ions in large ribozymes. *Met. Ions Life Sci.* **9,** 197–234 (2011).
14. Sigel, R. K. Group II intron ribozymes and metal ions – A delicate relationship. *Eur. J. Inorg. Chem.* **2005,** 2281–2292 (2005).
15. Sigel, A., Sigel, H. & Sigel, Roland K. O. *Structural and catalytic roles of metal ions in RNA* (Royal Society of Chemistry, Cambridge, U.K., 2011).

16. Batey, R. T., Gilbert, S. D. & Montange, R. K. Structure of a natural guanine-responsive riboswitch complexed with the metabolite hypoxanthine. *Nature* **432,** 411–415 (2004).

17. Wahl, M. C., Will, C. L. & Luhrmann, R. The spliceosome: design principles of a dynamic RNP machine. *Cell* **136,** 701–718 (2009).

18. Pyle, A. M. Metal ions in the structure and function of RNA. *J. Biol. Inorg. Chem.* **7,** 679–690 (2002).

19. Sigel, R. K. & Pyle, A. M. Alternative roles for metal ions in enzyme catalysis and the implications for ribozyme chemistry. *Chem. Rev.* **107,** 97–113 (2007).

20. Freisinger, E. & Sigel, R. K. From nucleotides to ribozymes—A comparison of their metal ion binding properties. *Coord. Chem. Rev.* **251,** 1834–1851 (2007).

21. Draper, D. E. A guide to ions and RNA structure. *RNA* **10,** 335–343 (2004).

22. Shiman, R. & Draper, D. E. Stabilization of RNA tertiary structure by monovalent cations. *J. Mol. Biol.* **302,** 79–91 (2000).

23. Sigel, A., Sigel, H. & Sigel, R. K. O. *Interplay between Metal Ions and Nucleic Acids* (Springer Netherlands, Dordrecht, 2012).

24. Zamir, A., Miskin, R. & Elson, D. Inactivation and reactivation of ribosomal subunits. Amino acyl-transfer RNA binding activity of the 30 s subunit of *Escherichia coli*. *J. Mol. Biol.* **60,** 347–364 (1971).

25. Misra, V. K. & Draper, D. E. On the role of magnesium ions in RNA stability. *Biopolymers* **48,** 113–135 (1998).

26. Steitz, T. A. & Steitz, J. A. A general two-metal-ion mechanism for catalytic RNA. *Proc. Natl. Acad. Sci. U. S. A.* **90,** 6498–6502 (1993).

27. Pechlaner, M. & Sigel, R. K. Characterization of metal ion-nucleic acid interactions in solution. *Met. Ions Life Sci.* **10,** 1–42 (2012).

28. Erat, M. C. & Sigel, R. K. Methods to detect and characterize metal ion binding sites in RNA. *Met. Ions Life Sci.* **9,** 37–100 (2011).

29. Harris, D. A. & Walter, N. G. Probing RNA structure and metal-binding sites using terbium(III) footprinting. *Curr. Protoc. Nucleic Acid Chem.* **6,** 6.8 (2003).

30. Alberti, E., Zampakou, M. & Donghi, D. Covalent and non-covalent binding of metal complexes to RNA. *J. Inorg. Biochem.* **163,** 278–291 (2016).

31. Michel, F. & Ferat, J. L. Structure and activities of group II introns. *Annu. Rev. Biochem.* **64,** 435–461 (1995).

32. Maria Pechlaner. PhD Thesis. University of Zurich, 2013.

33. Donghi, D., Pechlaner, M., Finazzo, C., Knobloch, B. & Sigel, R. K. The structural stabilization of the κ three-way junction by Mg(II) represents the first step in the folding of a group II intron. *Nucleic Acids Res.* **41,** 2489–2504 (2013).

34. Butcher, S. E., Dieckmann, T. & Feigon, J. Solution structure of a GAAA tetraloop receptor RNA. *EMBO J.* **16,** 7490–7499 (1997).

35. Donghi, D. & Sigel, R. K. Metal ion-RNA interactions studied via multinuclear NMR. *Methods Mol. Biol.* **848,** 253–273 (2012).

36. Waldsich, C. & Pyle, A. M. A folding control element for tertiary collapse of a group II intron ribozyme. *Nat. Struct. Mol. Biol.* **14,** 37–44 (2007).

37. Waldsich, C. & Pyle, A. M. A kinetic intermediate that regulates proper folding of a group II intron RNA. *J. Mol. Biol.* **375,** 572–580 (2008).

38. Fiore, J. L. & Nesbitt, D. J. An RNA folding motif: GNRA tetraloop-receptor interactions. *Q. Rev. Biophys.* **46,** 223–264 (2013).

39. Davis, J. H., Foster, T. R., Tonelli, M. & Butcher, S. E. Role of metal ions in the tetraloop-receptor complex as analyzed by NMR. *RNA* **13,** 76–86 (2007).

40. Davis, J. H., Tonelli, M., Scott, L. G., Jaeger, L., Williamson, J. R. & Butcher, S. E. RNA helical packing in solution: NMR structure of a 30 kDa GAAA tetraloop-receptor complex. *J. Mol. Biol.* **351,** 371–382 (2005).

41. Cate, J. H., Gooding, A. R., Podell, E., Zhou, K., Golden, B. L., Kundrot, C. E., Cech, T. R. & Doudna, J. A. Crystal structure of a group I ribozyme domain. Principles of RNA packing. *Science* **273,** 1678–1685 (1996).

42. Basu, S., Rambo, R. P., Strauss-Soukup, J., Cate, J. H., Ferre-D'Amare, A. R., Strobel, S. A. & Doudna, J. A. A specific monovalent metal ion integral to the AA platform of the RNA tetraloop receptor. *Nat. Struct. Biol.* **5,** 986–992 (1998).

43. Bartova, S., Alberti, E., Sigel, R. K. & Donghi, D. Metal ion binding to an RNA internal loop. *Inorg. Chim. Acta* **452,** 104–110 (2016).

44. Melnikov, S. V., Soll, D., Steitz, T. A. & Polikanov, Y. S. Insights into RNA binding by the anticancer drug cisplatin from the crystal structure of cisplatin-modified ribosome. *Nucleic Acids Res.* **44,** 4978–4987 (2016).

45. Rosenberg, B., van Camp, L. & Krigas, T. Inhibition of cell division in Escherichia coli by electrolysis products from a platinum electrode. *Nature* **205,** 698–699 (1965).

46. Rosenberg, B., van Camp, L., Grimley, E. B. & Thomson, A. J. The inhibition of growth or cell division in Escherichia coli by different ionic species of platinum(IV) Complexes. *J. Biol. Chem.* **242,** 1347–1352 (1967).

47. Orvig, C. & Abrams, M. J. Medicinal inorganic chemistry. Introduction. *Chem. Rev.* **99,** 2201–2204 (1999).

48. Wheate, N. J., Walker, S., Craig, G. E. & Oun, R. The status of platinum anticancer drugs in the clinic and in clinical trials. *Dalton Trans.* **39,** 8113–8127 (2010).

49. Alderden, R. A., Hall, M. D. & Hambley, T. W. The discovery and development of cisplatin. *J. Chem. Educ.* **83,** 728 (2006).

50. Dasari, S. & Tchounwou, P. B. Cisplatin in cancer therapy: molecular mechanisms of action. *Eur. J. Pharmacol.* **740,** 364–378 (2014).

51. Zhu, C., Raber, J. & Eriksson, L. A. Hydrolysis process of the second generation platinum-based anticancer drug cis-amminedichlorocyclohexylamineplatinum(II). *J. Phys. Chem. B* **109,** 12195–12205 (2005).

52. Spessard, G. O. & Miessler, G. L. *Organometallic chemistry.* 2nd ed. (Oxford University Press, New York, 2010).

53. Montana, A. & Batalla, C. The rational design of anticancer platinum complexes:The importance of the structure-activity relationship. *Curr. Med. Chem* **16,** 2235–2260 (2009).

54. Cleare, M. J. & Hoeschele, J. D. Studies on the antitumor activity of group VIII transition metal complexes. Part I. Platinum (II) complexes. *Bioinorg. Chem.* **2,** 187–210 (1973).

55. Boulikas, T. & Vougiouka, M. Cisplatin and platinum drugs at the molecular level (Review). *Oncol. Rep*. **10,** 1663–1682 (2003).

56. Hoeschele, J. D., Showalter, H. D. H., Kraker, A. J., Elliott, W. L., Roberts, B. J. & Kampf, J. W. Synthesis, structural characterization, and antitumor properties of a novel class of large-ring platinum(II) chelate complexes incorporating the cis-1,4-diaminocyclohexane ligand in a unique locked boat conformation. *J. Med. Chem.* **37,** 2630–2636 (1994).

57. Margiotta, N., Marzano, C., Gandin, V., Osella, D., Ravera, M., Gabano, E., Platts, J. A., Petruzzella, E., Hoeschele, J. D. & Natile, G. Revisiting $PtCl_2$(cis-1,4-DACH): an underestimated antitumor drug with potential application to the treatment of oxaliplatin-refractory colorectal cancer. *J. Med. Chem.* **55,** 7182–7192 (2012).

58. Kasparkova, J., Suchankova, T., Halamikova, A., Zerzankova, L., Vrana, O., Margiotta, N., Natile, G. & Brabec, V. Cytotoxicity, cellular uptake, glutathione and DNA interactions of an antitumor

large-ring Pt^{II} chelate complex incorporating the cis-1,4-diaminocyclohexane carrier ligand. *Biochem. Pharmacol.* **79,** 552–564 (2010).

59. Ranaldo, R., Margiotta, N., Intini, F. P., Pacifico, C. & Natile, G. Conformer distribution in (cis-1,4-DACH)bis(guanosine-5'-phosphate)platinum(II) adducts: a reliable model for DNA adducts of antitumoral cisplatin. *Inorg. Chem.* **47,** 2820–2830 (2008).

60. Margiotta, N., Petruzzella, E., Platts, J. A., Mutter, S. T., Deeth, R. J., Ranaldo, R., Papadia, P., Marzilli, P. A., Marzilli, L. G., Hoeschele, J. D. & Natile, G. DNA fragment conformations in adducts with Kiteplatin. *Dalton Trans.* **44,** 3544–3556 (2015).

61. Hall, M. D., Okabe, M., Shen, D.-W., Liang, X.-J. & Gottesman, M. M. The role of cellular accumulation in determining sensitivity to platinum-based chemotherapy. *Annu. Rev. Pharmacol. Toxicol.* **48,** 495–535 (2008).

62. Ishida, S., Lee, J., Thiele, D. J. & Herskowitz, I. Uptake of the anticancer drug cisplatin mediated by the copper transporter Ctr1 in yeast and mammals. *Proc. Natl. Acad. Sci. U. S. A.* **99,** 14298–14302 (2002).

63. Orton, D. M., Gretton, V. A. & Green, M. Acidity constants for cis-diaquadiammineplatinum(II), the aquated form of cisplatin. *Inorg. Chim. Acta* **204,** 265–266 (1993).

64. Jamieson, E. R. & Lippard, S. J. Structure, recognition, and processing of cisplatin−DNA adducts. *Chem. Rev.* **99,** 2467–2498 (1999).

65. Horacek, P. & Drobnik, J. Interaction of cis-dichlorodiammineplatinum (II) with DNA. *Biochim. Biophys. Acta* **254,** 341–347 (1971).

66. Elmroth, S. K. & Lippard, S. J. Platinum binding to d(GpG) target sequences and phosphorothioate linkages in DNA occurs more rapidly with increasing oligonucleotide length. *J. Am. Chem. Soc.* **116,** 3633–3634 (1994).

67. Arpalahti, J. & Lippert, B. Coordination of aquated cis-platinum(II) diamines to purine nucleosides. Kinetics of complex formation. *Inorg. Chem.* **29,** 104–110 (1990).

68. Kozelka, J. Molecular origin of the sequence-dependent kinetics of reactions between cisplatin derivatives and DNA. *Inorg. Chim. Acta* **362,** 651–668 (2009).

69. Gelasco, A. & Lippard, S. J. NMR solution structure of a DNA dodecamer duplex containing a cis-diammineplatinum(II) d(GpG) intrastrand cross-link, the major adduct of the anticancer drug cisplatin. *Biochemistry* **37,** 9230–9239 (1998).

70. Takahara, P. M., Frederick, C. A. & Lippard, S. J. Crystal structure of the anticancer drug cisplatin bound to duplex DNA. *J. Am. Chem. Soc.* **118,** 12309–12321 (1996).

71. Ahmad, S., Isab, A. A. & Ali, S. Structural and mechanistic aspects of platinum anticancer agents. *Transition Met. Chem.* **31,** 1003–1016 (2006).

72. Stehlikova, K., Kostrhunova, H., Kasparkova, J. & Brabec, V. DNA bending and unwinding due to the major 1,2-GG intrastrand cross-link formed by antitumor cis-diamminedichloroplatinum(II) are flanking-base independent. *Nucleic Acids Res.* **30,** 2894–2898 (2002).

73. Hambley, T. W. Platinum binding to DNA. Structural controls and consequences. *J. Chem. Soc., Dalton Trans.*, 2711–2718 (2001).

74. Fuertes, M. A., Alonso, C. & Perez, J. M. Biochemical modulation of cisplatin mechanisms of action: enhancement of antitumor activity and circumvention of drug resistance. *Chem. Rev.* **103,** 645–662 (2003).

75. Bischin, C., Lupan, A., Taciuc, V. & Silaghi-Dumitrescu, R. Interactions between proteins and platinum-containing anti-cancer drugs. *Mini Rev. Med. Chem.* **11,** 214–224 (2011).

76. Chapman, E. G., Hostetter, A. A., Osborn, M. F., Miller, A. L. & DeRose, V. J. Binding of kinetically inert metal ions to RNA: The case of platinum(II). *Met. Ions Life Sci.* **9,** 347–377 (2011).

77. Sharp, P. A. The centrality of RNA. *Cell* **136,** 577–580 (2009).

78. Guan, L. & Disney, M. D. Recent advances in developing small molecules targeting RNA. *ACS Chem. Biol.* **7,** 73–86 (2012).

79. Disney, M. D. Rational design of chemical genetic probes of RNA function and lead therapeutics targeting repeating transcripts. *Drug Discov. Today* **18,** 1228–1236 (2013).

80. Bennett, C. F. & Swayze, E. E. RNA targeting therapeutics: molecular mechanisms of antisense oligonucleotides as a therapeutic platform. *Annu. Rev. Pharmacol. Toxicol.* **50,** 259–293 (2010).

81. Fougerolles, A. de, Vornlocher, H.-P., Maraganore, J. & Lieberman, J. Interfering with disease: a progress report on siRNA-based therapeutics. *Nat. Rev. Drug Discov.* **6,** 443–453 (2007).

82. Thomas, J. R. & Hergenrother, P. J. Targeting RNA with small molecules. *Chem. Rev.* **108,** 1171–1224 (2008).

83. Davidson, A., Patora-Komisarska, K., Robinson, J. A. & Varani, G. Essential structural requirements for specific recognition of HIV TAR RNA by peptide mimetics of Tat protein. *Nucleic Acids Res.* **39,** 248–256 (2011).

84. Velagapudi, S. P., Vummidi, B. R. & Disney, M. D. Small molecule chemical probes of microRNA function. *Curr. Opin. Chem. Biol.* **24,** 97–103 (2015).

85. Tran, T., Childs-Disney, J. L., Liu, B., Guan, L., Rzuczek, S. & Disney, M. D. Targeting the r(CGG) repeats that cause FXTAS with modularly assembled small molecules and oligonucleotides. *ACS Chem. Biol.* **9,** 904–912 (2014).

86. Hostetter, A. A., Osborn, M. F. & DeRose, V. J. RNA-Pt adducts following cisplatin treatment of Saccharomyces cerevisiae. *ACS Chem. Biol.* **7,** 218–225 (2012).

87. Hagerlof, M., Hedman, H. K. & Elmroth, S. K. Platination of the siRNA sense-strand modulates both efficacy and selectivity in vitro. *Biochem. Biophys. Res. Commun.* **361,** 14–19 (2007).

88. Schmittgen, T. D., Ju, J.-F., Danenberg, K. D. & Danenberg, P. V. Inhibition of pre-mRNA splicing by cisplatin and platinum analogs. *Int. J. Oncol.* **23,** 785–789 (2003).

89. Danenberg, P. V., Shea, L. C., Danenberg, K. D. & Horikoshi, T. Inactivation of Tetrahymena rRNA self-splicing by cis-platin proceeds through dissociable complexes. *Nucleic Acids Res.* **19,** 3123–3128 (1991).

90. Rosenberg, J. & Sato, P. H. Messenger RNA loses the ability to direct in vitro peptide synthesis following incubation with cisplatin. *Mol. Pharmacol.* **33,** 611–616 (1988).

91. Rosenberg, J. M. & Sato, P. H. Cisplatin inhibits in vitro translation by preventing the formation of complete initiation complex. *Mol. Pharmacol.* **43,** 491–497 (1993).

92. Becker, J. P., Weiss, J. & Theile, D. Cisplatin, oxaliplatin, and carboplatin unequally inhibit in vitro mRNA translation. *Toxicol. Lett.* **225,** 43–47 (2014).

93. Osborn, M. F., White, J. D., Haley, M. M. & DeRose, V. J. Platinum-RNA modifications following drug treatment in S. cerevisiae identified by click chemistry and enzymatic mapping. *ACS Chem. Biol.* **9,** 2404–2411 (2014).

94. Chapman, E. G. & DeRose, V. J. Enzymatic processing of platinated RNAs. *J. Am. Chem. Soc.* **132,** 1946–1952 (2010).

95. Polonyi, C., Albertsson, I., Damian, M. S. & Elmroth, S. K. Comparison of cis- and oxaliplatin-induced destabilization of 15-mer DNA- and RNA duplexes by binding to centrally located GG- and GNG sequences. *Z. anorg. allg. Chem.* **639,** 1655–1660 (2013).

96. Alshiekh, A., Clausén, M. & Elmroth, S. K. Kinetics of cisplatin binding to short r(GG) containing miRNA mimics – influence of Na^+ versus K^+ , temperature and hydrophobicity on reactivity. *Dalton Trans.* **44,** 12623–12632 (2015).

97. Polonyi, C., Alshiekh, A., Sarsam, L. A., Clausén, M. & Elmroth, S. K. Cisplatin-induced duplex dissociation of complementary and destabilized short GG-containing duplex RNAs. *Dalton Trans.* **43,** 11941–11949 (2014).

98. Polonyi, C. & Elmroth, S. K. Time dependence of cisplatin-induced duplex dissociation of 15-mer RNAs and mature miR-146a. *Dalton Trans.* **42,** 14959 (2013).

99. Papsai, P., Aldag, J., Persson Tina, J. & Elmroth, S. K. Kinetic preference for interaction of cisplatin with the G–C-rich wobble basepair region in both $tRNA^{Ala}$ and Mh^{Ala}. *Dalton Trans.,* 3515–3517 (2006).

100. Papsai, P., Snygg, A. S., Aldag, J. & Elmroth, S. K. Platination of full length $tRNA^{Ala}$ and truncated versions of the acceptor stem and anticodon loop. *Dalton Trans.,* 5225–5234 (2008).

101. Hostetter, A. A., Chapman, E. G. & DeRose, V. J. Rapid cross-linking of an RNA internal loop by the anticancer drug cisplatin. *J. Am. Chem. Soc.* **131,** 9250–9257 (2009).

102. Rijal, K. & Chow, C. S. A new role for cisplatin: probing ribosomal RNA structure. *Chem. Commun.,* 107–109 (2009).

103. Dedduwa-Mudalige, G. N. P. & Chow, C. S. Cisplatin targeting of bacterial ribosomal RNA hairpins. *Int. J. Mol. Sci.* **16,** 21392–21409 (2015).

104. Rijal, K., Bao, X. & Chow, C. S. Amino acid-linked platinum(II) analogues have altered specificity for RNA compared to cisplatin. *Chem. Commun.* **50,** 3918–3920 (2014).

105. Carthew, R. W. & Sontheimer, E. J. Origins and mechanisms of miRNAs and siRNAs. *Cell* **136,** 642–655 (2009).

106. Hedman, H. K., Kirpekar, F. & Elmroth, S. K. Platinum interference with siRNA non-seed regions fine-tunes silencing capacity. *J. Am. Chem. Soc.* **133,** 11977–11984 (2011).

107. Dewan, J. C. Binding of the antitumor drug cis-diamminedichloroplatinum to crystalline tRNAPhe at 6-.ANG. resolution. *J. Am. Chem. Soc.* **106,** 7239–7244 (1984).

108. Rhodes, D., Piper, P. W. & Clark, B. Location of a platinum binding site in the structure of yeast phenylalanine transfer RNA. *J. Mol. Biol.* **89,** 469–475 (1974).

109. Rubin, J. R., Sabat, M. & Sundaralingam, M. Similar binding of the carcinostatic drugs cis-$[Pt[NH_3)_2]$ and $[Ru(NH_3)_5Cl]Cl_2$ to $tRNA^{phe}$ and a comparison w with the binding of the inactive trans -$[Pt(NH_3)_2Cl_2]$ complex - reluctance in binding to Watson-Crick base pain within doable helix. *Nucleic Acids Res.* **11,** 6571–6586 (1983).

110. Malinina, L., Tereshko, V., Ivanova, E., Subirana, J. A., Zarytova, V. & Nekrasov, Y. Structural variability and new intermolecular interactions of Z-DNA in crystals of d(pCpGpCpGpCpG). *Biophys. J.* **74,** 2482–2490 (1998).

2 Investigation of the platination reaction conditions and isolation of monoplatinated RNA

2.1 Aim

In the first half of this chapter it will be described the evaluation of cisplatin (cisPt) and oxaliplatin (oxaliPt) as possible platination agents for D1-27. Gel mobility shift assays together with MALDI-MS analysis were employed for this purpose. The desired final product is a homogeneously monoplatinated RNA, in which the platination binding site can be unambiguously identified. In the second half, the methods used for the isolation of monoplatinated RNA samples as well as the use of dephosphorylated RNA (deph-RNA) for the platination reactions will be described.

2.2 Introduction: Platination of RNA

RNA has received a lot of attention in the last few years as possible platinum binding target in an attempt to study platinum interactions with biomolecules other than DNA, in order to better understand their mechanism of action and probably the origin of their side effects[1,2]. Additionally, the inhibition of important RNA-based processes like transcription[3] and translation[4] in the presence of platinum(II) has further supported the importance of RNA as platinum(II) drug target (Chapter 1, Paragraph 1.3). Towards this direction we were aiming at investigating the interaction of platinum(II) anticancer drugs with RNA. Considering that RNA platination may be sequence and structure dependent[5], an RNA model was used (D1-27) (Figure 2.1) in which both structure and sequence dependency of platinum binding could be investigated (Chapter 1, Paragraph 1.1.4). This RNA derived from the mitochondrial group II intron ribozyme *Sc*.ai5γ from *Saccharomyces cerevisiae*, baker's yeast[6], and it has high content of guanines and adenines, which represent possible platinum binding sites[7], but it also contains various structural motifs which are common in many RNAs. In these motifs are included the very stable -UUCG- terminal loop[8], and an internal loop which in the context of the Group II intron is acting as a GAAA tetraloop-receptor[9] (Chapter 1, Paragraph 1.1.4). The presence of these biologically relevant structural motifs will allow us to investigate possible structural preference of the platination. Additionally, its NMR three dimensional structure in solution is known[10], thus making easier the NMR characterization of its platinated species. Lastly, NMR studies on Mg(II), Cd(II) and Co(III)hexammine binding to this specific RNA were recently reported[11] which gave us evidences about the sites which can accommodate divalent metal ions. After the recently reported crystal structure of cisplatin-ribosome which is suggesting that the Mg(II) binding sites could also represent possible platinum(II) binding sites[12] (Chapter 1, Paragraph 1.3.5), knowing where Mg(II) binds in our construct may give us a first indication of the possible platination sites.

The characterization of the Pt(II)-RNA adducts was performed with various biochemical methods and spectroscopic techniques. Gel mobility shift assays are widely used for the evaluation of the platination reactions with both RNA and DNA. For example, it was reported that the reaction of RNA or DNA with

platinum(II) complexes results in products which could migrate either slower or faster compared to unplatinated RNA[5,13,14] or DNA[15,16] when analyzed by denaturing PolyAcrylamide Gel Electrophoresis (dPAGE). Slower migration of the platinated species could be either due to their higher molecular weight or to the reduced overall negative charge of the nucleic acid upon binding of the platinum complex. Contrarily, faster migration could be caused by the formation of intrastrand cross-linking[13,15]. Moreover, least distorted Pt(II)-RNA adducts could be formed, with similar migration as the unplatinated RNA. In the current study, the presence of one or more new bands was used as indication of actual platination. The intensity of the new band was used to evaluate the platination efficiency. The higher the intensity, the higher the amount of platinated species formed. From the ratio of the intensity of the new band and the band corresponding to the unreacted RNA, a first evaluation of the reaction speed could be done. The faster the reaction was, the less intense was the band corresponding to the unreacted RNA, and new band(s) appeared on the gel, depending on the different RNA species formed. In order to get information about the platinated RNA species migrating in the gel bands, the gel pieces were cut and the Pt(II)-RNA species were isolated (Chapter 5, Paragraph 5.4) and characterized with MALDI-MS. From the mass spectra we could get information about the number and the identity of the formed species (Paragraph 2.7). The RNA with one platinum moiety will be called monoplatinated and the RNA sample with two platinum moieties diplatinated. The expected and measured m/z for each species (monoplatinated, diplatinated etc.) are given in Appendix 1.

The optimization of the platination reaction conditions that will be described below has as a target to obtain a homogeneously platinated RNA sample in reasonable yield, which will be used later on for further characterization. More specifically, we investigated the presence of a preferential binding site. The RNA molecule chosen for this study offers several platination sites (Figure 2.1), and only the presence of a strong preferential platinum binding site would indeed ideally lead to the formation of a single monoplatinated RNA species. The investigation of the platination reaction conditions involved optimization of parameters like RNA and platinum concentration, temperature, time of incubation and reaction buffer.

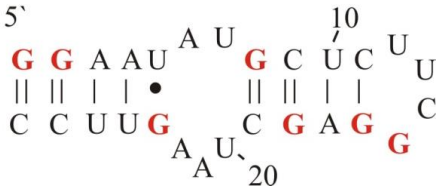

Figure 2.1: *The secondary structure of D1-27. In red are denoted the guanines, which could be possible platination sites.*

The platination reactions were performed at pH 6 – 6.5. Indeed, on the one hand, RNA stability decreases at alkaline pH[17], therefore staying within this range we avoided RNA degradation. On the other hand, aquation rates and species, and binding of cisplatin and oxaliplatin depend on pH and ionic

environment[18,19]. For example, in the case of monoaquated cisplatin and its derivatives the pK_a of the monoaquated species is between 6 to 7 and therefore under the pH conditions used here the formation of the less reactive hydroxyl species is avoided[20–24] (Figure 2.2). For oxaliplatin the pK_a for the oxalate monodentate complex (ring-opening) was estimated at 7.2 and therefore within this pH range the use of the intact complex is assured[19].

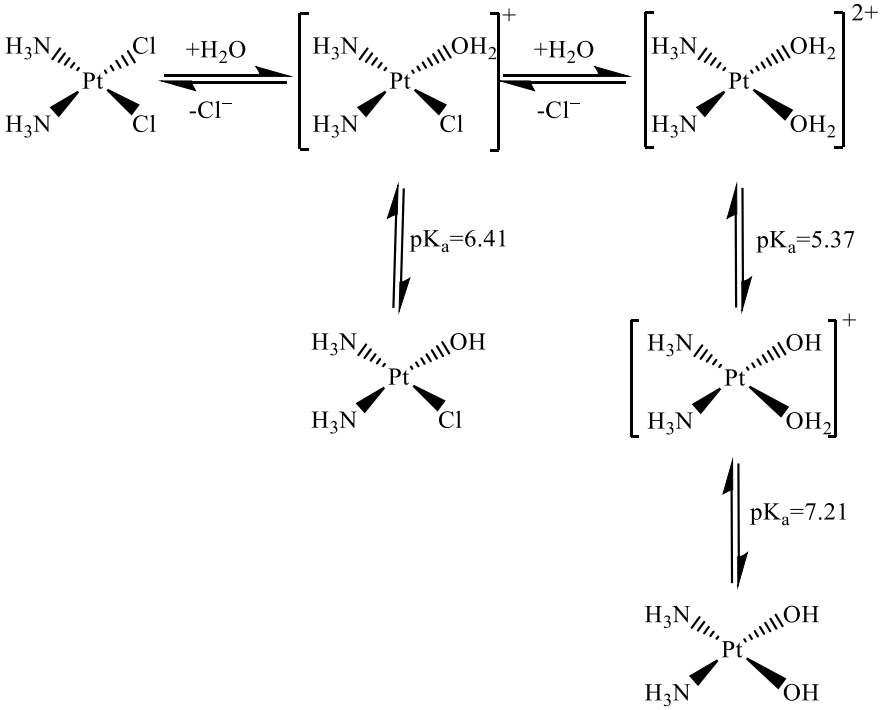

Figure 2.2: *Cisplatin speciation in aqueous solutions[20].*

2.3 Platination reactions of D1-27 with cisplatin

The first platinum(II) complex used for platination studies was cisplatin, both in its non-activated and its activated form, as monoaquo complex (Figure 2.3). The aquation / activation of cisPt is described in detail in the experimental part (Chapter 5, Paragraph 5.2.4*)*.

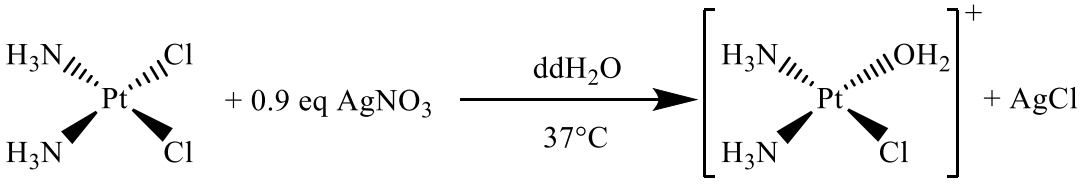

Figure 2.3: *Activation of cisplatin and formation of the monoaquated complex.*

2.3.1 Platinum concentration dependent experiments at 25 °C

Preliminary data on the interaction of D1-27 with cisPt were collected by the master student Dania Marthaler[25]. These data showed that 1 equivalent (eq) of cisPt was enough to give rise to the formation of a new slower migrating band which though was very low in intensity. Trying to increase the intensity of the band and consequently the platination yield an excess of platinum complex (5 eq and 10 eq) as well as the activated monoaquated cisPt were used. Higher reaction rates are expected by increasing the concentration either of RNA or platination agent, since more molecules are available to react. This would in turn lead to the formation of a higher amount of platinated species, then contributing to increasing the platination yield. The use of monoaquated cisPt instead of its parent compound was also expected to increase the platination rate. It is indeed known that activated platinum(II) complexes react faster compared to their parent compounds[7]. At first, 1 eq, 5 eq and 10 eq of cisPt and monoaquated cisPt were reacted with 0.1 mM D1-27 in 60 mM $KClO_4$ / 10µM EDTA for 5 days at 25 °C (Figure 2.4). No second band was observed on the gel in the case of 1 eq of cisPt and monoaquated cisPt, while for 5 eq and 10 eq a not defined band (smear) was observed for both platinum complexes. Smear is formed when there are differently multiplatinated species which are not properly separated in a gel to give a compact band. For 10 eq of cisPt and monoaquated cisPt additionally to the formation of a smeary band there was also not unreacted RNA left. That indicates that the reaction with 10 eq of platinum(II) complex proceeded faster compared to the reaction with 5 eq. Comparing the behaviour of the two platinum(II) complexes using 10 eq it is also worth noting that the smeary band observed in the case of the reaction performed with monoaquated cisPt migrated slower compared to the one with cisPt. This slower migration may be indicative of the presence of higher content of different multiplatinated RNA species suggesting faster reaction rate. This is in accordance with what is reported in the literature about the speed of the activated and non-activated platinum(II) complexes[7,18].

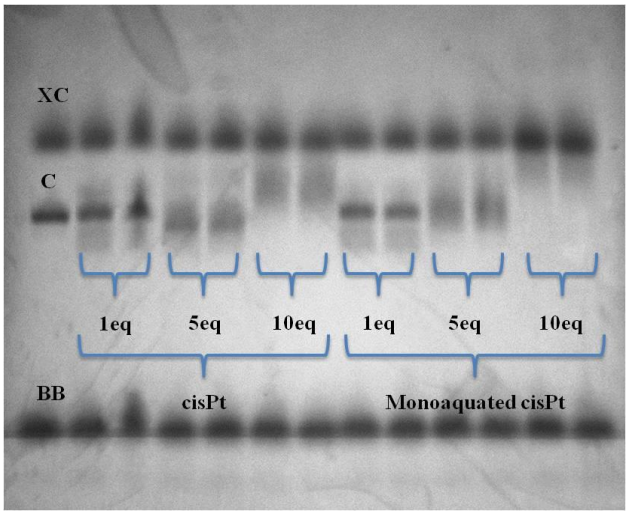

Figure 2.4: *18 % denaturing PAGE for the platinum concentration dependent experiments at 25 °C. 1 eq, 5 eq and 10 eq of cisPt and monoaquated cisPt were tested in 60 mM $KClO_4$ / 10 µM EDTA for 5 days. Both lanes correspond to the repetition of the same reaction. The gel was run at room temperature.*

2.3.2 Platinum concentration dependent experiments at 37 °C

At 25 °C there was no formation of a well-defined second band. So similar experiments, as above, were performed at higher temperature (37 °C) attempting to enhance the formation of platinated RNA species, which were homogeneous enough to form a compact band. Now only monoaquated cisPt was used considering that it reacts faster than cisPt[7,18]. 1 eq, 5 eq and 10 eq of monoaquated cisPt were reacted with 0.1 mM D1-27, for 5 days in 60 mM $KClO_4$ / 10 μM EDTA and in MOPS buffer (Figure 2.5). MOPS buffer is widely used for platination reactions[5]. Also in this case, no second band was observed on the gel when the reaction was performed in the presence of 1 eq of monoaquated cisplatin. Conversely, the use of 5 eq and 10 eq of monoaquated cisplatin led to the formation of smeary bands on the gel (Figure 2.5). There was no significant difference in the behaviour of the reactions in MOPS and in $KClO_4$ / EDTA solution (Figure 2.5) but for the slower migrating smeary band that is observed when 10 eq of monoaquated cisPt are used in the presence of MOPS. This suggests that the content of platinum per RNA was higher in the presence of MOPS, likely due to higher platination speed. Interestingly, in the presence of 5 eq of monoaquated cisplatin in $KClO_4$ / EDTA, the band corresponding to unreacted RNA is stronger at 25 °C (Figure 2.4) than at 37°C (Figure 2.5), suggesting that the reaction at this temperature proceeded faster, as expected. Unfortunately, the platination reactions performed so far at 25 °C and 37 °C, whatever the reaction conditions and the platinum complex used, did not result in the formation of a clear second band.

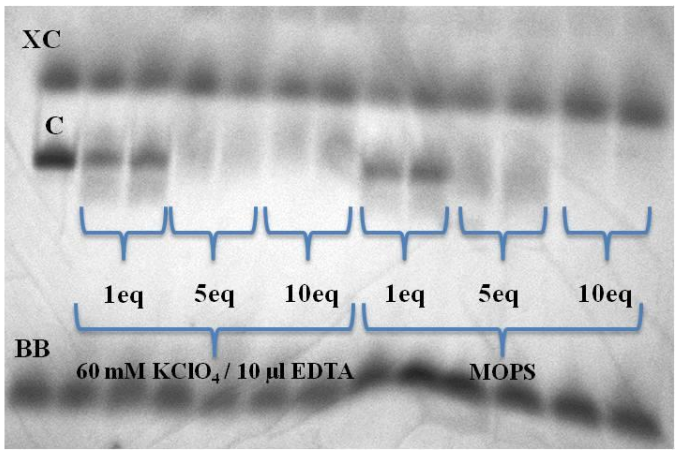

Figure 2.5: *18 % denaturing PAGE for the platinum concentration dependent experiments at 37 °C. 1 eq, 5 eq and 10 eq of monoaquated cisPt were tested in 60 mM $KClO_4$ / 10 μM EDTA and in MOPS buffer. Both lanes correspond to the repetition of the same reaction. The gel was run at room temperature.*

The behaviour was different when instead of 60 mM $KClO_4$ / 10 μM EDTA, double distilled water (ddH_2O) was used. When 5 eq, 10 eq and 15 eq of monoaquated cisPt were reacted with 0.1 mM D1-27 at 37 °C for 15 h in ddH_2O, there was formation of a second band in the case of 5 eq (Figure 2.6, blue frame). In the other two cases, not defined bands were observed, indicative of a mixture of multiple

platinated RNAs. As already commented above, the slower the migration of these bands, the higher their platinum content (Figure 2.6). In the platination reaction in ddH_2O the incubation time was significantly reduced (15 h), because folding and stability of D1-27 are expected to be lower in the absence of monovalent metal ions, and the platination sites are likely to be better accessible, thus leading to easier and faster platination (Chapter 4, Paragraph 4.4 - 4.5).

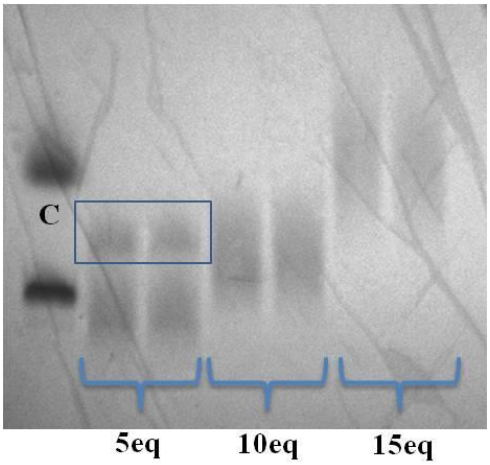

Figure 2.6: *18 % denaturing PAGE for the platinum concentration dependent experiments at 37 °C. 5 eq, 10 eq and 15 eq of monoaquated cisPt were tested in ddH_2O. Both lanes for each reaction correspond to the repetition of the same reaction. The gel was run at room temperature.*

2.3.3 Platinum concentration dependent experiments at 50 °C

In the previous paragraphs it was shown that at 25 °C and 37 °C there was not formation of a clear second band and there were only smeary bands when 60 mM $KClO_4$ / 10 μM EDTA or MOPS buffer were used. The next temperature tested was 50 °C. This corresponds to the first melting temperature of D1-27 (Tm_1 = 53.8 ± 2.1 °C). The melting temperature profile of D1-27 shows two transitions, which may be attributed to the denaturing of the first and the second part of the construct, respectively (Chapter 4, Paragraph 4.4). At 50 °C partial denaturing of the first part of the construct is expected[26,27], thus making possible binding sites more accessible. The reactions were performed in both 60 mM $KClO_4$ / 10 μM EDTA and in ddH_2O (Figure 2.7). Thermal melting studies show that D1-27 stability increases upon addition of potassium ions. Moreover, CD spectra recorded in the presence of increasing potassium(I) concentration suggest that the fraction of folded RNA increases upon potassium(I) addition (Chapter 4, Paragraph 4.4 - 4.5). Since faster reaction is expected at higher temperature, especially in water, the reaction time was reduced from 5 days to 15 h and cisplatin was used instead of the monoaquated derivative.

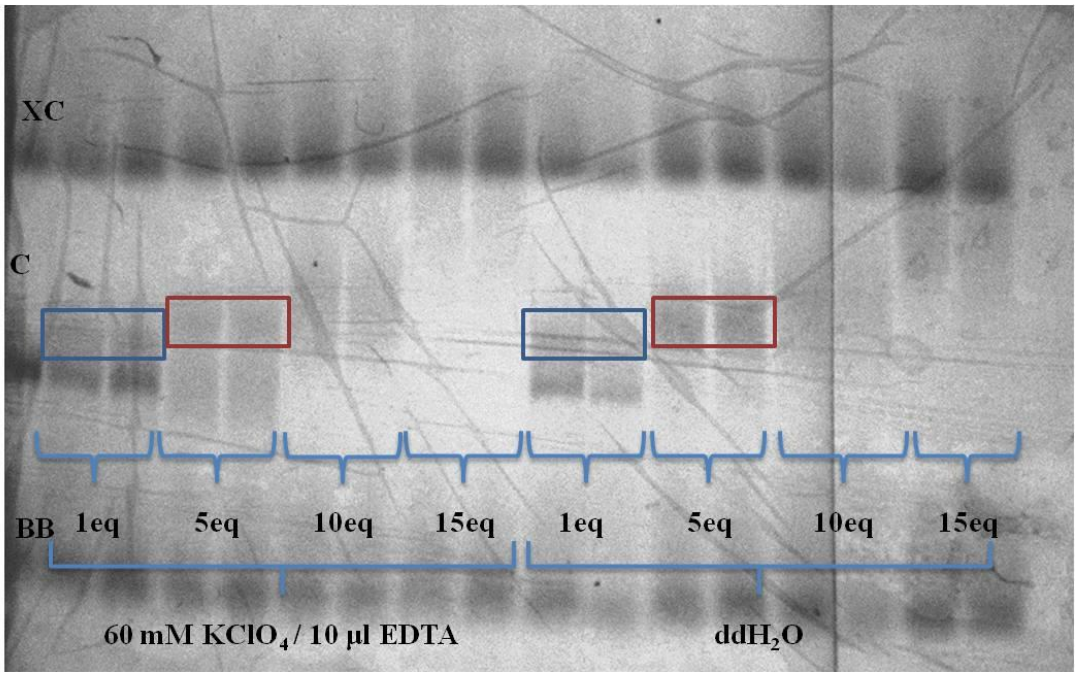

Figure 2.7: *18 % denaturing PAGE for the platinum concentration dependent experiments at 50 °C. 1 eq, 5 eq 10 eq and 15 eq of cisPt were tested in 60 mM $KClO_4$ / 10 µM EDTA and in ddH_2O. Both lanes correspond to the repetition of the same reaction. The gel was run at room temperature.*

Both in the presence and in the absence of monovalent ions, a new slower migrating band was observed in the gel when the reaction was performed using 1 eq of cisPt and 0.1 mM D1-27 at 50 °C (Figure 2.7, blue frame). This band was more pronounced in the reaction with ddH_2O. With 5 eq -15 eq there were only undefined bands which by increasing the platinum concentration were migrating slower (Figure 2.7). Comparing the reaction of 5 eq of cisPt with RNA in 60 mM $KClO_4$ / 10 µM EDTA and in ddH_2O, formation of a new slower migrating band was observed in both cases (Figure 2.7, red frame). The difference was that for the reaction in ddH_2O there was no unreacted RNA left suggesting that the platination reaction was faster. This was not surprising, since in the absence of monovalent ions D1-27 is expected to be less stable, making the platination sites more available. Moreover, the absence of cations which could compete with platinum for RNA binding is expected to favour platination[13]. Based on the collected results until now, the best picture was obtained using 5 eq of cisPt in ddH_2O, at which the formation of a new band and no band for unreacted RNA was observed. Consequently, less than 5 eq had to be tested in order to investigate when the new band appears.

The next set of experiments included the platination of 0.1 mM D1-27 with 0.5, 1, 2, 3, 4 and 5 eq of monoaquated cisPt, at 50 °C, for 15 h in ddH_2O (Figure 2.8). Monoaquated cisPt was used instead of cisPt attempting to further increase the platination yield in the presence of less equivalents of platination agent. In the following gel (Figure 2.8) is depicted the formation of the upper band with increasing platinum concentration (blue frame). The upper bands corresponding to the reactions performed in the

presence of 2 to 5 eq were intense enough to be cut (Figure 2.8, blue frame). The platinated RNA species were isolated from the gel pieces and purified (Chapter 5, Paragraph 5.4). Due to low recovery of the samples corresponding to the reactions performed with 2 eq and 3 eq of cisPt only the upper bands obtained in the case of 4 eq and 5 eq were characterized with MALDI-MS. The MS spectrum of the two samples combined showed that they contained mixture of multiplatinated RNA species (monoplatinated, diplatinated, triplatinated and tetraplatinated RNA) (Appendix 1, A 1.1). Summing up, these experiments showed that the platination of D1-27 with 4 and 5 eq of monoaquated cisPt at 50 °C, for 15 h in ddH_2O on the one hand resulted in the formation of a well-defined new band but on the other hand the reaction was fast enough to lead to the formation of multiplatinated species.

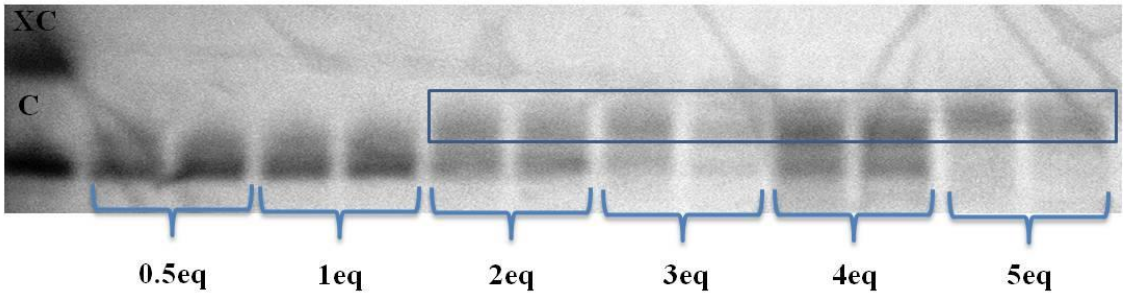

Figure 2.8: *18 % denaturing PAGE for the platinum concentration dependent experiments at 50 °C. 0.5 eq -5 eq of monoaquated cisPt were tested in ddH_2O. Both lanes correspond to the repetition of the same reaction. The gel was run at room temperature.*

2.3.4 Time and temperature dependent experiments in the presence of 1 eq and 2 eq of monoaquated cisplatin in ddH_2O

The experiments commented in paragraph 2.3.3 showed that the use of 4 eq or 5 eq of monoaquated cisPt led to multiplatinated species. Consequently, 1 and 2 eq of monoaquated cisPt were tested, with 0.1 mM D1-27, at 25, 37 and 50 °C for 15 h, 1 day and 2 days in ddH_2O (Figures 2.9 and 2.10). At 25 °C using 1 eq of monoaquated cisPt the band corresponding to unreacted D1-27 was almost intact and a faint smear close to this band was observed (Figure 2.9, right). That suggests that the formation of platinated RNA species was slow and the species formed were not separated sufficiently on the gel. However, formation of species which were not significantly distorted and therefore had mobility similar to the unreacted RNA could also be the reason for the observed behaviour[14]. On the contrary, at 37 °C and 50 °C, using 1 eq of monoaquated cisPt there was formation of a second slower migrating band which was better defined (Figure 2.9, centre and left). These gel bands were cut and the platinated RNA samples were isolated and characterized with MALDI-MS. The upper bands corresponding to the reactions performed at 37 °C contained unreacted RNA and monoplatinated species (Appendix 1, A 1.2), while the corresponding upper bands at 50 °C contained a mixture of unreacted, monoplatinated and diplatinated RNA with the monoplatinated being the major species (Appendix 1, A 1.3).

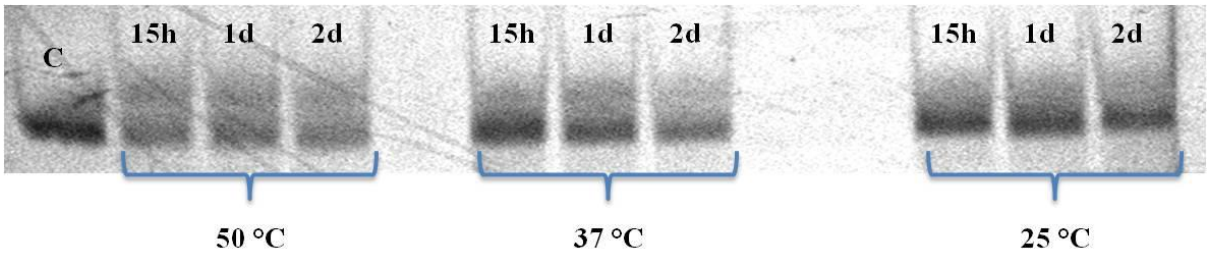

Figure 2.9: *15 % denaturing PAGE for time and temperature dependent experiments for 1 eq of monoaquated cisplatin. Reaction of 1 eq monoaquated cisPt was tested at 25 °C, 37 °C and 50 °C in ddH_2O. The reaction time varied from 15 h to 1 day and 2 days. The gel was run at room temperature.*

A similar behaviour was observed when the reaction was repeated at 25 °C in the presence of 2 eq of monoaquated cisplatin (Figure 2.10, right). At 37 °C and 50 °C using 2 eq of monoaquated cisPt the behaviour was also similar to 1 eq but the bands seem to be slightly more intense, suggesting that higher amount of platinated RNA was formed (Figure 2.10, middle, left). At 50 °C there was less unreacted RNA and the new band was more intense compared to the new band at 37 °C, indicating that the reaction was faster (Figure 2.10, middle, left). The platinated RNA from the new upper bands at 50 °C and 37 °C were isolated and characterized with MALDI-MS. They both contained a mixture of mostly monoplatinated and, to a lesser extent, diplatinated as well as triplatinated and tetraplatinated RNA (Appendix A 1.4 - A 1.5). By increasing the temperature, the reaction was faster and more platinated species were formed; the upper bands were better defined but they all contained a mixture of monoplatinated and diplatinated RNA. The presence of a better-defined second band could be the result of the formation of more similarly platinated RNA species possibly suggesting the existence of a preferable platination site.

Putting together the results from the abovementioned comparison using 1 eq and 2 eq of platinum complex, the upper bands which did not contain multiplatinated RNA resulted from the reaction of 1 eq of monoaquated cisPt with 0.1 mM D1-27 at 37 °C (Figure 2.9, middle) and these were the conditions chosen. The platinated RNA species from the upper bands in all cases were mixed in order to have enough sample to be characterized by MALDI-MS. Therefore, a safe conclusion about the time dependency could not be done.

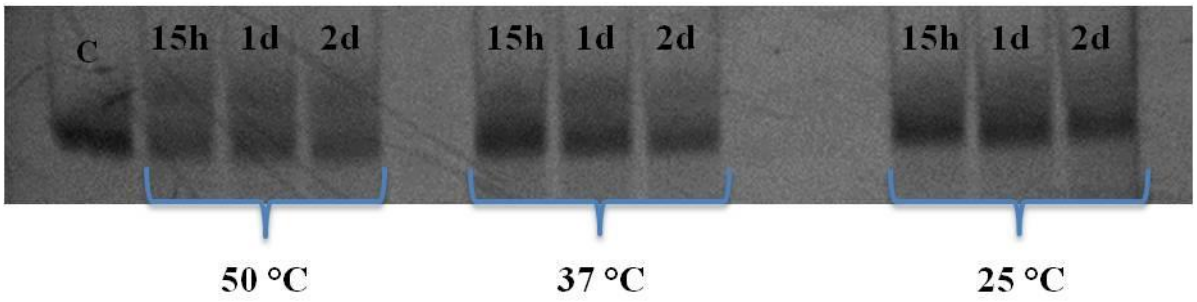

Figure 2.10: *15 % denaturing PAGE for time and temperature dependent experiments for 2 eq of monoaquated cisplatin. Reaction of 2 eq of monoaquated cisPt was tested at 25 °C, 37 °C and 50 °C in ddH_2O. The reaction time varied from 15 h to 1 day and 2 days. The gel was run at room temperature.*

2.3.5 RNA concentration dependent experiments

Based on the results commented in paragraph 2.3.4, the platination reactions were repeated using 1 eq of monoaquated cisPt in the presence of different concentration of D1-27, namely 0.1 mM, 0.25 mM and 0.5 mM (Figure 2.11). The reaction mixtures were incubated at 37 °C and the reaction was allowed to proceed for 2 days. For all three RNA concentrations new slower migrating bands (upper bands) were observed in the gel, together with a band corresponding to unreacted RNA and undefined faster migrating bands. All bands were similar in intensity suggesting that the platination reaction proceeded comparably for all the three tested RNA concentrations. Interestingly, this time two upper bands were visible on the gel, and they could be analysed separately. Indeed, for the reaction performed in the presence of 0.5 mM D1-27, enough sample could be recovered from the gel and analysed by MALDI-MS. Interestingly, the faster migrating upper band seems to contain a mixture of monoplatinated and diplatinated RNA, with the monoplatinated RNA being the major species, whereas the slower migrating upper band seems to contain monoplatinated and diplatinated RNA but in this case the diplatinated RNA was the major specie (Appendix 1, A 1.6 - A 1.7). Considering that with all different concentrations tested, the bands appeared were similar (intensity and number of the bands), the lower RNA concentration was chosen as the working concentration (0.1 mM). The quality of this gel was good enough to allow the quantification of the bands with the use of the software ImageJ 1.50i. With this software, the relative band area is calculated and from the comparison of the band area of the two bands, a percentage for each is given. Considering that the upper bands correspond to the platinated RNA species, this percentage can be used as an indication of the platination yield. The gel bands from the reaction using 0.5 mM were the better-defined ones and were analysed with ImageJ 1.50i. The platination yield in this case was found to be around 25 %.

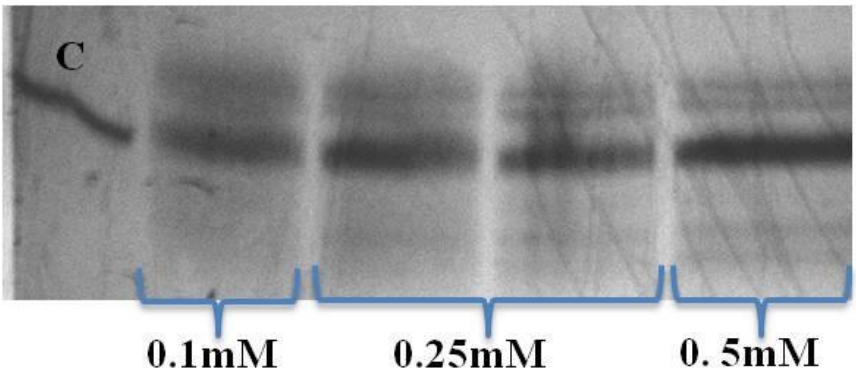

Figure 2.11: *15 % denaturing PAGE for RNA concentration dependent experiments. 0.1 mM, 0.25 mM and 0.5 mM D1-27 were tested with 1 eq of monoaquated cisPt at 37 °C for 2 days in ddH_2O. Both lanes for 0.25 mM correspond to the repetition of the same reaction. The gel was run at room temperature. The presence of two slower migrating bands as well as several faster migrating bands was observed here for the first time.*

2.3.6 Time dependent experiments

All the experiments commented above showed that a good combination of experimental conditions in order to get mostly monoplatinated D1-27 with cisPt was: 1 eq monoaquated cisPt, 0.1 mM D1-27, 37 °C, incubation for 2 days in ddH_2O. Aiming at improving the platination yield, different incubation times were tested with the same reaction conditions. Namely, the incubation time was increased from 2 days to 3 days and 4 days. The gel obtained from these reactions (Figure 2.12) was similar to the one obtained for 2 days incubation (Figure 2.11), showing two main bands. The upper band contained the platinated D1-27 and the other band corresponded to unreacted D1-27. However, despite the increased incubation time, the platination yield did not improve (23 % for both 3 days and 4 days). MALDI-MS characterization of the platinated D1-27 recovered from the upper band corresponding to 4 days incubation showed that the main species were the diplatinated ones (Appendix 1, A 1.8). These data suggest that the increased incubation time, instead of leading to a higher number of monoplatinated species, favoured multiplatination. This behaviour suggests lack of strong binding preference of cisPt for a platination site, and advices against the use of long incubation time. Therefore, 2 days were kept as the optimal incubation time for the platination reactions of monoaquated cisPt with D1-27. Similarly to the previous experiment, (Figure 2.11) a faster migrating undefined band was also observed, but unfortunately, the identity of the species giving rise to this band could not be identified due to very low recovery from the gel.

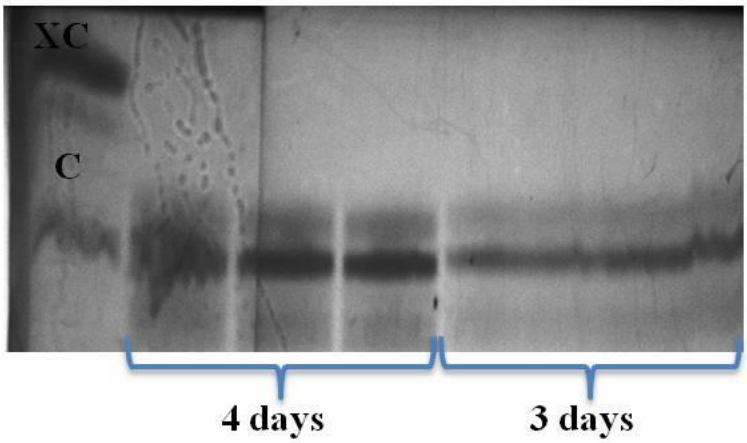

Figure 2.12: *15 % denaturing PAGE for time dependent experiments. D1-27 was incubated with 1 eq of monoaquated cisPt at 37 °C for 3 and 4 days in ddH_2O. All lanes for 4 days of incubation correspond to the repetition of the same reaction. The gel was run at room temperature.*

2.3.7 Conclusions for cisplatin platination reactions

For the platination of D1-27 with monoaquated cisPt the platination conditions which allowed the best separation of the Pt(II)-RNA adducts on the gel and the highest platination yield with the least possible multiplatinated species formed were: 1 eq of monoaquated cisPt, 0.1 mM D1-27, 37 °C, 2 days incubation in ddH_2O (Figure 2.13). The maximum platination yield achieved using these reaction conditions was around 25 %. Several problems were encountered while investigating the platination reactions involving D1-27 and cisPt. First, the platinated D1-27 species isolated from the upper band were not homogeneous. From their MALDI-MS characterization it was found that the newly formed slower migrating band contained a mixture of monoplatinated and diplatinated D1-27 with the monoplatinated being the major species. The formation of a mixture of differently platinated RNAs migrating together in the newly formed band was also reported in the literature[13]. Second, the platination yield was always rather low (25 %). Any attempt to increase the platination yield resulted in the formation of more multiplatinated species (Figures 2.11 and 2.12). This behaviour may be related to the lack of a preferential binding site for cisplatin, together with the presence of similarly accessible platination sites within D1-27, which resulted in the formation of multiplatinated RNA species. Having as a target to obtain high amount of homogeneous Pt(II)-D1-27 sample for studying the possible sequence and / or structural preferences of platinum(II) complexes, the use of cisPt was not ideal. The next platinum(II) complex to be tested was oxaliplatin (oxaliPt).

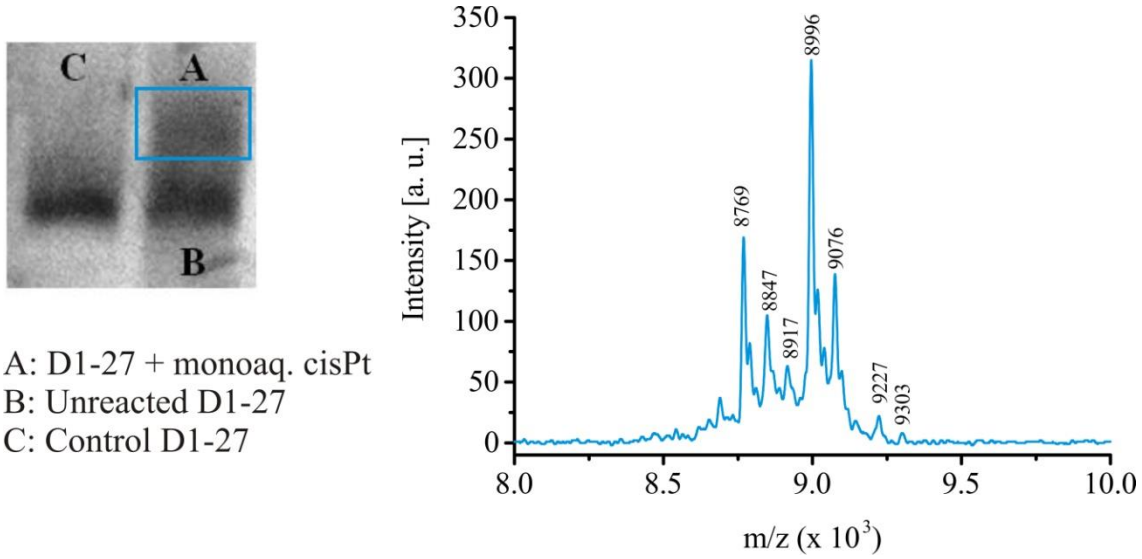

Pt-RNA species (upper band)	Predicted mass (m/z)	Experimental mass (m/z)
D1-27 – {HPO_3} [a]	8768	8769
D1-27	8848	8847
Monoplatinated D1-27 – 2 {HPO_3}	8917	8917
Monoplatinated D1-27 – {HPO_3}	8997	8996
Monoplatinated D1-27	9076	9076
Diplatinated D1-27 – {HPO_3}	9226	9227
Diplatinated D1-27	9306	9303

[a] *{HPO_3}: Its molecular mass (80) corresponds to the loss of a phosphate group*[28].

Figure 2.13: *15 % denaturing PAGE for the platination reaction of D1-27 with cisPt, using the following experimental conditions: 0.1 mM D1-27 incubated with 1 eq of monoaquated cisPt at 37 °C for 2 days in ddH_2O. The gel was run at room temperature. A characteristic mass spectrum of the platinated species isolated from the upper band is depicted on the right.*

In the mass spectrum of the platinated D1-27 with cisPt (Figure 2.13) in addition to the peaks corresponding to monoplatinated and diplatinated RNA there are also peaks for the monoplatinated and diplatinated RNA with different number of phosphate groups. The RNA used (D1-27) after transcription is expected to have a triphosphate group at the 5′-end. However, the presence of Mg(II) in the transcription mixture enhances the hydrolysis of the triphosphate leading to a mixture of RNA molecules having triphosphate and diphosphate groups at the 5′-end (Figure 2.14). Therefore, a mixture of platinated RNAs containing three or two phosphate groups was observed. Additionally, cleavage of phosphate ester bonds have been reported during the ionization procedure of MALDI-MS[28,29]. These molecules are differing by 80 Da and the phosphate group lost will be noted as

{HPO_3}. The behaviour of the RNA during the MALDI-MS measurements will be further discussed in paragraph 2.7.

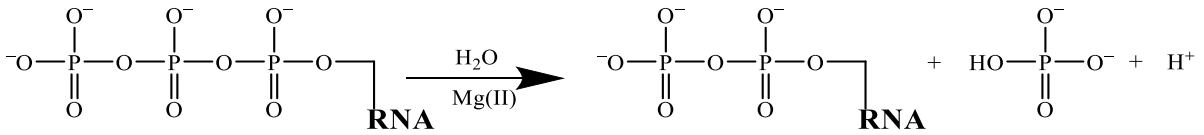

Figure 2.14: *Representation of the hydrolysis of the 5'-end triphosphate, which leads to the presence of RNAs with different number of phosphate groups*

2.4 Platination reactions of D1-27 with oxaliplatin

OxaliPt {[Pt (oxalato) (1R, 2R-cyclohexane-1,2-diamine)]} is a third-generation platinum(II) complex, which was developed in order to show less side effects and better cytotoxicity compared to cisPt[7,30–32]. OxaliPt is not side effect free but it shows activity against cisPt resistant cancers[32]. CisPt is believed to exert its anticancer activity by covalent binding to nuclear DNA. Upon platinum binding the induced DNA distortion and its inability to be fixed is leading to apoptosis. The main cisPt-DNA adducts formed consist of 1,2-d(GG) and 1,2-d(AG)[7] (Chapter 1, Paragraph 1.2.3). The exact mechanism of action of oxaliPt is not clear and is mostly extrapolated from the understanding of the cisPt one. Compared to cisPt, oxaliPt has a 1,2-diaminocyclohexane (DACH) as non-leaving group instead of ammine groups and an oxalate ligand as leaving group instead of chlorides[32] (Figure 2.15, left). The different reactivity observed for oxaliPt may be attributed to its different non-leaving group, DACH[31,33]. The sterical hindrance introduced by the bulky DACH moiety leads to significant conformational changes between the cisPt and oxaliPt DNA adducts[34]. It is hypothesized that these conformational differences result in discrimination from the various DNA repair proteins which could explain their differences in reactivity[34,35]. It was shown that the same type of adducts at similar abundance are formed upon DNA platination with both cisplatin and oxaliplatin[32] but oxaliPt has been also found to form additional adducts involving adenine when reacting with RNA[36]. Considering that, upon platination of D1-27 with oxaliPt the formation of platinated species at adenine sites was also expected. CisPt reacts with DNA upon hydrolysis which leads to the formation of the monoaquated complex[7,32]. However, the active form of oxaliPt is considered to be its diaquated complex[31,37]. The exact route by which the diaquated complex is formed is complicated and not completely understood, but it is suggested that, following oxalate ring opening, the dichloride complex [Pt(DACH)Cl_2] is first formed. This dichloride complex is hydrolysed, similarly to cisPt, to the monoaquated and finally diaquated active form[37–40]. The hydrolysis of oxaliPt to its active form is longer compared to the cisPt, therefore slower reaction with DNA / RNA is expected. This is probably explaining the fewer oxaliPt-DNA adducts formed compared to cisPt when the reactions is performed under the same conditions[37]. Therefore, the combination of the

slower kinetics of oxaliPt together with its increased bulkiness compared to cisPt, could lead to the formation of homogeneous Pt(II)-RNA adducts considering that less platinum moieties could be accommodated per RNA. In principle, these characteristics of oxaliPt make it a better candidate for the current study. The optimization of the experimental conditions, which would lead to the formation of homogeneously platinated D1-27 species, was performed using gel mobility shift assays and the newly formed species were analysed by MALDI-MS, similarly to the procedure explained for cisPt.

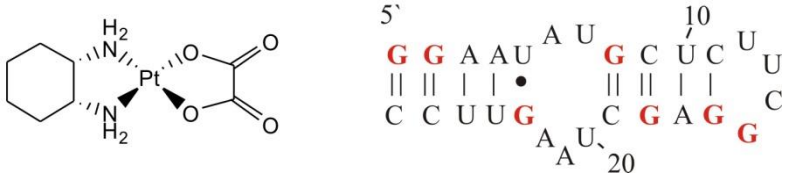

Figure 2.15: *Chemical structure of oxaliplatin (left) and secondary structure of D1-27 (right). In red are denoted the guanines, which could be possible platination sites.*

2.4.1 Oxaliplatin concentration, temperature and time dependent experiments

Based on the procedure followed in the case of cisPt, similar experiments were performed for the investigation of the platination conditions with oxaliPt. At first, 1 eq, 5 eq and 10 eq of oxaliplatin were reacted with 0.1 mM D1-27. The mixtures were incubated for 15 h, 1 day and 2 days at 25 °C, 37 °C and 50 °C in ddH_2O. The reaction of D1-27 with 1 eq of oxaliPt at 25 °C and 37 °C, independently of the reaction time, showed intense bands for the unreacted RNA as well as a smeary band very close to the band of the unreacted RNA (Figure 2.16).

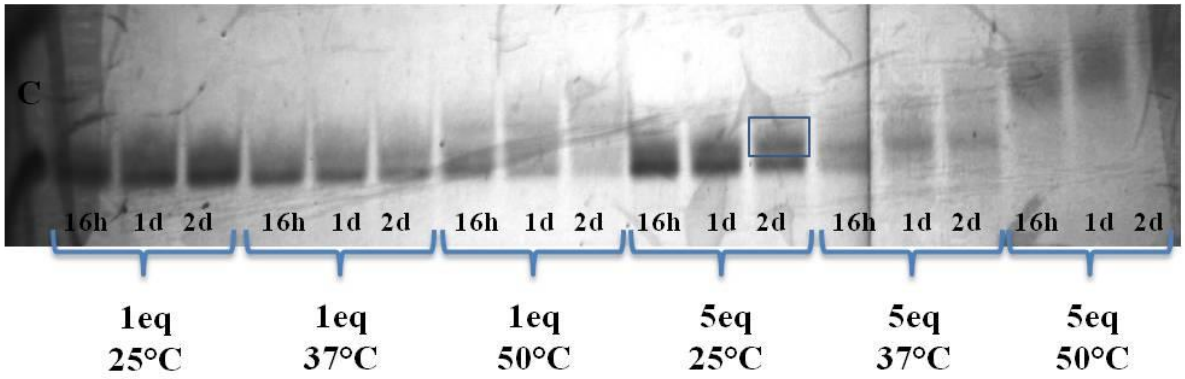

Figure 2.16: *15 % denaturing PAGE for time, platinum concentration and temperature dependent experiments of oxaliPt in ddH_2O. 1 eq and 5 eq of oxaliPt were incubated with 0.1 mM D1-27 for 16 h, 1 day and 2 days, at 25 °C, 37 °C and 50 °C in ddH_2O. The gel was run at room temperature.*

The formation of smeary bands suggests that similarly platinated RNAs are formed, which cannot be sufficiently separated on the gel. At 50 °C, with increasing incubation time, the band corresponding to

the unreacted RNA becomes weaker and the smeary band is more extended. The decrease of the amount of unreacted RNA at 50 °C indicates higher reaction speed compared to the other two temperatures. However, the presence of an extended smear suggests that several differently platinated species were formed which could not be separated.

With 5 eq of oxaliPt at 25 °C after 16 h there was a not well-defined band which was poorly separated from the band of the unreacted RNA. However, after 1 day of incubation there was formation of a more compact second band on the gel whose intensity was further increased after 2 days of incubation (Figure 2.16, blue frame). The upper band corresponding to the reaction performed for 2 days was cut and analysed via MALDI-MS. The mass spectrum showed that the major species was the monoplatinated D1-27 while there were minor peaks corresponding to diplatinated D1-27 and unreacted D1-27 (Appendix 1, A 1.9). The presence of unreacted D1-27 in the sample isolated from the upper band may be due to not sufficient separation on the gel and could be eliminated with optimization of the gel running conditions (see below). On this gel, these two bands were intact enough to allow their quantification with the use of ImageJ 1.50i. From the comparison of the band area, it was found that the upper band and therefore the platination yield was around 50 %. An intense band for the unreacted D1-27 was observed for all three reaction times investigated, but in the case of the reactions performed for 16 hours and 1 day, quantification was not possible due to their not sufficient separation from the upper band (Figure 2.16). At 37 °C after 16 h of incubation, there was a clear second band and a band for the unreacted RNA while after 1 day and 2 days there was only one band and no unreacted RNA left. The content of the upper band corresponding to the reactions performed for 16 h was analysed by MALDI–MS. The spectrum showed the presence of a mixture of monoplatinated and diplatinated RNA (Appendix 1, A 1.10). Under all the incubation times tested, 5 eq of oxaliplatin at 50 °C resulted in a very slow migrating undefined smeary band, indicative of a mixture of multiplatinated RNA species. The longer the incubation time the slower the band was migrating, suggesting higher degree of multiplatination (Figure 2.16).

The use of 10 eq of oxaliPt at 25 °C resulted in the formation of a second well-separated band only after 1 day and 2 days of incubation while the band of the unreacted RNA was still visible. At 37 °C and 50 °C there were only undefined smeary bands and no band for unreacted RNA indicating that the reaction proceeded very fast. The smeary bands formed migrate slower at 50 °C suggesting that there were more platinum moieties per RNA (Figure 2.17).

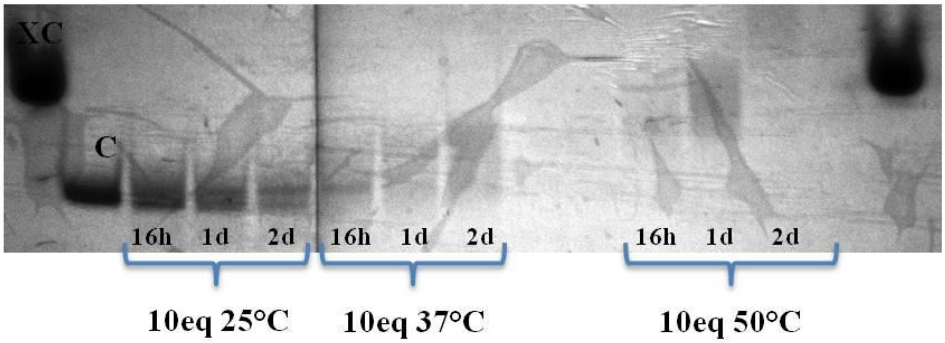

Figure 2.17: *15 % denaturing PAGE for time, platinum concentration and temperature dependent experiments of oxaliPt in ddH_2O. 10 eq of oxaliPt were incubated with 0.1 mM D1-27 for 16 h, 1 day and 2 days at 25 °C, 37 °C and 50 °C in ddH_2O. The gel was run at room temperature.*

Summing up, the most promising results were obtained by using 5 eq of oxaliPt, incubating for 2 days with 0.1 mM D1-27 at 25 °C in ddH_2O (Figure 2.16, blue frame). Under these conditions, the platination yield was almost 50 % and the upper slower migrating band contained mostly monoplatinated RNA. However, a small amount of diplatinated RNA was also formed, which could be possibly eliminated with further optimization of the reaction conditions.

2.4.2 RNA concentration and time dependent experiments

In order to reduce the amount of diplatinated RNA, the reaction time was reduced to 1 day. Moreover, different RNA concentrations were tested (0.1 mM, 0.25 mM and 0.5 mM) in order to increase the amount of platinated sample formed which then could be used for further characterization. Incubation for 1 day with 0.1 mM D1-27 resulted in bands with similar intensity as observed before (Figure 2.18). With 0.25 mM and 0.5 mM D1-27 for 1 day of incubation upper bands with similar intensity were observed (Figure 2.18). The overall different migration of the bands obtained using 0.5 mM D1-27 was due to mishandling of the gel during the gel pocket preparation. The MALDI-MS spectrum of the upper band obtained using 0.25 mM D1-27 for 1 day reaction showed that it consisted mostly of monoplatinated RNA but a small amount of diplatinated RNA was still present (Appendix A 1.11). Therefore, even at reduced incubation time the diplatinated RNA species were already formed. Despite the presence of a small amount of diplatinated species, 0.25 mM D1-27 and 1 day of incubation were kept as the conditions of choice. Due to very low recovery it was not possible to characterize the species from the upper band obtained using 0.5 mM D1-27.

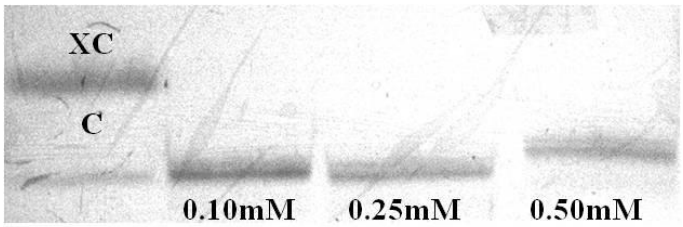

Figure 2.18: *15 % denaturing PAGE for RNA concentration and time dependent experiments. 5 eq of oxaliPt were incubated with 0.1 mM, 0.25 mM and 0.50 mM D1-27 for 1 day at 25 °C in ddH_2O. The gel was run at room temperature.*

2.4.3 Influence of salt concentration on platination reaction efficiency

All the experiments performed during the optimization procedure with oxaliPt were carried out in ddH_2O. The reason for that was that during the corresponding reactions with cisPt, it was found that the replacement of 60 mM $KClO_4$ solution for ddH_2O resulted in the formation of a clear second band (Paragraph 2.3.3, Figure 2.7). As discussed before, in the absence of monovalent cations the RNA does not have its compact secondary structure, and the possible platination sites are more exposed, which leads to the enhancement of the platination reaction (Chapter 4, Paragraph 4.4). Also in the case of oxaliplatin a second clear band is observed when the reaction is performed in water. However, the mass spectrum of the sample isolated from the upper band showed that it contained a mixture of mono- and diplatinated RNA. In the attempt of reducing the amount of diplatinated species, ddH_2O was replaced with 60 mM $KClO_4$, to reduce platination kinetics and possibly favour a single platination site. For these reactions 5 eq and 10 eq of oxaliPt were used and the incubation times tested were 1 day and 2 days at 25 °C using 0.25 mM D1-27.

By reacting 5 eq of oxaliPt with 0.25 mM D1-27 for 1 day in 60 mM $KClO_4$ the formation of a smear, migrating very close to the band of the unreacted RNA, was observed. That shows that the few platinated RNA species formed were not separated on the gel (Figure 2.19). No clear upper band was observed, suggesting that the platination yield was reduced. In the presence of 5 eq (2 days) and 10 eq (1 day) of oxaliPt a second well-defined band was visible on the gel, in both cases. The MS characterization of the platinated RNAs extracted from these upper bands showed that they consisted of a mixture of multiplatinated RNAs (Appendix 1, A 1.12- 1.13). The formation of multiplatinated species may be attributed to longer platination time and increased platinum concentration. Upon reaction of 10 eq of oxaliPt for 2 days, the band corresponding to the unreacted RNA was significantly reduced, showing that the reaction proceeded faster, and a slower migrating band was well visible on the gel. As expected, the content of the upper bands was a mixture of multiplatinated RNAs (Appendix 1, A 1.14). Summing up, the use of 5 eq oxaliPt incubating for 2 days and 10 eq of oxaliPt incubating for 1 and 2 days, all lead to the formation of a second band on the gel but all bands contained a mixture of multiplatinated RNAs. However, no clear upper band was observed on the gel when the reaction was

performed with 5 eq of oxaliPt for 1 day. Therefore, the use of 60 mM $KClO_4$ does not seem to be ideal for the formation of measurable amount of a homogeneously platinated RNA.

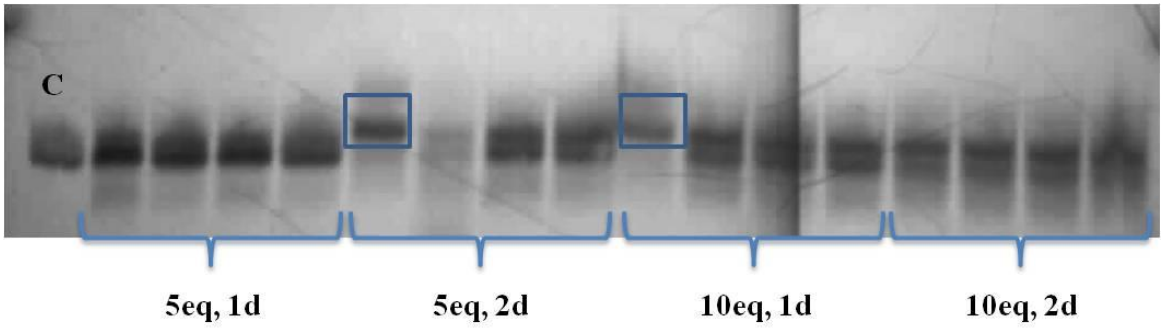

Figure 2.19: *15 % denaturing PAGE for RNA concentration and time dependent experiments. 5 eq and 10 eq of oxaliPt were incubated with 0.25 mM D1-27, for 1 day and 2 days, at 25 °C in 60 mM $KClO_4$. All four lanes correspond to the repetition of the same reaction. The gel was run at room temperature.*

In addition to improving the platination yield, much effort was put in order to have a better gel separation between the bands of the unreacted and the platinated RNA. Better separation could be achieved by reducing the speed at which the gel was running. A way to do that was to run the gels at lower power and for longer time. Towards this direction, longer gel plates were used and the electric power was reduced to 1-2 W from 5-8 W used before. By increasing the length of the plates and by reducing the electric power the two bands on the gel were more compact but still very close to each other (Figure 2.19). Another way that could further improve the separation was to run the gel at 4 °C instead of room temperature and use higher percentage of denaturing gel solution, like 20 % instead of 15 %. The lower temperature, similarly to the lower electric power and longer gel plates, would lead to longer running time. The higher gel solution percentage is expected to favour more compact and better resolved gel bands, thus improving the separation[41]. The reaction was then repeated (5 eq of oxaliplatin, 0.25 mM D1-27, 1 day of incubation at 25 °C) both in ddH_2O and in 60 mM $KClO_4$ and the gel was run at 4 °C, using 20 % denaturing gel solution (instead of 15 %). This significantly improved the separation of the two bands (Figure 2.20). The good quality of this gel allows for a few important comments. Firstly the platination yield is higher in the presence of ddH_2O (35 %) than in the presence of $KClO_4$ (16 %), as previously observed for cisPt (Paragraph 2.3.3). Additionally, the platination yield of the reaction in ddH_2O seemed to be reduced with respect to the previous experiments (35 % vs 50 %, compare Figure 2.20 with Figure 2.16). Of course, the platination yield is not related to the improved separation, but now, because of that the yield could be evaluated more precisely. Finally, the 5th lane of each reaction shows only one band corresponding to the platinated D1-27, thus suggesting that 100 % platination was achieved (Figure 2.20, blue boxes). The reaction mixture for these two platination reactions was prepared in different Eppendorf tubes and the pH was measured only in one of them, whose content was loaded on the 5th lane of the gel. Similar behaviour was observed also in a previous

gel (Figure 2.19, blue boxes). These bands were cut and the platinated RNA species were isolated and analysed with MALDI-MS. They contained a mixture of monoplatinated and diplatinated RNA (Appendix 1, A 1.15).

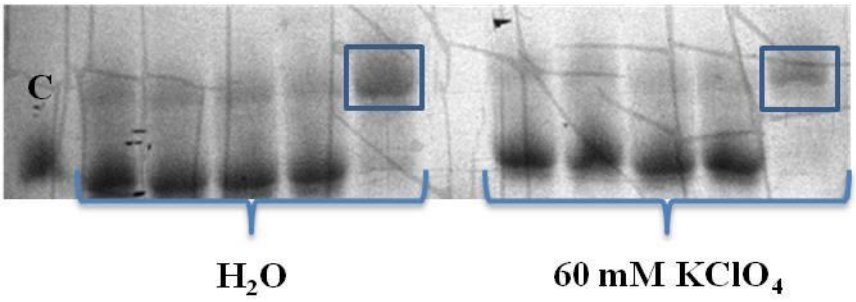

Figure 2.20: *20 % denaturing PAGE for platination reactions in ddH_2O and in 120 mM $KClO_4$. 5 eq of oxaliPt were incubated with 0.25 mM D1-27 for 1 day at 25 °C. All five lanes correspond to the repetition of the same reaction. The gel was run at 4 °C.*

A pH electrode (Minitrode glass electrode from Hamilton) contains saturated solution of KCl, which is released in very small amount through the membrane in the measured samples. Consequently, traces of KCl are expected to be present in the samples in which the pH was measured. The final volume of the reaction mixtures loaded in the above commented gel was 10 µL. To investigate the effect of KCl concentration, the reaction was repeated using larger volumes (10 µL, 20 µL, 30 µL, 40 µL). The pH electrode was dipped in all samples to check the pH, the reactions were allowed to proceed for 1 days and the reaction mixtures were then loaded on the gel (Figure 2.21). Interestingly, the strongest effect on platination yield is observed when the reaction is performed in 10 µL final volume, compared to the other volumes tested. Even if a faint band corresponding to unreacted RNA was still visible (Figure 2.21), while only one band corresponding to the platinated RNA was observed in the previous gels (Figure 2.19 - 2.20), the platination yield was around 68 %, which is considerably higher than in all previous cases. When the reaction was performed in larger volumes, around 40 % platination yield was obtained. Assuming that the same amount of KCl is released by the pH electrode each time, the data commented above suggest that the final concentration of KCl, expected to be higher in the smaller volume samples, has a strong influence on the platination yield.

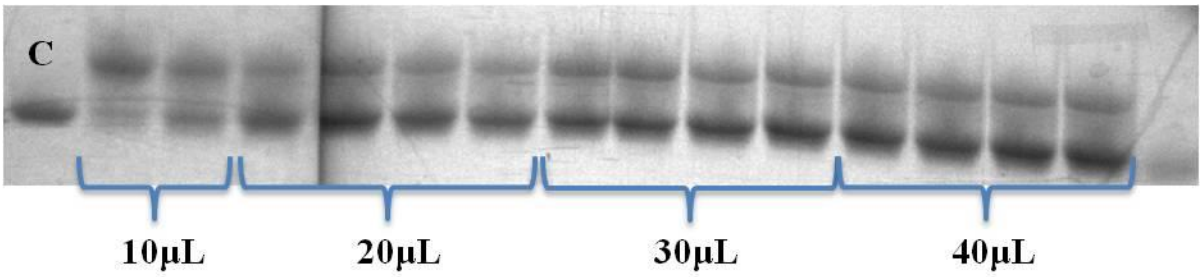

Figure 2.21: *20 % denaturing PAGE for the investigation of the influence of the volume on the platination reaction. Increasing volumes of platination reactions were used: 10 μL, 20 μL, 30 μL and 40 μL. Both lanes for the 10 μL volume, as well as all four lanes for the rest, correspond to the repetition of the same reaction. The gel was run at 4 °C.*

Having established that the presence of KCl in the platination reaction increases the platination yield and that this behaviour seems to depend on KCl concentration, the next platination reactions were performed in 60 mM KCl as well as in 60 mM $KClO_4$ in the presence of 5 mM KCl (Figure 2.22). In the first case, high platination yield was observed (60 %), similarly to what reported above (Figure 2.21) while the presence of 5 mM KCl in the reaction mixture did not improve the platination yield, which remained rather low (25 %).

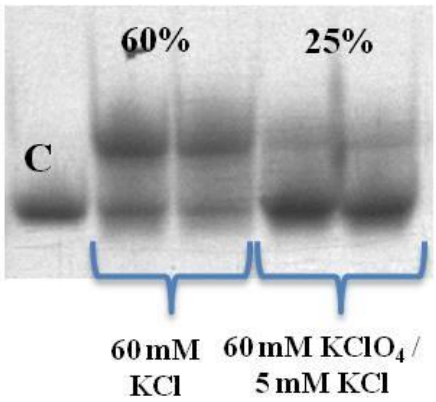

Figure 2.22: *20 % denaturing PAGE for the investigation of the influence of KCl. The platination reactions were performed in 60 mM KCl (left) and in 60 mM $KClO_4$ / 5 mM KCl (right). Both lanes correspond to the repetition of the same reaction. The gel was run at 4 °C.*

Since it was found that 60 mM of KCl could enhance the platination (Figure 2.22), increased amounts of Cl^- were tested. More specifically 60 mM, 80 mM, 120 mM and 200 mM of KCl were used (Figure 2.23). The reaction performed in the presence of 60 mM KCl behaved as expected, reaching almost 70 % platination yield. Similar platination yield was obtained in the presence of 80 mM and 120 mM KCl, while significantly higher platination yield (85 %) was observed with 200 mM KCl. The platinated species from the upper bands corresponding to the reactions performed in the presence of 80 mM,

120 mM and 200 mM KCl were isolated and analysed with MALDI-MS (Appendix 1, A 1.16 - A 1.18), while in all the other cases the amounts collected were not sufficient for any characterization. The major platinated species in all samples was monoplatinated RNA, but diplatinated RNA was also present. Despite the presence of diplatinated RNA in the samples, 120 mM KCl was chosen as the salt concentration to be used for the platination reactions. The lower salt concentrations were not chosen because of the lower platination yield and the higher, even if the yield was better, due to higher content of diplatinated species. The mass spectra of the platinated species resulting from the reactions commented above suggest that the relative intensity of the diplatinated RNA increase with the increase of the KCl concentration used (Appendix 1, A 1.16 - A 1.18). Aiming at reducing the amount of diplatinated RNA species, the reaction was repeated for shorter time, e.g. only for 15 h, in the presence of 120 mM KCl (Figure 2.24). However, the platination yield was lower and similar amount of diplatinated RNA was formed. The evaluation of the amount of the diplatinated RNA formed when the reaction was carried out for 15 h and 1 day was performed via HPLC (Paragraph 2.8.1).

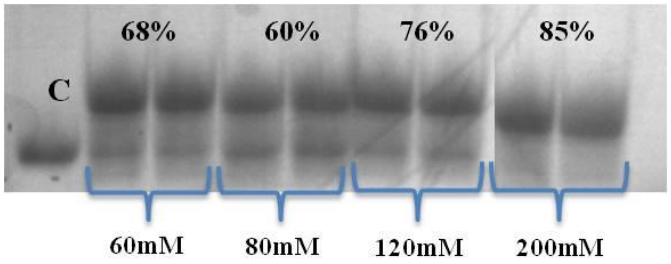

Figure 2.23: *20 % denaturing PAGE for the investigation of the influence of different KCl concentrations. The platination reactions were performed in the presence of 60 mM, 80 mM, 120 mM and 200 mM KCl. Both lanes for each condition correspond to the repetition of the same reaction. The gel was run at 4 °C.*

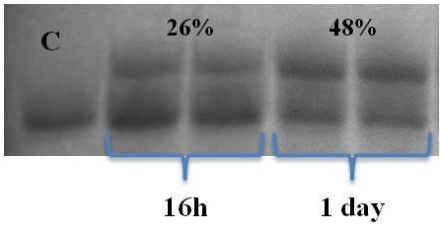

Figure 2.24: *20 % denaturing PAGE for the time dependency of the platination reaction of D1-27 with 5 eq of oxaliPt, at 25 °C in 120 mM KCl. Both lanes correspond to the repetition of the same reaction. The gel was run at 4 °C.*

By replacing ClO_4^- with Cl^- in the platination reaction a noticeable increase of the platination yield was observed. Platination reactions of cisPt take place in chloride free medium in order to avoid the replacement of water molecules of the activated cisPt with chloride which slows down the reaction[42]. In our study, all the reactions with cisPt were performed indeed in chloride free medium but it was found that, in the case of oxaliPt, the presence of the Cl^- enhanced the platination reaction. More particularly the higher the concentration of Cl^- the higher the yield was (Figure 2.23). A possible explanation for this behaviour relays on the fact that the oxalate group of oxaliPt is lost in the presence of Cl^-[40,43]. The mechanism of action of cisPt is well-established[7,32,44,45] but it is unclear the way oxaliPt reacts and the mechanism of action proposed is mostly deduced from the one of cisPt[44,45]. Latest findings suggest that oxaliPt rapidly reacts with Cl^- forming a ring opened intermediate ([Pt(DACH)Cl(ox)]) which is then converted to [Pt(DACH)Cl_2]. The last one could be then hydrolysed to its monoaquated and diaquated complex. The diaquated species is supposed to be the most active one[40,46] (Figure 2.25). This could explain the behaviour observed in our study where upon KCl addition the platination yield increased. Most probably the presence of Cl^- leads to the formation of [Pt(DACH)Cl_2]. This complex, after replacement of the Cl^- ligands, forms aquated complexes, which are known to be more reactive compared to the parent compound[47]. However, the complete mechanism of action of oxaliplatin is more complicated than that. For example, it has been reported that the oxalate ligand can be detached also in aqueous solution leading to the formation of the aquated platinum complexes[37,46,48,49]. Additionally, computational studies have shown that under neutral conditions the oxalate ring-opening is the rate-determining step[49]. Summing up, the increased platination yield observed in our study is most probably related to oxaliPt degradation in the presence of KCl. Interestingly, the use of NaCl to increase the speed of the formation of active species in reactions containing oxaliplatin was already reported in the literature[50].

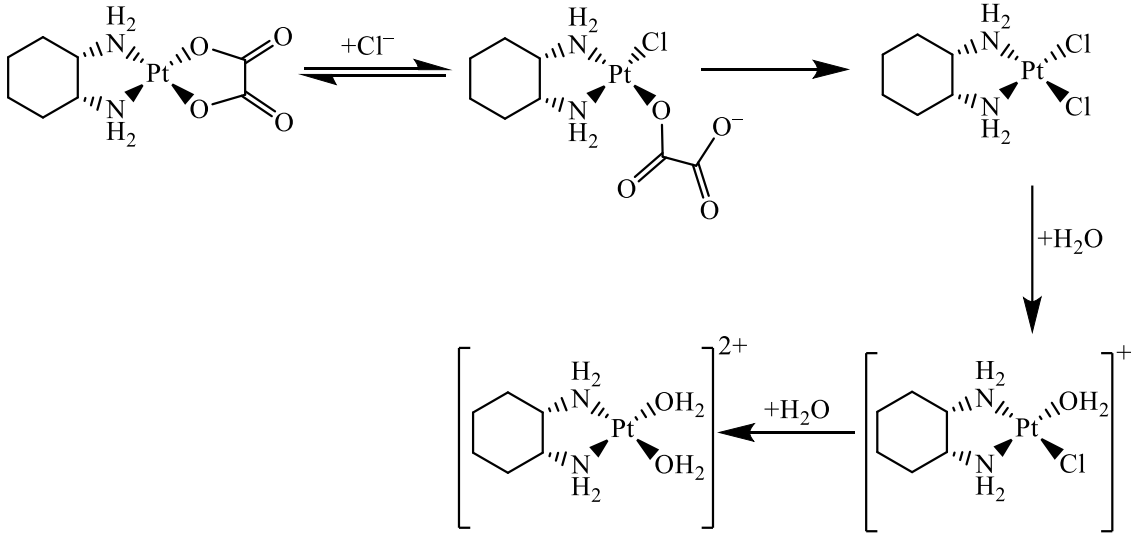

Figure 2.25: *Proposed reaction mechanism for the activation of oxaliplatin in the presence of chloride[40].*

2.4.4 Conclusion for the oxaliplatin platination reactions

The experiments commented above showed that the reaction of 5 eq of oxaliplatin with 0.25 mM D1-27, in the presence of 120 mM KCl, for 1 day at 25 °C led to the formation of platinated species responsible for a well-defined upper band in the gels. The platination yield was about 50 %, and mass spectra confirmed that the platinated species consisted mainly of monoplatinated RNA. During the investigation of the platination conditions it was found that the presence of Cl^- was beneficial for the increase of the platination yield. The quality of the gels was significantly improved by running the gel at lower temperature (4 °C) and increasing the percentage of the gel solution from 15 % to 20 %. Because of the better gel band separation, unreacted RNA was not anymore present in the samples isolated from the upper band. However, the upper band always contained a small amount of diplatinated RNA together with monoplatinated RNA species. Effort was put to separate the diplatinated RNA species from the monoplatinated ones using HPLC, and this will be described in detail in the next part of this chapter (Paragraph 2.8). In Figure 2.26, it is depicted an example gel obtained for the platination reaction of oxaliPt with D1-27 using the experimental conditions mentioned above. Upon platination a slower migrating band, containing platinated RNA was formed. All the three bands on the gel were cut and the RNA samples were characterized with MALDI-MS. The band corresponding to the control (Figure 2.26, blue frame) consisted, as expected, of unreacted RNA. The extra peaks on its MS spectrum (Figure 2.26, blue line spectrum) correspond to RNAs with different number of phosphate groups at the 5′-end, which results from the hydrolysis of the phosphate groups during *in vitro* transcription (Paragraph 2.3.7, Figure 2.14). The behaviour of the RNA during the MS measurement will be discussed in detail in the next part of this chapter (Paragraph 2.7). The upper band (Figure 2.26, red line spectrum) contains monoplatinated and diplatinated D1-27, with the monoplatinated one being the major specie. The extra peaks are due to platinated D1-27 containing different number of phosphate groups. Finally, the lower band (Figure 2.26, green line), which was expected to contain only unreacted RNA, consisted mainly of unreacted RNA, but minor peaks were present in the mass spectrum, which could be attributed to monoplatinated and diplatinated RNA species. The presence of platinated RNA species in both upper and lower band was also reported upon RNA platination with cisPt, and it was justified as secondary products which were created from slower platination reactions once the main platination sites were occupied[13]. Only the platinated species contained in the upper band, which corresponds to the major species, was further characterized. Unfortunately, the Pt(II)-RNA adducts found in the lower band were always in little amount and migrate together with unreacted RNA. Consequently, no further characterization on these species was performed.

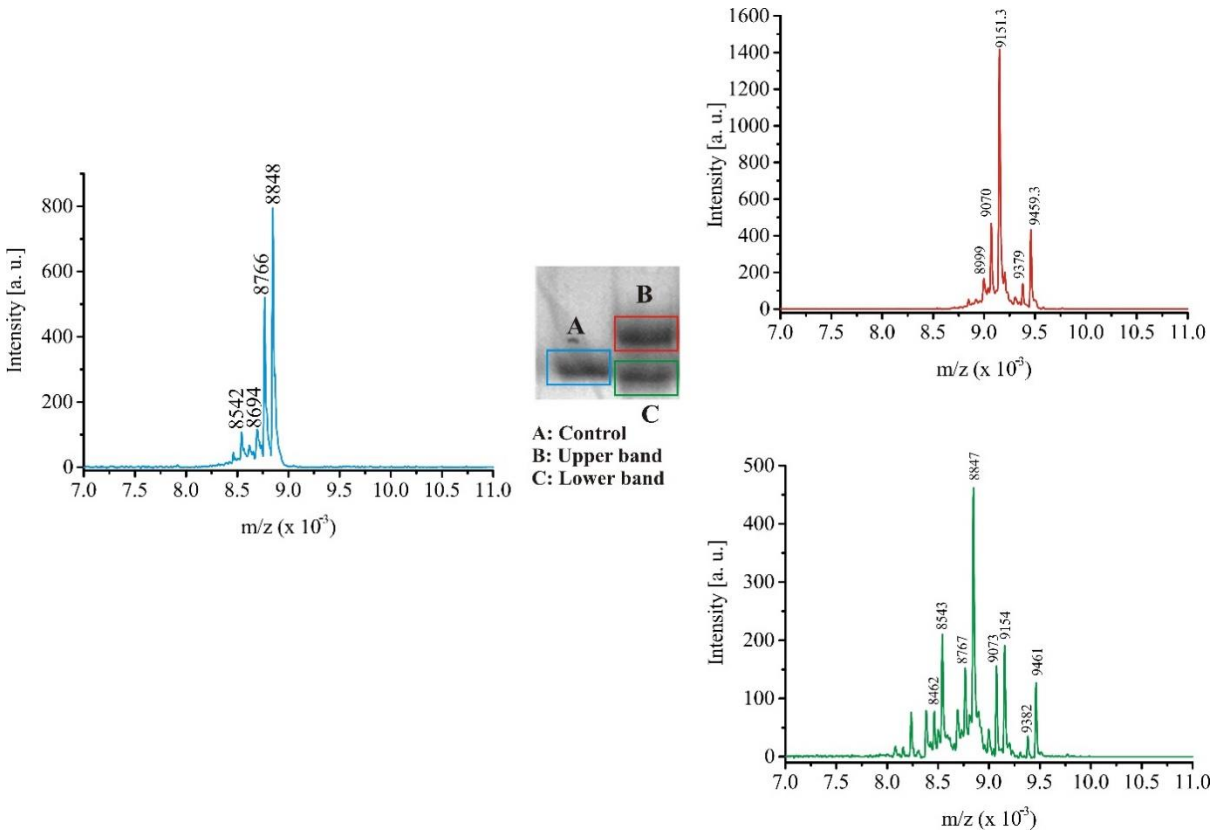

Figure 2.26: *20 % denaturing PAGE for the platination reaction of D1-27 with oxaliPt, using the optimal experimental conditions found for oxaliPt. These conditions are: 0.25 mM D1-27 incubated with 5 eq of oxaliPt at 25 °C for 1 day in 120 mM KCl solution. The gel was run at 4 °C. Characteristic mass spectra from the control, upper and lower bands are depicted (Appendix 1, A 1.19 - A 1.21).*

2.5 Comparison of cisPt and oxaliPt platination reactions – Conclusions

Sections 2.3 and 2.4 described the optimization of the platination conditions carried out in order to 1) obtain a well-defined and well-separated upper band on the gel, which would likely corresponds to single monoplatinated species, and to 2) obtain the highest platination yield, with the lowest number of multiplatinated products. In the case of cisplatin, the best separation between unreacted and platinated species and the highest platination yield was obtained by reacting 0.1 mM of D1-27 with 1 eq of monoaquated cisPt for 2 days at 37 °C in ddH_2O, while in the case of oxaliplatin by reacting 0.25 mM of D1-27 with 5 eq of oxaliPt, in the presence of 120 mM KCl, for 1 day at 25 °C. The platination yield in the case of cisPt was about 20 – 25 % while for oxaliPt was varying between 50 and 60 %. The first advantage of oxaliPt over cisPt was the higher platination yield achieved. Additionally, the slower migrating band appearing upon platination in the case of cisPt was always less defined compared to the one from the reaction with oxaliPt. This not well-defined band may be due to the absence of a preferential binding site or to the fact that, upon platination of a preferable site, other slower platination reactions are taking place at other sites, giving rise to products, which are not well-

separated on the gel. This behaviour could be related to both faster kinetics compared to oxaliPt as well as to the lack for a strong preferential binding site. The platinum(II) complexes are bound to DNA upon hydrolysis of their leaving group[7,45,49]. Cisplatin leaving groups are the two chloride ligands while for oxaliplatin is the oxalate ligand[7,30]. The chlorides of cisPt are good leaving groups and are faster substituted by water molecules compared to the oxalate group of oxaliPt[7,49]. Additionally, as discussed before (Paragraph 2.4.3) the formation of the active oxaliPt species is not really well understood but it is supposed to be more complicated compared to cisPt given that more steps are required before the formation of the aquated species[31,37–40,43,46,48,49]. Therefore, cisPt is expected to react faster compared to oxaliPt. The Pt(II)-RNA species formed with oxaliPt are more bulky compared to the adducts with cisPt[32,34,35] meaning that, in principle, less platinum moieties could be accommodated per RNA in the case of oxaliPt compared to cisPt. It has been suggested that the different non-leaving groups contribute to the different anticancer activity of the two platinum drugs[7,32,45,49]. The more compact bands formed upon RNA platination with oxaliPt suggest that similar Pt(II)-RNA species were formed, which could indicate the existence of a preferential binding site for oxaliplatin. To get a better picture about the different behaviour of the two platinum(II) complexes, platination of RNA was performed with both complexes, using the experimental conditions which led to the formation of a well-separated upper band on the gel in the case of oxaliPt (Figure 2.27, conditions commented in Paragraph 2.4.4). Interestingly, under these conditions, only a dispersed smeary band was visible in the case of cisPt, suggesting the formation of many differently multiplatinated RNA species. This behaviour may be due to the faster kinetics of cisPt as well as the lack of a specific binding site, which would prevent the formation of a homogeneously platinated RNA sample.

For all these reasons, this work focuses on oxaliplatin as RNA platination agent, and the discussion about the methods used for the isolation of monoplatinated RNA, in the next part of this chapter (2.7 - 2.9), as well as the characterization of the Pt(II)-RNA adducts, that will be described in chapter 4 will all be referred to the platinated RNA species formed upon RNA reaction with oxaliPt.

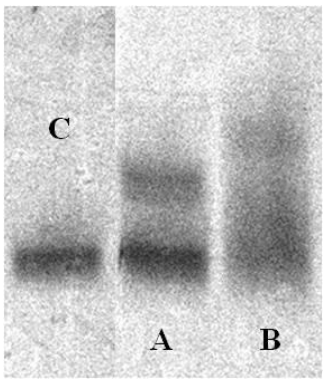

Figure 2.27: *15 % denaturing PAGE for the platination reaction of D1-27 with oxaliPt (lane A) and cisPt (lane B) using the optimal conditions found for oxaliPt. (0.25 mM D1-27 incubated with 5 eq of oxaliPt at 25 °C for 1 day in 120 mM KCl solution). C=control. The gel was run at room temperature.*

2.6 Platination of RNA 26 with oxaliplatin

Once oxaliPt was chosen as an appropriate platination agent for our study and the platination reaction conditions which could lead to well separated and homogeneous Pt(II)-RNA adducts were found using D1-27, the next step was to study the influence of structural RNA features on the platination reaction. For that reason, a 26nt long RNA construct (RNA 26) was used (Figure 2.28, right). RNA 26 is the analogue of D1-27 without the internal loop. Internal loops are structural motifs which can be found in many RNAs and are important for RNAs functions and folding[51,52]. D1-27 contains an asymmetric loop, with three stacked adenines capped by a U-U mismatch and a G-U wobble base pair[53] (Chapter 1, Paragraph 1.1.4). The aim of the platination of RNA 26 was to obtain information on the influence of this internal loop on the platination sites.

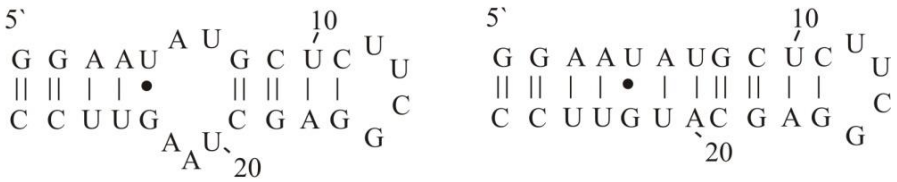

Figure 2.28: Secondary structures of D1-27 (left) and RNA 26 (right).

The platination of RNA 26 was performed using 5 eq of oxaliPt, 0.25 mM RNA, and incubation for 1 day at 25 °C in 120 mM KCl. The gel picture corresponding to this platination reaction was different compared to what observed in the case of D1-27. Indeed, no well-defined slower migrating band was observed. However, the band corresponding to Pt(II)-RNA 26 was cut, and the platinated RNA species were isolated and analysed with MALDI–MS. They consisted of monoplatinated RNA species and unreacted RNA (Appendix 1, A 1.22). In this case, contrarily to what observed in the case of D1-27, no diplatinated RNA species were formed. The absence of a second well-defined band in the case of RNA 26 may be due to different distortion of the two constructs upon platination, and therefore different migration on the gel. However, it should be noted that RNA 26 migrates much faster than expected in the denaturing PAGE. Indeed, the two RNAs differ only by one nucleotide, and much lower separation in their migration was to be expected. The faster migration of RNA 26 indicates that probably it was not fully denatured under our working conditions, and this may also influence the gel migration of the corresponding platinated species.

In order to be able to expand the comparison of the two RNAs and get information on the platinum binding sites, their platinated adducts must be characterized. The use of RNA 26 as RNA target for oxaliPt will be discussed in chapter 3 (Paragraph 3.3.3).

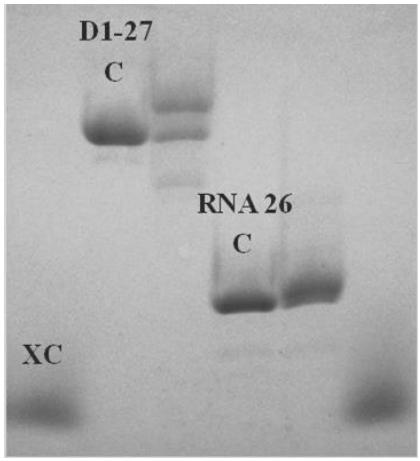

Figure 2.29: *20 % denaturing PAGE for the platination reaction of deph-D1-27 and deph-RNA 26 with oxaliPt, using the optimal experimental conditions found for oxaliPt. These conditions are: 0.25 mM RNA incubated with 5 eq of oxaliPt at 25 °C for 1 day in 120 mM KCl solution. The gel was run at 4 °C.*

2.7 Matrix-assisted laser desorption ionization (MALDI-MS) for the characterization of the platinated RNA

As described in the previous paragraphs, upon platination a new slower migrating band was observed on the gel (Paragraphs 2.3 - 2.4). The platinated RNA species were extracted from the gel pieces and MALDI-MS was used for their identification. Application of MS-based techniques such as MALDI and ESI are widely used to acquire information about the sequence and fragmentation of oligonucleotides[54] as well as metal-DNA[55] and metal-RNA interactions[56]. In MALDI mass spectrometry singly charged oligonucleotide ions are formed. In the positive-ion mode, protonated ions of the form $(M+H)^+$ are formed while in the negative ion-mode the corresponding deprotonated ions are formed $(M-H)^-$. Unlike MALDI, with ESI a range of multiply charged ions of the form $(M+nH)^{n+}$ or $(M-nH)^{n-}$ are produced, depending on whether the positive or negative ion-mode is used. This tendency to form multiply charged ions, increases the complexity of ESI spectra compared to MALDI spectra. Additionally, the ESI instrumentation is more complex making the MALDI-based approach more favourable[57]. MALDI-MS can be used in general for the characterization of oligonucleotides and nucleic acids[58]. It has been used for the analysis of RNA cleavage[54], for the identification of RNA modifications[59], as well as for the characterization of metallated DNA and RNA. For example, it was employed for the characterization of platinum(II)-RNA[13,56,60,61] and platinum(II)-DNA complexes[2,58,62,63]. Literature data

on the interaction of nucleic acids with metal complexes other that platinum(II) compounds, like Ru(II) and Rh(III) complexes, are also available[55,64].

In MALDI-MS in order to improve the spectra quality factors like sample preparation, matrices, matrices additives, laser wavelength as well as laser power should be taken into consideration. For our study, the sample preparation had a key role. RNA has the tendency to form Na(I) and K(I) adducts; for this reason it is important to eliminate residual cations during the sample preparation procedure[57]. This is normally achieved by desalting the samples. The desalting was performed either by NAP columns or electroelution (Chapter 5, Paragraphs 5.1.2.3 - 5.1.2.4). Additionally to this, C18 reverse-phase pipette tips such as ZipTips were used. An important source of cations during the preparation of the platinated RNAs was the "crush and soak" buffer. This buffer was used in order to extract the RNA samples from the gels. It consisted of 250 mM NaOAc, 10 mM MOPS and 1 mM EDTA. Using this buffer, despite the desalting step, the quality of the mass spectra was low due to the presence of numerous Na(I) adducts (Figure 2.30, left). To overcome this problem, NaOAc was replaced by NH_4OAc at the same concentration. The ammonium salts of the oligonucleotides can easier lose ammonia after proton loss during the desorption process resulting in homogeneous oligonucleotide ions[28]. With the use of the new buffer, the quality of the mass spectra was improved (Figure 2.30, right).

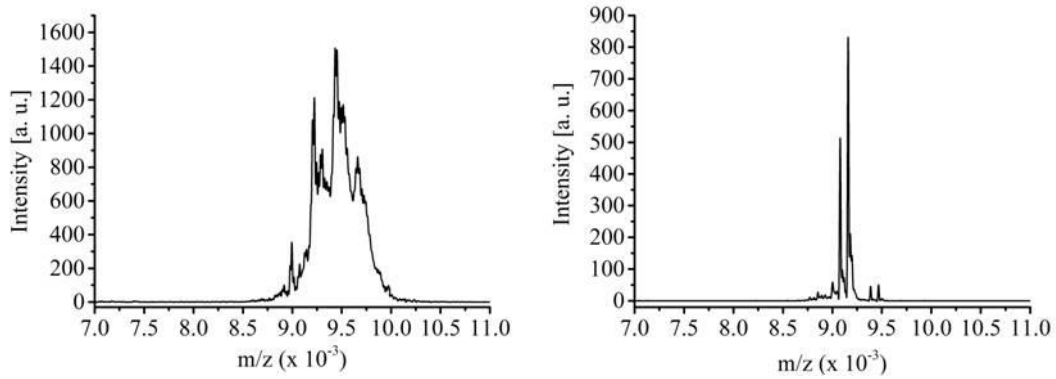

Figure 2.30: *Mass spectra of samples that were isolated with the use of NaOAc (left) and NH_4OAc (right).*

The RNA and Pt(II)-RNA samples were analysed in the negative-ion mode with THAP (2,3,4-trihydroxyacetophenone) as matrix. A typical mass spectrum of D1-27 is given in Figure 2.31. In addition to the peak corresponding to D1-27 (m/z = 8848), peaks for the RNA with different number of phosphate groups were also observed (m/z = 8766 and m/z = 8694) (Table 2.1). As it was previously mentioned, the RNA used was transcribed *in vitro* and upon transcription there was a triphosphate group at the 5′-end. Under the experimental conditions of the transcription, hydrolysis of the phosphate group could take place (Figure 2.14). The hydrolysis of the phosphates occurs by S_N2 mechanism and is dependent on Mg(II) ions. The presence of RNA molecules containing different number of phosphates is confirmed by analytical denaturing gels run on freshly transcribed RNA (Figure 2.31). The

appearance of more than one band on the gels resulted from the longer running time (2 days instead of 1 day) used. Additionally to this, it is known that the phosphate ester bonds of the triphosphate could be cleaved during the ionization process of MS measurement leading also to the formation of RNA species with different number of phosphate groups[28].

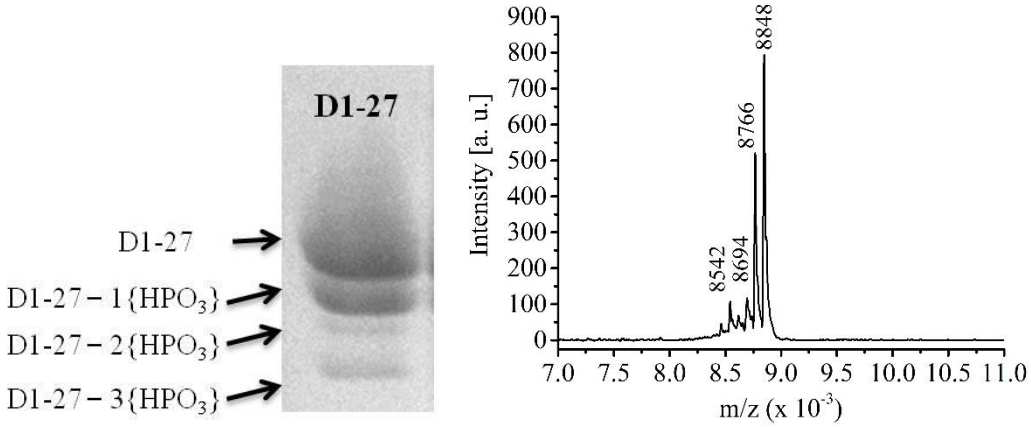

Figure 2.31: *20 % denaturing PAGE corresponding to D1-27 (left) and a characteristic mass spectra of D1-27 (right). The gel was run for 2 days at 4 °C. In Table 2.1 are given the expected and measured m/z values for this sample.*

Table 2.1

RNA species	Expected m/z	Measured m/z
D1-27	8848	8848
D1-27 − {HPO$_3$}	8768	8766
D1-27 − 2{HPO$_3$}	8688	8694
D1-27 − CMP	8542	8542

Besides these peaks, a peak corresponding to D1-27 missing a cytidine monophosphate (m/z = 8542) unit was often observed in the mass spectra. The fragmentation of RNA during MS measurements is well established[28,29]. The possible fragmentation sites in oligonucleotides are given in Figure 2.32. There are four possible sites along the phosphodiester backbone, denoted as *w*, *x*, *y*, *z* when the fragment ion contains the 3′ terminus. The number in subscript gives the number of bases from the termini. The C indicates the cytosine. In the case of D1-27 the x_1 fragment was observed, which corresponds to the loss of 305 Da.

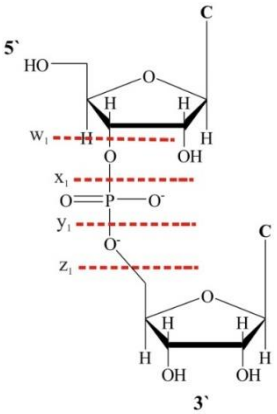

Figure 2.32: *Possible fragmentation sites in oligonucleotides and nomenclature proposed by McLuckey et al*[65].

In the case of oxaliPt, an increase in mass by 309 or 618 Da is expected upon coordination of one or two Pt(DACH) moieties respectively, accompanied by the loss of the oxalate ligand. Due to the presence of a triphosphate group at the 5′-end of D1-27, additional peaks, which corresponded to monoplatinated and diplatinated RNAs with different number of phosphate groups at their 5′-end could also be observed (Figure 2.33). For example in the case of monoplatinated D1-27, peaks corresponding to [RNA + 1Pt – 1{HPO_3}] (m/z = 9070), [RNA + 1Pt – 2{HPO_3}] (m/z = 8999) could be observed additionally to the major peak for the [RNA + 1Pt] (m/z = 9151) species (Figure 2.34). Unfortunately, the isotopic pattern of platinum is not observed in the MS spectra, the reason for that being the use of the linear ionization mode which shows reduced resolution compared to the reflectron mode[58]. The experimental masses obtained were in accordance with the predicted masses. For small oligonucleotides, typical errors are between 0.03 % - 0.05 % while for larger oligonucleotides the mass errors could reach 0.3 %. Therefore, the measurement errors observed here (< 0.1 %) were all within the limit[58].

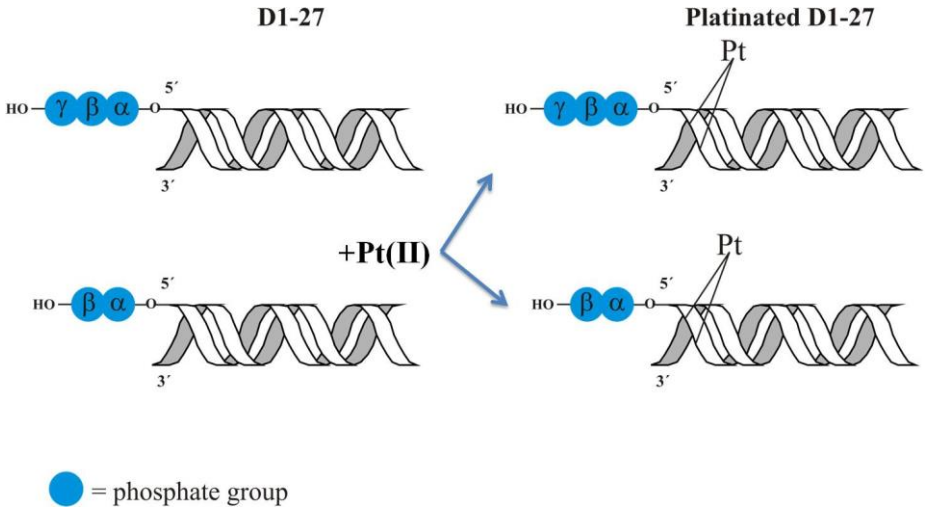

Figure 2.33: *Schematic representation of an A-form RNA with different number of 5'-phosphate groups together with possible monoplatinated species formed. α, β, γ indicate the three phosphates in the triphosphate group. Cartoons prepared with ChemDraw Pro 13.0.*

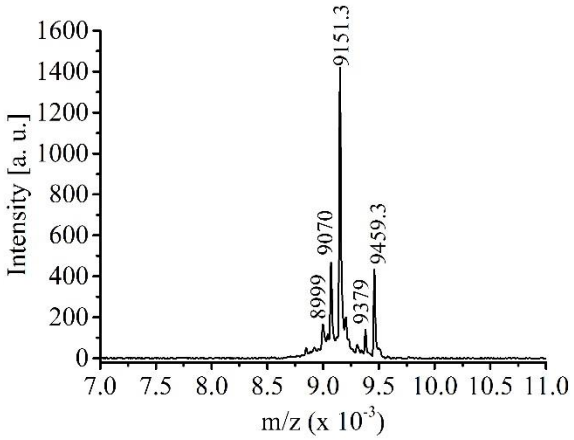

Figure 2.34: *A characteristic mass spectrum of platinated D1-27 with oxaliPt. In Table 2.2 are given the expected and measured m/z values for this sample.*

Table 2.2

Pt-RNA species	Expected m/z	Measured m/z
Monoplatinated D1-27	9157	9151
Monoplatinated D1-27 − {HPO_3}	9077	9070
Monoplatinated D1-27 − 2{HPO_3}	8998	8999
Diplatinated D1-27	9467	9459
Diplatinated D1-27 − {HPO_3}	9387	9379

2.8 Isolation of the monoplatinated RNA

As commented in section 2.4, when the platination was performed in the presence of 5 eq of oxaliPt, in 120 mM KCl at 25 °C for 1 day, a slower migrating band was observed on the gels. This band was cut and the platinated RNA was isolated and characterized with MALDI–MS. The MS measurements showed that under these reaction conditions the predominant species was the monoplatinated RNA; however, there were always additional lower-intensity peaks corresponding to diplatinated RNA (Figure 2.34). It was not possible to avoid the formation of the diplatinated species nor to separate them from the monoplatinated ones via denaturing PAGE. For this reason, we explored the use of High Performance Liquid Chromatography (HPLC) for the separation of our various platinated RNA species[66]. HPLC has been widely used to assess the purity of oligonucleotides[67], to separate differently platinated DNA species[68] as well as to perform kinetic measurements of platination reactions[68,69].

2.8.1 Ion-Pair Reversed Phase HPLC (IP RP HPLC)

IP RP HPLC is a well-recognized method for the analysis of RNA[66]. It is used for the separation of different RNA species, quantification and purification. Ion-pairing agents are large ionic molecules which have a charge which is opposite of the sample of interest. These reagents are added in small concentrations to the mobile phase; their hydrophobic region associates with the non-polar stationary phase while the charged region interacts with the sample of interest. This interaction affects the affinity of the sample for the stationary phase leading to higher resolution[67]. Since we work with RNA, which is negatively charged, the positively charged triethylammonium acetate (TEAA) (buffer A) was used as ion-pairing agent. The negatively charged RNA backbone is ion paired with the triethylammonium ions resulting in the separation of the charged species according to their charged state. The molecules are released from the stationary phase by increasing the amount of a nonpolar solvent. For our study acetonitrile was used (buffer B). The order of elution depends mostly on: 1) the charge of the oligonucleotide: the retention time increased proportionally to the number of charges in the oligonucleotide, 2) the length of alkyl chain in the ion-pairing reagent: extended retention is the result of increased hydrophobicity in the ion-pairing reagent, 3) the proportion of the organic solvent in the mobile phase: the retention time is decreased while the concentration of organic solvent is increased[67]. By using HPLC we were aiming at separating the monoplatinated from the diplatinated D1-27. In order to do that, it was necessary to first establish a method, which could give rise to a single well-resolved peak for D1-27 alone. For that reason, different stationary phases and gradients of buffer B were tested. All the columns used contained C18 bonded phase packing. C18 columns are mostly used in studies of RNA platination[5,69]. The first method for testing them was method 1 (Chapter 5, Paragraph 5.5.3_ Method 1) and the columns tested were:

RP cross-linked poly(styrene-co-divinylbenzene) polymer PRP® –h1 column (5 μm, 4.6 x 250 mm) from Hamilton
RP Ultraphere® (5 μm, 4.6 x 250 mm) from Beckman & Coultier
Macherey-Nagel Nucleodur column, Gravity column (5 μm, 4 x 250 mm)
RP X-Bridge column (3.5 μm, 4.6 x 150 mm) from Waters

D1-27 was dissolved in ddH_2O and a 0.4 nmol sample was injected. In the case of column 1, a low resolution peak corresponding to D1-27 was eluted at 19.7 min while by using column 2 a very small broad peak was observed at 19.4 min. The RNA peak was better when column 3 was used, but it was still too broad and asymmetric (Figure 2.35).

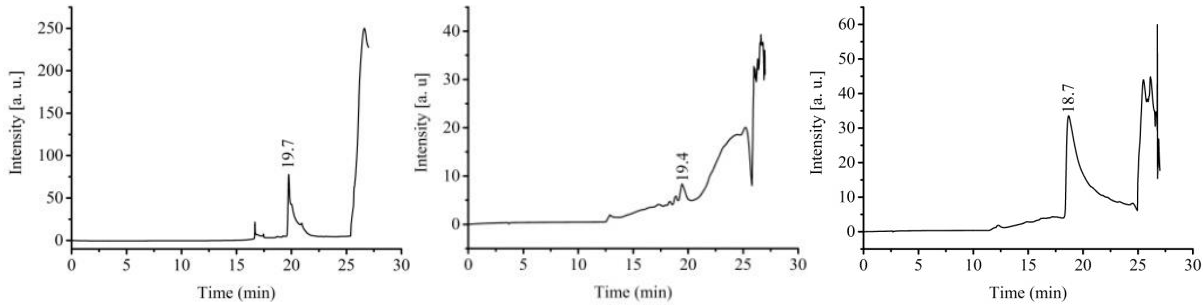

Figure 2.35: *HPLC traces obtained for D1-27 using column 1 (left), column 2 (middle) and column 3 (right). Method 1, Flow rate: 1 mL / min, Buffer A: 23 mM TEAA, pH 7, Buffer B: Acetonitrile.*

The best result was achieved by using column 4. A well resolved but tailing peak appeared after 21 min (Figure 2.36, left). The difference in retention time observed for the four different C18 columns may be attributed to differences in silica support or to the stationary phase chemistry[67]. The best performance was obtained with column 4, which was then used for the rest of the study. The shape of the peak was improved by increasing the gradient slope as well as by changing the TEAA concentration from 23 mM to 100 mM (Chapter 5, Paragraph 5.5.3_ Method 2) (Figure 2.36, right).

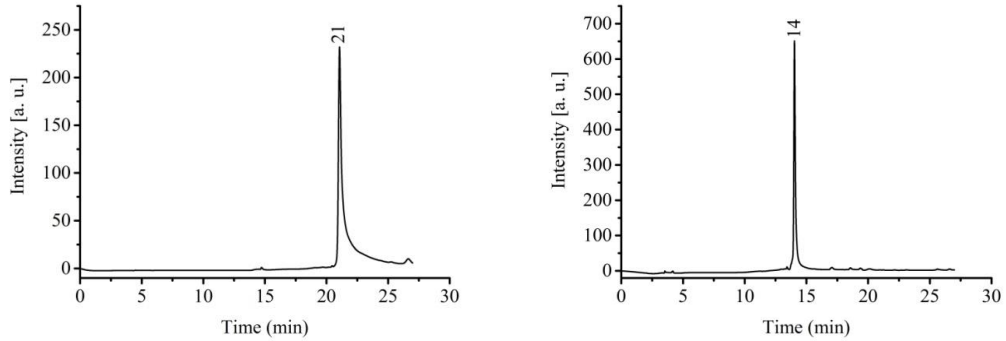

Figure 2.36: *HPLC traces obtained for D1-27 with column 4 using method 1 (left) and method 2 (right). Left chromatogram: Method 1, Flow rate: 0.5 mL / min, Buffer A: 23 mM TEAA, pH 7, Buffer B: Acetonitrile; Right chromatogram: Method 2, Flow rate: 0.5 mL / min, Buffer A: 100 mM TEAA, pH 7, Buffer B: Acetonitrile.*

Upon platination of D1-27 with oxaliPt (5 eq of platinum(II) complex, 0.25 mM RNA, 120 mM KCl, 1 day at 25 °C) the sample was purified with a denaturing gel and the upper band was cut. The platinated RNA species were isolated from the band and injected in the HPLC machine (method 2) giving the red chromatogram in Figure 2.37. An RNA sample was injected separately and the chromatograms were overlaid. As shown in Figure 2.37 the retention time of the RNA and the Pt(II)-RNA species are very close, even if the two peaks correspond to two different species. The shorter retention time for RNA in Figure 2.37 compared to Figure 2.36 (10.8 *vs* 14 min) was due to the fact that a higher flow rate was used (1 mL / min *vs* 0.5 mL / min). Interestingly, the platinated RNA had shorter retention time

compared to the unreacted one. It is known that with the use of IP RP HPLC by increasing the gradient of the organic solvent, the smaller fragments are eluting first from the column. Here the platinated molecules were eluted first independently of their higher molecular weight. Similar behaviour was reported also by Papsai et al[5] when using similar experimental conditions. This is likely because the mechanism by which the RNA samples are separated is more complicated, and does not simply rely on mass differences. Instead, more variables, like the overall charge as well as structural conformation, have to be taken into consideration. For instance, it is known that dsRNA elute faster compared to dsDNA species. Due to the different structural conformation that they adopt (A-form for RNA and B-form for DNA) the hydrophobicity of RNA is decreased compared to DNA and therefore RNA elutes first[70].

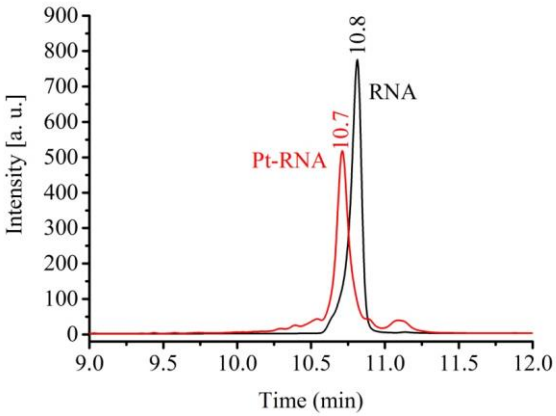

Figure 2.37: *Chromatograms of D1-27 (black) and platinated D1-27 (red). Method 2, Flow rate: 1 mL / min, Buffer A: 100 mM TEAA, pH 7, Buffer B: Acetonitrile.*

From MALDI-MS analysis of the sample before injection, it was known that it consisted of a mixture of monoplatinated and diplatinated RNA (Figure 2.34), with the monoplatinated species being the main one. With the use of HPLC we were aiming at separating and quantifying these two species.

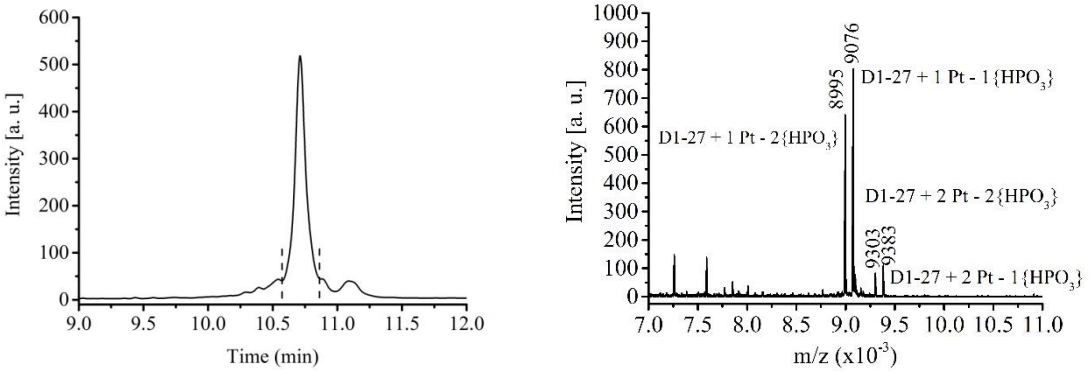

Figure 2.38: *Chromatogram of the platinated D1-27 (left) and the MALDI mass spectrum (right) of the sample collected between 10.6 and 10.8 minutes, corresponding to the main peak in the chromatogram. Method 2, Flow rate: 1 mL / min, Buffer A: 100 mM TEAA, pH 7, Buffer B: Acetonitrile.*

First, the attribution of the peaks appearing in the chromatogram had to take place. The main peak, which was thought to contain the monoplatinated RNA, was collected (from 10.6 to 10.8 min, Figure 2.38) and analysed by MALDI-MS. A mixture of monoplatinated and diplatinated RNA was again the result of the MALDI-MS characterization (Figure 2.38, right). This result suggests that the two species eluted together and they were not separated. To solve this problem, the gradient used had to be further optimized in order to achieve a better separation of the two species. Towards this direction, the slope of the gradient was decreased. This had as a result to increase the peak resolution[71] and a shoulder corresponding to the diplatinated RNA species appeared (Figure 2.39, black line). To confirm that the shoulder corresponds to diplatinated RNA, the platination reaction was repeated using 10 eq of oxaliPt instead of 5 eq, and it was allowed to proceed for 2 days instead of 1, which leads to the formation of more diplatinated RNA species (Appendix 1, A 1.23). The presence of increased amount of diplatinated RNA resulted in the increase of its peak on the chromatogram. Indeed, the intensity of the shoulder besides the main peak increased, confirming its attribution to the diplatinated species (Appendix 1, A 1.24). Different gradients were tested to obtain the best separation between monoplatinated and diplatinated species: the smaller the slope used, the more pronounced the shoulder was (Figure 2.39). The method used in the case of the blue chromatogram (Figure 2.39) led to a better separated peak for the diplatinated species, and was then chosen for the following experiments (Method 5).

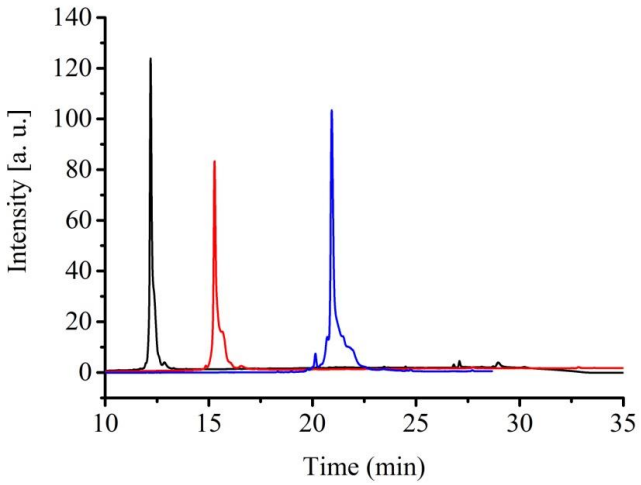

Figure 2.39: *Method optimization for the separation of monoplatinated and diplatinated D1-27. The gradient slope is decreasing from the left to the right. Black line: Method 3, Red line: Method 4, Blue line: Method 5, Flow rate: 1 mL / min, Buffer A: 100 mM TEAA, pH 7, Buffer B: Acetonitrile.*

A new platinated sample was prepared and it was injected in the HPLC machine using this new method (Method 5). The chromatogram obtained is shown in Figure 2.40. The main peak was collected and analyzed via MALDI-MS (Figure 2.40, right). The mass spectrum showed that the collected sample contained only monoplatinated RNA (m/z = 9154) (Figure 2.40). The procedure was repeated in order

to collect higher amounts of monoplatinated RNA for further studies but the result was unfortunately not reproducible, and a small amount of diplatinated species was always present in the collected samples. The chromatograms of the mixture was used to quantify the two platinated species. From that, it was found that the diplatinated species corresponded the 12 % of the sample while the monoplatinated one was the 88 %. The quantification of the platinated RNA species was however not very precise due to the presence of Pt(II)-RNA adducts with different number of phosphate groups, which are all expected to have different retention time. The way that we approached and solved this problem will be discussed in paragraph 2.9. Finally, considering that this amount of diplatinated RNA was the smallest possible that we could achieve, this mixture was used for further characterization (Chapter 4).

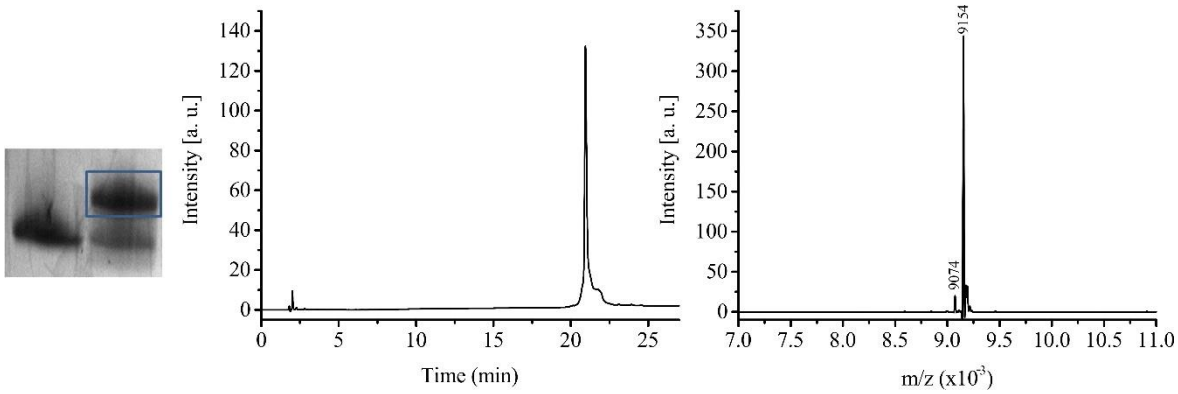

Figure 2.40: *Experimental procedure followed for the isolation of monoplatinated D1-27. From the left to the right are depicted the gel corresponding to the platination reaction, the HPLC chromatogram of the platinated RNA species isolated from the upper band (blue frame) and the mass spectrum corresponding to the species responsible for the main peak in the chromatogram. Method gradient 5, Flow rate: 1 mL / min, Buffer A: 100 mM TEAA, pH 7, Buffer B: Acetonitrile. The higher platination yield observed with respect to the previous gels is because of the use of 200 mM KCl instead of 120 mM.*

2.8.2 Use of IP RP HPLC for sample isolation and purification

By using denaturing PAGE the separation of the unreacted from the platinated species was successful but no separation between monoplatinated and diplatinated RNA was ever achieved. Since IP RP HPLC can be successfully used to separate various platinated species (see above), we evaluated the possibility of substituting dPAGE separation with HPLC separation. The platination reaction was performed following the experimental conditions commented above (5 eq of platinum, 0.25 mM RNA, 120 mM KCl, 1 day at 25 °C) and then, instead of using denaturing PAGE, the reaction mixture was directly injected in the HPLC machine. The chromatogram obtained this time corresponds to the whole platination reaction mixture, and therefore two main peaks were observed (one for the unreacted and one for the platinated RNA, Figure 2.41, black line). Since the aim was to collect the platinated RNA, the retention times of the two peaks had to be further separated. Indeed, by using the methods explored until now, the retention times of the RNA and the Pt(II)-RNA species were very close (Figure 2.37),

making difficult the collection of only platinated RNA species. The optimization of the method took place by changing the slope of the gradient. More specifically, by decreasing the slope, better separation of the unreacted from the platinated RNA was achieved (Figure 2.41). The method chosen corresponds to the red chromatogram (Method 7) in which the main peak (15.6 min), which corresponds to the platinated RNA, was well-separated from the peak corresponding to the unreacted RNA (17.4 min) (Figure 2.41).

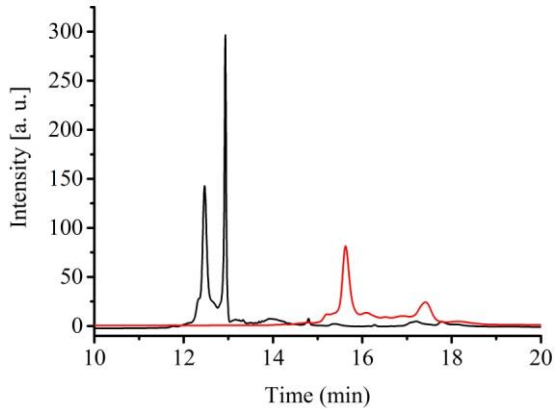

Figure 2.41: *Chromatograms corresponding to two different methods tested to optimize the separation of the peaks of platinated and unreacted RNA. The gradient slope is decreasing from the left to the right. Black line: Method 6, Flow rate: 1 mL / min, Buffer A: 100 mM TEAA, pH 7, Buffer B: Acetonitrile. Red line: Method 7, Flow rate: 1 mL / min, Buffer A: 100 mM TEAA, pH 7, Buffer B: Acetonitrile. Both chromatograms in Figure 2.41 correspond to the same sample and the different peak shape is due to the use of a different gradient slope.*

Having a good HPLC method, which allowed a better separation of the untreated from the platinated RNA (Figure 2.41, red line), the platination reaction mixture was prepared and injected once immediately after the start of the reaction (Figure 2.42, upper panel, left) and once after 1 day of incubation (Figure 2.42, upper panel, right). The comparison between the two chromatograms obtained at the beginning and at the end of the platination reaction confirmed the attribution of the peak at 17.4 min to the unreacted RNA. This was indeed the main peak at the beginning of the reaction, which after 1 day of incubation was reduced, whereas the intensity of the peak at 15.6 min increased, confirming its attribution to the platinated RNA. The area below the peaks denoted with a circle and with a square (Figure 2.42, upper panel, right) were collected and analysed with MALDI-MS. The mass spectrum of the sample corresponding to the main peak (yellow circle, Figure 2.42, lower panel, left) showed as major species the monoplatinated RNA [(m/z = 9156: (D1-27 + 1Pt), m/z = 9075: (D1-27 + 1Pt – 1{HPO_3})], in addition to a smaller peak corresponding to diplatinated species [(m/z = 9383: (D1-27 + 2Pt – 1{HPO_3}), m/z = 9463: (D1-27 + 1Pt)]. On the contrary, the mass spectrum of the sample corresponding to the peaks denoted with a square in the chromatogram (Figure 2.42, lower panel, right) shows a mixture of monoplatinated and diplatinated RNA species with similar intensity.

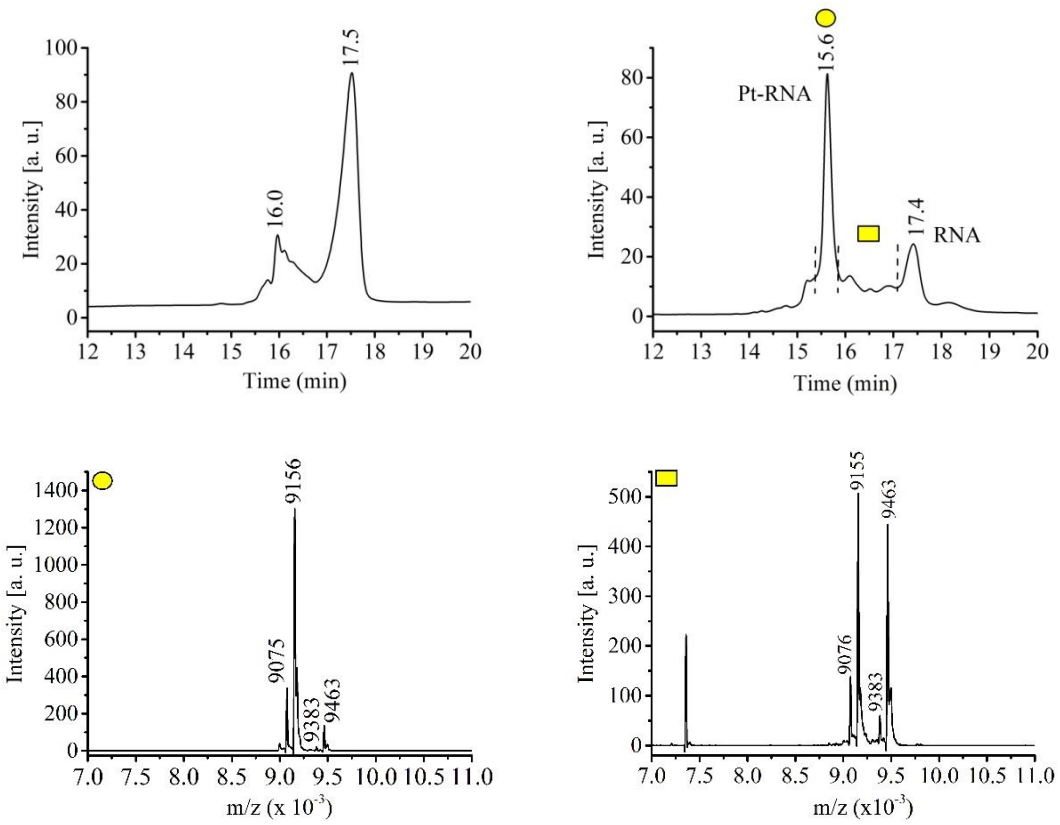

Figure 2.42: *Upper panels: Chromatograms from the direct injection of the platination reaction mixture in the beginning of the reaction (left) and after 1 day of incubation (right). An improved gradient (method 7) was employed to better separate the unreacted from the platinated RNA. The peak under the circle and the square were collected and analysed with MALDI-MS. Lower panels: The MALDI-MS spectra of the collected peaks.*

Interestingly, even if the gradient used in this case (Figure 2.41, red line, method 7) was less steep compared to the one used while attempting to separate monoplatinated from diplatinated RNA (Figure 2.39, blue line), it was still not possible to separate the diplatinated RNA from the monoplatinated one. Additionally, mass spectra showed that both collected samples contained a mixture of mono- and diplatinated RNAs. A reason for this behaviour could be the heterogeneity of D1-27 due to the presence of a different number of phosphate groups at the 5´-end. Indeed, the RNA samples in aqueous solution consist mostly of the species with the triphosphate, but RNA species with two or only one phosphate group at the 5′-end are present (Paragraph 2.7, Figure 2.33). Upon platination there is formation of platinated species with three, two or one phosphate group and all of them, due to different overall negative charge, interact with the stationary phase of the column differently and therefore are eluted at different times. According to the information from MS data, the main peak observed in the chromatogram corresponds to a sample containing mostly the monoplatinated species with 5′-triphosphate (Figure 2.42). Indeed, the mass spectrum shows a main peak corresponding to the monoplatinated specie with 5′-triphosphate together with a peak with lower intensity, corresponding to diplatinated species with 5′-triphosphate. Additionally to these peaks, lower intensity peaks were

observed, corresponding to monoplatinated and diplatinated species with two phosphate groups at the 5′-end. The different number of the phosphate groups may then be the reason why it was not possible to separate the monoplatinated from the diplatinated RNA with IP RP HPLC (Paragraph 2.8.1). Summing up, the use of HPLC as an alternative way to separate the platinated RNA species from the unreacted ones, instead of denaturing PAGE, was explored. With this approach, the separation of the monoplatinated from the diplatinated RNAs was also attempted. However, due to the heterogeneity of the RNA used and, consequently, of the platinated RNA species formed, the separation of the differently platinated RNA species was not feasible. Since there was no advantage in using HPLC instead of dPAGE for sample separation, the latter was used for the rest of this study.

2.9 Use of dephosphorylated RNA for platination reactions

The data above suggest that the heterogeneity due to the presence of different number of phosphate groups per RNA could be the reason for not separating the monoplatinated from the diplatinated RNA. In the direction of obtaining a homogeneous RNA sample, D1-27 was dephosphorylated before being used for the platination reactions. The large scale RNA dephosphorylation is described in detail in the experimental part (Chapter 5, Paragraph 5.1.4). Upon dephosphorylation, 1D ^{31}P-NMR experiments, MALDI-MS and HPLC analysis were performed in order to evaluate the quality of the sample (Figure 2.43). The ^{31}P-NMR spectrum shows that upon dephosphorylation the three peaks corresponding to α, β and γ phosphate are not present anymore (Figure 2.43, left). The MALDI-MS spectrum of the dephosphorylated RNA (deph-RNA) has a peak with m/z = 8612 that corresponds to the deph-D1-27. The other peak with m/z = 8307 corresponds to deph-D1-27 without the CMP from the 3′- end (Figure 2.43, middle). As mentioned before this could be either due to fragmentation during the ionization process (Paragraph 2.7) or possibly due to malfunction of the T7 polymerase during the *in vitro* transcription. Finally, the HPLC chromatogram shows only one peak that corresponds to deph-D1-27, unlike the chromatogram of triphosphate-D1-27 (triph-D1-27), where peaks for all the species with different number of phosphates were observed (Figure 2.43, right). The chromatogram in Figure 2.43 corresponding to triph-D1-27 (black line, right) is different compared to the one showed above, which has only one peak and not four (Figure 2.37). The difference observed is because different methods were used in each case. The gradient slope that was used for the sample whose chromatogram is reported in Figure 2.37 was steeper compared to the one used in the case of Figure 2.43 (Method 7), and no separation of the various RNAs with different phosphate groups was achieved.

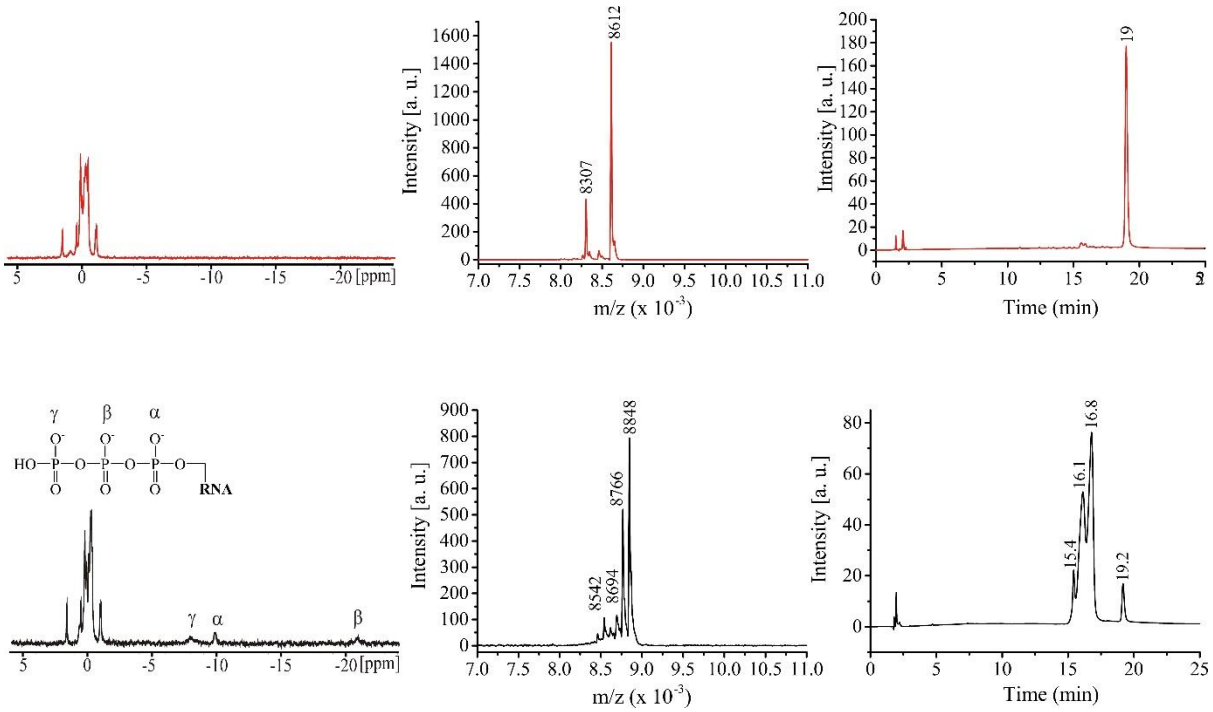

Figure 2.43: *Characterization of deph-D1-27 with ^{31}P-NMR (left), MALDI-MS (middle) and HPLC (right). The black line corresponds to triph-D1-27 and the red to dephosphorylated one.*

The platination of deph-RNA with oxaliPt was performed using 5 eq of oxaliplatin, 0.25 mM RNA, 1 day of incubation at 25 °C in 120 mM KCl. Interestingly the gel picture obtained upon platination of deph-D1-27 is different from the gel picture obtained in the case of triph-D1-27 (Figure 2.44). More specifically when triph-D1-27 was platinated two main bands were visible on the gel and from the MALDI-MS analysis the one corresponded to the mixture of monoplatinated and diplatinated RNA (upper band) and the second corresponded to a mixture of mostly unreacted RNA as well as monoplatinated and diplatinated species (lower band) (Figure 2.26). Upon dephosphorylation three main bands were observed and named as upper, middle and lower band (Figure 2.44).

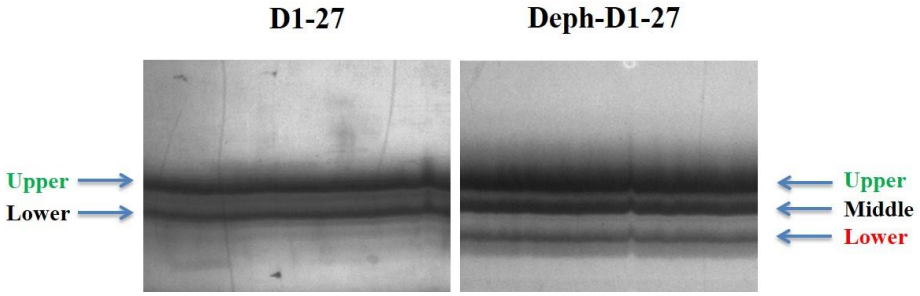

Figure 2.44: *20% denaturing PAGE (19:1 gel solution) for the platination reaction of triph-D1-27 (left) and deph-D1-27 (right) with oxaliPt. In the same colours are indicated the bands which had similar MS spectra. The gel was run at 4 °C.*

The three bands were cut and the samples were isolated and characterized via MALDI-MS (Figure 2.45, lower panel). The mass spectra showed that the upper band consisted of a mixture of monoplatinated (m/z = 8917) and diplatinated deph-RNA (m/z = 9225) (like the upper band obtained in the case of triph-RNA) (Figure 2.45, lower panel, left); the middle band was a mixture of unreacted (m/z = 8612), monoplatinated (m/z = 8919) and diplatinated deph-RNA species (m/z = 9226) (like the lower band obtained in the case of triph-RNA) (Figure 2.45, lower panel, middle) and the lower band contained species with the same molecular weight as the upper band, but in different ratio (Figure 2.45, lower panel, right). In the lower band the intensity of the peak for the diplatinated deph-RNA (m/z = 9226) was higher compared to the sample extracted from the upper band (See Appendix 1, A 1.25 - A 1.27). Analysis of the samples from all three bands was performed also via HPLC (Figure 2.45, upper panels).

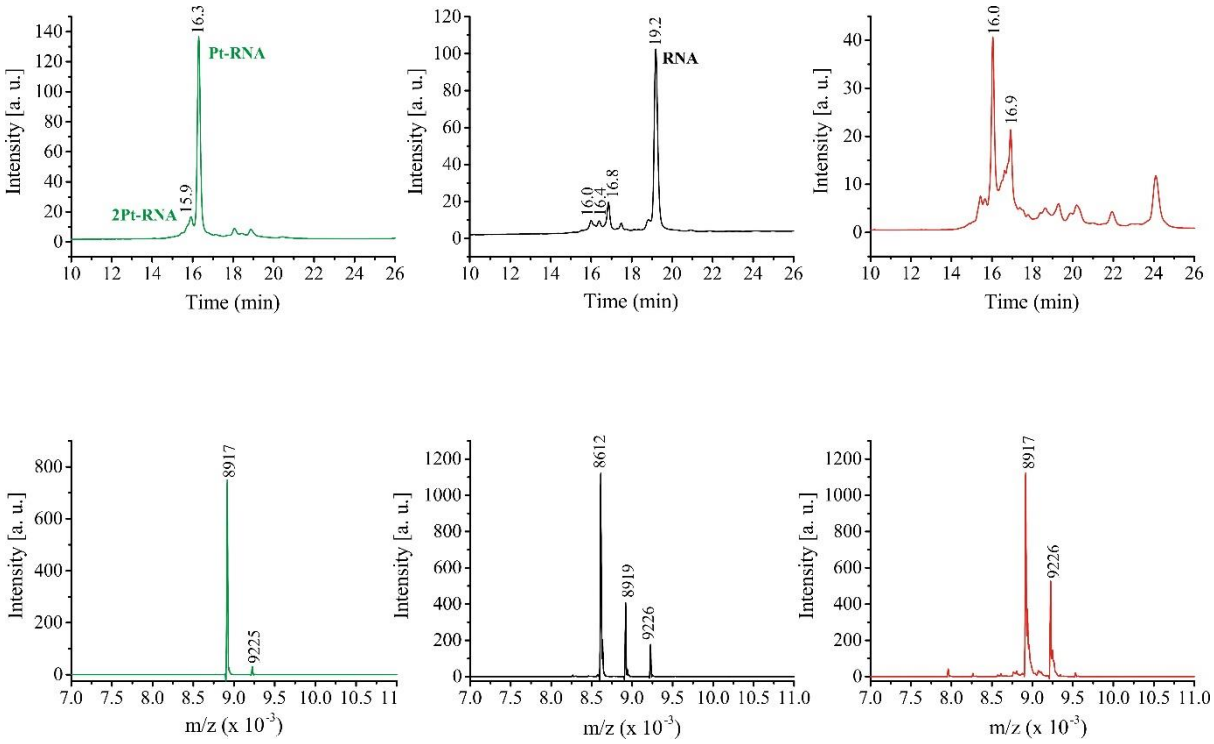

Figure 2.45: *Upper panels: HPLC traces of the platinated species extracted from the upper (green), middle (black) and lower (red) band of the denaturing gel. The method 7 was used. Lower panels: MALDI-MS spectra of the samples extracted from the three bands (colour code as above).*

In the case of the upper band, a main peak was observed at 16.3 min, which was assigned to the monoplatinated deph-D1-27, whereas the smaller peak at 15.9 min was assigned to diplatinated deph-RNA (Figure 2.45, upper panel, left). This attribution was confirmed by mass spectra recorded on the isolated samples, collected at 15.9 and 16.3 minutes (Figure 2.46). The sample eluting at 15.9 min consisted of monoplatinated (m/z= 8992) and diplatinated deph-RNA (m/z= 9200), with the

latter being the major species (Figure 2.46, left), whereas the sample eluting at 16.3 min consisted almost completely of monoplatinated deph-RNA (m/z= 8890) and only a minor peak was attributed to diplatinated species (m/z= 9202) (Figure 2.46, right). Given that the two peaks can be confidently attributed to monoplatinated (16.3 min) and diplatinated (15.9 min) deph-D1-27, their integration was used to roughly quantify the two RNA species. The peak integration was performed automatically by the HPLC software (Chromeleon 7.1) and it was found that the sample consisted of 84 % of monoplatinated and 16 % of diplatinated deph-RNA.

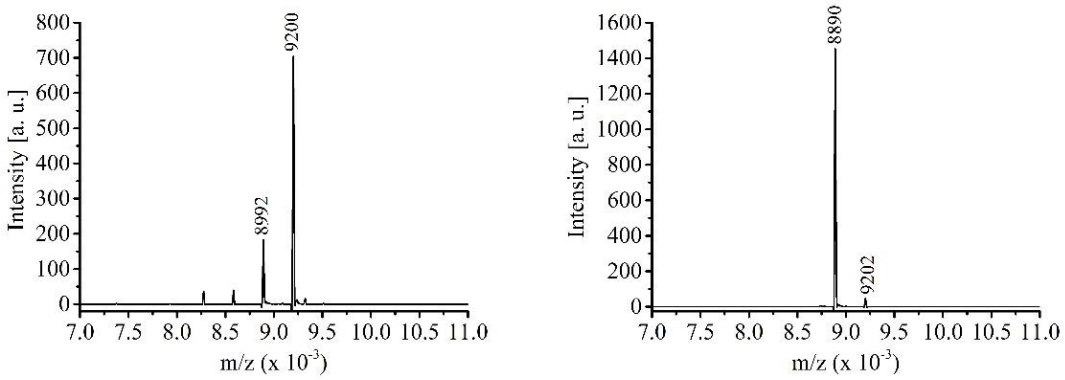

Figure 2.46: *The MALDI-MS spectra of the sample collected from the peak at 15.9 min (left) and 16.3 min (right).*

The HPLC chromatogram of the middle band had a main peak for the unreacted RNA (19.2 min) and some minor peaks which could be attributed to monoplatinated and diplatinated RNA (Figure 2.45, upper panel, middle), based on the assignments commented above. The chromatogram of the lower band (Figure 2.45, upper panel, right) was more crowded compared to the one from the upper band even if their mass spectra were similar. This could be due to either the lower concentration of the sample (the HPLC trace of the sample has indeed similar intensity as the impurities), or to the fact that this sample consisted of a mixture of RNA species platinated at different sites. The two main peaks at 16 min and 16.9 min, based on the assignment of the peaks from the upper band (Figure 2.45, upper panel, left) and considering the ratio of the products from the mass spectrum, can be attributed to diplatinated and monoplatinated RNA respectively. The peaks between 18 and 24 minutes can be considered as impurities (the same peaks were present also in the chromatogram of the sample from the upper band). Further assignment of the peaks was not performed.

Concluding, upon platination of deph-D1-27 there was formation of three bands, two of which contained monoplatinated and diplatinated species. The main platinated species migrating in the upper band was further characterized, and compared with the corresponding one obtained when the platination was performed with triph-RNA (Chapter 4). However, to understand the origin of the newly appeared band (lower), the platinated species from the lower band was also characterized using various techniques, as described in detail at the end of chapter 4.

2.10 Conclusions

In the first part of the chapter, the reasons why this study was conducted using oxaliplatin as platination agent have been discussed. Upon platination, a slower migrating band (upper) was formed and from MALDI-MS characterization it was found that it contained a mixture of monoplatinated and diplatinated RNA, with the first being the major species. Since no separation between the two species was achieved using denaturing PAGE, the use of HPLC was attempted. At first, the appropriate stationary phase as well as a method which would allow to obtain well resolved peaks for both RNA and platinated RNA were found. Once the HPLC method was optimized, the platinated samples extracted from the gel were analysed by HPLC. Unfortunately, despite the optimization, the retention time of the mono- and diplatinated RNA were very close, and no successful separation was obtained. Next, the use of HPLC for the isolation and purification of the platinated RNAs instead of dPAGE was attempted. The platination mixture was directly HPLC injected after the end of the reaction. However, no advantage with respect to dPAGE separation was obtained, and all the samples were then purified and isolated using denaturing gels. Unfortunately, isolation of pure monoplatinated RNA was not possible, likely because of the heterogeneity of the reaction mixture. However, HPLC could be used to quantify the diplatinated species (12 %). The heterogeneity observed was the result of the use of RNA samples with triphosphate and diphosphate groups at the 5′-end (Figure 2.33), which led to the formation of platinated RNA species with different number of phosphate groups (Figure 2.33). In order to have a homogeneous starting material for our studies, D1-27 was dephosphorylated before being used for platination. The platination of deph-D1-27 resulted in a gel with three bands (Figure 2.44). In addition to the slower migrating band observed also in the previous case, a new faster migrating band (lower), which consisted of monoplatinated and diplatinated RNA, appeared. By using deph-RNA the chromatogram of the platinated RNA species from the upper band was improved (Figure 2.45, left, green line) and two main peaks were observed corresponding to monoplatinated and diplatinated RNA. Now, contrary to what previously observed, a more homogeneously platinated sample could be isolated (Figure 2.46, right), which corresponds to the species eluting at 16.3 min (Figure 2.45, left, up). However, this result is preliminary, and further optimization is likely required if the method is to be used to obtain large amount of homogeneous sample. Consequently, in all cases the main species that will be characterized contain monoplatinated RNA (88 %), but also a small percentage of diplatinated RNA (12 %) is present. Chapter 4 is dedicated to the characterization of the platinated species which were isolated from the upper band of denaturing gels run on reaction mixtures performed with both triph- and deph-D1-27.

In the next chapter, time evolution NMR experiments will be employed as a way to directly follow the platination reactions and get a first indication about which nucleobases are affected upon platination.

2.11 References

1. Alberti, E., Zampakou, M. & Donghi, D. Covalent and non-covalent binding of metal complexes to RNA. *J. Inorg. Biochem.* **163,** 278–291 (2016).
2. Chapman, E. G., Hostetter, A. A., Osborn, M. F., Miller, A. L. & DeRose, V. J. Binding of kinetically inert metal ions to RNA: The case of platinum(II). *Met. Ions Life Sci.* **9,** 347–377 (2011).
3. Jordan, P. & Carmo-Fonseca, M. Cisplatin inhibits synthesis of ribosomal RNA in vivo. *Nucleic Acids Res.* **26,** 2831–2836 (1998).
4. Heminger, K. A., Hartson, S. D., Rogers, J. & Matts, R. L. Cisplatin inhibits protein synthesis in rabbit reticulocyte lysate by causing an arrest in elongation. *Arch. Biochem. Biophys.* **344,** 200–207 (1997).
5. Papsai, P., Snygg, A. S., Aldag, J. & Elmroth, S. K. Platination of full length tRNA(Ala) and truncated versions of the acceptor stem and anticodon loop. *Dalton Trans.*, 5225–5234 (2008).
6. Michel, F. & Ferat, J. L. Structure and activities of group II introns. *Annu. Rev. Biochem.* **64,** 435–461 (1995).
7. Alderden, R. A., Hall, M. D. & Hambley, T. W. The discovery and development of cisplatin. *J. Chem. Educ.* **83,** 728 (2006).
8. Sheehy, J. P., Davis, A. R. & Znosko, B. M. Thermodynamic characterization of naturally occurring RNA tetraloops. *RNA* **16,** 417–429 (2010).
9. Waldsich, C. & Pyle, A. M. A kinetic intermediate that regulates proper folding of a group II intron RNA. *J. Mol. Biol.* **375,** 572–580 (2008).
10. Maria Pechlaner. PhD Thesis. University of Zurich, 2013.
11. Bartova, S., Alberti, E., Sigel, R. K. & Donghi, D. Metal ion binding to an RNA internal loop. *Inorg. Chim. Acta* **452,** 104–110 (2016).
12. Melnikov, S. V., Soll, D., Steitz, T. A. & Polikanov, Y. S. Insights into RNA binding by the anticancer drug cisplatin from the crystal structure of cisplatin-modified ribosome. *Nucleic Acids Res.* **44,** 4978–4987 (2016).
13. Hostetter, A. A., Chapman, E. G. & DeRose, V. J. Rapid cross-linking of an RNA internal loop by the anticancer drug cisplatin. *J. Am. Chem. Soc.* **131,** 9250–9257 (2009).
14. Papsai, P., Aldag, J., Persson Tina, J. & Elmroth, S. K. Kinetic preference for interaction of cisplatin with the G–C-rich wobble basepair region in both $tRNA^{Ala}$ and Mh^{Ala}. *Dalton Trans.*, 3515–3517 (2006).

15. Redon, S. Platinum cross-linking of adenines and guanines on the quadruplex structures of the $AG_3(T_2AG_3)_3$ and $(T_2AG_3)_4$ human telomere sequences in Na^+ and K^+ solutions. *Nucleic Acids Res.* **31,** 1605–1613 (2003).

16. Meroueh, M., Kjellström, J., Mårtensson, K., Elmroth, S. K. & Chow, C. S. Reactions of platinum(II) complexes with a DNA hairpin, d(CGCGTTGTTCGCG):Structural characterization and kinetic studies. *Inorg. Chim. Acta* **297,** 145–155 (2000).

17. Li, Y. & Breaker, R. R. Kinetics of RNA degradation by specific base catalysis of transesterification involving the 2‘-hydroxyl group. *J. Am. Chem. Soc.* **121,** 5364–5372 (1999).

18. Ahmad, S., Isab, A. A. & Ali, S. Structural and mechanistic aspects of platinum anticancer agents. *Transition Met. Chem.* **31,** 1003–1016 (2006).

19. Jerremalm, E., Eksborg, S. & Ehrsson, H. Hydrolysis of oxaliplatin—evaluation of the acid dissociation constant for the oxalato monodentate complex. *J. Pharm. Sci.* **92,** 436–438 (2003).

20. Berners-Price, S. J., Ronconi, L. & Sadler, P. J. Insights into the mechanism of action of platinum anticancer drugs from multinuclear NMR spectroscopy. *Prog. Nucl. Magn. Reson. Spectrosc.* **49,** 65–98 (2006).

21. Alshiekh, A., Clausén, M. & Elmroth, S. K. Kinetics of cisplatin binding to short r(GG) containing miRNA mimics – influence of Na^+ versus K^+ , temperature and hydrophobicity on reactivity. *Dalton Trans.* **44,** 12623–12632 (2015).

22. Polonyi, C., Alshiekh, A., Sarsam, L. A., Clausén, M. & Elmroth, S. K. Cisplatin-induced duplex dissociation of complementary and destabilized short GG-containing duplex RNAs. *Dalton Trans.* **43,** 11941–11949 (2014).

23. Polonyi, C. & Elmroth, S. K. Time dependence of cisplatin-induced duplex dissociation of 15-mer RNAs and mature miR-146a. *Dalton Trans.* **42,** 14959 (2013).

24. Rijal, K. & Chow, C. S. A new role for cisplatin: probing ribosomal RNA structure. *Chem. Commun.*, 107–109 (2009).

25. Dania Marthaler. Master Thesis. University of Zurich, 2012.

26. *Encyclopedia of Life Sciences. Nucleic Acids: Thermal Stability and Denaturation* (John Wiley & Sons, Ltd, Chichester, UK, 2001).

27. Jean-Louis Mergny, Laurent Lacroix. Analysis of thermal melting curves. *Oligonucleotides* **13,** 515–537 (2003).

28. Wu, J. & McLuckey, S. A. Gas-phase fragmentation of oligonucleotide ions. *Int. J. Mass Spectrom.* **237,** 197–241 (2004).

29. Nordhoff, E., Cramer, R., Karas, M., Hillenkamp, F., Kirpekar, F., Kristiansen, K. & Roepstorff, P. Ion stability of nucleic acids in infrared matrix-assisted laser desorption/ionization mass spectrometry. *Nucleic Acids Res.* **21,** 3347–3357 (1993).

30. Alcindor, T. & Beauger, N. Oxaliplatin: a review in the era of molecularly targeted therapy. *Curr. Oncol.* **18,** 18–25 (2011).

31. Raymond, E., Faivre, S., Chaney, S. G., Woynarowski, J. & Cvitkovic, E. Cellular and molecular pharmacology of oxaliplatin. *Mol. Cancer Ther.* **1,** 227–235 (2002).

32. Mehmood, R. K. Review of Cisplatin and oxaliplatin in current immunogenic and monoclonal antibody treatments. *Oncol. Rev.* **8,** 256 (2014).

33. Wang, Z., Wu, M. & Gou, S. Toward a better understanding of the oxaliplatin mode of action upon the steric hindrance of 1,2-diaminocyclohexane and its analogue. *J. Inorg. Biochem.* **157,** 1–7 (2016).

34. Wu, Y., Bhattacharyya, D., King, C. L., Baskerville-Abraham, I., Huh, S.-H., Boysen, G., Swenberg, J. A., Temple, B. R., Campbell, S. L. & Chaney, S. G. Solution structures of a DNA dodecamer duplex with and without a cisplatin 1,2-d(GG) intrastrand cross-link: comparison with the same DNA duplex containing an oxaliplatin 1,2-d(GG) intrastrand cross-link. *Biochemistry* **46,** 6477–6487 (2007).

35. Bhattacharyya, D., Ramachandran, S., Sharma, S., Pathmasiri, W., King, C. L., Baskerville-Abraham, I., Boysen, G., Swenberg, J. A., Campbell, S. L., Dokholyan, N. V. & Chaney, S. G. Flanking bases influence the nature of DNA distortion by platinum 1,2-intrastrand (GG) cross-links. *PLoS One* **6,** e23582 (2011).

36. Snygg, A. S. & Elmroth, S. K. Expanding the chemical nature of siRNAs: oxaliplatin as metalation reagent. *Biochem. Biophys. Res. Commun.* **379,** 186–190 (2009).

37. Jerremalm, E., Wallin, I. & Ehrsson, H. New insights into the biotransformation and pharmacokinetics of oxaliplatin. *J. Pharm. Sci.* **98,** 3879–3885 (2009).

38. Alberto, M. E., Lucas, M. F., Pavelka, M. & Russo, N. The degradation pathways in chloride medium of the third generation anticancer drug oxaliplatin. *J. Phys. Chem. B* **112,** 10765–10768 (2008).

39. Jerremalm, E., Eksborg, S. & Ehrsson, H. Hydrolysis of oxaliplatin-evaluation of the acid dissociation constant for the oxalato monodentate complex. *J. Pharm. Sci.* **92,** 436–438 (2003).

40. Mehta, A. M., Van den Hoven, J M, Rosing, H., Hillebrand, M. J. X., Nuijen, B., Huitema, A. D. R., Beijnen, J. H. & Verwaal, V. J. Stability of oxaliplatin in chloride-containing carrier solutions used in hyperthermic intraperitoneal chemotherapy. *Int. J. Pharm.* **479,** 23–27 (2015).

41. Barril, P. & Nates, S. in *Gel Electrophoresis - Principles and Basics*, edited by S. Magdeldin (InTech2012).

42. Horacek, P. & Drobnik, J. Interaction of cis-dichlorodiammineplatinum (II) with DNA. *Biochim. Biophys. Acta* **254,** 341–347 (1971).

43. Jerremalm, E., Hedeland, M., Wallin, I., Bondesson, U. & Ehrsson, H. Oxaliplatin degradation in the presence of chloride: Identification and cytotoxicity of the monochloro monooxalato complex. *Pharm. Res.* **21,** 891–894 (2004).

44. Küng, A., Strickmann, D. B., Galanski, M. & Keppler, B. K. Comparison of the binding behavior of oxaliplatin, cisplatin and analogues to 5′-GMP in the presence of sulfur-containing molecules by means of capillary electrophoresis and electrospray mass spectrometry. *J. Inorg. Biochem.* **86,** 691–698 (2001).

45. Kozelka, J. Molecular origin of the sequence-dependent kinetics of reactions between cisplatin derivatives and DNA. *Inorg. Chim. Acta* **362,** 651–668 (2009).

46. Hah, S.-S., Sumbad, R. A., de Vere White, Ralph W, Turteltaub, K. W. & Henderson, P. T. Characterization of oxaliplatin-DNA adduct formation in DNA and differentiation of cancer cell drug sensitivity at microdose concentrations. *Chem. Res. Toxicol.* **20,** 1745–1751 (2007).

47. Verstraete, S., Heudi, O., Cailleux, A. & Allain, P. Comparison of the reactivity of oxaliplatin, Pt(diaminocyclohexane)Cl_2 and Pt(diaminocyclohexane^{I})$(OH_2)_2^{2+}$with guanosine and L-methionine. *J. Inorg. Biochem.* **84,** 129–135 (2001).

48. Kim, Y.-S., Shin, S.-M., Cheong, M.-S. & Hah, S.-S. Mechanistic insights into in vitro DNA adduction of oxaliplatin. *Bull. Korean Chem. Soc.* **31,** 2043–2046 (2010).

49. Lucas, M. F., Pavelka, M., Alberto, M. E. & Russo, N. Neutral and acidic hydrolysis reactions of the third generation anticancer drug oxaliplatin. *J. Phys. Chem. B* **113,** 831–838 (2009).

50. Woynarowski, J. M., Faivre, S., Herzig, Maryanne C. S., Arnett, B., Chapman, W. G., Trevino, A. V., Raymond, E., Chaney, S. G., Vaisman, A., Varchenko, M. & Juniewicz, P. E. Oxaliplatin-induced damage of cellular DNA. *Mol. Pharmacol.* **58,** 920–927 (2000).

51. Butcher, S. E. & Pyle, A. M. The molecular interactions that stabilize RNA tertiary structure: RNA motifs, patterns, and networks. *Acc. Chem. Res.* **44,** 1302–1311 (2011).

52. Fiore, J. L. & Nesbitt, D. J. An RNA folding motif: GNRA tetraloop-receptor interactions. *Q. Rev. Biophys.* **46,** 223–264 (2013).

53. Donghi, D., Pechlaner, M., Finazzo, C., Knobloch, B. & Sigel, R. K. The structural stabilization of the κ three-way junction by Mg(II) represents the first step in the folding of a group II intron. *Nucleic Acids Res.* **41,** 2489–2504 (2013).

54. Joyner, J. C., Keuper, K. D. & Cowan, J. A. Analysis of RNA cleavage by MALDI-TOF mass spectrometry. *Nucleic Acids Res.* **41,** 2–11 (2013).

55. Chifotides, H. T., Koomen, J. M., Kang, M., Tichy, S. E., Dunbar, K. R. & Russell, D. H. Binding of DNA purine sites to dirhodium compounds probed by mass spectrometry. *Inorg. Chem.* **43,** 6177–6187 (2004).

56. Chapman, E. G. & DeRose, V. J. Enzymatic processing of platinated RNAs. *J. Am. Chem. Soc.* **132,** 1946–1952 (2010).

57. Thomas, B. & Akoulitchev, A. V. Mass spectrometry of RNA. *Trends Biochem. Sci.* **31,** 173–181 (2006).

58. Limbach, P. A., Crain, P. F. & McCloskey, J. A. Characterization of oligonucleotides and nucleic acids by mass spectrometry. *Curr. Opin. Biotechnol.* **6,** 96–102 (1995).

59. Douthwaite, S. & Kirpekar, F. Identifying modifications in RNA by MALDI Mass spectrometry. *Methods Enzymol.* **425,** 3–20 (2007).

60. Hedman, H. K., Kirpekar, F. & Elmroth, S. K. Platinum interference with siRNA non-seed regions fine-tunes silencing capacity. *J. Am. Chem. Soc.* **133,** 11977–11984 (2011).

61. Dedduwa-Mudalige, G. N. P. & Chow, C. S. Cisplatin targeting of bacterial ribosomal RNA hairpins. *Int. J. Mol. Sci.* **16,** 21392–21409 (2015).

62. Nyakas, A., Eymann, M. & Schurch, S. The influence of Cisplatin on the gas-phase dissociation of oligonucleotides studied by electrospray ionization tandem mass spectrometry. *J. Am. Soc. Mass Spectrom.* **20,** 792–804 (2009).

63. Iannitti-Tito, P., Weimann, A., Wickham, G. & Sheil, M. M. Structural analysis of drug–DNA adducts by tandem mass spectrometry. *Analyst* **125,** 627–634 (2000).

64. Hostetter, A. A., Miranda, M. L., DeRose, V. J. & McFarlane Holman, K. L. Ru binding to RNA following treatment with the antimetastatic prodrug NAMI-A in Saccharomyces cerevisiae and in vitro. *J. Biol. Inorg. Chem.* **16,** 1177–1185 (2011).

65. McLuckey, S. A., Berker, Gary J. Van & Glish, G. L. Tandem mass spectrometry of small, multiply charged oligonucleotides. *J. Am. Soc. Mass Spectrom.* **3,** 60–70 (1992).

66. Azarani, A. RNA analysis by ion-pair reversed-phase high performance liquid chromatography. *Nucleic Acids Res.* **29,** 7e–7 (2001).

67. Cramer, H., Finn, K. & Girindus, E. in *Handbook of Analysis of Oligonucleotides and Related Products,* edited by G. Srivatsa (CRC Press2011), pp. 1–46.

68. Spingler, B., Whittington, D. A. & Lippard, S. J. 2.4 Å Crystal structure of an oxaliplatin 1,2-d(GpG) intrastrand cross-link in a DNA dodecamer duplex. *Inorg. Chem.* **40,** 5596–5602 (2001).

69. Kjellström, J. & Elmroth, S. K. Similar rates for platination of hairpin loops and single-stranded DNA. *Dalton Trans.*, 2867–2871 (2003).

70. Waghmare, S. P., Pousinis, P., Hornby, D. P. & Dickman, M. J. Studying the mechanism of RNA separations using RNA chromatography and its application in the analysis of ribosomal RNA and RNA:RNA interactions. *J. Chromatogr. A* **1216,** 1377–1382 (2009).

71. Bonilla, J. V. & Srivatsa, S. *Handbook of analysis of oligonucleotides and related products* (CRC Press, Boca Raton, FL, 2011).

3 Screening of platination reactions with the use of time evolution NMR experiments, PAGE and plasmid binding assays

3.1 Aim

The main topic of this chapter is the use of time evolution NMR experiments as a way to directly monitoring the platination reactions, which will provide us with a first indication of the possible platination sites. In chapter 2 the experimental conditions that allowed to obtain homogeneous monoplatinated species (Paragraph 2.5) by reacting D1-27 with oxaliplatin were described. We here followed the same platination reactions directly into the NMR tube. The effect of changing platinum concentration was also investigated. Towards this direction, time evolution ^{1}H-NMR experiments were used to study the interaction of oxaliplatin with different RNA constructs, namely an RNA construct without the internal loop (RNA 26), an RNA construct with a different tetraloop (D1-27$_{GAAA}$) and dephosphorylated D1-27 (deph-D1-27). The behaviour of different platination agents, namely oxaliplatin, cisplatin and kiteplatin, towards D1-27, was compared via both NMR experiments and gel mobility shift assays. Finally, gel mobility shift assays were also used to obtain information about the role of Cl^{-} and K(I) ions in the platination reactions. Further comparison of the behaviour of these three platinum complexes took place by screening of their reaction kinetics with DNA plasmids using plasmid binding assays.

3.2 Introduction

A quick and easy way to detect RNA-platinum(II) interactions is to record time evolution NMR experiments and to follow the changes induced in the imino proton region upon platinum(II) addition. Figure 3.1 shows the four common RNA nucleobases with the imino protons NH1 of guanine (G) and NH3 of uracil (U) indicated in red. Adenine (A) and cytidine (C) do not have imino protons. In free bases the imino protons are in fast exchange with the solvent and can therefore not be detected by NMR under normal ambient conditions. However, when these protons are involved in stable hydrogen bonding the exchange rate slows down and the resonances can be observed in the ^{1}H chemical shift range of 10 - 15 ppm[1].

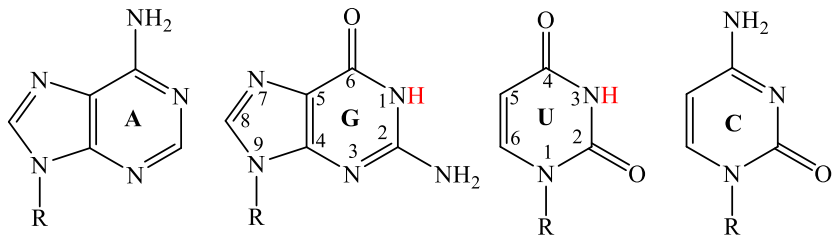

Figure 3.1: *Structure of the four common bases of RNA, with imino protons in red. Numbering is indicated only for guanine and uracil.*

In folded RNAs stable hydrogen bonds are typically found in double helical regions due to canonical base pairing (Figure 3.2, top). However, also loop or bulge regions can have an extensive hydrogen bonding network mainly caused by non-canonical base pairing[1,2]. Consequently, changes in chemical shifts and /or intensity of imino resonances upon addition of the platinum reagent can be indicative for platination or platinum-induced structural changes[3,4]. Unfortunately, it is very hard and often even not possible to distinguish between direct platination and structural changes induced by close-by platination using 1D ^{1}H-NMR experiments. Another drawback of this method is that the imino proton resonances are also easily affected by changes in temperature or pH[1,2]. However, despite these drawbacks, looking at the changes of the imino proton resonances is a good qualitative method to identify regions affected by interaction with small molecules[5] and/ or by platination. In our case, the combination of these data with complementary approaches allowed the identification of the platination site(s) (Chapter 4).

In Figure 3.2 the ^{1}H-NMR imino proton region of D1-27 is depicted at 4 °C (top, red line) and 25 °C (bottom, blue line) and all imino proton assignments are indicated[6]. For the imino proton resonances of the nucleobases found in stable base-pairing like U10, U24, G18, G8. G1, G16 and G2 strong peaks are observed between 12 and 15 ppm while the imino proton resonances of the nucleobases involved in the G-U wobble and -UUCG- tetraloop (U5, G23, U12) were found in the 9 - 12 ppm range. In general, lowering the temperature leads to stronger hydrogen bonding and accordingly to a decrease of the imino proton exchange rate. Therefore, the resonances at 4 °C have slightly increased overall intensities compared to 25 °C. The low intensity of G1NH1 at 25 °C is due to weak hydrogen bond close to 5′-end[7]. Similar behaviour was observed also for G23NH1, U5NH3 (G-U wobble) and U12NH3 (terminal -UUCG- loop) due to their location in non-Watson-Crick regions, and therefore they will not be commented during the description of the time evolution NMR experiments. As the optimal platination reaction temperature was found to be 25 °C (Chapter 2, Paragraph 2.4.4) all time evolution NMR experiments were recorded at this temperature.

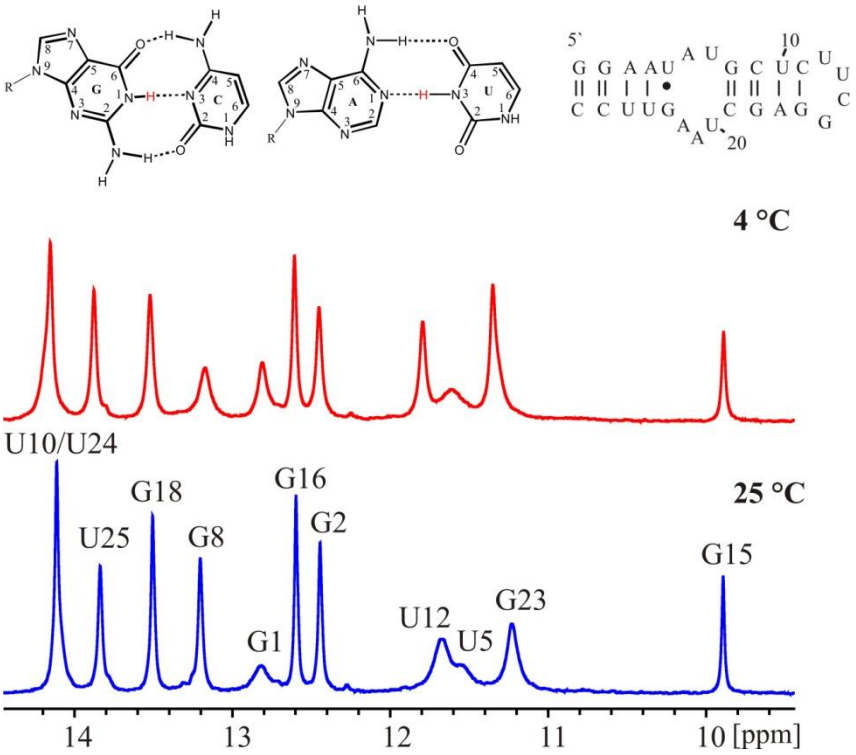

Figure 3.2: *Stack plot of the imino proton region of ^{1}H-NMR spectra of D1-27 at 25 °C (blue line) and 4 °C (red line). Top left: Canonical base-pairing between G-C and U-A, Top right: Secondary structure of D1-27. (120 mM KCl, pH 6, 600 MHz)*

3.3 Time evolution NMR experiments: Oxaliplatin

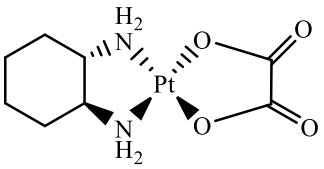

OxaliPt (chemical structure on the right) was found to be the most appropriate platination agent for this study (Chapter 2, Paragraph 2.5) and therefore time evolution NMR experiments were performed to follow its platination reaction in the attempt to identify which nucleobases are affected upon platination. For these experiments, the experimental conditions used were the ones, which were found to favour the maximum platination yield, with the minimum amount of diplatinated RNA, i.e. 5 eq of oxaliplatin, 0.25 mM RNA, 1 day of incubation at 25 °C in the presence of 120 mM KCl (Chapter 5, Paragraph 5.9). However, for the time evolution NMR experiments lower RNA concentration was used. 0.1 mM RNA results in the formation of the same platination adducts like 0.25 mM and therefore it was the concentration used for all the time evolution NMR experiments. After studying the behaviour of D1-27 in the presence of 5 eq of oxaliplatin, its reaction with different amount of platinum(II) complex was also briefly investigated. Then, several RNA constructs (Chapter 1, Paragraph 1.1.4) were employed in order to study the influence of different structural features on the platinum binding sites. At the end, the platination of deph-D1-27 was followed in order to investigate

the role of the 5′-end triphosphate group in platinum binding specificity. For all these last reactions, 5 eq of oxaliplatin were used and the experimental procedure is described in chapter 5 (Paragraph 5.9).

3.3.1 Investigation of platinum(II) binding sites for the platination of D1-27 with oxaliplatin

All the reactants were mixed in an NMR tube according to the experimental conditions mentioned above. 1D ^{1}H-NMR spectra, focusing on the imino proton region, were recorded before and after the addition of oxaliPt every 1 hour for 22 hours (Figure 3.3). The first spectrum (Figure 3.3, blue line) corresponds to D1-27 prior the addition of oxaliPt. The overall pattern of the imino proton region after 22 h of reaction was very similar to the one of the non-platinated sample, but for changes in intensity for some peaks. Interestingly, no chemical shift changes were observed (Figure 3.3). To evaluate more easily the changes induced upon platination a plot of the percentage of the intensity of each resonance over time is shown in Figure 3.3 and the percentage of the intensity decrease for each peak is given in Table 3.1. The imino proton resonances of G2, G8 and U25 seem to be the most affected by platination. Indeed, after 10 h, their intensity was already significantly decreased, and at the end of the reaction (after 22 h) it was reduced by around one half (Figure 3.3, green and red dotted frames, Table 3.1). Interestingly, a new peak appeared close to the resonance of G8 (Figure 3.3, green dotted frame). Significant intensity reduction was observed also for U10/U24 (Figure 3.3) but given their resonance overlap no safe conclusion could be done and they will generally not be considered for the discussion. The imino proton resonances of G16 and G18 were only moderately affected while the lowest decrease of intensity was observed for the G15 imino proton resonance (Figure 3.3, black dotted frame, Table 3.1).

Table 3.1: *The percentage of the intensity decrease of the imino proton resonances at the end of the time evolution NMR experiment for the platination reaction of D1-27 with 5 eq of oxaliPt.*

Resonance	Intensity decrease (%)
U25	59.9
G2	58.8
G8	54.6
G18	21.3
G16	19.7
G15	10.3
U10/U24	41.5

G2 and U25 are found in the first helical part of D1-27 while G8 is located in the beginning of the second one and is very close to the internal loop (Figure 3.3, top, right). Since guanines are possible platination targets, considering the significant decrease of the intensity of the imino proton resonances of G2 and G8, they could represent possible platination sites. On the other hand, the changes of the imino proton resonance of U25 could be linked to local structural distortions provoked by close-by platination. Taking into consideration that the most abundant Pt(II)-RNA/DNA adducts observed are the 1,2-GG[8], if platination occurred at G2, G1 would be most likely also involved in platination. Unfortunately the G1 imino proton resonance is very weak at this temperature[7] therefore it was not possible to obtain any information about its behaviour in these conditions. In the case of G8 the possible platination patterns

could be either G8-G18 or G8-G23 interstrand cross-links. However, the first scenario is excluded by the fact that G18NH1 is only moderately affected by platination. The second is also not very probable, first due to the large distance between the two nucleobases and second due to the presence of the stacked adenines in the internal loop (Chapter 1, Paragraph 1.1.4) which most probably prohibits the formation of a cross-link. However, monodentate interaction at G8 could not be excluded based on these data only, and further data will be needed to exclude direct G8 platination (Chapter 4). The intensity of G15 was almost stable over time suggesting that the terminal loop remained unaffected upon platination (Figure 3.3, black dotted frame).

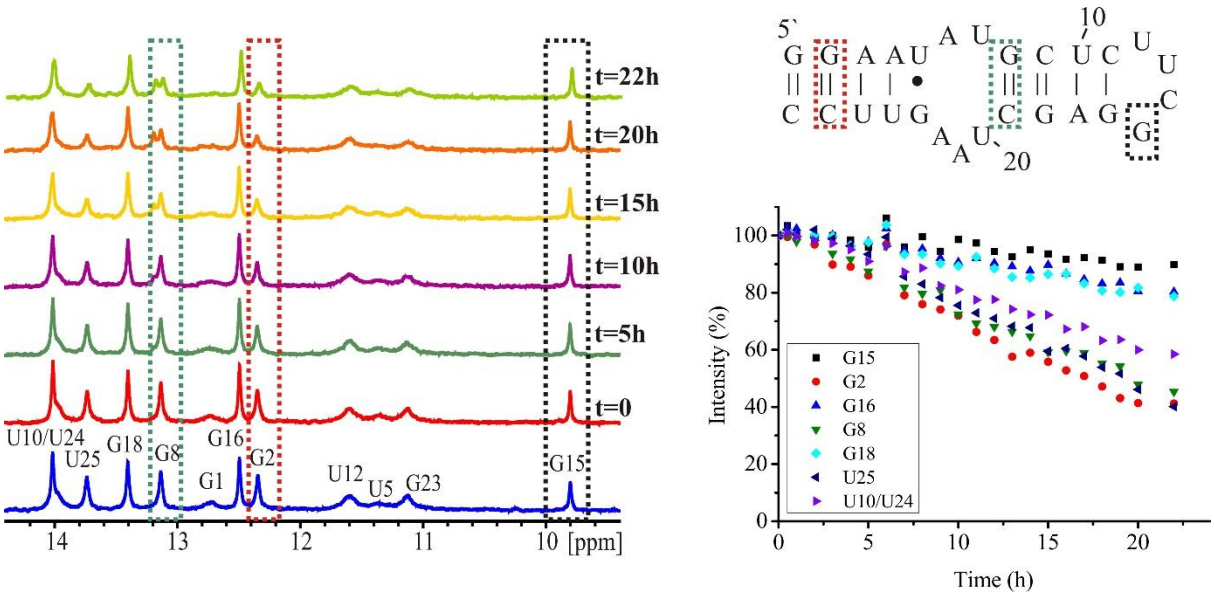

Figure 3.3: *Time evolution ^{1}H-NMR experiments for the platination of D1-27 with oxaliPt (left panel). Right Top: Secondary structure of D1-27, Right Bottom: Plot of the percentage of the intensity of the imino proton resonances over time. (5 eq of oxaliPt, 0.1 mM RNA, 25 °C, 120 mM KCl, pH 6, 600 MHz)*

The same experiment was performed using 1 eq and 20 eq of oxaliPt (Figure 3.4). Only little changes are observed in the spectra using 1 eq of oxaliPt, with only a slight decrease for the imino proton resonances of G2, G8 and U25, in line with the results commented above (Figure 3.3, green and red dotted frames). Using 20 eq of oxaliPt, the imino proton resonances of G2, G8 and U25 almost disappear within the first 10 h suggesting preferential interaction at these sites, but afterwards all resonances exhibited a strong broadening indicating that non-specific, generalized interaction took place (Figure 3.4, right panel, green and red dotted frames). Because of the high platinum(II) excess the reaction proceeded faster and after the preferential binding sites were occupied, within the first 10 h, platination also took place in all possible sites. This led to a strong overall decrease of the intensity or complete disappearance of the imino proton resonances in the spectrum, likely indicating the presence of multiplatinated species (Figure 3.4, right panel). The latter was also confirmed by running small scale platination in the presence of 1, 5 and 10 eq of oxaliplatin (Chapter 2, Paragraph 2.4.1),

using the same experimental conditions used here. Gels run on the platination mixtures showed that, with increasing platinum(II) concentration, the gel bands moved from non-defined / non-separated to the formation of a well-defined and better separated gel band which contained mostly monoplatinated RNA. At 10 eq of oxaliplatin the band corresponding to unreacted RNA was reduced in intensity, indicating faster platination rates while the new well-defined new band formed (upper) contained higher amount of diplatinated RNA species (Chapter 2, Paragraph 2.4.1, Figures 2.16 - 2.17).

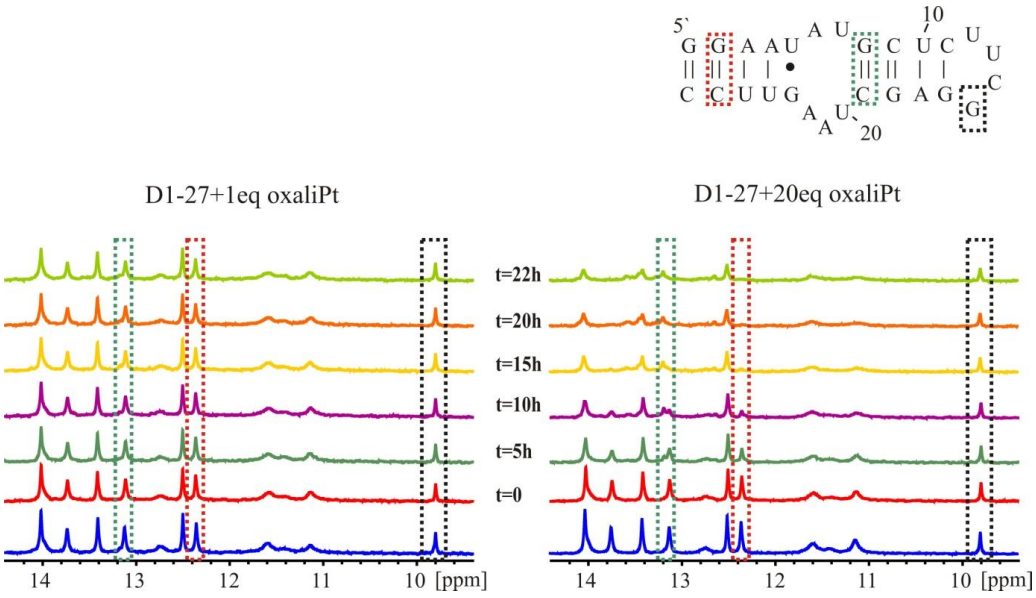

Figure 3.4: *Comparison of the time evolution NMR experiments for the platination of D1-27 with 1 eq and 20 eq of oxaliPt. Right Top: Secondary structure of D1-27. In the dotted frames are the resonances, which are commented in the text. (1 eq and 20 eq of oxaliPt, 0.1 mM RNA, 25 °C, 120 mM KCl, pH 6, 600 MHz)*

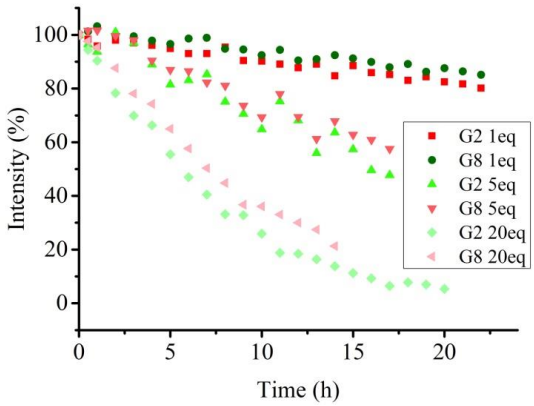

Figure 3.5: *Plot of the percentage of the intensity of G2 and G8 imino proton resonances over time for 1 eq, 5 eq and 20 eq of oxaliPt.*

Figure 3.5 shows the decrease of the intensity percentage of the imino proton resonances of G2 and G8 in the three cases. As expected, concentration dependency of the reaction is observed, with faster platination in the presence of higher amount of oxaliplatin. Moreover, very interestingly, in all the three cases, G2 and G8 behave very similarly to each other. This may be due to contemporary platination of G2 and G8, without preferential binding, or to the fact that platination at only one binding site affects also the other nucleotide. This second hypothesis will be confirmed by combining these data with data obtained by NMR and different analytic techniques collected on isolated monoplatinated samples (Chapter 4).

Summing up, the time evolution NMR experiment for the platination reaction of oxaliPt with D1-27 using the reaction conditions found for oxaliPt (Chapter 2, Paragraph 2.4.4) revealed that G2 and G8 imino proton resonances were the most affected ones, suggesting interaction at these sites. All other resonances, especially the ones of the -UUCG- tetraloop did not show significant changes upon platination. Only in the presence of 20 eq of oxaliPt a substantial overall broadening of all resonances was observed suggesting non-specific interaction.

3.3.2 Influence of the terminal tetraloop on platination (-UUCG- *vs* -GAAA- tetraloop)

Upon platination of D1-27, the imino proton resonance of G15 in the -UUCG- tetraloop remained mostly unaffected but this could be expected taking into consideration the high stability (more compact structure) of this tetraloop[9]. To investigate whether this behaviour was related to this specific tetraloop, the -UUCG- was replaced for a -GAAA- one. The new RNA used was named D1-27$_{GAAA}$ (Figure 3.6, right panel, top). The -GAAA- tetraloop belongs to the group of GNRAs (N=any nucleotide, R=purines) tetraloops, which are the most abundant tetraloop sequences in some catalytic RNAs as well as in rRNAs[10]. The -GAAA- tetraloop is thermodynamically less stable and can accommodate more substitutions compared to the -UUCG- one. Additionally this tetraloop often makes long-range interactions to other RNA structural elements, with the most famous being the tetraloop receptors[10] (Paragraph 1.1.4).

Before running the platination reaction, its 1D ^{1}H-NMR spectrum was assigned. Upon replacement of the -UUCG- for a -GAAA- tetraloop, changes were expected for G16NH1 resonance, the imino proton resonance of G15 should not be present anymore and a new peak for G12 from the -GAAA- tetraloop, should appear. Indeed, as shown in Figure 3.6, a new peak appeared at 10.5 ppm corresponding to G12NH1, while G16NH1 was upfield shifted with respect to the spectrum of D1-27. All the other resonances remained the same. The assignment was confirmed by a [^{1}H,^{1}H]-NOESY recorded at 4 °C.

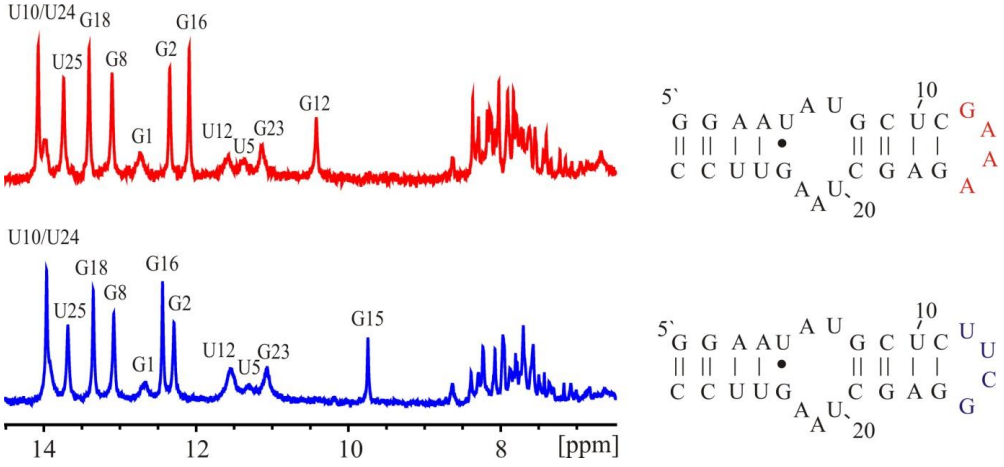

Figure 3.6: *Left panel: Comparison of the imino proton region of ^{1}H-NMR spectra of D1-27 (bottom) and D1-27$_{GAAA}$ (top). Right panel: Secondary structure of D1-27 (bottom) and D1-27$_{GAAA}$ (top).*

The D1-27$_{GAAA}$ construct was platinated with oxaliPt under the same experimental conditions as above (Chapter 2, Paragraph 2.4.4) and the reaction was followed by time evolution ^{1}H-NMR experiments (Figure 3.7). Similar to the previous experiment, upon platination of D1-27$_{GAAA}$ the imino proton resonances of G2, G8 (Figure 3.7, green and red dotted frames) and U25 showed the largest decrease in intensity (Figure 3.7, Table 3.2). The imino proton resonance of G12, which is located at the terminal loop, was the next mostly affected resonance (Figure 3.7, black dotted frame) followed by the imino proton resonances of G16 and G18. Changes at the G12 site suggests that the -GAAA- tetraloop region was affected upon platination. Moreover, G16, which in the previous case remained almost unchanged, showed a significant decrease in intensity (Table 3.2).

***Table 3.2**: The percentage of the intensity decrease of the imino proton resonances at the end of the time evolution NMR experiment for the platination reaction of D1-27$_{GAAA}$ with 5 eq of oxaliPt.*

Resonance	Intensity decrease (%)
G2	61.1
G8	56
U25	60.4
G12	47.8
G16	39.5
G18	31
U10	34.3
U24	11.6

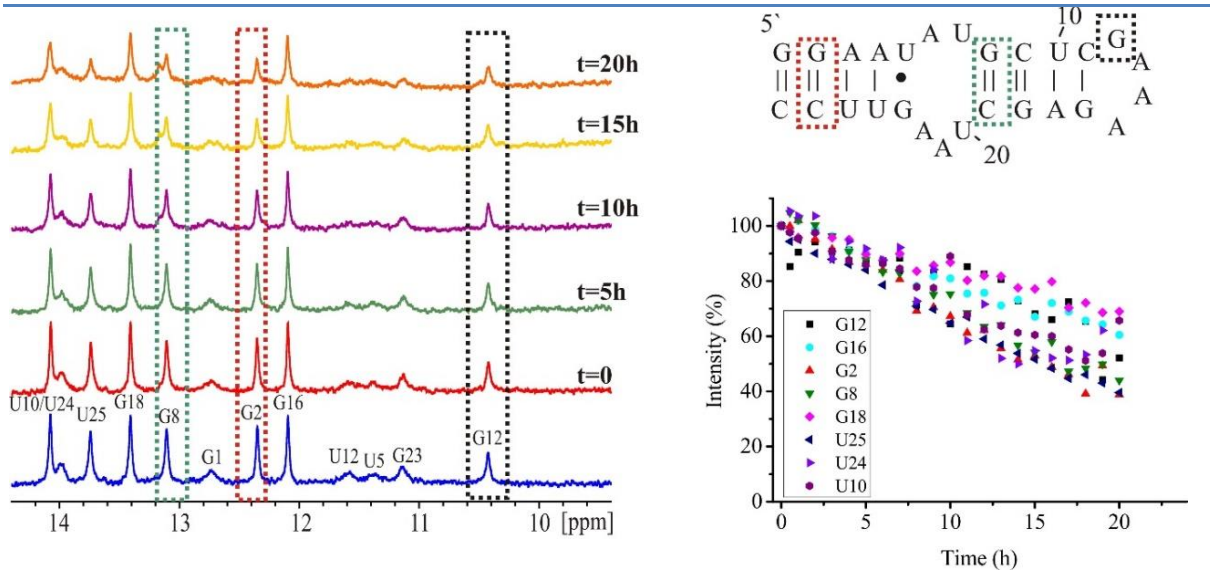

Figure 3.7: *Time evolution 1H-NMR experiment for the platination of D1-27$_{GAAA}$ with oxaliPt (left). Right Top: Secondary structure of D1-27$_{GAAA}$, Right Bottom: Plot of the percentage of the intensity of the imino proton resonances over time. (5 eq of oxaliPt, 0.1 mM RNA, 25 °C, 120 mM KCl, pH 6, 600 MHz)*

The replacement of the very stable -UUCG- tetraloop for a less stable one (-GAAA-)9 resulted in changes at the tetraloop region (G12) and in the neighbouring guanine (G16) suggesting that this area became more susceptible to platination. In addition to the high degree of compaction, resulting in great stability, the absence of platination at G15-G16 observed in the presence of the -UUCG- tetraloop may be due to the relative orientation of the two guanines (Figure 3.8). From the comparison of the NMR solution structures of the two tetraloops, as shown in Figure 3.8, it can be seen that in the case of the-UUCG- tetraloop the N7 atoms of G15 and G16 (which represent possible platination sites) are pointing at different directions making difficult the formation of intrastrand crosslink while in the-GAAA- loop the N7 of the G12 is more exposed.

In conclusion, the replacement of the -UUCG- tetraloop for the -GAAA- one resulted in similar behaviour concerning the changes of the imino proton resonances of the first part of the RNA construct, but upon tetraloop replacement, the -GAAA- region was more affected upon platination.

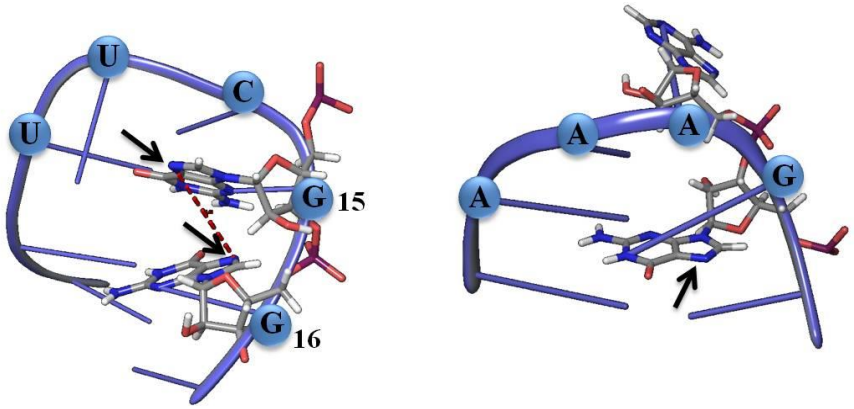

***Figure 3.8**: NMR solution structures of the -UUCG- tetraloop[6] (left) and -GAAA- tetraloop[11] (right). The N7 atoms are indicated with a black arrow. The pictures were prepared with Maestro Schrödinger Version 10.5.014 using PDB file 2LUO for the -GAAA- tetraloop.*

3.3.3 Influence of the internal loop on platination (D1-27 *vs* RNA 26)

All time evolution experiments commented until now showed that the imino proton resonances of G2, G8 and U25 were always the ones mostly affected. G2 represents a feasible platination site because of several reasons. First, it is located at the 5′-end which is a flexible region[12]; second, the presence of the adjacent G1 offers the possibility to form intrastrand platinum cross-link; finally, due to the presence of the triphosphate group, the interaction could be favoured by electrostatic attraction. Contrarily, G8 is located very close to the internal loop and formation of bidentate species would require the formation of interstrand cross linked adducts. A possible scenario for the significant changes observed at this site could be that platination at the first part of D1-27 causes distortions which, due to the presence of the internal loop, could influence the base-pairing at the G8 site. In order to investigate whether the presence of the loop plays a role in the observed behaviour, another RNA construct was used which is the analogue of the D1-27 without an internal loop (RNA 26) (Figure 3.9, right panel, top).

The time evolution NMR experiments on RNA 26 were performed using the same experimental conditions used for D1-27. The assignment of the imino proton resonances was performed by comparison of the imino proton resonances of D1-27, and confirmed by [^{1}H,^{1}H]-NOESY experiments run at 4 °C and 10 °C. After 22 h of interaction most of the imino proton resonances were affected and several new peaks appeared. The behaviour observed here refers to the whole platination mixture, and the assignment of new peaks would require an isolated homogeneously platinated sample. Isolation of a homogeneously platinated sample was not possible in the case of RNA 26 because the platinated RNA sample was migrating together with the unreacted RNA (Chapter 2, Paragraph 2.6, Figure 2.29). Moreover, after *in vitro* transcription of this construct, it seemed that a heterogeneous sample was obtained which consisted of a mixture of the full length RNA 26 together with a shorter RNA species, missing the first nucleotide. The heterogeneity of the starting RNA did not allow any further study of this RNA, and only the changes of the G8 imino proton resonance in the ^{1}H-NMR time evolution experiments will be commented. Interestingly, despite the several changes observed, the imino proton resonance of G8 remained unaffected compared to the rest (Figure 3.9, blue dotted frame).This resonance in the case of D1-27 showed similar behaviour to G2 resonance, which could possibly be the platination site (Figure 3.3). In the absence of the internal loop this behaviour was not observed. In Figure 3.9 (right panel, bottom), it is clearly illustrated the different behaviour of the imino proton resonance of G8 in the presence (D1-27) and in the absence (RNA 26) of the internal loop. A possible explanation for this could be the following. Internal loops are common RNA structural motifs, which consist of unpaired nucleotides on both strands and which are more destabilized compared to normal Watson-Crick base paired double helical structures. Also, it is known that when platination takes place local distortion is observed which can affect 4-5 nucleobases away[13]. Combining these two information, it could be very probable that the changes observed at the G8 site are due to the presence of the internal loop, which allows the local structural changes induced from platination at, e.g., G2 to influence the base-pairing at the G8 site. The fact that the imino proton resonance of G8 remains unaffected during platination of RNA 26 supports this scenario.

Summing up, the data commented above suggest platination at G2 in the case of D1-27 and suggest that the changes of the imino proton resonance of G8 may be the effect of structural rearrangement rather than the result of direct platination. The characterization of the isolated platinated D1-27 further confirms these findings (Chapter 4). The same experiment was performed using 5′-end dephosphorylated RNA 26 (deph-RNA 26) and the results obtained for the behaviour of G8 imino proton resonance were identical (Appendix 2, Figure A 2.1).

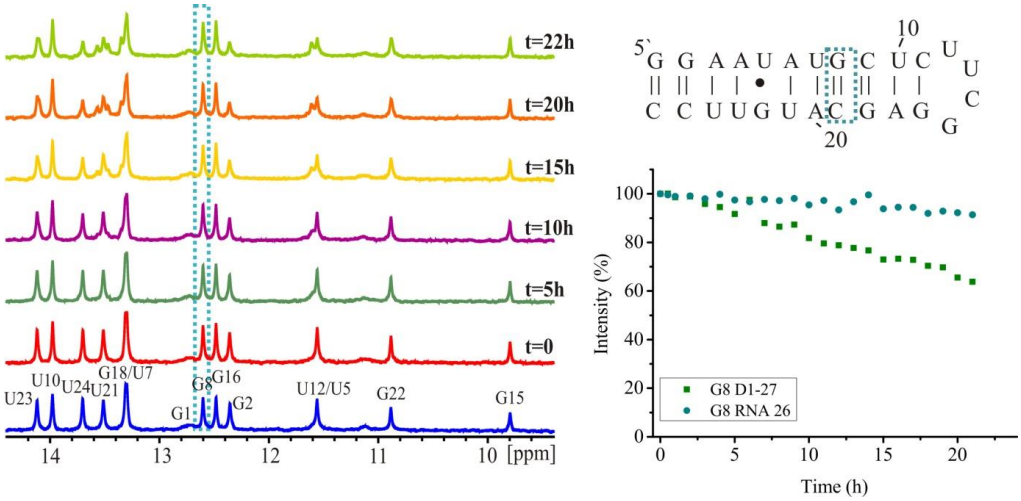

Figure 3.9: *Time evolution NMR experiment for the platination of RNA 26 with oxaliPt (left). Right Top: Secondary structure of RNA 26, Right Bottom: Plot of the intensity of the imino proton resonances over time for the comparison of the G8 behaviour in D1-27 and RNA 26. (5 eq of oxaliPt, 0.1 mM RNA, 25 °C, 120 mM KCl, pH 6, 600 MHz)*

3.3.4 The role of the 5′-triphosphate group on platination

In order to perform platination reactions starting from a homogeneous starting material, deph-RNA was used instead of triph-RNA (Chapter 2, Paragraph 2.9). The platination reactions of deph-D1-27 with oxaliPt were performed using the experimental conditions previously optimized using triph-D1-27. Interestingly, instead of the appearance of only one new slower migrating band (upper), as it was observed from the platination of triph-D1-27, another new faster migrating band appeared (Chapter 2, Paragraph 2.9, Figure 2.44). To get a first insight into this different behaviour time evolution NMR experiments were performed. The ^{1}H-NMR spectra of the two RNA constructs (with and without phosphate group) are very similar (Figure 3.10). The only difference observed is that the imino proton resonance of G1 is shifted upfield upon dephosphorylation, which could be related to the absence of the triphosphate group.

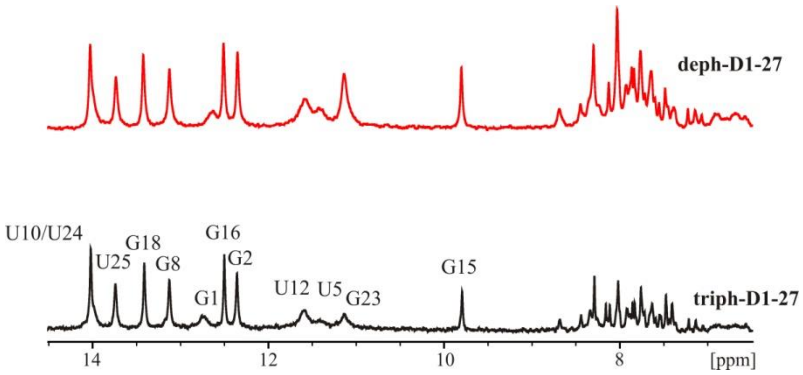

Figure 3.10: *^{1}H-NMR spectra, (imino proton and aromatic region), including labelling of the imino proton resonances, of triph-D1-27 (black line) and deph-D1-27 (red line). The spectra were recorded at 25 °C, in the presence of 120 mM $KClO_4$, pH 6, 600 MHz.*

The time evolution NMR experiment was performed under the same experimental conditions as mentioned above. From the stack plot and the plot of the intensity decrease of the imino proton resonances over time for all the nucleobases (Figure 3.11, Table 3.3) it is again evident that G2, G8 (green and red frame) and U25 are the ones which are mostly affected by platination. Indeed, the intensity of their imino proton resonances is reduced by almost 50 %, while less affected, but in a similar manner, are the imino proton resonances of G15, G16 and G18.

Table 3.3: *The percentage of the intensity decrease of the imino proton resonances at the end of the time evolution NMR experiment for the platination reaction of deph-D1-27 with 5 eq of oxaliPt.*

Resonance	Intensity decrease (%)
G2	49.5
G8	49.1
U25	45.8
G15	15.1
G18	13.1
G16	11.9
U10/U24	40.3

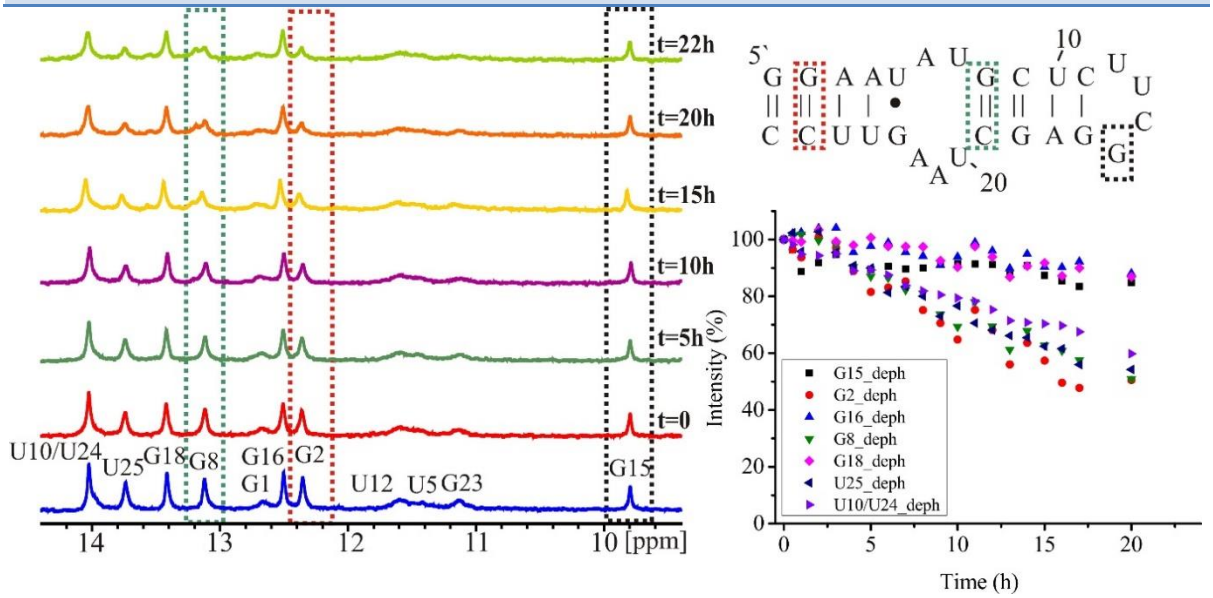

Figure 3.11: *Time evolution NMR experiment for the platination of deph-D1-27 with oxaliPt (left). Right Top: Secondary structure of D1-27, Right Bottom: Plot of the percentage of the intensity of the imino proton resonances over time. (5 eq of oxaliPt, 0.1 mM RNA, 25 °C, 120 mM KCl, pH 6, 600 MHz)*

To understand the different behaviour observed in the gels performed using deph-RNA, the intensity decrease found during its time evolution NMR experiment was compared with the corresponding values obtained from the platination reaction using triph-D1-27 (Table 3.4). The imino proton resonances of G2, G8 and U25 are in both cases the most affected but for deph-D1-27 their intensities are decreased to a smaller extend. A possible explanation for this could be that upon removal of the negatively charged triphosphate group from the 5′-end, a possible interaction at the G2 site could still took place but not as fast as before thus reducing the intensity decrease of the corresponding imino proton signals. U25 that is close-by and G8 which probably is not directly platinated as discussed in the previous paragraph were also analogously affected. Upon RNA dephosphorylation the G15 imino proton resonance seems to be a bit more affected (Table 3.4) without though its intensity decrease being very important suggesting that the region of the -UUCG- terminal loop is not significantly influenced from platination, in line with previous observations.

Table 3.4: *Comparison of the percentage of the intensity decrease of the imino proton resonances at the end of the time evolution NMR experiment for the platination reaction of triph-D1-27 and deph-D1-27 with 5 eq of oxaliPt.*

Resonance	Intensity decrease (%) triph-D1-27	Intensity decrease (%) deph-D1-27
G2	58.8	49.5
G8	54.6	49.1
U25	59.9	45.8
G15	10.3	15.1
G18	21.3	13.1
G16	19.7	11.9
U10/U24	41.5	40.3

In conclusion, the platination of deph-D1-27 with oxaliPt resulted in significant changes at the same nucleobases as when triph-D1-27 was used (G2, G8 and U25) while the resonances at the terminal loop remained almost unaffected. The differences of the intensity decrease observed may be connected with the removal of the negatively charged triphosphate from the 5′-end which resulted in still preferable interaction at the 5′-end region (probably at G2) but not with the same specificity as before. The reduced specificity at the first part of the RNA could probably lead to the formation of other less preferable species which are the ones forming the new faster migrating gel band appeared upon platination of deph-D1-27.

3.4 Conclusions from the investigation of the interaction between oxaliplatin and D1-27

OxaliPt is the platination agent that is chosen for this study and its interaction with D1-27 was screened using time evolution NMR experiments. With this approach, we were aiming at finding which could be the nucleobases, which were affected upon platination monitoring the changes induced during the platination reaction at the imino proton resonances. In addition to that, the influence of various structural features on platination as well as the role of the phosphate group at the 5′-end were investigated. In all experiments G2, G8 and U25 imino proton resonances were the ones strongly affected. Using an RNA without the internal loop (RNA 26), G8 was excluded as directly platinated site and the changes observed were attributed to structural rearrangements caused by platination close-by, which due to the presence of the loop affected the G8 resonance as well. Uracils do not represent a platination site and therefore U25 is not expected to be platinated, suggesting that the G2 site could be the one that is directly platinated. Considering that the 1,2-GG are the most commonly found platinated adducts, in our case the platination could take place at the G1-G2 site. As mentioned also before, at the temperature that the experiments were performed the resonance of G1 is hardly visible (Figure 3.2). To see if there are changes at the G1 site upon platination, the imino proton spectra of D1-27 before platinum(II) addition and after 22 h of reaction were recorded at 4 °C at which the imino proton resonance of G1 is more pronounced (Figure 3.12). Indeed, the imino proton resonance of G1 at the end of the reaction (Figure 3.12, red line, purple frame) was significantly broadened and reduced in intensity, which could be attributed to platination at this site. Factors which could enhance the platination at the G1-G2 site are the presence of the triphosphate, which being negatively charged attracts the positively charged platinum(II) complex, and the fact that the 5′-end of the construct is flanking[12], thus making this area more flexible and therefore easier for the platinum(II) complex to bind.

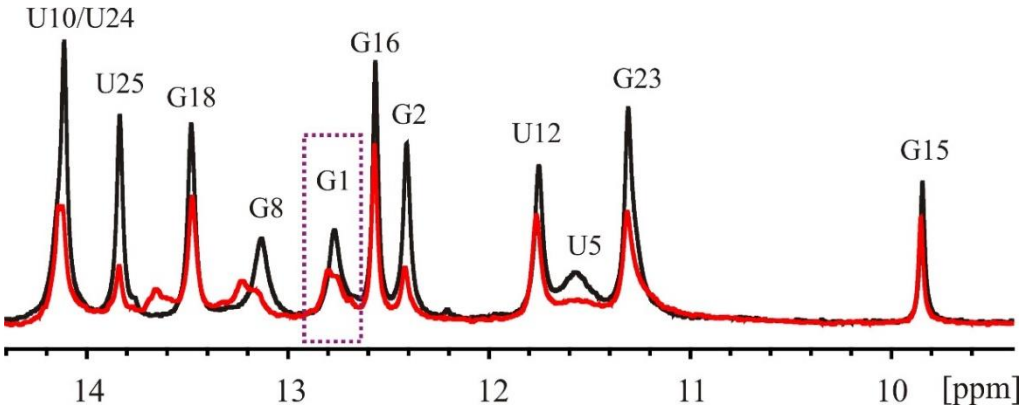

Figure 3.12: *Comparison of the imino proton region of ^{1}H-NMR spectra of unreacted D1-27 (black line) and D1-27 after 22 h of reaction (red line) at 4 °C. (5 eq of oxaliPt, 0.1 mM RNA, 25 °C, 120 mM KCl, pH 6, 600 MHz)*

From the platination of D1-27 it was also found that the area of the -UUCG- terminal loop remained mostly unaffected which, as discussed above, could be the result of the stability of this tetraloop and/ or could be due to the orientation of the N7 atoms of the possible platination sites (G15, G16) (Figure 3.8). Its replacement with another less stable tetraloop (-GAAA-) indeed changed the accessibility of the region with both G12 (which is part of the loop) and G16 (which is very close to the tetraloop) being more affected than before. In the end the removal of the triphosphate group from the 5′-end led to similar changes like when triph-RNA was used with the difference that the changes in intensity of the imino proton resonances of G2, G8 and U25 was less pronounced. Despite the removal of the negatively charged phosphate group platination was again taking place at the 5′-end region but with less specificity compared to when it was present.

From these experiments, we are suggesting that the possible platination site could be G1-G2. However, in order to confirm this isolation of the pure monoplatinated sample is necessary considering that the picture of the time evolution NMR experiments corresponds to the whole platination reaction mixture. The characterization of the platinated RNA species isolated from the upper gel band is described in chapter 4.

3.5 Time evolution NMR experiments: Monoaquated cisplatin

The choice of oxaliPt over monoaquated cisPt (chemical structure on the right) as possible platination agent was done based on its more specific RNA binding (Chapter 2, Paragraph 2.4.4). This was concluded from the appearance of a new band on the gel, which in the case of oxaliPt was well-defined and compact while for monoaquated cisPt it was more smeary and less compact, suggesting formation of various similarly platinated RNA species. Applying the same experimental reaction conditions (best conditions for oxaliPt) the gel obtained showed a clear second band for oxaliPt and a dispersed smear for the monoaquated cisPt. This is suggesting that under the same conditions the monoaquated cisPt was reacting faster and less specific forming various platinated species (Chapter 2, Figure 2.27). To further confirm this behaviour, time evolution NMR experiments were performed using the experimental conditions found for oxaliPt.

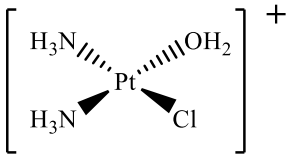

3.5.1 Time evolution NMR experiments of the platination reaction of D1-27 with monoaquated cisPt and comparison with oxaliPt

The platination reaction of D1-27 with monoaquated cisPt was followed with time evolution NMR experiments using the same experimental conditions used for oxaliPt. Under these conditions as it can be seen in Figure 3.13, the platination reaction evolved very fast. Already after platinum(II) addition (Figure 3.13, red line) most of the imino proton resonances were strongly affected (broader and decreased in intensity). After 22 h of reaction G2, G8 and U25 imino proton resonances disappeared

while strong decrease in intensity was observed also for the G18 resonance. The intensity of G15 and G16 resonances decreased but they were less affected compared to the rest. The least affected area of the terminal loop (G15, G16) is a common characteristic between the platination reaction of oxaliPt and monoaquated cisPt. However, the reaction of cisPt evolved much faster and less specific as it can be seen from the reduced intensity of the majority of the resonances already immediately after addition of cisPt (Figure 3.13, red line). Under the same experimental conditions oxaliPt reacts more specifically with D1-27, with G2 and G8 resonances (Figure 3.13, green and red dotted frames) being the ones, which were mostly affected, as it was shown in paragraph 3.3.1 (Figure 3.3). This behaviour is in accordance with the behaviour observed using PAGEs for the comparison of the reactivity of the two platinum(II) complexes (Chapter 2, Paragraph 2.5, Figure 2.27). Under these experimental conditions, the use of oxaliPt resulted in the formation of two well separated distinct bands while for the monoaquated cisPt an extended smeary band was formed. As it was discussed there, the presence of the smeary band could be reflecting the formation of various differently platinated RNA species, which was now further confirmed from the significant change of almost all imino proton resonances. It is worth noting that the platination reaction progressed very fast despite the fact that it was performed in the presence of Cl^-, which is known to reduce the platination reaction rate of cisPt[14]. Consequently, this comparison further supports the choice of oxaliPt as a better platination agent for this study.

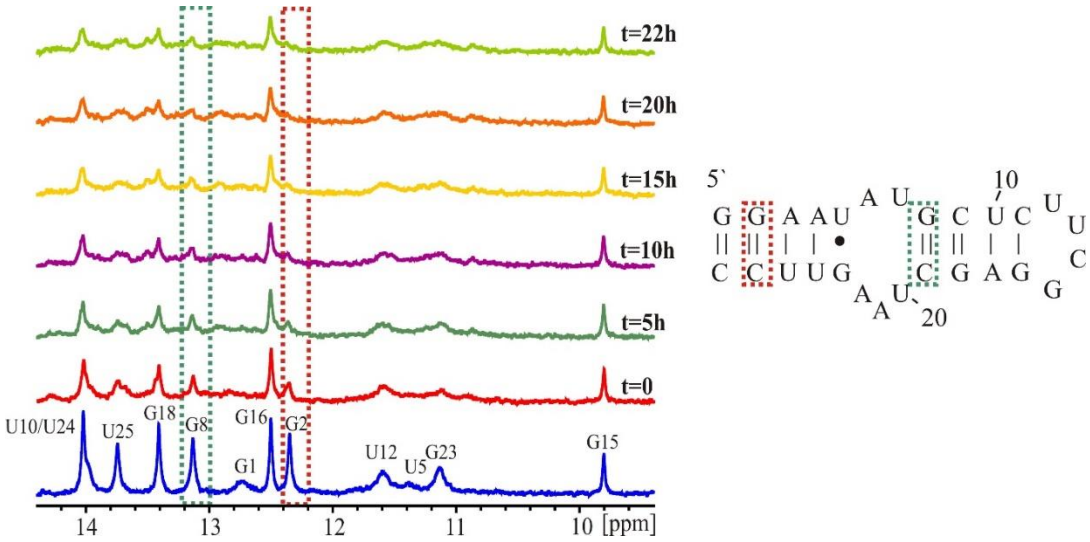

Figure 3.13: *Time evolution NMR experiment for the platination of D1-27 with 5 eq of monoaquated cisPt in 120 mM KCl (left). Right: Secondary structure of D1-27. The dotted frames correspond to the nucleobases, which were mostly affected upon platination with oxaliplatin. (5 eq of monoaquated cisPt, 0.1 mM RNA, 25 °C, 120 mM KCl, pH 5.9, 600 MHz)*

3.6 Platination reactions with kiteplatin ($PtCl_2$ (*cis*-1,4-DACH)]

In chapter 2 it was discussed the evaluation of cisPt and oxaliPt as possible platination agents towards D1-27 (Paragraphs 2.3 - 2.5). Additionally to these two complexes, the interaction of kiteplatin (kitePt) with D1-27 was also briefly investigated, even if no optimization of its platination conditions in order to get a homogeneously platinated RNA was performed. For our study the complex [$PtCl_2$(cis-1,4-DACH)] (kitePt) (chemical structure on the right) was kindly provided by Prof. James Hoeschele (University of Michigan Chemistry Department, USA) and Prof. Nicola Margiotta (University of Bari, Department of Chemistry, Italy). We aimed at comparing its interaction with D1-27 with the behaviour of cisPt and oxaliPt. Therefore, before performing time evolution NMR experiments, a platination reaction was performed and analyzed via PAGE. KitePt was activated to its monoaquated complex (Chapter 5, Paragraph 5.2.4) before usage, and it was reacted with D1-27 using

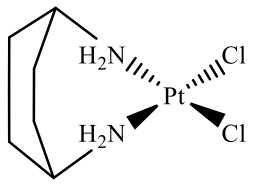

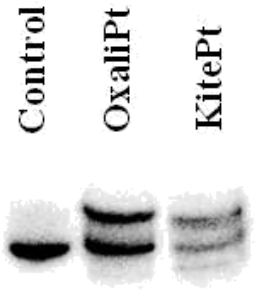

Figure 3.14: *20 % denaturing PAGE for the platination reaction of ^{32}P-5′-end labelled D1-27 with oxaliPt and kitePt using the experimental conditions found for oxaliPt. (0.1 mM RNA incubated with 5 eq of oxaliPt at 25 °C for 1 day in 120 mM KCl solution). The gel was run at 4 °C. For preparation of the platination reactions using labelled RNA see Chapter 5, Paragraph 5.10.4.*

the experimental conditions used for oxaliPt (5 eq of platinum(II) complex, 0.1 mM RNA, 1 day of incubation at 25 °C in the presence of 120 mM KCl). Interestingly, under these conditions a slower migrating band (upper) was formed on a denaturing gel similarly, to what was found for oxaliPt (Figure 3.14). The platinated RNA isolated from the upper band was analysed with MALDI-MS and it was found to consist of a mixture of monoplatinated (m/z = 9080), diplatinated (m/z = 9388) and triplatinated RNA (m/z = 9695), with the diplatinated ones being the major species. Despite the fact that oxaliPt and kitePt showed similar gel patterns, the products of the upper bands were different. Indeed, while the upper band in the case of oxaliplatin contains monoplatinated species, which were further characterized (chapter 4), in the case of kitePt contains a mixture of species, with the diplatinated ones being the major species.

3.7 Time evolution NMR experiments: kiteplatin [$PtCl_2$ (*cis*-1,4-DACH)]

A first comparison of kitePt and oxaliPt was performed by using the same experimental platination conditions and utilizing PAGE for visualization of the platination adducts (Paragraph 3.6). To get further insights into kitePt-RNA adducts and to attempt a comparison with the oxaliPt-RNA ones, time evolution NMR experiment was performed (Figure 3.15). The imino proton resonance of G8 was the most affected (Figure 3.15, green dotted frame), followed by U25, G2 and G18 resonances, which showed similar decrease in intensity (Figure 3.15, red and green dotted frames, Table 3.5). The imino proton resonance of G15 and G16 were the least affected suggesting no interaction at the -UUCG- tetraloop region similarly, to what was found for oxaliPt. However, it should be noticed that G15 resonance during kitePt reaction is more affected compared to the corresponding one in oxaliPt reaction (Table 3.5). G2 imino proton resonance in the case of oxaliPt is expected to be an actual platinum binding site and as such, it is strongly affected upon platination. For kitePt the most affected imino proton resonance was G8, while G2 and G18 imino proton resonances showed similar decrease (Table 3.5). Expecting to have diplatinated RNA as the major species (from MALDI-MS data, Paragraph 3.6) we could assume direct platination at both G1-G2 and G8-G18, the latter leading to formation of intrastrand adducts. Nevertheless, formation of a mixture of monodentate adducts at different sites could not be excluded. However, to further evaluate the possible platinum binding sites characterization of the isolated platinated RNA sample is necessary.

Table 3.5: *Comparison of the intensity decrease of the imino proton resonances during the time evolution NMR experiments for the platination of D1-27 with kitePt and oxaliPt.*

Resonance	Intensity decrease (%) D1-27 + 5eq kitePt	Intensity decrease (%) D1-27 + 5eq oxaliPt
G8	42.6	54.6
U25	37	59.9
G2	35.1	58.8
G18	34.5	21.3
G16	18.8	19.7
G15	17.3	10.3
U10/U24	31	41.5

From Table 3.5 it should be also noted that the decrease in intensity of the imino proton resonances in the case of kitePt is more equally distributed between the various nucleobases, while for oxaliPt there are significant differences for example between G2 and G15. This, together with the presence of

diplatinated RNA species as the major species, suggests that the platination pattern between the two platinum(II) complexes is different, with kitePt exhibiting reduced specificity.

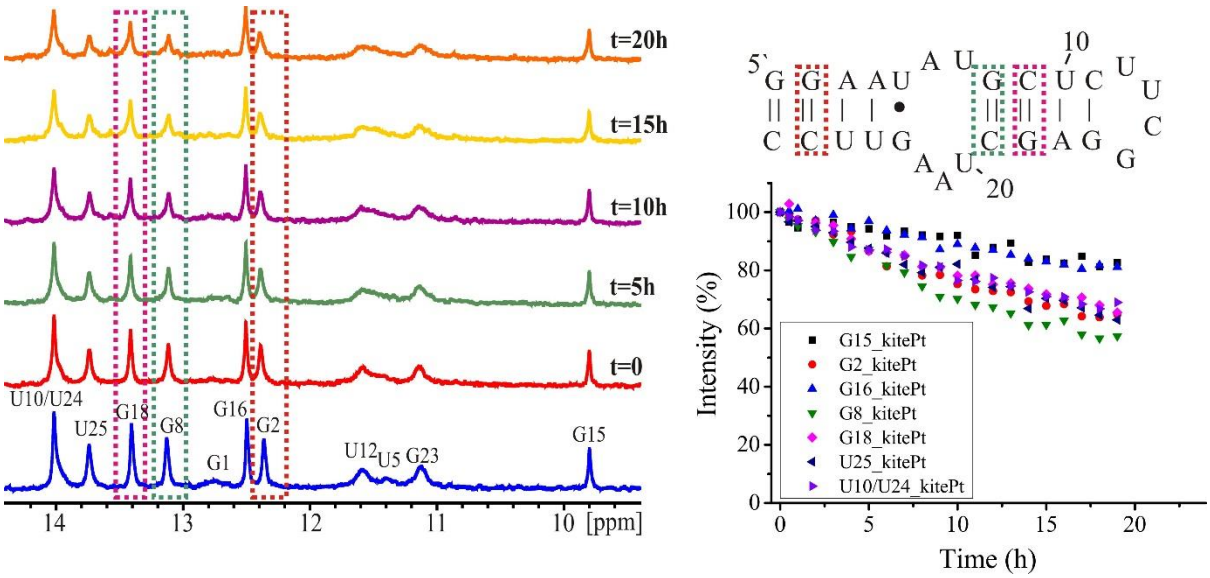

Figure 3.15: *Time evolution NMR experiment for the platination of D1-27 with 5 eq of monoaquated kitePt in the presence of 120 mM KCl (left). Right Top: Secondary structure of D1-27, Right Bottom: Plot of the percentage of the intensity of the imino proton resonances over time. (5 eq of monoaquated kitePt, 0.1 mM RNA, 25 °C, 120 mM KCl, pH 6, 600 MHz)*

3.8 Plasmid binding studies for cisplatin, oxaliplatin and kiteplatin

Gel mobility shift assays and ^{1}H-NMR time evolution experiments show strong differences in the behaviour of kiteplatin, oxaliplatin and cisplatin towards our short RNA construct. Driven by these findings, we decided to directly compare the behaviour of the three complexes also towards DNA, using DNA plasmid binding assays. These studies were part of a STSM project, which took place in the laboratory of Prof. Sofi K. C. Elmroth in Lund, Sweden (Appendix 4). Utilizing the ability of the platinum(II) anticancer drugs as DNA unwinding agents[15] we studied the DNA binding affinity of the monoaquated complexes of cisPt, kitePt and [Pt(DACH)Cl_2] with the negatively supercoiled pUC18 plasmid. The [Pt(DACH)Cl_2] was used as activated form of oxaliPt[16] and its synthesis and complete characterization is described in chapter 5 (Paragraphs 5.2.2-5.2.5). Their behaviour was studied in two different phosphate buffers namely 200 mM Na_2HPO_4 / NaH_2PO_4 (NaPi) and 200 mM K_2HPO_4 / KH_2PO_4 (KPi) which were simulating the extracellular and intracellular environment. Upon platination, supercoiled and relaxed forms can be visualized by agarose gel electrophoresis (Figure 3.16). By increasing the amount of platinum(II) complexes bound to DNA the appearance of a slower migrating supercoiled plasmid band could be detected. The point at which the supercoiled and relaxed forms coincide is called coalescence point (Figure 3.16, white frame). These studies were performed using experimental conditions previously reported from the Elmroth's group[17]. The ratio of nucleotide

concentration (C_{DNA}) and concentration of platinum(II) compounds (C_{Pt}) ($r_f = C_{Pt}/C_{DNA}$) was varied from 0 to 0.5. Each platinum(II) complex has its coalescence point at the same r_f in NaPi and KPi buffer, meaning that they exhibit similar behaviour in both buffers (Figure 3.16). Cisplatin reacted the fastest, as expected, having the coalescence point much earlier (Figure 3.16, lane 5) compared to the other two complexes (Figure 3.16, lane 8 in both cases). Among the other two, kiteplatin was faster than oxaliplatin, considering that the slower migrating supercoiled band appeared earlier (lane 4 over lane 7 for [Pt(DACH)Cl_2]). It is worth noting that here kitePt reacted faster than the dichlorido analogue of oxaliPt, even if the oxalate group, whose hydrolysis was probably slowing down the platination reaction in the case of the interaction with D1-27, was not present[18]. Studies on the reaction rates of these three platinum(II) complexes with double-stranded DNA led to comparable results to the ones observed here. More specifically it was shown that kitePt and [Pt(DACH)Cl_2] exhibit similar behaviour while cisplatin has higher reactivity. Their lower reactivity compared to cisplatin was suggested to be connected with the greater steric effect introduced by their bulky non-leaving groups[16].

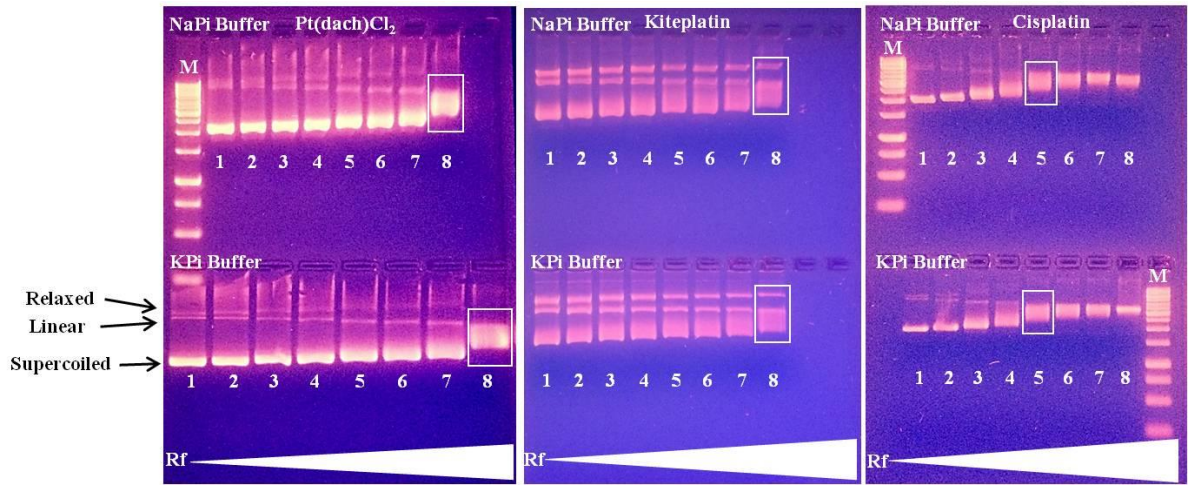

Figure 3.16: *Gel mobility shift assay of platinum(II) complexes with supercoiled and relaxed forms of the pUC18 plasmid. The r_f varied from 0 to 0.5 with 1 = 0, 2 = 0.01, 3 = 0.05, 4 = 0.076, 5 = 0.15, 6 = 0.2, 7 = 0.0.3, 8 = 0.5. In the white frame are the bands at which the coalescence point is observed. With M is indicated the marker lane.*

3.9 Summary of the differences between the platination reactions using oxaliPt, monoaquated cisPt, and monoaquated kitePt

3.9.1 Comparison of cisPt *vs* oxaliPt

From the data commended above, it was concluded that cisPt was reacting faster compared to oxaliPt and in a non-specific manner with D1-27. This was observed from the appearance of a non-well defined gel band (Chapter 2, Paragraphs 2.3 - 2.5, Figure 2.27) and from the change of intensity of the majority of the imino proton resonances during the time evolution experiments (Chapter 3, Paragraph 3.5). On

the contrary, for the platination reaction using oxaliPt, a well-defined new band was formed (Chapter 2, Figure 2.26) and from the time evolution experiments it was concluded that most probably a possible platination site is G1-G2 (Chapter 3, Paragraph 3.4). The origin of this different behaviour is mostly connected with their different non-leaving groups (a bulky DACH moiety and an ammine group) which due to the different sterical hindrance are affecting the conformation of the formed adducts[19]. Finally, the faster reaction rate observed for cisplatin is the result of faster hydrolysis of its leaving groups compared to the oxalate group of oxaliplatin[20] (Chapter 2, Paragraphs 2.4 - 2.5).

3.9.2 Comparison of oxaliPt *vs* kitePt

OxaliPt and kitePt have in common a different isomer of the same non-leaving group (1,2-DACH for oxaliPt and 1,4-DACH for kitePt) and oxaliPt has an oxalate ligand as leaving group, while kitePt has two chlorides. On the denaturing gels under the same experimental conditions, both complexes exhibited the same behaviour, meaning that there was formation of a new slower migrating band (Figure 3.14). Despite that, the MALDI-MS analysis of the Pt(II)-RNA species from these upper bands were different with oxaliPt major species being the monoplatinated RNA, while for kitePt the major species was the diplatinated one. Considering the data from the MALDI-MS analysis different behaviour was also expected in the time evolution NMR experiments. Indeed, for oxaliPt the mostly affected imino proton resonances were the ones corresponding to G2, G8 and U25 while for kitePt they were the ones corresponding to G2, G8 and G18. In both cases, no interaction was detected at the terminal -UUCG- tetraloop. OxaliPt binds more specifically compared to kitePt and this was observed from the general decrease of the majority of the imino proton resonances intensity for kitePt compared to oxaliPt (Table 3.5). The reduced specificity observed for kitePt might be connected with the presence of the very labile chloride ligands, as leaving groups, which based on studies with cisplatin are hydrolyzed faster compared to the oxalate group of oxaliplatin[19,20].

3.9.3 Comparison of cisPt *vs* kitePt

CisPt and kitePt have in common that both possess two chloride ligands as leaving groups while the first have two ammines as non-leaving groups and the second has a 1,4-DACH ammine-ligand. Under the same experimental conditions the two platinum(II) complexes showed that they do not have strong preference for a binding site as it was observed for oxaliPt and in both cases most of the imino proton resonances were affected upon platination. The important difference between the two was the fact that monoaquated cisPt reacted faster compared to monoaquated kitePt. Being both monoaquated and therefore being to the same extent ready to react, the difference observed should result from the difference in bulkiness of their non-leaving groups similarly to what is known for the differences observed between the cisplatin and oxaliplatin DNA adducts[19].

3.10 Investigation of the role of K(I) and Cl^- in the platination reactions using PAGE analysis and time evolution NMR experiments

To improve the platination reactions for both cisPt and oxaliPt the choice of the reaction solution was important. For cisPt the use of ddH_2O instead of $KClO_4$ solution resulted in the formation of a slower migrating band while for oxaliPt the use of KCl significantly improved the platination reaction yield (Chapter 2, Paragraph 2.4.4). The presence of K(I) could on the one hand stabilize the secondary structure of the RNA and on the other hand it could reduce the platination efficiency due to competition with the also positively charged platinum(II) for the same binding sites at the RNA (Chapter 4, Paragraph 4.4 - 4.5). The presence of Cl^- has also a double role. It can replace the water molecules of the activated cisPt and kitePt reducing the platination reaction speed[14], while in the case of oxaliPt it boosted the platination efficiency due to degradation of the oxalate ligand and the formation of the activated oxaliPt species[18,21–24] (Chapter 2, Paragraph 2.4.3). To have an overview of the behaviour of all the platinum(II) complexes used until now, based on the use of different reaction solution (ddH_2O, 120 mM $KClO_4$ and 120 mM KCl), platination reactions were performed using the experimental conditions found for oxaliPt (5 eq of platinum(II) complex, 0.1 mM RNA, 1 day of incubation at 25 °C) and all samples were run in the same denaturing gel (Figure 3.17). Additionally to the three platinum(II) complexes discussed until now carboplatin (carboPt)[25] was also used for this comparison (Chapter 1, Paragraph 1.2.2).

Using carboPt no formation of a new gel band was observed meaning either that it does not react under these experimental conditions or that the platinated-RNA species formed migrate similarly to the control. For oxaliPt, it could be nicely observed the difference in the platination yield upon variation of the reaction conditions. In the absence of K(I) (only ddH_2O) there is a moderate platination yield, which was significantly reduced when K(I) was added (120 mM $KClO_4$). This is connected most probably with the competition of the two cations for binding to RNA and with the more compact form that the RNA adopts in the presence of cations. The yield is again greatly increased when Cl^- is used, which as discussed before can degrade the oxalate group forming the activated complex of oxaliplatin.

When platination with monoaquated cisPt was performed in ddH_2O and in 120 mM $KClO_4$ formation of a new slower migrating band and appearance of a smear were observed on the gel in both cases, suggesting that the presence or absence of K(I) does not influence the product formation. However, in 120 mM KCl, in which the reaction was expected to proceed slower, two different new bands appeared; a faster migrating one, which was not formed before, and a slower migrating one much closer to the unreacted RNA compared to the other two reactions. Interestingly this behaviour suggests formation of differently platinated adducts upon addition of Cl^-.

The platination reaction with kitePt took place very fast in ddH_2O with no unreacted RNA being left and an extended slowly migrating smeary band being formed. The platination speed was reduced

gradually in the presence of K(I) (120 mM $KClO_4$) with the smeary slowly migrating band migrating faster than before. In the presence of 120 mM KCl two well-separated and well-defined bands were present with the one corresponding to unreacted RNA and the other slower migrating one (upper) to the platinated RNA species. Therefore, kitePt exhibits an intermediate behaviour between oxaliPt and cisPt, with the presence of K(I) reducing its reaction rate, similarly to what was observed for oxaliPt, and the presence of Cl^- having the same effect as for cisPt. The transition from a smeary band to a well-defined one suggests that the reaction was more specific and platinated RNA species with similar gel mobility were formed upon reduction of the reaction speed.

Summing up, all the above observations are in line with what was found from the time evolution NMR experiments and the preliminary DNA plasmid binding studies discussed above (Paragraph 3.9). Performing a denaturing PAGE useful conclusions could be made about the reactivity of the different platinum(II) complexes in various reaction solution conditions together with a quick first comparison of their kinetic behaviour.

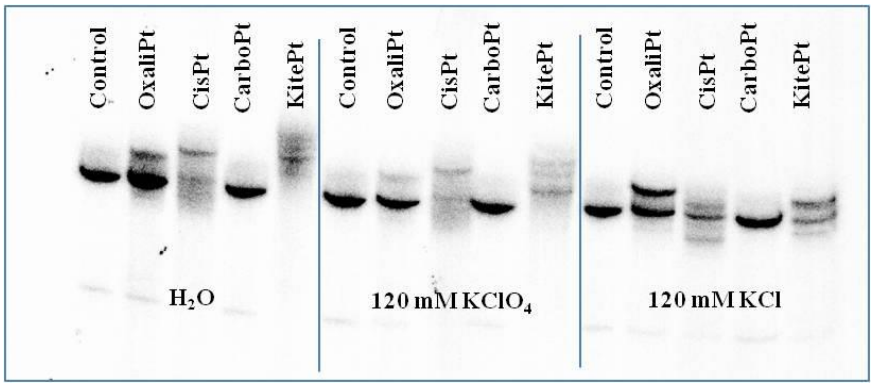

Figure 3.17: *20 % denaturing gel for the evaluation of the platination behaviour of various platinum(II) complexes with D1-27 using different reaction solution conditions. Platination conditions: 5 eq of platinum(II) complex, 0.1 mM D1-27 and 1 nM 5'-end labelled D1-27, incubation for 1 day at 25 °C. The gel was run at 4 °C.*

3.10.1 Investigation of the role of K(I) and Cl^- in the platination reactions of monoaquated cisPt using time evolution NMR experiments

Using 5 eq of monoaquated cisPt in 120 mM KCl the platination reaction was very fast with all the imino proton resonances being affected, despite the presence of Cl^- (Paragraph 3.5). In chapter 2 (Paragraph 2.3) from the investigation of the platination reaction conditions of cisPt it was concluded that 1 eq of monoaquated cisPt, 0.1 mM RNA incubated for 2 days at 37 °C in ddH_2O results in a slower migrating gel band (upper) which contains mostly monoplatinated RNA. The low resolution of this upper band (Chapter 2, Figure 2.13) is probably related with the formation of several similarly platinated

RNA species indicating the low specificity of cisPt in binding to RNA. From what was described in the current chapter following the platination reactions using time evolution NMR experiments is a good way to probe the mostly affected nucleobases and to get an indication of the reaction kinetics. Aiming at understanding the platination behaviour of cisPt under the best experimental conditions found for it, time evolution experiments were then employed. Towards this direction, the reaction was monitored for 1 day at 25 °C using 1 eq of monoaquated cisPt, 0.1 mM RNA, in the presence of 120 mM $KClO_4$. Having already performed a similar experiment using 5 eq of monoaquated cisPt in 120 mM KCl (Paragraph 3.5) and having seen that the reaction was very fast and unspecific, by reducing the platinum(II) concentration we were aiming at slowing down the reaction. However, not significant reduction could be expected considering that Cl^- which usually reduces the reaction rate, was replaced by ClO_4^-. In line with this, the time evolution experiment showed that the majority of the imino proton resonances were again extensively affected immediately after the addition of the platinum(II) complex (Figure 3.18, red line). However, comparing it with the reaction performed using 5 eq of platinum(II) in the presence of 120 mM of KCl (Paragraph 3.5, Figure 3.13), now the reaction seemed to be slightly slower, because even after 20 h of reaction the imino proton resonance of G2 was still visible, while when 5 eq were used this resonance disappeared after 10 h.

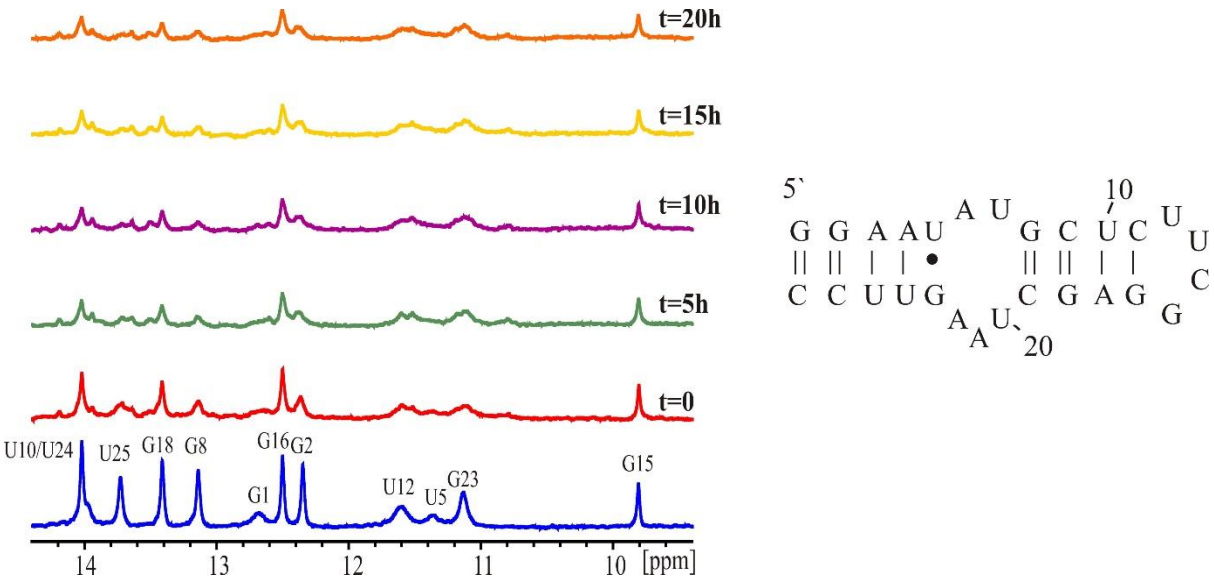

Figure 3.18: *Time evolution NMR experiment for the platination of D1-27 with 1 eq of monoaquated cisPt in 120 mM $KClO_4$ (left). Right: Secondary structure of D1-27. (5 eq of monoaquated cisPt, 0.1 mM RNA, 25 °C, 120 mM $KClO_4$, pH 5.9, 600 MHz)*

To be even closer to the experimental conditions optimized for cisPt, $KClO_4$ was replaced by ddH_2O. In the absence of cations the RNA is less compact and for that reason the imino proton resonances of the untreated D1-27 were broader and less sharp (Figure 3.19, blue line). Similarly to the previous

experiment, the platination reaction proceeded very fast and in a non-specific manner in the absence of cations with the majority of the imino proton resonances being affected to the same extent as when 120 mM $KClO_4$ was used (Figure 3.18). The formation of similar platinum-RNA adducts under these conditions was also suggested from the PAGE analysis of these two reactions where similar gel band patterns were observed for both (Figure 3.17).

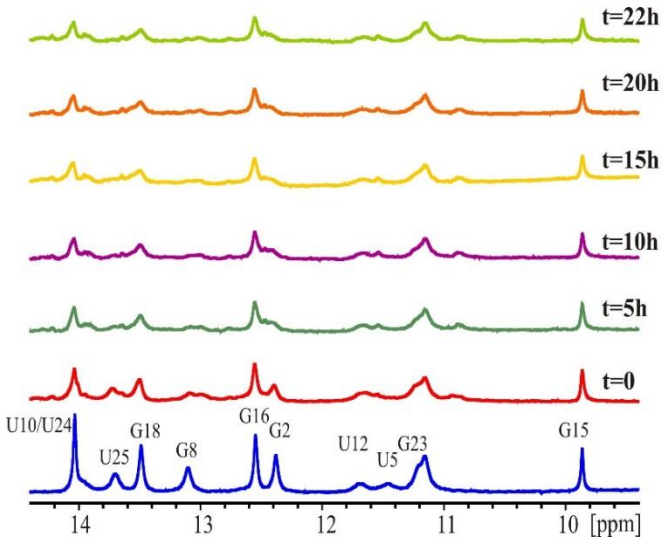

Figure 3.19: *Time evolution NMR experiment for the platination of D1-27 with 1 eq of monoaquated cisPt in ddH_2O. (1 eq of monoaquated of cisPt, 0.1 mM RNA, 25 °C, dH_2O, pH 5.9, 600 MHz)*

Summing up, the time evolution NMR experiments recorded with monoaquated cisPt showed that independently of the presence of Cl^-, the reaction took place much faster compared to oxaliPt (Paragraph 3.5). This behaviour did not change significantly when the platinum(II) concentration was reduced (1 eq) and Cl^- was replaced by ClO_4^- or only water. These data are in line with the data obtained from the PAGE analysis of the platination reactions. The time evolution NMR experiment performed with 1 eq monoaquated cisPt in ddH_2O (Figure 3.19) is the one closer to the experimental conditions used for cisPt and showed that upon platination various differently platinated RNAs were formed. The heterogeneity of the sample was also suggested by denaturing gels, where not well-defined gel band appeared (Chapter 2, Paragraph 2.3, Figure 2.13). Interestingly the MALDI-MS analysis of the sample isolated from this band showed that it consisted of mostly monoplatinated RNA (Chapter 2, Paragraph 2.3, Figure 2.13), which, based on the current data, may be a mixture of RNA species monoplatinated at different positions.

3.11 Conclusions

The main part of this chapter was devoted to the time evolution NMR experiments as a quick way to follow and evaluate the platination reactions. For the platination of D1-27 with oxaliPt the influence of the terminal tetraloop, the presence of the internal loop and the role of the 5′-end phosphate group on the platinum(II) binding sites were investigated. From this study, it was concluded that there is not interaction at the terminal -UUCG- tetraloop and a very possible target is the G1-G2 site while the changes observed at the G8 site could be linked to structural changes induced upon platination at, for example, G1-G2, which were affecting G8 because of the presence of the internal loop. To similar conclusion led the removal of the triphosphate group (deph-D1-27), with the difference that the reaction at the G1-G2 site was not as fast as before. Lastly, the replacement of the -UUCG- tetraloop for the -GAAA- one made the terminal loop region more prone to platinum binding (Paragraph 3.3.2). This approach cannot be used alone for the evaluation of the platination reactions because the imino proton resonances are influenced by many different experimental factors and additionally, as shown for example for G8, are very sensitive to local structural changes. With oxaliPt being the platination agent chosen for this study, further isolation and characterization of its platinated RNA species is following in chapter 4. A first evaluation of the different platinum binding preferences and reaction kinetics of monoaquated cisPt and monoaquated kitePt compared to oxaliPt was performed with the combination of time evolution NMR experiments and PAGE analysis under the same platination reaction conditions. Information about the platination reaction rates of all three platinum(II) complexes were also gathered from DNA unwinding experiments (Paragraph 3.8). CisPt was found to be the agent, which was binding faster and less specific with RNA and oxaliPt was the one with good specificity and good reaction kinetics. KitePt exhibited an average behaviour between the other two, because it seemed to be more specific than cisPt but less than oxaliPt. Plasmid binding assays confirmed also the above-mentioned behaviour. In the end the kinetics and the role of K(I) and Cl^- in the platination reactions of all three platinum(II) complexes was investigated using PAGE analysis. In addition, time evolution NMR experiments were employed for the platination reaction of monoaquated cisPt under different K(I) and Cl^- conditions, which supported its high reactivity and reduced specificity which did not allow its further characterization.

3.12 References

1. Figueroa, N., Keith, G., Leroy, J. L., Plateau, P., Roy, S. & Gueron, M. NMR study of slowly exchanging imino protons in yeast $tRNA^{Asp}$. *Proc. Natl. Acad. Sci. U. S. A.* **80,** 4330–4333 (1983).
2. Höbartner, C. & Micura, R. Bistable secondary structures of small RNAs and their structural probing by comparative imino proton NMR spectroscopy. *J. Mol. Biol.* **325,** 421–431 (2003).
3. Varani, G. & Tinoco, I. RNA structure and NMR spectroscopy. *Q. Rev. Biophys.* **24,** 479 (1991).
4. Shamsi, M. H. & Kraatz, H.-B. Interactions of metal ions with DNA and some applications. *J. Inorg. Organomet. Polym.* **23,** 4–23 (2013).
5. Lee, M.-K., Bottini, A., Kim, M., Bardaro, M. F., JR, Zhang, Z., Pellecchia, M., Choi, B.-S. & Varani, G. A novel small-molecule binds to the influenza A virus RNA promoter and inhibits viral replication. *Chem. Commun.* **50,** 368–370 (2014).
6. Maria Pechlaner. PhD Thesis. University of Zurich, 2013.
7. Vogtherr, M. & Limmer, S. NMR study on the impact of metal ion binding and deoxynucleotide substitution upon local structure and stability of a small ribozyme. *FEBS Lett.* **433,** 301–306 (1998).
8. Alderden, R. A., Hall, M. D. & Hambley, T. W. The discovery and development of cisplatin. *J. Chem. Educ.* **83,** 728 (2006).
9. Sheehy, J. P., Davis, A. R. & Znosko, B. M. Thermodynamic characterization of naturally occurring RNA tetraloops. *RNA* **16,** 417–429 (2010).
10. Cheong, H.-K., Kim, N.-K. & Cheong, C. in *eLS*, edited by J. W. &. S. Ltd (John Wiley & Sons, Ltd, Chichester, UK, 2001), pp. 1–6.
11. Donghi, D., Pechlaner, M., Finazzo, C., Knobloch, B. & Sigel, R. K. The structural stabilization of the κ three-way junction by Mg(II) represents the first step in the folding of a group II intron. *Nucleic Acids Res.* **41,** 2489–2504 (2013).
12. Romaniuk, P. J., Hughes, D. W., Gregoire, R. J., Neilson, T. & Bell, R. A. Stabilizing effect of dangling bases on a short RNA double helix as determined by proton nuclear magnetic resonance spectroscopy. *J. Am. Chem. Soc.* **100,** 3971–3972 (1978).
13. Stehlikova, K., Kostrhunova, H., Kasparkova, J. & Brabec, V. DNA bending and unwinding due to the major 1,2-GG intrastrand cross-link formed by antitumor cis-diamminedichloroplatinum(II) are flanking-base independent. *Nucleic Acids Res.* **30,** 2894–2898 (2002).
14. Horacek, P. & Drobnik, J. Interaction of cis-dichlorodiammineplatinum (II) with DNA. *Biochim. Biophys. Acta* **254,** 341–347 (1971).

15. Malina, J., Hofr, C., Maresca, L., Natile, G. & Brabec, V. DNA interactions of antitumor cisplatin analogs containing enantiomeric amine ligands. *Biophys. J.* **78,** 2008–2021 (2000).

16. Margiotta, N., Marzano, C., Gandin, V., Osella, D., Ravera, M., Gabano, E., Platts, J. A., Petruzzella, E., Hoeschele, J. D. & Natile, G. Revisiting $PtCl_2$(cis-1,4-DACH): an underestimated antitumor drug with potential application to the treatment of oxaliplatin-refractory colorectal cancer. *J. Med. Chem.* **55,** 7182–7192 (2012).

17. Damian, M. S., Hedman, H. K., Elmroth, S. K. & Diederichsen, U. Synthesis and DNA interaction of platinum complex/peptide chimera as potential drug candidates. *Eur. J. Org. Chem.* **2010,** 6161–6170 (2010).

18. Lucas, M. F., Pavelka, M., Alberto, M. E. & Russo, N. Neutral and acidic hydrolysis reactions of the third generation anticancer drug oxaliplatin. *J. Phys. Chem. B* **113,** 831–838 (2009).

19. Malina, J., Novakova, O., Vojtiskova, M., Natile, G. & Brabec, V. Conformation of DNA GG intrastrand cross-link of antitumor oxaliplatin and its enantiomeric analog. *Biophys. J.* **93,** 3950–3962 (2007).

20. Kasparkova, J., Vojtiskova, M., Natile, G. & Brabec, V. Unique properties of DNA interstrand cross-links of antitumor oxaliplatin and the effect of chirality of the carrier ligand. *Chem. Eur. J.* **14,** 1330–1341 (2008).

21. Jerremalm, E., Hedeland, M., Wallin, I., Bondesson, U. & Ehrsson, H. Oxaliplatin degradation in the presence of chloride: Identification and cytotoxicity of the monochloro monooxalato complex. *Pharm. Res.* **21,** 891–894 (2004).

22. Jerremalm, E., Wallin, I. & Ehrsson, H. New insights into the biotransformation and pharmacokinetics of oxaliplatin. *J. Pharm. Sci.* **98,** 3879–3885 (2009).

23. Kim, Y.-S., Shin, S.-M., Cheong, M.-S. & Hah, S.-S. Mechanistic insights into in vitro DNA adduction of oxaliplatin. *Bull. Korean Chem. Soc.* **31,** 2043–2046 (2010).

24. Mehta, A. M., Van den Hoven, J M, Rosing, H., Hillebrand, M. J. X., Nuijen, B., Huitema, A. D. R., Beijnen, J. H. & Verwaal, V. J. Stability of oxaliplatin in chloride-containing carrier solutions used in hyperthermic intraperitoneal chemotherapy. *Int. J. Pharm.* **479,** 23–27 (2015).

25. Di Pasqua, A. J., Goodisman, J. & Dabrowiak, J. C. Understanding how the platinum anticancer drug carboplatin works. From the bottle to the cell. *Inorg. Chim. Acta* **389,** 29–35 (2012).

4 Characterization of the isolated oxaliplatin-RNA adducts

4.1 Aim

In this chapter it will be described the characterization of the platinated RNA species, using various techniques, mainly focusing on Pt-RNA adducts migrating in the upper band, obtained using deph-RNA (Pt-deph-RNA adducts). The platinated RNA species of the triph-RNA, which were isolated from the upper band, were also characterized and very similar behaviour was observed. Finally, the last part of the chapter will be dedicated to the characterization of the Pt(II)-RNA species deriving from the faster migrating band, which appears using deph-RNA as starting material.

4.2 Introduction

Upon platination of D1-27 with oxaliPt using the experimental conditions optimized (Chapter 2, Paragraph 2.4.4), the platinated RNA adducts were isolated and purified with denaturing PAGE. A slower migrating band was formed upon platination (upper band), which, according to MALDI-MS analysis, contained monoplatinated RNA as major product. As discussed before in order to have a homogeneous starting RNA sample, D1-27 was dephosphorylated before use (Chapter 2, Paragraph 2.9). Because of the homogeneity of deph-RNA over triph-RNA (Chapter 2, Paragraph 2.9), the species deriving from the upper band obtained in the first case will be mainly described herein. However, upon description of the Pt-deph-RNA adducts a comparison with the corresponding species prepared using triph-RNA will follow. It should be reminded that in both cases the platinated samples consisted of a mixture of monoplatinated (88 %) and diplatinated RNA (12 %) and they were characterized as such. Besides the upper band, the gel corresponding to platination of the deph-RNA showed a third, faster migrating band, which also contained platinated adducts (Chapter 2, Paragraph 2.9, Figure 2.44). The characterization of the Pt-deph-RNA species responsible for this faster migrating band (Figure 2.44, lower band) was also performed in order to get insights into the platinum(II) binding sites, and it will be discussed separately, at the end of this chapter.

4.3 Characterization methods of platinated RNA

In chapter 2 it was described the use of denaturing PAGE for the separation of the platinated RNA species and the use of MALDI-MS for their identification. Upon isolation, the platinated RNA species were characterized using different techniques, as described in the current chapter. Thermal melting studies were performed to determine the effect of platination on RNA stability while circular dichroism (CD) was employed for the monitoring of conformational changes upon platination. Moreover, enzymatic digestion followed by HPLC analysis was used in order to identify the nucleobases, which were involved in platination. Towards the same direction, 5′-end and 3′-end radiolabelled RNA samples were platinated and the radiolabelled platinated RNAs were enzymatically and chemically digested

giving information about the possible platination sites. Finally, from NMR spectroscopy, information about the platination sites with atomic resolution were obtained.

4.4 Thermal melting studies

The nucleic acids, when are present as random coils, have the ability to pair with a complementary strand, based on the intrinsic pairing capabilities of the nucleobases, forming a double stranded helical structure. The aromatic bases of the nucleic acids have lower absorbance at 260 nm when a duplex is formed compared to when they are in a random coil form. This phenomenon is called hypochromicity of nucleic acids and on that are based the thermal melting studies. The stability of the duplexes is affected by several factors like the type of nucleic acid (DNA or RNA), the length, the base composition, the ionic strength and the pH of the solution[1]. A melting curve is obtained by monitoring the increase of UV absorption at 260 nm over increasing temperature. The thermal melting temperature, Tm, of a nucleic acid duplex is defined as the point where half of the oligonucleotides are found in the random coil conformation[2]. The melting curve of D1-27 shows two melting temperatures (Tm_1 = 52.2 ± 2.1 °C and Tm_2 = 74.2 ± 3.0 °C, Figure 4.1), suggesting the presence of a complex melting profile, including at least two steps.

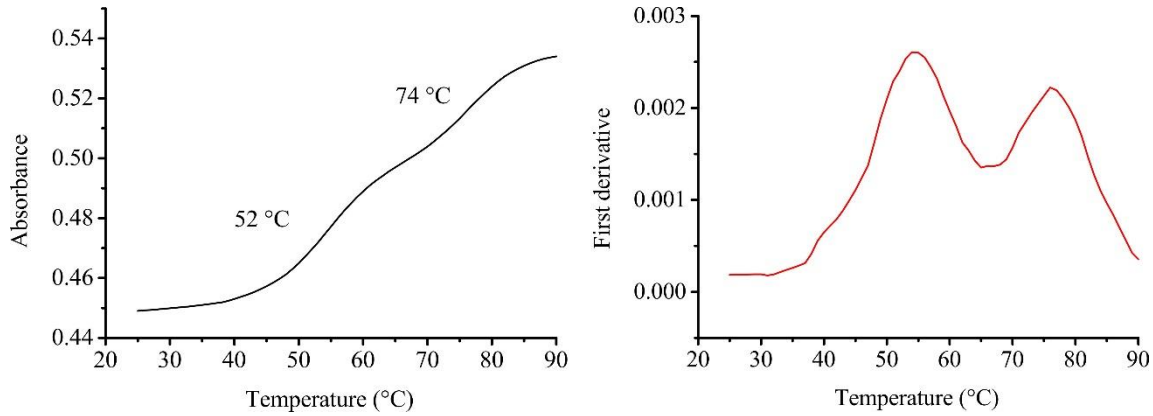

Figure 4.1: *Representative thermal melting curve of deph-D1-27 (left panel) and representation of Tm determination by the first derivative method (right panel).*

Although the unfolding of this construct was not studied in detail, a qualitative simplified interpretation of the two observed melting temperatures may be attempted. There are two potential scenarios: 1) Tm_1 corresponds to the opening of the first part of the construct and Tm_2 to the complete denaturation of the RNA (Figure 4.2, panel A), 2) Tm_1 corresponds to the opening of the second part of the RNA, without the construct being fully denatured, and Tm_2 to the complete denaturing of the RNA (Figure 4.2, panel B). The first hypothesis is likely to be the most probable one. Indeed, first of all, hairpins are very stable constructs[3,4]. For example, the theoretical Tm of the 14 nucleotide long RNA hairpin corresponding to the second part of D1-27 is 85.1 °C (https://eu.idtdna.com/calc/analyzer), this value being well in agreement with Tm_2 observed for our RNA construct. Second, the first part of the D1-27 construct

consists of an internal loop and a G-U wobble, and it is known that these structural elements are less stable compared to a duplex construct[1,3,4]. Finally, the base pairing at the 5′- and 3′-end are known not to be stable[4]; therefore they contribute little to the stabilization of the first part. Consequently, the first part of D1-27 is expected to melt first compared to the second part, thus supporting the first model. The thermal melting point was determined by the derivative method[2], and corresponds to the maximum of the first derivative curve (Figure 4.1).

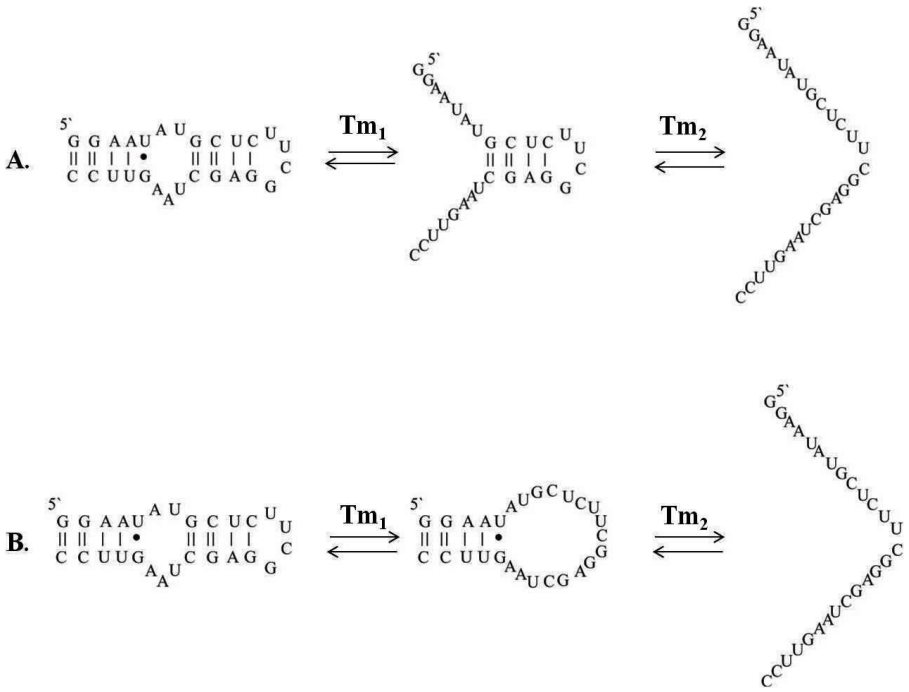

Figure 4.2: *Schematic representation of the two hypothesis about the attribution of the two melting temperatures[3,4].*

Thermal melting curves were recorded both for the unreacted and platinated RNA in order to investigate the effect of platinum(II) binding on RNA stability. At first, the effect of increasing monovalent salt concentration on RNA structure stabilization was evaluated. Thermal melting studies were performed with 0 mM, 20 mM, 60 mM and 120 mM $KClO_4$ (Figure 4.3). Only one low melting temperature is observed when the melting curve is recorded in the presence of 0 mM $KClO_4$ (44.7 ± 2.7 °C). The shape of the curve changes already upon addition of 20 mM $KClO_4$, and two higher melting temperatures can be identified. By further increasing salt concentration (60 - 120 mM), a slight increase of the melting temperatures is observed, suggesting additional RNA stabilization (Table 4.1). Melting profiles of unreacted and platinated RNAs were recorded in the presence of 120 mM $KClO_4$. This K(I) concentration was also used for the platination reaction and is closer to the physiological conditions.

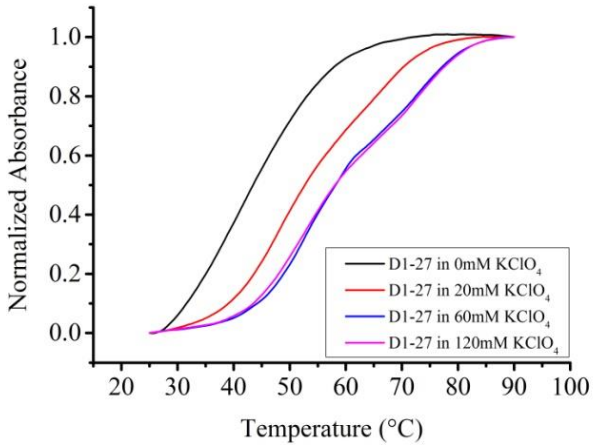

Figure 4.3: *Thermal melting profiles for D1-27 in the presence of different $KClO_4$ concentrations. They were monitored at 260 nm, data collected from 20 °C to 90 °C at a rate of 1 °C / min. C_{RNA} = 1.3 μM.*

Table 4.1: *Melting temperatures of triph-D1-27 at different $KClO_4$ concentrations. These measurements were performed in duplicates. The errors are corresponding to standard deviation.*

$KClO_4$ concentration (mM)	**Tm_1 (°C)**	**Tm_2 (°C)**
0	44.7 ± 2.7	-
20	51.7 ± 1.9	67.8 ± 1.3
60	53.7 ± 1.9	73.8 ± 2.4
120	53.8 ± 2.1	74.5 ± 1.9

Upon platination of deph-D1-27 only Tm_1 was significantly changed towards a lower temperature (ΔTm_1 = 7.4 ± 3.3) (Table 4.2) while almost no change was observed for Tm_2, whose variation was within the experimental error (ΔTm_2 = 3.6 ± 3.2). Similar behaviour was also observed for the platinated species obtained using triph-RNA (Table 4.2). In this latter case the measurements were performed at lower pH, which led to lower absolute values for the melting temperatures for both unreacted and platinated samples. However, similar destabilization was observed as before, with 8 °C decrease of the first melting temperature, while the second melting temperature was almost not affected by platination, with its variation being within the experimental error (Table 4.2). Similar behaviour was also reported for the platination of other RNAs with platinum(II) complexes[5–7] as well as for DNA[5,7]. Platinum(II) induced destabilization may be attributed to local distortion, as observed in the case of DNA, where structural data confirm strong distortion of double stranded oligonucleotides at the platination site[8–14]. The here observed destabilization may derive from intrastrand cross-link, as suggested also by the presence of a slower migrating band on the platination gels, likely attributed to intrastrand binding mode[15]. Platinum(II) intrastrand binding causes base pairing weakening, possibly leading to an easier

denaturation of the construct. In the case of interstrand cross-linked products, a faster migrating band would be expected on the gel[15] and the melting profile should show increased melting temperature[16,17]. Similar destabilization (ΔTm = 10.7 °C) as the one here found (ΔTm ≈ 8 °C) was observed for a 15nt long duplex RNA containing two central consecutive guanines upon platination with oxaliPt. When a similar duplex RNA containing GNG was used instead, the ΔTm was significantly increased (– 19.4 °C). Similar behaviour was reported also for the corresponding DNA-oxaliPt adducts[5].

Table 4.2: *Summary of the melting temperatures for triph- and deph-D1-27 as well as for their platinated adducts. The given Tm values are the average of at least five measurements, and are reported together with their standard deviation. The errors reported for ΔTms values were estimated using the standard error propagation calculations[18].*

RNA construct	Tm_1 (°C)	ΔTm_1 (°C)	Tm_2 (°C)	ΔTm_2 (°C)
Triph-D1-27_pH 6.5	53.8 ± 2.1		74.5 ± 1.9	
Triph-D1-27_pH 5	50.5 ± 0.8	8.1 ± 2.1	69.9 ± 1.2	1.6 ± 1.8
Pt-triph-D1-27_pH 5	42.4 ± 1.9		68.3 ± 1.4	
Deph-D1-27_pH 6.5	52.2 ± 2.1	7.4 ± 3.3	74.2 ± 3.0	3.6 ± 3.2
Pt-deph-D1-27_pH 6.5	44.8 ± 2.5		77.8 ± 1.0	

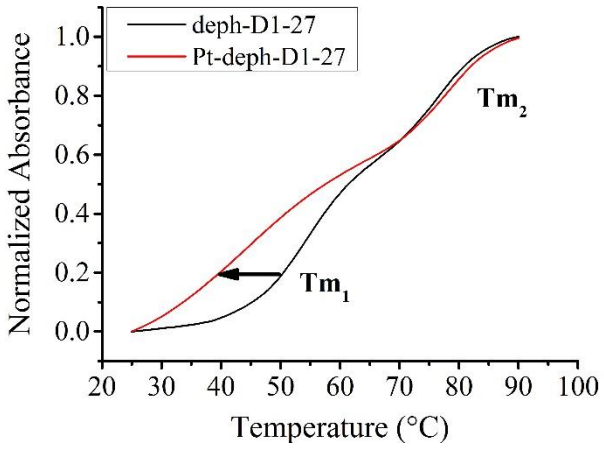

Figure 4.4: *Indicative thermal melting profiles for unreacted deph-RNA (black line) and platinated deph-RNA (red line). They were monitored at 260 nm, data collected from 20 °C to 90 °C at a rate of 1 °C / min.* C_{RNA} *= 1.3 μM, 120 mM* $KClO_4$*, pH 6.5.*

In addition to the information about the stability of the RNA upon platination, these thermal melting profiles also give a hint about the possible location of the platination site. The only very slightly affected Tm_2 indeed suggests that the stable hairpin and the terminal loop in the second part of the D1-27 construct are not (or only slightly) influenced by platination. The significant change observed only for the first melting temperature suggests that the first part of the RNA construct is the one mostly affected from platination, and likely contains the platination site.

4.5 Circular Dichroism (CD)

Circular dichroism (CD) is the difference in the absorption of left-handed circularly polarized light and right-handed circular polarised light and is observed for chiral molecules. Ellipticity (θ) is the quantity used to describe this phenomenon and is measured in degrees (deg)[19]. In CD spectroscopy the CD of molecules is measured over a range of wavelengths and is used to monitor structural changes in proteins as well as in nucleic acids[19,20]. DNA and RNA have specific CD signatures[20]. A regular A-form RNA has a characteristic spectrum showing a large positive ellipticity at 260 nm and a large negative one at 210 nm (Figure 4.5). Changes in the band at 260 nm corresponds to hyperchromism of nucleobases resulting from the helical stacking, and the band at 210 nm is connected to changes in loop structures[21–23]. Therefore, changes in the shape of the CD spectrum are directly related to conformational changes of the RNA.

The CD spectrum of triph-D1-27 shows the two typical bands due to A-form RNA, at 210 nm and 260 nm. CD spectra were recorded in 0 mM $KClO_4$ and 120 mM $KClO_4$ in order to investigate the effect of K(I) on D1-27 structure. It was found that already without adding K(I) the spectrum of D1-27 had the typical shape corresponding to an A-form RNA. Upon K(I) addition, the band at 260 nm and mostly the one at 210 nm were getting more intense, probably due to more properly structured RNA formed or higher percentage of folded species (Appendix 2, Figure A 2.2). Next the spectrum of triph-D1-27 was compared to the CD spectrum of a RNA hairpin lacking the internal loop (RNA 26) (Chapter 2, Figure 2.28, right), therefore representing a properly A-form RNA (Figure 4.5). The slight differences observed between the two spectra can be attributed to the presence of the internal loop in D1-27.

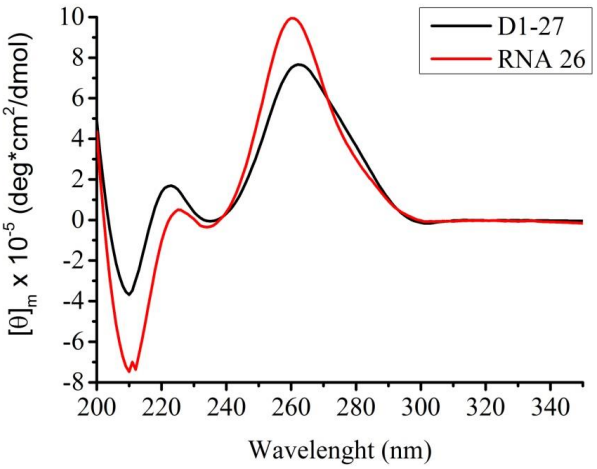

Figure 4.5: *CD signal of D1-27 and RNA 26 constructs. C_{RNA} = 1.3 μM, in 120 mM KCl, pH 6.5 The raw data obtained were given in ellipticity (θ) and were measured in mdeg. To compare the CD spectra of different RNAs or of the same RNA under different concentrations the ellipticity is converted to molar ellipticity [θ] (deg. cm^2.$dmol^{-1}$) (Chapter 5, Paragraph 5.6).*

CD spectroscopy as method of conformational analysis has been widely employed for the study of metal ion-nucleic acids interactions[23], RNA-antibiotic interactions[21,22] as well as platinum(II) anticancer drugs-RNA[7] and platinum(II) anticancer drugs-DNA interactions[7,24–29]. In the current study CD spectroscopy has been employed to monitor the conformational changes induced on D1-27 upon platination.

The CD spectra of the platinated RNA with oxaliPt exhibits the features characteristic for an A-form RNA, meaning a positive band at 260 nm and a negative one at 210 nm[20] showing that platination did not influence the overall conformation of the RNA (Figure 4.6). In previous studies it was reported that the interaction of monoaquated cisPt with DNA resulted in transformation of B-form DNA to Z-form[7]. In our case, only small changes were observed. Compared to unreacted RNA, the negative band at 210 nm was only slightly changed, while for the positive band at 260 nm there was always a bathochromic shift (from 260 nm to 266 nm). However, the intensity of the band was not consistent, as it was observed to be either increased with respect to the unreacted RNA or remained almost unaffected (Figure 4.6, upper and lower panel). Changes of the negative band can be related to changes at the loop structures[21,22]. Here, the change of the negative band was not significant even if, based on the thermal melting studies, the first part of the RNA construct, and therefore the internal loop, could be affected by platination. More interesting is the red shift of the positive band, which was described also in the case of DNA platination with cisPt, and it was related to *cis*-bidentate platinum fixation[25]. Finally, the behaviour of the intensity of the positive band is not clear. The increase of the intensity suggests local changes at the stacking of the duplex, and suggests higher stacking (see D1-27 *vs* RNA 26 in Figure 4.5). However, intrastrand cross-linking caused by platination is expected to reduce the stacking, resulting in a lower intensity band at 260 nm. Similar behaviour is observed when different spectra are recorded at increasing temperature (Figure 4.7). Interestingly, the spectrum of deph-D1-27 at 50 °C, which is close to its Tm_1, shows a bathochromic shift together with a reduction in the intensity of the band at 260 nm, as well as a significant change for the band at 210 nm. Upon further heating both bands greatly decreased until spectra corresponding to almost unstructured RNAs were observed. Based on these data, the increase in intensity of the band at 260 nm, whenever observed, is difficult to be explained, and experimental mishandling and/or artefacts during the measurements could not be excluded.

Summing up, these results suggest an overall retain of the A-form features with the observed changes most probably reflecting local disruption of the structure at the platination sites, with only little effects on the overall stacking of the entire construct. The red shift of the band at 260 nm, together with the previously commented decrease of the first melting temperature, strongly support intrastrand platination.

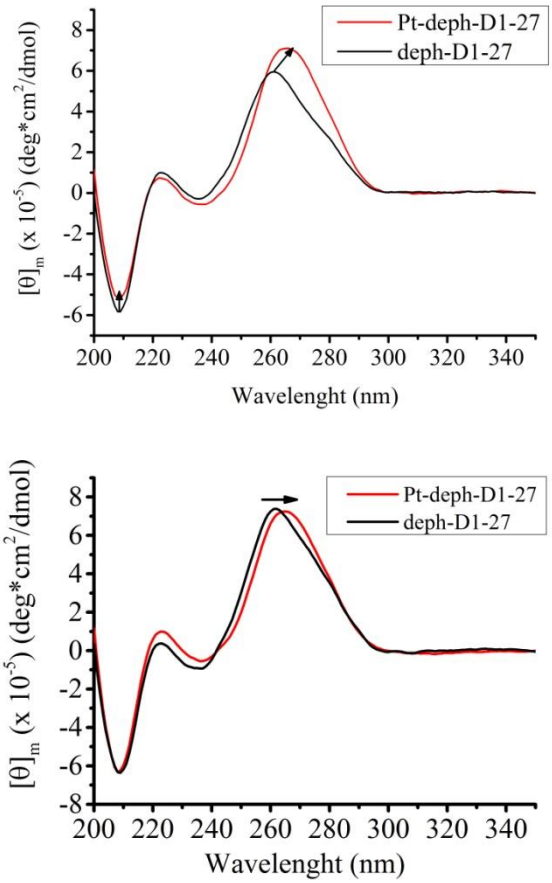

Figure 4.6: *Comparison of the CD spectra of D1-27 (black) and the platinated D1-27 (red). C_{RNA} and $C_{Pt\text{-}RNA}$ = 1.3 μM, in 120 mM $KClO_4$, pH 6.5. CD spectra from different platination reactions are represented in which the band at 260 nm could be either increased in intensity (upper panel) or remained almost unaffected (lower panel)*

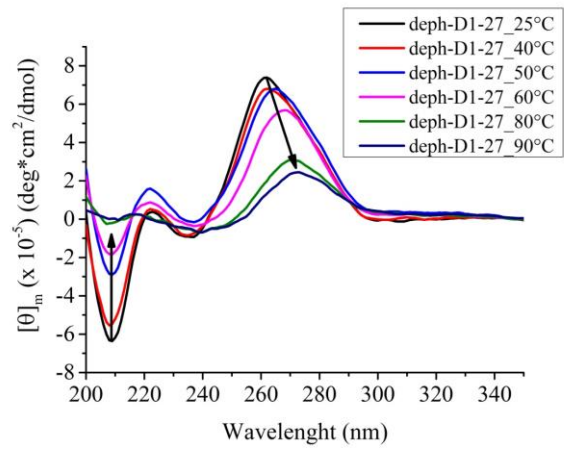

Figure 4.7: *Changes of the CD spectra of deph-D1-27 with increasing temperature.*

The results above correspond to the platinated species originating from the upper band from the platination of deph-D1-27. CD spectra were also recorded on the corresponding species from the platination of triph-RNA. First, it was investigated whether the presence of the triphosphate group could have an influence on the conformation of our RNA construct. For that reason, the CD spectra of triph- and deph-D1-27 were compared. Not significant differences were observed between the two spectra (Figure 4.8) confirming that the triphosphate group does not play a role on the RNA conformation. The same behaviour as for the deph-platinated RNA species was observed for the Pt-RNA adducts obtained when triph-RNA was used as starting material, with the difference that a clearer decrease in intensity of the band at 260 nm was observed (Appendix 2, Figure A 2.3).

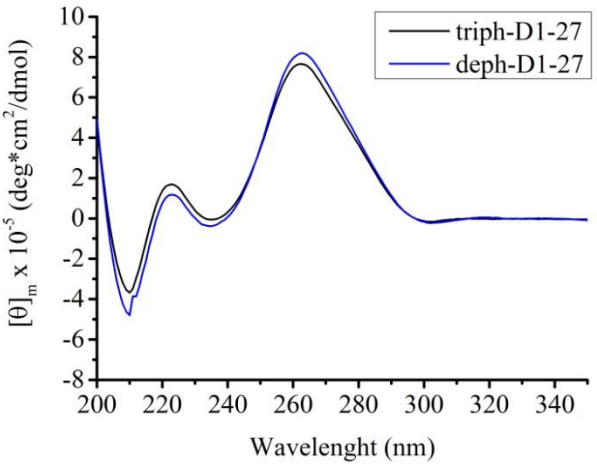

Figure 4.8: *Comparison of the CD spectra of D1-27 (black) and deph-D1-27 (blue).* C_{RNA} *= 1.3 μM, in 120 mM KCl, pH 6.5.*

4.6 Enzymatic digestion and HPLC analysis

To evaluate which nucleobases are affected by platination, D1-27 was digested before and after platination with a non specific enzyme (P1 nuclease), dephosphorylated using an alkaline phosphatase (TSIAP) and injected into the HPLC machine. The combination of P1 digestion and HPLC is very often used for the quantification of DNA[30] as well as for its composition analysis[31]. The P1 nuclease forms nucleoside-5′-monophosphates, which upon dephosphorylation with an alkaline phosphatase (TSIAP) result in a mixture of nucleosides. The removal of the 5′-phosphate with the alkaline phosphatase leads to products which are less polar and have improved separation on a C18 column[32]. The chromatogram obtained from the digestion of D1-27 corresponded to the four different nucleosides. The four peaks of the chromatogram were assigned to cytidine (C), uridine (U), guanine (G) and adenine (A) by comparing them with the retention time of standard nucleoside solutions.

4.6.1 Optimization of the digestion and dephosphorylation conditions of D1-27

The HPLC column used was analytical X-Bridge C18 RP column from Waters and the buffers were: buffer A: 40 mM NH_4OAc, pH 6.5 and buffer B: methanol. The combination of NH_4OAc / methanol is extensively used for this kind of studies[32,33]. First, a HPLC method had to be optimized in order to achieve good separation of the four nucleosides. For the method development, mixture of standard nucleoside solutions was utilized. A linear gradient of increasing amount of buffer B was used (Chapter

5, Paragraph 5.5.3, Methods 8 and 9). After having a method, which allows the separation of the four nucleosides, the optimal digestion conditions had to be found. The choice of the P1 nuclease was based on the fact that it is widely used for digesting DNA, it is very stable and relatively low in cost[30,33]. For the digestion reaction, the amounts of the reactants as well as the incubation times had to be optimized. The amount of RNA used was 0.2 nmol and 1 U/µL of P1 nuclease was tested. The mixture was incubated at 37 °C for 15 min and afterwards 2 U/µL of alkaline phosphatase (TSIAP) were added. The dephosphorylation was performed at 37 °C for 15 min. Afterwards the TSIAP was thermally deactivated by heating at 74 °C for 15 min. The mixture was analyzed with HPLC and the chromatogram obtained is shown in Figure 4.9 (left panel). In addition to the four main peaks, which were assigned to the four nucleosides, several peaks appeared within the first seven minutes (Figure 4.9, left panel, blue frame), whose origin had to be investigated. The absence of late-eluting peaks (after 30 min) in the chromatogram indicates that the digestion was complete[33]. This was further confirmed by repeating the experiments using longer incubation times (1 h, 2 h, 22 h), which led to similar chromatograms, with no extra late-eluting peaks. Therefore, 1 U/µL of P1 nuclease and the incubation for 15 min were sufficient.

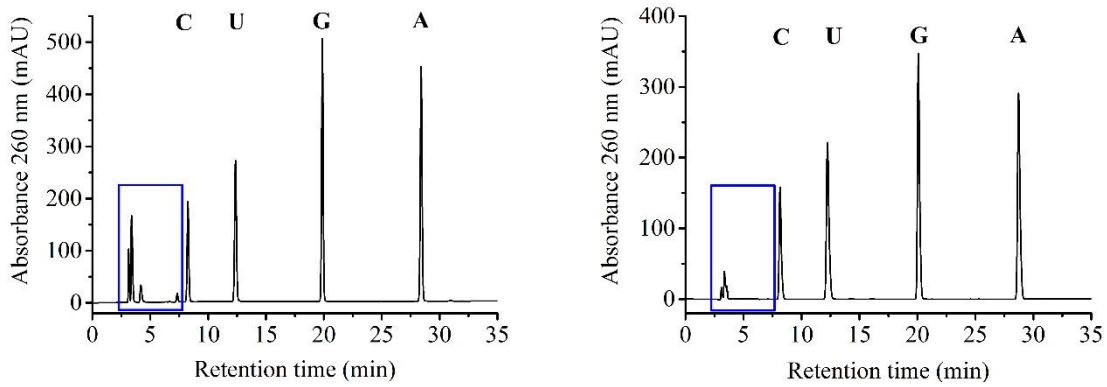

Figure 4.9: *Left panel: HPLC chromatogram of the digested D1-27 using 1 U/µL P1 nuclease (15 min incubation) + 2 U/µL TSIAP (15 min incubation), Right panel: HPLC chromatogram of the digested D1-27 using 1 U/µL P1 nuclease (15 min incubation) + 2 U/µL TSIAP (30 min incubation). By increasing the dephosphorylation time the intensity of the early-eluting peaks decreased suggesting more efficient dephosphorylation.*

The early-eluting peaks could not be the result of incomplete digestion due to their very short retention time but they could be the result of insufficient dephosphorylation. As mentioned before upon P1 digestion there is a mixture of nucleotides, which after dephosphorylation are transformed into nucleosides. Insufficient dephosphorylation could result in a mixture of nucleotides and nucleosides. The nucleotides, due to the presence of a phosphate group should elute faster compared to nucleosides[32]. To confirm this, the RNA was digested and directly injected without dephosphorylation. The corresponding chromatogram shows four peaks with the same retention time as the early-eluted ones

observed above (Figure 4.9, left panel, blue frame, and Figure 4.10). From the direct injection of AMP and GMP, as well as from literature data[31,34], the four peaks were assigned to the four nucleotides (Figure 4.10). Consequently, in order to decrease the intensity of the early-eluting peaks, the dephosphorylation had to be improved. This took place by testing different amounts of TSIAP and different incubation times. Higher concentration of TSIAP was tested (4 U/μL instead of 2 U/μL) which was found to favour the decrease of the intensity of the extra peaks. However, the use of higher concentration and therefore higher volume of TSIAP led to increased glycerol amount in the reaction solution, making it too viscous, which could cause inhibition of the enzyme diffusion, thus reducing its activity[1]. Therefore, the amount of TSIAP was kept to 2 U/μL and the incubation time was varied. Already from increasing the time to 30 min, the extra peaks were significantly decreased (Figure 4.9, right panel, blue frame). Consequently, the optimal combination of conditions leading to the decrease of the early-eluting peaks was 2 U/μL of TSIAP and incubating for 30 min at 37 °C (Figure 4.9, right panel).

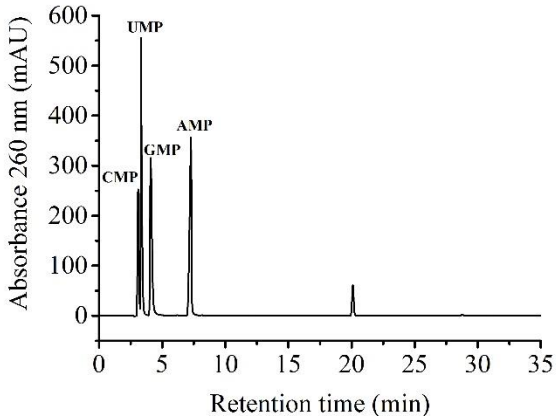

Figure 4.10: *HPLC chromatogram of the digested D1-27 using 1 U/μL P1 nuclease (15 min incubation) without dephosphorylation. The peak with retention time around 20 min corresponds to guanosine, because, since the sample used was the dephosphorylated RNA, not all the 5'-end guanines do contain the phosphate group.*

4.6.2 Digestion of the platinated D1-27

The same digestion conditions used for the unplatinated RNA were also applied to the platinated one. Upon digestion of the platinated deph-RNA originating from the upper slower migrating band a new peak was observed (Figure 4.11, left panel, blue frame). From the comparison of the relative peak areas of the four main peaks before and after platination it was found that the relative peak area of the guanines was reduced, and this reduction corresponded to the loss of two guanines. To confirm that the newly formed peak contained the Pt-GG fragment, a comparison was performed with the adducts obtained

[1] https://ch.promega.com/resources/product-guides-and-selectors/restriction-enzyme resource/applications-and-reaction-conditions-for-restriction-enzymes/

upon reaction of the GpG dinucleotide with oxaliPt. The GpG dinucleotide was incubated with an excess of oxaliPt at 37 °C for 1 day[35] and the reaction mixture was analyzed by HPLC. The chromatogram of the reaction mixture shows three peaks, two of which were assigned to unreacted oxaliPt and GpG dinucleotide upon comparison with the chromatograms of the pure starting materials. The third peak has the same retention time as the new peak observed upon digestion of the platinated RNA (Figure 4.11, right panel, blue box), suggesting that this peak contains the Pt-GG moiety. This is also in accordance with the reduction of the guanosine relative peak area upon platination. Interestingly, after 1 day of incubation the dinucleotide was almost fully converted into the platinated adduct.

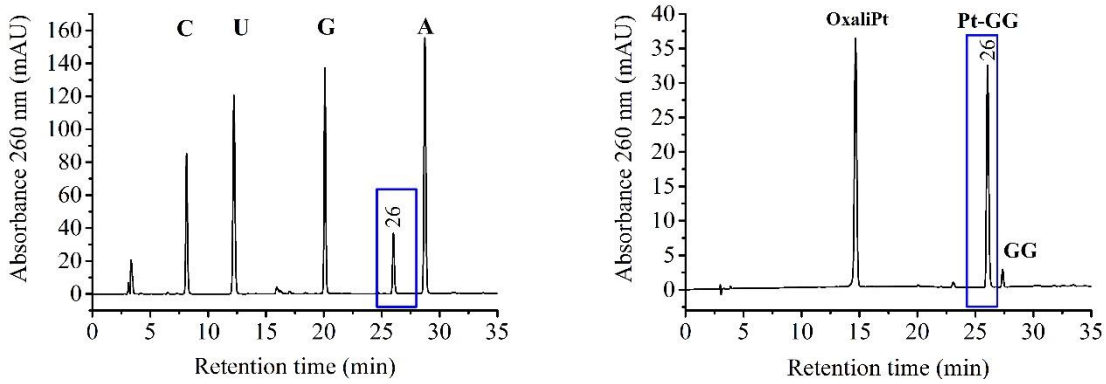

Figure 4.11: *Left panel: HPLC chromatogram of the digestion of the platinated deph-D1-27, which led to the appearance of a new peak at 26 min., Right panel: HPLC chromatogram of the reaction of the GpG dinucleotide with oxaliPt. After 1 day of interaction, a new peak appeared at 26 min. From the comparison of the two chromatograms, the peak at 26 min was assigned to the Pt-GG species.*

The Pt(II)-RNA adducts from the upper band using the triph-D1-27 were also digested and injected into the HPLC machine. Similarly to what previously commented, an additional peak appeared, and from the comparison of the relative peak area before and after platination, loss of two guanines was suggested (Figure 4.12, left panel). The difference of this sample was that the retention time of the new main peak was 17 min, instead of 26 min, which was observed previously. However, in the present case, a minor peak at 26 min was also observed. Interestingly, by increasing the dephosphorylation time from 30 min to 1 day the peak at 17 min decreased while the peak at 26 min increased (Figure 4.12, right panel), resulting in the same picture obtained for the Pt-deph-RNA species. The extra-peak at 17 min likely corresponds to the Pt-GG-triphosphate species, while the peak at 26 min corresponds to its dephosphorylated form, whose formation was indeed favoured upon extensive dephosphorylation. The fact that the Pt-GG-triphosphate species elute faster from the column is not surprising, since they have increased negative charge with respect to their dephosphorylated counterpart. Interestingly, the fact that stronger dephosphorylation conditions are needed to obtain the Pt-GG species in this case suggests that the presence of platinum(II) partially inhibits the activity of the phosphatase.

All the above commented results suggest that the platinated RNA species migrating in the upper band on denaturing gels are platinated at a GG site. The thermal melting studies, described above, suggested that the first part of D1-27 was mainly affected upon platination. The only platination site that satisfies both requirements is G1-G2. This was further supported by the digestion data obtained from platinated triph-RNA, which clearly showed that the platination fragment includes the 5′-end phosphate. Summing up, all the data collected so far strongly support that G1-G2 is the platination site of the species migrating in the upper band on denaturing gels.

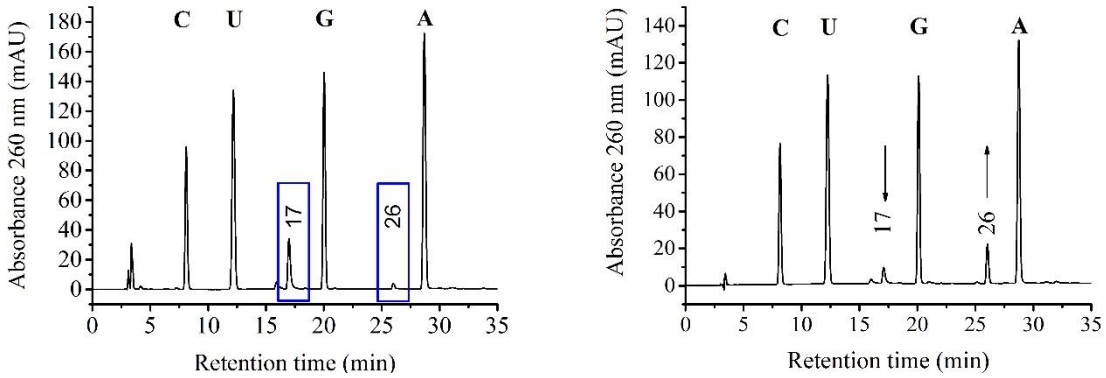

Figure 4.12: *Left panel: HPLC chromatogram of the digestion of platinated triph-D1-27, Right panel: HPLC chromatogram of the same reaction with increased dephosphorylation time from 30 min to 1 day.*

4.7 ^{32}P-3′-end and ^{32}P-5′-end radiolabelling of RNA

The use of ^{32}P-3′-and ^{32}P-5′-end radiolabelled RNAs in RNA platination studies is extensively exploited[7,15,36–41]. The radioactive labelling allows high-resolution detection of the cleavage pattern of RNA or platinated RNA samples. ^{32}P-end labelling can be performed either at 3′- or at 5′-end[42]. Both techniques were employed for this study. Independently of the labelling method used, the labelled RNA was purified by denaturing PAGE and was detected on a phosphorimager. To identify the possible platination sites, the untreated and platinated RNA samples were subjected to alkaline hydrolysis and enzymatic digestions, analyzed by denaturing PAGE and their cleavage patterns were compared (Chapter 5, Paragraph 5.10). This strategy is used very often to identify platination sites in RNA and DNA[15,37–41]. Upon RNA alkaline hydrolysis, single 2′- and 3′-monophosphate nucleotides are formed and the number of bands appearing on the PAGE corresponds to the number of nucleotides. The ribonuclease T1 (RNase T1) is used to map the solvent accessible guanine residues of the RNA[43]. This nuclease cleaves between the 3′-phosphate group of a guanidine ribonucleotide and 5′-hydroxyl of the adjacent nucleotide[43]. The initial product is a 2′,3′-cyclic phosphate nucleoside that is hydrolysed to the corresponding 3′-nucleoside phosphate. Additionally to RNase T1, S1 nuclease was used to map

mismatches and loops. This nuclease cleaves at mismatches and loops of double stranded nucleic acids releasing 5'-phosphoryl monoligonucleotides or oligonucleotides.

4.7.1 ^{32}P-5′-end radiolabelling of RNA

In the 5′-end labelling method the 5′-terminal phosphate group is removed and a ^{32}P-labelled monophosphate nucleotide is transferred to the 5′-end by an enzyme[40,42]. In the first step, the RNA is dephosphorylated using an alkaline phosphatase. This step is not required for the 3′-end labelling while is mandatory for the 5′-end one. Upon dephosphorylation, the T4 polynucleotide kinase is used to transfer the γ-phosphate group from the γ-^{32}P-ATP to the 5′-end of the RNA (Figure 4.13, left panel).

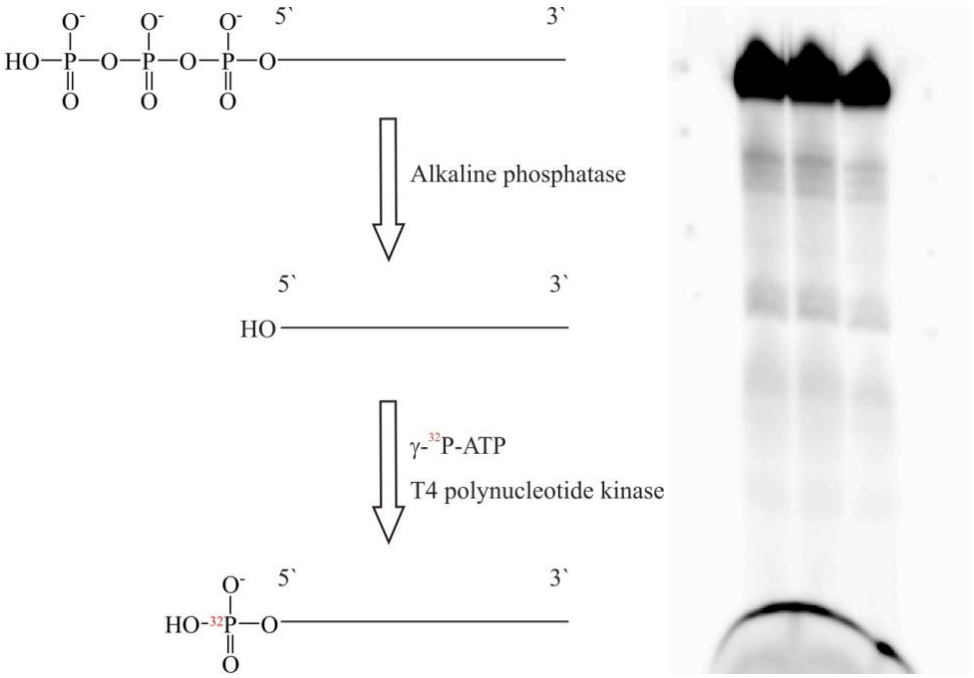

Figure 4.13: *Left panel: Schematic representation of the steps leading to 5'-end labelling[42]. Right panel: Denaturing PAGE of 5'-end labelled D1-27. The main band corresponds to the full-length construct. The gel was run at room temperature using 15 % denaturing PAGE.*

The 5′-end labelling of D1-27 was improved upon optimization of the dephosphorylation and labelling reactions. It was crucial to have efficient dephosphorylation in order to have enough molecules to be labelled. Increasing the amount of alkaline phosphatase (from 2 U/μL to 4 U/μL) the labelling efficiency was increased from 0.01 % to 3 %. Additionally, using 6 U/μL instead of 4 U/μL of the PKN kinase the labelling was improved with labelling efficiency reaching the 25 %. The labelled D1-27 was purified by denaturing PAGE (Figure 4.13, right panel) and isolated with the crush and soak method (Chapter 5, Paragraph 5.10.2). The concentration of the labelled RNA was measured by scintillation counting and it was compared to the total RNA concentration measured by UV. The dephosphorylation and labelling procedures are described in detail in chapter 5 (Paragraph 5.10).

4.7.2 Optimization of partial alkaline hydrolysis and enzymatic digestion of ^{32}P-5′-end labelled D1-27

The isolated ^{32}P-5′-end labelled RNA was subjected to partial alkaline hydrolysis and enzymatic digestions (Chapter 5, Paragraph 5.10.5). The parameters to be optimized were the concentration of the reactants as well as the incubation time and the temperature. The RNA concentration used in all experiments was 0.1 nM. For the alkaline hydrolysis a stock of 0.5 M of sodium carbonate (Na_2CO_3) was used and the reaction temperature was kept at 90 °C. The concentration of Na_2CO_3 was varied from 0.2 M to 0.4 M and the incubation time tried first was 10 min. In the presence of 0.4 M Na_2CO_3 twenty-four bands were visible on the gel (Figure 4.14, left panel). The bands corresponding to the first nucleotides were not visible because small fragments (1-5nt) migrate too fast on the gel[15,44]. Despite that, in order to ensure the maximum efficiency of alkaline hydrolysis, the incubation time was increased from 10 min to 15 min. However, no extra bands appeared on the gel (Figure 4.14, right panel). Moreover, aiming at increasing the resolution of the gel picture, which could eventually result in better defined bands leading to easier attribution, the gel solution used was increased from 15 % to 25 % (Figure 4.14, right panel). However, very similar picture was obtained in the two cases.

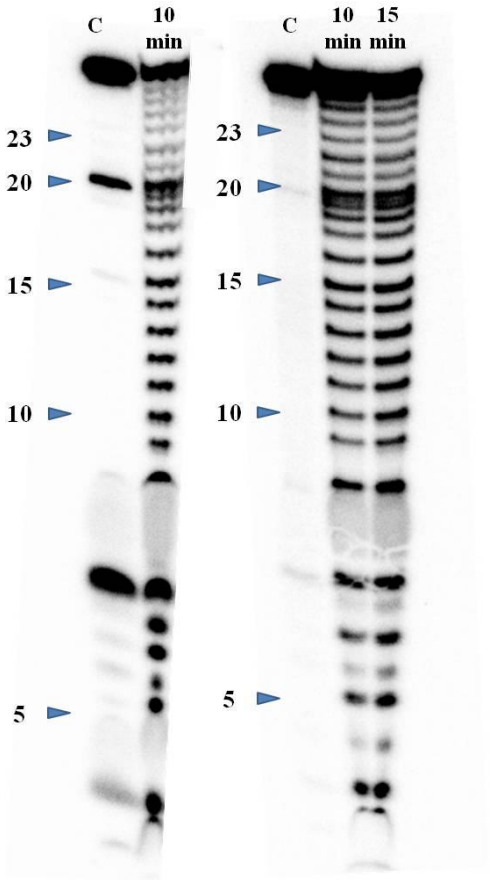

Figure 4.14: *Left panel: Partial alkaline hydrolysis ladder for ^{32}P-5′-end labelled D1-27. The reaction took place in 0.4 M Na_2CO_3, for 10 min at 90 °C. 15 % denaturing PAGE. Right panel: Partial alkaline hydrolysis ladder for ^{32}P-5′-end labelled D1-27. The reaction took place in 0.4 M Na_2CO_3, for 10 min and 15 min at 90 °C. 25 % denaturing PAGE. C indicates the control lane in the two cases.*

To confirm the numbering of the partial alkaline hydrolysis ladder and to assign the guanines of the RNA construct the RNase T1 was used. Concentration and incubation time were optimized, whilst the temperature was kept at 55 °C[45], which is the recommended working temperature for this enzyme. The reaction was performed under native conditions. The RNase T1 concentration used varied from 0.1 U/µL to 10 U/µL and the incubation times were 20 (1), 30 (2) and 40 (3) min (Figure 4.15). Under these conditions only two bands were visible, corresponding to G23 (Figure 4.15, blue frame) and U5 (Figure 4.15, green frame). This suggests that G23 was the only guanine accessible to RNase T1 for digestion. The cleavage at the U5 site was not expected, but cleavage of uridines from RNase T1 is often reported in the literature[7,38]. Higher concentration of RNase T1 as well as higher incubation times were screened in order to test the possibility of cleavage at the other guanine residues. The RNase T1 concentration varied from 10 U/µL to 100 U/µL. In the case of 10 U/µL and 20 U/µL, 20 min (1), 40 min (2) and 60 min (3) digestion time was used, while for the 50 U/µL and 100 U/µL the reaction was run for 10 min (1), 20 min (2), 30 min (3) and 40 min (4) (Figure 4.16). Despite the increased enzyme concentration and incubation time, the same two bands were visible. The new band appearing in the lower part of the gel does not correspond to any guanine (Figure 4.16, purple frame). The conditions for the RNaseT1 digestion chosen were then: 20 U/µL of RNase T1 and incubation for 20 min at 55 °C. The RNase T1 is known to specifically cleave guanines in single stranded DNA/RNA, and it is used to map solvent accessible guanines[43]. Our results suggest that under the used experimental conditions only G23 in the G-U wobble is accessible to cleavage. G15, even if located within a tetraloop, was not cleaved probably due to the compact structure that the -UUCG- tetraloop adopts. This characteristic of the -UUCG- tetraloop makes it also an unfavourable metal ion binding site[46]. Digestions with RNase T1 were performed also under denaturing conditions without though leading to the appearance of more bands, suggesting that the RNA was not properly denatured under the experimental conditions used. Due to flanking 5'-end, G1 and G2 may be cleaved by T1 RNase, but the absence on the gel of fragments shorter than 5 nucleotides prevented their evaluation. Next, the use of the S1 nuclease (S1) was aiming at mapping the looped and bulged regions. Time and concentration dependent experiments were performed in order to find the best reaction conditions. For this purpose 0.5 U/µL to 1 U/µL of S1 were used and the incubation time was varied from 10 min to 40 min at 25 °C (Figure 4.17). Long incubation times (30 - 40 min) seemed to have negative effect on the activity of the enzyme with the observed bands becoming more faint upon longer incubation (Figure 4.17). With S1 nuclease it was possible to map the internal loop (U5 - U7 and U20 - A22, Figure 4.17, light blue and blue frames) and a part close to the terminal loop (G15 - A17, Figure 4.17, brown frame). The experimental conditions chosen were 0.8 U/ µL of S1 and 10 min of incubation at 25 °C.

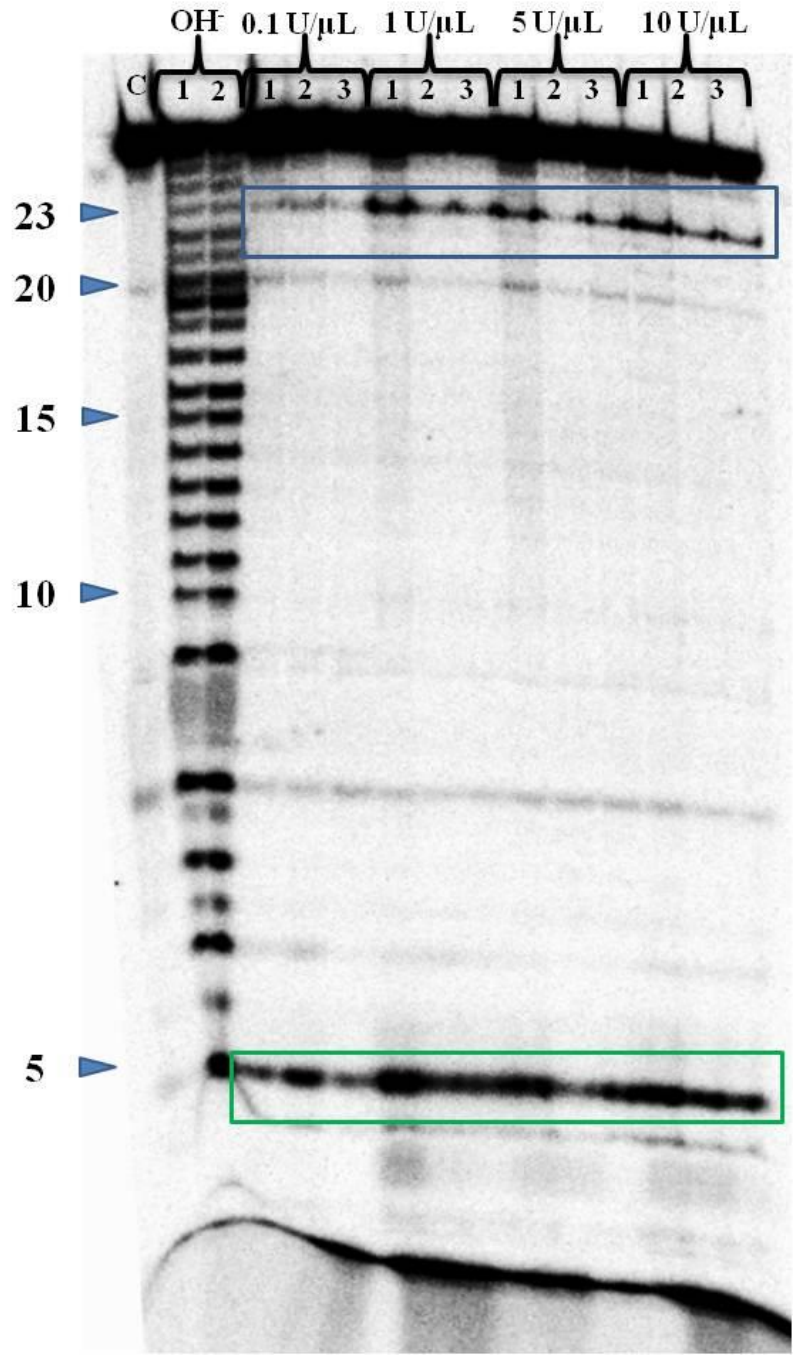

Figure 4.15: *Autoradiogram illustrating partial alkaline hydrolysis and RNase T1 cleavage pattern obtained for ^{32}P-5'-end labelled D1-27. The C stands for the control RNA, OH^- for the partial alkaline hydrolysis lane. OH^- lane: 1 corresponds to 10 min and 2 to 15 min of digestion at 90 °C with 0.4 M Na_2CO_3. T1 RNase lanes: concentration and time dependent experiments were performed in the presence of citrate buffer under denaturing conditions at 55 °C. The concentrations used are reported directly above the gel image, while 1, 2, and 3 correspond to 20 min, 30 min and 40 min of digestion. 25 % denaturing PAGE.*

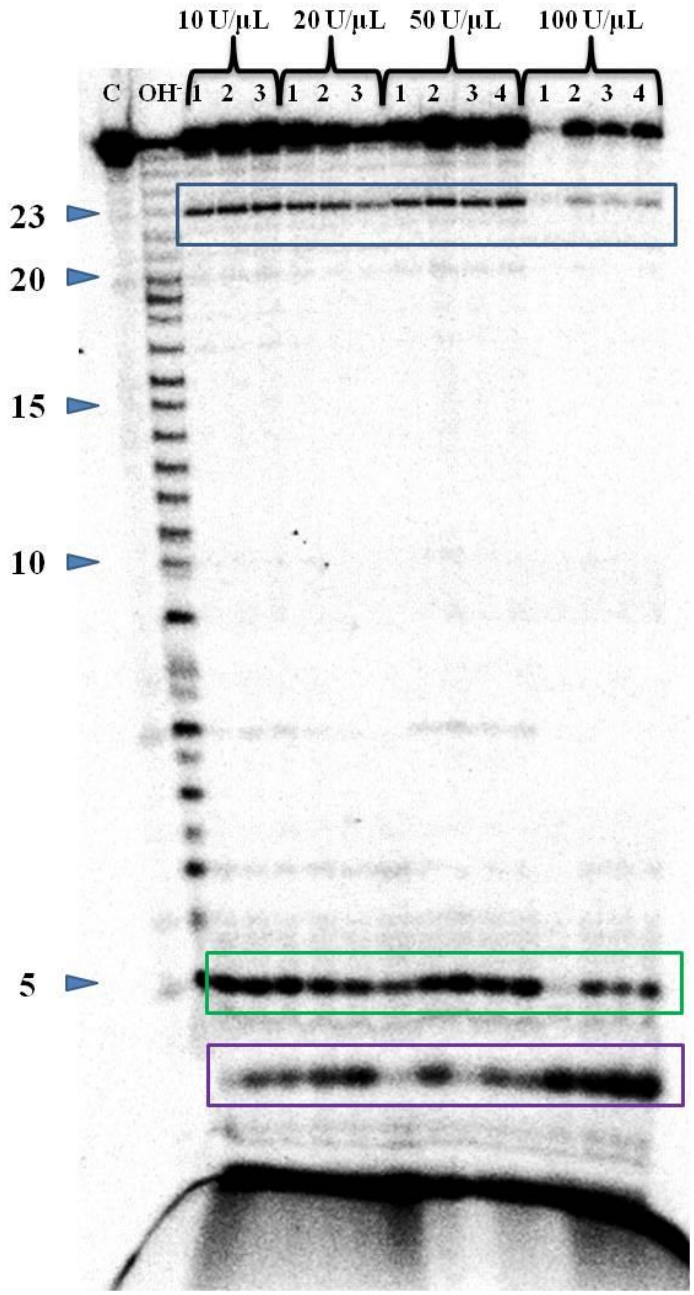

Figure 4.16: *Autoradiogram illustrating partial alkaline hydrolysis and RNase T1 cleavage pattern obtained for ^{32}P-5'-end labelled D1-27. The C stands for the control RNA, OH^- for the partial alkaline hydrolysis. The OH^- lane corresponds to 15 min of digestion at 90 °C with 0.4 M Na_2CO_3. T1 RNase lanes: concentration and time dependent experiments were performed in the presence of citrate buffer under denaturing conditions at 55 °C. The concentrations used are reported directly above the gel image. In the case of 10 U/ µL and 20 U/ µL, 1, 2, and 3 correspond to 20 min, 40 min and 60 min of digestion, whereas in the case of 50 U/ µL and 100 U/ µL, 1, 2, 3 and 4 correspond to 10 min, 20 min, 30 min and 40 min of digestion respectively. 25 % denaturing PAGE.*

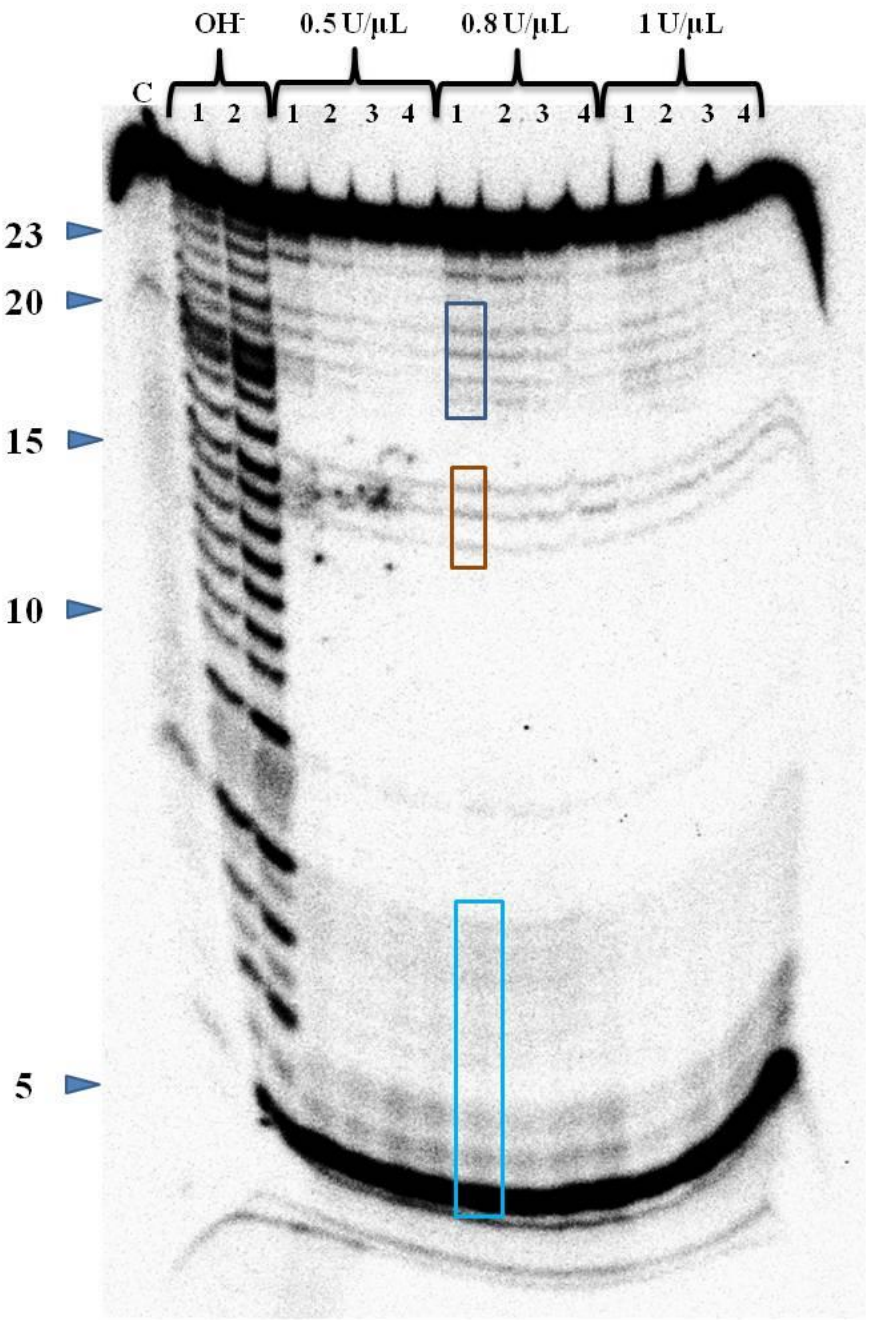

Figure 4.17: *Autoradiogram illustrating partial alkaline hydrolysis and nuclease S1 cleavage pattern obtained for ^{32}P-5'-end labelled D1-27. The C stands for the control RNA, OH^- for the alkaline hydrolysis lane. Both OH^- lanes correspond to 15 min digestion at 90 °C with 0.4 M Na_2CO_3. S1 lanes: concentration and time dependent experiments for the S1 were performed in the presence of zinc sulphate under denaturing conditions at 25 °C. The concentrations used are reported directly above the gel image, while 1, 2, 3 and 4 correspond to 10 min, 20 min, 30 min and 40 min of incubation respectively. 25 % denaturing PAGE.*

4.7.3 Partial alkaline hydrolysis and enzymatic digestions of ^{32}P-5′-end labelled platinated D1-27

Once the reaction conditions for the partial alkaline hydrolysis and enzymatic digestion of D1-27 were optimized, they were also applied to labelled platinated RNA samples. At first, platinated samples were prepared using the same experimental conditions as for the not radiolabelled RNA (5 eq of oxaliPt, 0.25 mM RNA, 1 day of incubation, 25 °C, in 120 mM KCl (Chapter 2, Paragraph 2.4.4 and Chapter 5, Paragraph 5.10.2). The gel obtained from the platination reaction with ^{32}P-5′-end radiolabelled RNA is shown in Figure 4.18. Despite the fact that deph-RNA was used, always only two bands were observed on the gel upon platination, contrarily to what was observed for the platination of unlabelled deph-D1-27 (Chapter 2, Paragraph 2.9. Figure 2.44). A possible explanation for this behaviour is the shorter running time used for the analysis of the labelled samples. Indeed, in the latter case the gel was running for only 15 h, while for the unlabelled samples the running times varied between one to two days.

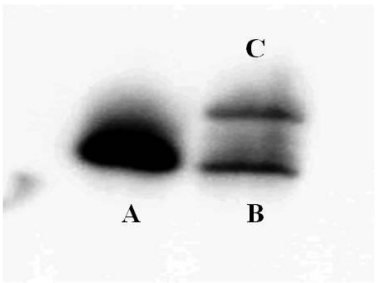

Figure 4.18: *25 % denaturing gel for the platination reaction of ^{32}P-5'-end labelled D1-27 with oxaliplatin. A: Control, B: lower band, C: upper band. The gel was run at 4 °C.*

After platination the reaction mixture was purified via denaturing PAGE, and isolated with crush and soak (Chapter 5, Paragraph 5.4). The platinated samples from both upper and lower bands were subjected to partial alkaline hydrolysis and enzymatic digestions (Figure 4.19). RNase T1 and S1 nuclease enzymatic cleavage as well as partial alkaline hydrolysis of unplatinated RNA were also performed and the corresponding samples were loaded on the gel for comparison. The OH^- lane of the lower band shows an overall cleavage pattern very similar to that obtained for the control sample. Similar behaviour was observed also for the RNase T1 ladder and S1 nuclease lane (Figure 4.19, dark blue, brown and light blue frames). This behaviour was expected considering that the lower band contains mostly unreacted RNA. The little differences observed may be due to the presence of small amounts of platinated RNA, expected to be present in the lower band based on MS experiments performed on unlabelled samples (Chapter 2, Figure 2.26). The upper band contains only platinated adducts and therefore the OH^- cleavage pattern was expected to be different compared to the control. Indeed, the bands corresponding to shorter fragments were very faint (U5-G8, green frame in Figure 4.19) and cleavage products with slower mobility were observed, probably due to platinum(II) presence. This different cleavage pattern suggests conformational changes likely caused by platination. In the RNase T1 lane, the band corresponding to G23 shows higher intensity with respect to the control lane, suggesting increased accessibility of this nucleotide upon platination. This may indicate platination close-by, and excludes direct platination because less efficient cleavage is expected upon direct

platination[44]. Moreover, new bands appeared in the RNase T1 lane, indicating that this part became accessible for cleavage upon platinum(II) binding (Figure 4.19, black dotted frame). The S1 nuclease lane showed increased intensity bands in the area corresponding to G16-A17 (Figure 4.19, brown frame) suggesting higher accessibility of this area upon platination. Moreover, also in this case, novel cleavage sites were detected (Figure 4.19, red dotted line). The appearance of new cleavage sites both in the RNase T1 as well as in the nuclease S1 lanes is often reported in the literature and justified as areas which became more accessible for digestion upon platination due to different conformation of the platinated RNA species compared to the unplatinated ones[7,37,38,44].

In conclusion, the digestions performed on the ^{32}P-5′-end labelled platinated RNA samples originating from the upper band suggest that G23 is not a direct platination site and that the conformational changes caused by platination affect the solvent accessibility of the loops. Platination at G1, G2 could not be investigated, since short fragments could not be detected with this labelling approach. For that reason, ^{32}P-3′-end labelling technique was used.

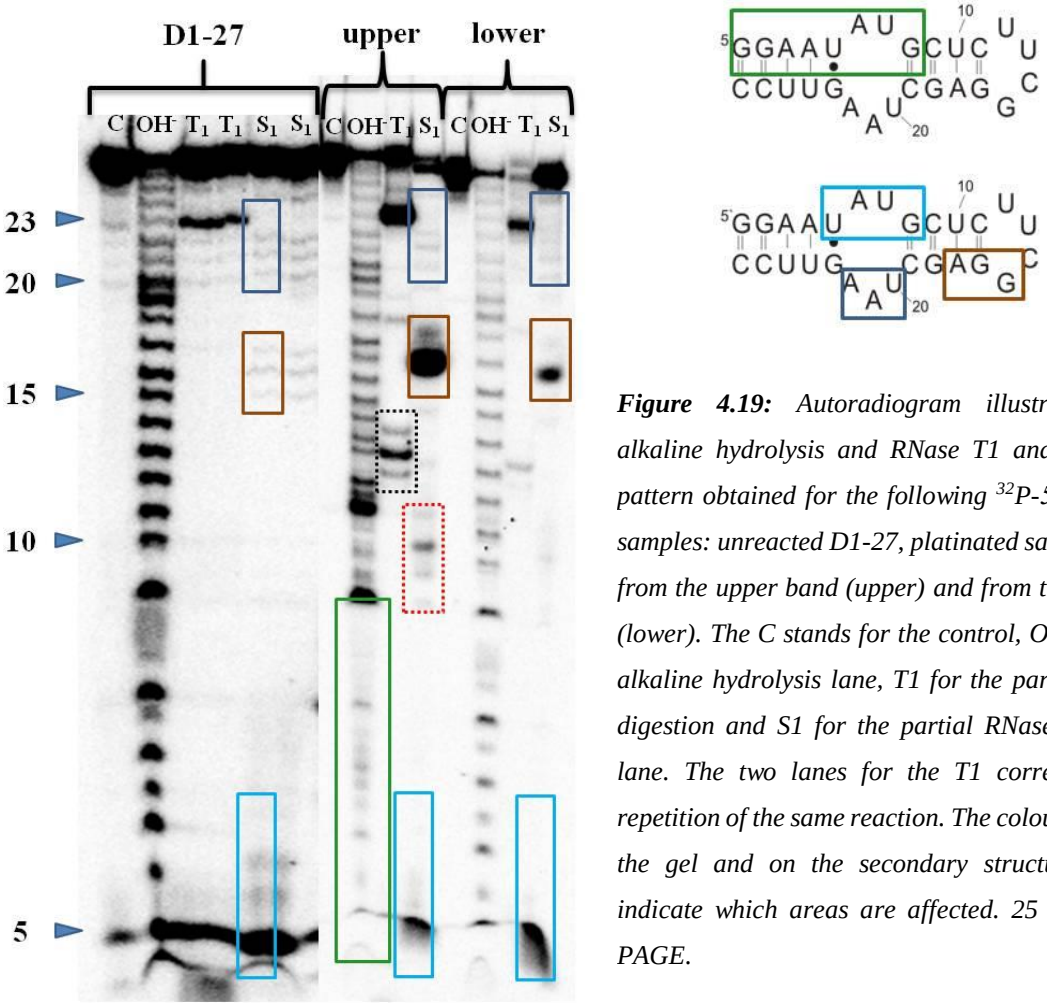

Figure 4.19: *Autoradiogram illustrating partial alkaline hydrolysis and RNase T1 and S1 cleavage pattern obtained for the following ^{32}P-5′-end labelled samples: unreacted D1-27, platinated samples isolated from the upper band (upper) and from the lower band (lower). The C stands for the control, OH^- for partial alkaline hydrolysis lane, T1 for the partial RNase T1 digestion and S1 for the partial RNase S1 digestion lane. The two lanes for the T1 correspond to the repetition of the same reaction. The coloured frames on the gel and on the secondary structure of D1-27 indicate which areas are affected. 25 % denaturing PAGE.*

4.7.4 ^{32}P-3′-end radiolabelling of D1-27

The "splint-method" was used for the ^{32}P-3′-end labelling of D1-27[42,47]. In this method a short DNA template, which is complementary to the 3′-end of the RNA to be labelled and contains three nucleotide overhang (5′-CCG-3′), is hybridized to the RNA. Afterwards, by using the Klenow fragment of DNA polymerase I the 3′-end of the RNA is extended with a single α-^{32}P-labelled dCTP nucleotide (Figure 4.20, left panel).

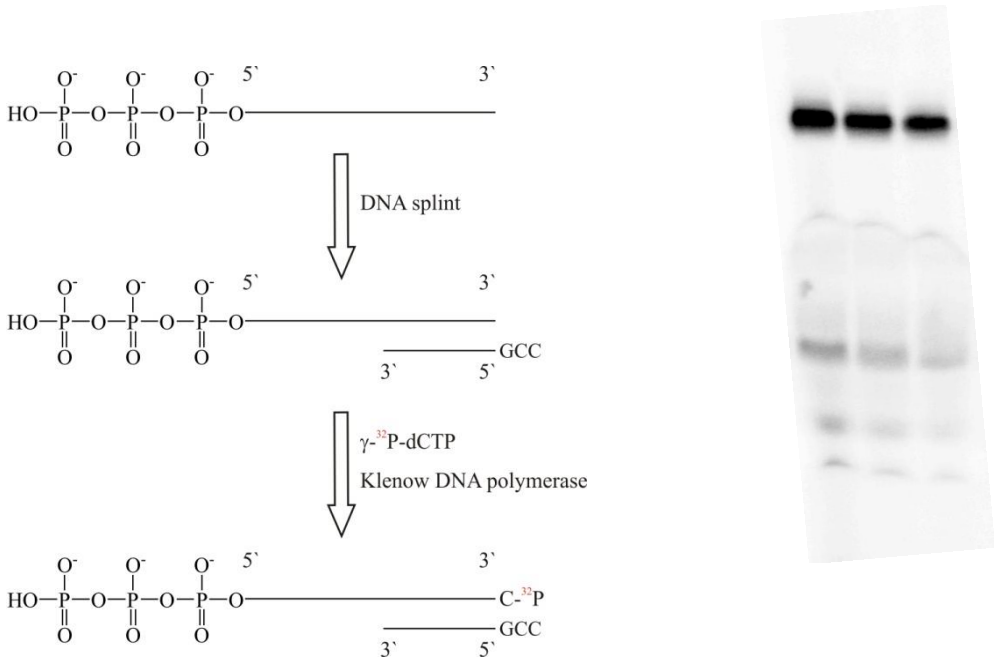

Figure 4.20: *Left panel: Schematic representation of the steps leading to RNA 3′-end labelling[47]. Right panel: Denaturing PAGE of ^{32}P-3′-end labelled D1-27. All three bands correspond to the same reaction. The gel was run at room temperature. 15 % denaturing PAGE.*

This labelling reaction, contrarily to the ^{32}P-5′-end labelling, is template dependent. To obtain a single labelled product it was necessary to find the correct length of the DNA splint as well as the correct number of the overhang nucleotides. For that purpose a 20nt long DNA template with one (5′-G-3′) and three (5′-CCG-3′) nucleotide overhang as well as a 13nt long DNA with three nucleotide overhang (5′-CCG-3′) were tested (Chapter 5, Paragraph 5.10.3). The DNA template that allowed to obtain a single labelled species was the 13nt long DNA with three nucleotide overhang (5′-CCG-3′). Using that DNA template, time dependent and DNA template dependent experiments were performed. From these experiments, the optimal incubation time was found to be 1 h, and the best DNA template concentration was found to be 10 μM. All the labelling reactions were performed at 37 °C. These experimental conditions were used for large scale labelling, in order to get enough material for RNA platination. Even if the labelling efficiency of the 3′-end labelling was lower compared to the 5′-end one, the recovered amount was enough for the platination reactions (Figure 4.20, right panel). The isolation of the 3′-end

labelled RNA from the gel as well as the platination reactions and the isolation of the platinated samples were performed as described above for the 5′-end labelled samples.

4.7.5 Partial alkaline hydrolysis and enzymatic digestions of unreacted and platinated ^{32}P-3′-end labelled D1-27

Partial alkaline hydrolysis and enzymatic digestions were performed for both untreated and platinated RNA (upper and lower band) using the reaction conditions commented above (Paragraph 4.7.2). Twenty-three bands (G1-G23) could be counted on the control lane (D1-27) corresponding to partial alkaline hydrolysis. The most intense bands of the RNase T1 ladder lane corresponded to G1-G2 (Figure 4.21, green frame) and G23 (Figure 4.21, dark blue frame) indicating that these guanines are the most accessible ones. A band corresponding to G23 was observed also during the cleavage studies performed on ^{32}P-5′-end labelled platinated RNA samples. Other faint bands were also observed but did not all correspond to guanines (G15, A17, A22)[15,38,44]. The S1 nuclease lane shows cleavage at the terminal loop (Figure 4.21, brown frame). As in the previous case, the cleavage pattern observed in the case of partial alkaline hydrolysis and of RNase T1 digestion of the species isolated from the lower band was very similar to the control due to the presence of mostly unreacted RNA. However, the internal loop seems to be more accessible to cleavage, as new bands appear in the A4-A6 region (Figure 4.21, light blue frame, S1 lane). This part of the construct is cleaved also in the case of the platinated species of the upper band, suggesting that the lower band contains traces of platinated RNA in addition to the unreacted species, which was in line with the results from the MALDI-MS measurements (Chapter 2, Figure 2.26). The OH^- lane of the species isolated from the upper band shows reduced cleavage intensity at G1-G2 (Figure 4.21, compare red frames) and all the bands were overall less intense compared to the control. The RNase T1 lane suggests that G23 remains the most accessible guanine but reduced cleavage intensity was observed for G1-G2 (Figure 4.21, compare green frames), which was very pronounced for the control. The inhibition of the cleavage at G1-G2 as well as the increased accessibility of A4-A6 upon platination could indicate platination at G1-G2 which made the neighbouring nucleobases (A4 - A6) more accessible. These data are in agreement with the results obtained from the thermal melting studies and enzymatic digestions followed by HPLC analysis, which also suggested G1-G2 as possible platination site.

In conclusion, the experiments performed on both 5′-end and 3′-end labelled samples exclude G23 as possible platination site, since its accessibility remains either similar (in the case of 3′-end labelled samples) or is even increased (in the case of 5′-end labelled samples) upon platination. Moreover, in both cases, different loop accessibility was found upon platination but no consistent behaviour was observed for 5′-end and 3′-end labelled samples, thus preventing detailed comments. Finally, the experiments carried on using 3′-end labelled samples allowed to identify G1-G2 as possible platination site, as previously suggested by other techniques (Paragraphs 4.4 - 4.6).

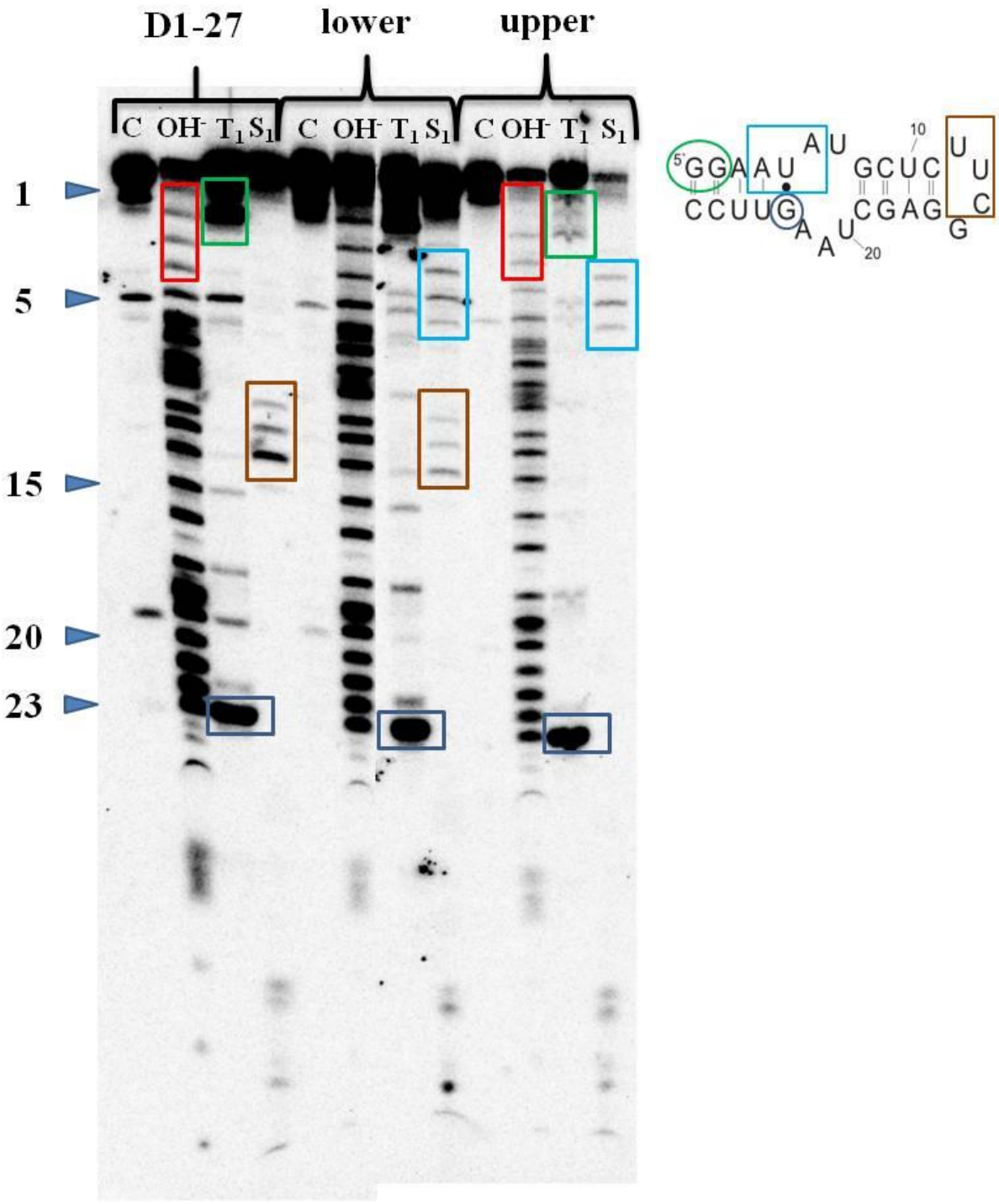

Figure 4.21: *Autoradiogram illustrating partial alkaline hydrolysis and RNase T1 and S1 cleavage pattern obtained for the following ^{32}P-3'-end labelled samples: unreacted D1-27, platinated samples isolated from the upper band (upper) and from the lower band (lower). The C stands for the control, OH^- for partial alkaline hydrolysis, T1 for the partial RNase T1 digestion and S1 for the partial RNase S1 digestion. The coloured frames on the gel and on the secondary structure of D1-27 indicate which areas are affected. 25 % denaturing PAGE. The drawback of the use of ^{32}P-3'-end labelled RNA was the reduced stability of the labelled products, which led to multiple bands at the control lanes that does not allow us to have a better gel picture.*

4.8 NMR characterization of the platinated RNA species isolated from the upper band

1D ^{1}H-NMR experiments were first used to characterize the platinated RNA samples. Large-scale platination reactions were performed in order to obtain the large amounts of platinated RNA samples needed for NMR analysis. An easy and quick way to detect possible platinum(II)-RNA interactions was by comparing the changes of the imino proton resonances of uracil NH3 and guanine NH1 in the unreacted and platinated RNA samples. The changes of the imino proton resonances during the platination reaction were also utilized for the time evolution NMR experiments, which were described in the previous chapter (Chapter 3). Imino protons can exchange rapidly with water, making their signals hardly visible in the spectra. However, when they are involved in stable base-pairing, the exchange is slowed down and the imino proton resonances become sharper and well observable[48]. All the experiments that will be described below were performed in 90 % H_2O:10 % D_2O in the presence of 120 mM $KClO_4$, pH 6.5 at 25 °C (Chapter 5, Paragraph 5.9.2). Spectra were also recorded at lower temperature (4 °C) at which, due to slower molecular tumbling, sharper signal were observed (Chapter 3, Figure 3.2). Imino proton resonances were previously assigned by combining [^{1}H,^{1}H]-NOESY experiments on exchangeable and non-exchangeable protons at different temperatures[49].

^{1}H-NMR spectra of dephosphorylated and 5'-triphosphate D1-27 were first compared. As shown in the previous chapter (Chapter 3, Paragraph 3.3.4, Figure 3.10) the imino proton resonances of the two species were very similar, with the difference that the G1NH1 resonance was slightly upfield shifted upon dephosphorylation. This upfield shift can be related to the absence of the triphosphate. In the same manner, the imino proton resonances of the platinated RNA species isolated from the upper band show very similar behaviour, using either deph-D1-27 or triph-D1-27 as starting material (Appendix 2, Figure A 2.4). For this reason, the NMR characterization which follows refers mainly to platinated triph-RNA adducts, which showed the best spectrum resolution.

In Figure 4.22, are compared the ^{1}H-NMR spectra (imino proton and aromatic region) for 1) non-platinated triph-D1-27 (black line), 2) platinated triph-RNA sample from the upper band (red line) and 3) the corresponding sample from the lower band (magenta line). The imino proton resonances profile of the upper band is different compared to the one of the unreacted RNA. More specifically, the imino proton peaks corresponding to G2 and U25 disappeared, while G8NH1 resonance was reduced in intensity and slightly shifted. The intensity of G23NH1 resonance was also slightly reduced, whereas the imino proton resonances of G15, G16 and G18 remained mostly unaffected. Since U10NH3 and U24NH3 resonances overlap, no safe conclusion on their behaviour can be drawn at this point. Upon platinum(II) binding to RNA the base-pairing at the binding site, as well as the overall RNA structure, could be affected[10] with these changes to be reflected on the changes of the imino proton resonances.

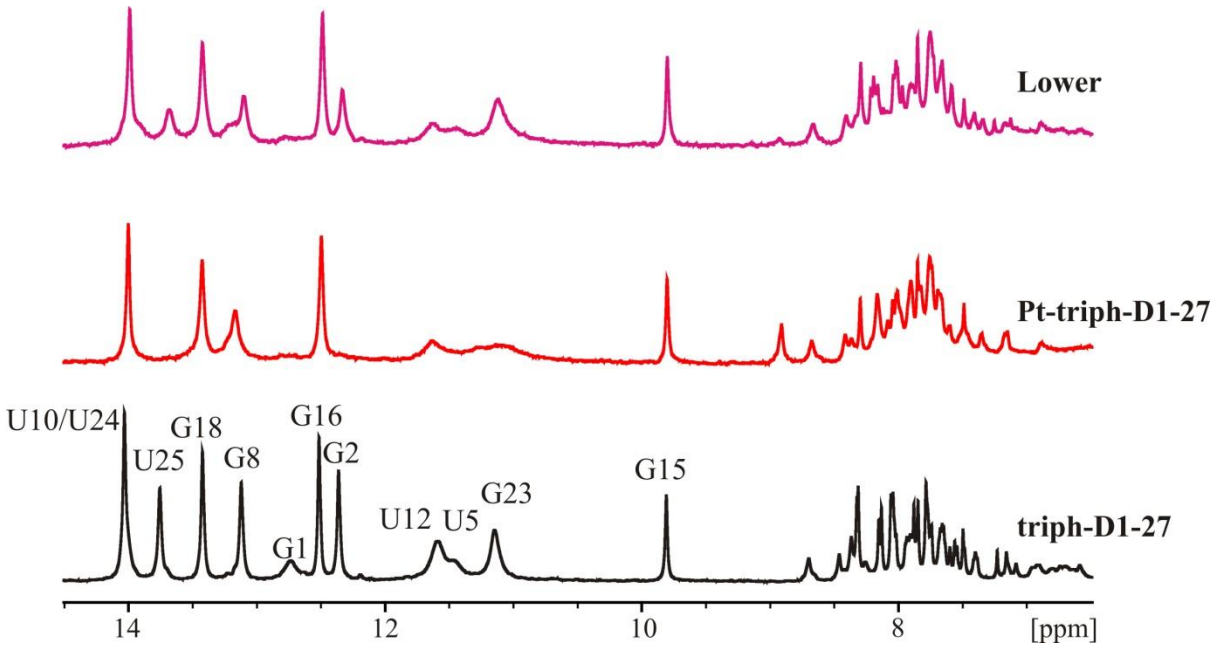

Figure 4.22: *^{1}H-NMR spectra (aromatic and imino proton regions), including imino proton assignment of the untreated D1-27 (black line), Pt-RNA sample isolated from the upper band (red line) and Pt-RNA sample isolated from the lower band (magenta line). The spectra were recorded at 25 °C, in 120 mM $KClO_4$, pH 6, 600 MHz.*

The results commented in the previous paragraphs (Paragraphs 4.4 - 4.7) suggest platination at G1-G2. From the ^{1}H-NMR spectrum of the upper band the disappearance of G2NH1 supports direct platination at this site. In order to get information for the behaviour of the imino proton resonance of G1 (this imino proton resonance is rather low at 25 °C due the dangling bases at the 5′-end[50]) the ^{1}H-NMR spectrum of the isolated Pt-triph-D1-27 sample as well as the unreacted triph-D1-27 were recorded at 4 °C (Appendix 2, Figure A 2.5). At this temperature, the resonance of G1NH1 is sharper and better visible in the unreacted RNA. The absence of G1 and G2 imino proton resonances in the ^{1}H-NMR spectrum of the isolated upper band at this temperature further supports direct platination at this site. As discussed above platination results in hydrogen bond breakage, followed by disappearance of their imino proton resonances. The absence of the U25 imino proton resonance is likely due to structural changes induced locally upon G1-G2 platination, which eventually lead to base-pairing disruption and therefore disappearance of U25NH3 resonance. The shift and intensity decrease of the imino proton peak of G8NH1 may be due to local conformational change of the internal loop, following G1-G2 platination as was also suggested from the time evolution NMR experiments (Chapter 3, Paragraph 3.3.3). The imino proton resonances of the nucleotides located in the second part of the construct (U10-G18) remain mostly unaffected, suggesting little destabilization upon platination, being in line with the thermal melting studies. As far as the aromatic region of the spectra is concerned, the most significant change is the appearance of one (or two) new strongly down-field shifted peak(s) at

around 8.5 - 9 ppm, which may confidently be attributed to H8 of the platinated guanosines[51]. Interestingly, the shift is stronger in the samples prepared using triph-D1-27 as starting material (Appendix 2, Figure A 2.4, black dotted frame). A [^{1}H,^{13}C]-HSQC experiment performed on an isolated platinated sample (Appendix 2, Figure A 2,6, lower panel) confirmed the findings so far commented. As far as guanines are concerned, strong down-field shifts are observed only for C8 resonances of G1 and G2, suggesting direct metal binding to the neighbouring N7 atoms (Appendix 2, Table A 2.1, red boxes in Figure A 2.6, lower panel)[52]. The C8 resonance of G8 does not significantly shift, further suggesting absence of direct platination at this site, while the resonance of G23, barely visible already for the unreacted RNA, is no longer visible in the spectrum of the platinated sample, suggesting dynamics at this site (Appendix 2, Table A 2.1). Similarly, a [^{1}H,^{1}H]-NOESY spectrum recorded on the same sample shows changes in the first part of the construct, and generally sharp peaks are visible in the sequential walk region. Interestingly, a cross peak between A6H2 and A21H2 is present, suggesting that platination does not completely break adenine stacking in the internal loop (Appendix 2, Figure A 2.7).

From the MALDI-MS, it was known that the lower band consists mostly of unreacted RNA, but there was also a small amount of platinated species. As such, the imino proton resonances in the ^{1}H-NMR spectra of the samples isolated from the lower band are very similar to the ones of unreacted D1-27, with a few peaks with reduced intensity and / or shifted (G2, G8 and U25), likely due to the presence of little amount of platinated RNA species (Figure 4.22, magenta line).

The above commented data further support G1-G2 as the preferential platinum(II) binding site of the species which migrates in the upper band, no matters the presence of the triphosphate at the 5′-end. It should be considered though that the appearance of the new faster migrating band observed upon platination of the deph-RNA could be related to the absence of the triphosphate group. Indeed, although G1-G2 remains the preferential binding site, the decreased negative charge at the 5′-end could lead to the formation of other differently platinated RNA species, responsible for the newly observed faster migrating band. The results obtained from all the above mentioned techniques suggest that platinum(II) strongly prefers G1-G2 as binding site. In general, metal ions are crucial for RNA structure and activity and several studies, mostly utilizing NMR spectroscopy, were focused on the elucidation of RNA metal ion binding sites[46,52–55]. The RNA used for this study (D1-27) derives from D1κζ, a three way junction RNA representing the catalytic core of the group II intron ribozyme *Sc*.ai5γ from baker`s yeast (Chapter 1, Paragraph 1.1.4). NMR solution structure and metal ion binding properties of D1κζ were recently reported[52,54]. D1-27 comprises a well-known internal loop, which acts as GAAA tetraloop receptor, and contains three stacked adenines and a U-U mismatch[56,57]. A recent study reported on binding preferences of Mg(II), Cd(II) and Co(III)hexammine towards D1-27. The latest two were used as mimics of inner-sphere and outer-sphere Mg(II) binding respectively. All three metal ions were reported to bind to the 5′-end, favoured by the presence of the negatively charged triphosphate group, while no interactions

was detected in the -UUCG- tetraloop. Generalized electrostatic interaction was observed at the internal loop, with slightly different behaviour between the divalent and trivalent species[46]. Similar behaviour was observed also in our study: platinum(II) binds mainly at the 5′-end, with G1-G2 being the preferential binding site, whereas no interaction was observed at the -UUCG- tetraloop, with the imino proton resonance of G15 remaining almost unaffected upon platination (Figure 4.22). Direct interaction at the internal loop cannot be investigated by looking at the imino proton resonances. However, the results from the different analytic techniques commented so far seem to exclude direct platination at uracil or adenines in the internal loop.

As it was already mentioned in chapter 3, concerning the time evolution NMR experiments, observing the changes of the imino proton resonances is a quick way to determine whether the platinum(II) has an influence on the RNA structure[58] but it also has drawbacks. First, the imino proton resonances are strongly sensitive to different pH and temperature, therefore small changes of the experimental conditions could cause peak shift and broadening. For this reason, special care should be taken, that all the NMR spectra are recorded at the same temperature and pH, in order to be able to attribute the observed differences only to platinum(II) binding. Second, and most important point, changes in the imino proton resonances only give indirect information on platination sites. Indeed, being indicators of base-pairing and therefore used for monitoring the existence or not of a secondary structure, the imino proton resonances could shift or disappear not necessarily due to direct metal-RNA interaction, but due to general structural changes induced by platination close-by. For example, in the case of G8 and U25, their imino proton resonances shifted and disappeared, respectively, without those nucleotides being directly platinated. Direct platination can be identified using different NMR techniques, or other analytical methods. In our case, enzymatic digestion (Paragraph 4.6) excluded platination at adenines, which are known to be possible platination sites for oxaliplatin, and confirmed GG platination.

Summing up, even if the changes in imino proton resonances do not allow to distinguish between direct platination and platination close-by, they give fast qualitative information on the binding site, which can be confirmed by combining data from other analytic techniques.

4.9 Sequence- and structure specificity of oxaliplatin with RNA

Guanine and adenine bases represent the main target for platinum(II) complexes both for DNA[59] and RNA[6]. In the case of cisPt, the most frequently observed platinated adducts with DNA are the 1,2-d(GG) (65 %) and the 1,2-d(AG) (25 %) intrastrand cross-links. However, recent studies on oxaliPt-RNA interactions have revealed that it tends to form both intrastrand adducts but also adducts involving only adenines have been indentified[6,60]. Our study showed that the main platinated adduct obtained by reacting D1-27 with oxaliplatin contains a 1,2-(GG) intrastrand crosslink at the 5'-end, involving G1 and G2. G1-G2 binding was preferred over G15-G16, located at the terminal loop. The

absence of platination in this latter case is likely due to the arrangement of the two guanosines, which point their N7 opposite from each other, thus not offering the ideal geometry for GG intrastrand platination (Chapter 3, Figure 3.8). Our results suggest that the presence or absence of the triphosphate group did not play a role in the G1-G2 binding of oxaliPt, given that similar platination behaviour was observed in both cases. Indeed, the main platinated RNA species formed are platinated at G1-G2, and migrate in the upper band, by using both triph-RNA and deph-RNA (Chapter 2, Figure 2.26 and 2.45) as starting material. Structure specificity of platinum(II) binding has been reported[61]. For example, Elmroth and co-workers suggested the G-U wobble base pair as binding site for cisPt[37,44]. DeRose and co-workers reported the cross-linking by cisPt of two guanines located at opposite site of an internal loop[15]. A very recent 2.6 Å-resolution crystal structure of a cisplatin-modified 70S ribosome provided us with new insights into platinum(II)-RNA interactions[62] (Chapter 1, Paragraph 1.3.5). Nine platinum(II) modifications were found in the whole ribosome, despite the presence of two thousand two hundred N7-atoms with similar solvent accessibility as the nine platinated sites. This finding suggests that RNA platination is not only defined by spatial accessibility. Additionally, it was suggested that specific structural motifs may represent preferential platination sites, and differences in adenine *vs* guanine binding were described.

The RNA used in the current study contains several common RNA structural features like G-U wobble base pair, internal and terminal loop as well as various guanines and adenines which could act as platinum(II) binding sites. Despite its complicated profile and the many platination sites available, a strong preference for the 5′-end G1-G2 site was observed for oxaliplatin. This high selectivity of oxaliPt for GG sites is in line with similar results reported recently from cisplatin interaction of bacterial ribosomal RNA hairpins[38].

4.10 RNA UU

To study the effect of platination at the G1-G2 site a new RNA construct, which is an analogue of D1-27, was used, in which the first two G-C base-pairs were replaced by U-A base-pairs (RNAUU) (Figure 4.23, bottom). ^{1}H-NMR spectra, thermal melting studies and CD measurements were recorded on this new construct. The data obtained were compared with the corresponding data from non-platinated and platinated D1-27. The ^{1}H-NMR spectrum of RNAUU showed less imino proton resonances than expected (Figure 4.24, red line). Their assignment was based on comparison with the imino proton resonances of D1-27, and confirmed by a [^{1}H,^{1}H-NOESY]

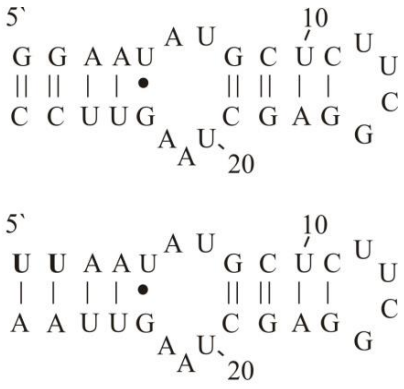

Figure 4.23: Secondary structures of D1-27 (top) and RNAUU (bottom).

spectrum recorded at 4 °C. Interestingly, no clear imino proton resonances for U1, U2, U24 and U25 could be identified, suggesting that the first part of the construct is very unstable. This is likely due to the presence of consecutive U-A base-pairs at the 5'-end, which resulted in destabilizing the first part of the construct and led to the disappearance of the imino proton peaks of the first nucleotides. Interestingly, the pattern of the ^{1}H-NMR spectrum of the RNAUU construct was almost identical to the one of the platinated RNA species isolated from the upper band, suggesting that the presence of platinum(II) at the G1-G2 site has similar effect on the stability of the RNA construct like the replacement of a stable G-U for an U-A base-pair (Figure 4.24, blue and red lines).

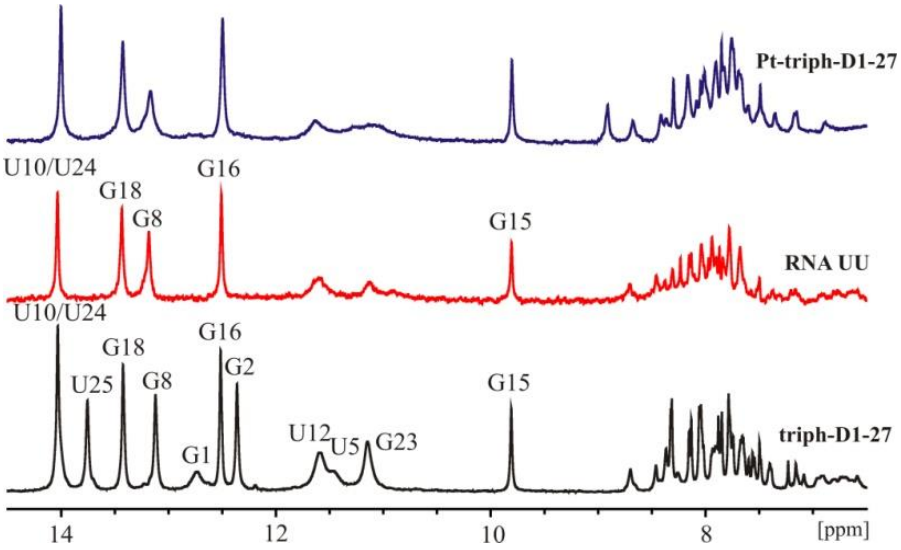

Figure 4.24: *^{1}H-NMR spectra (aromatic and imino proton regions), including imino proton assignment, of RNAUU (red line), Pt-triph-D1-27 (blue line) and non-platinated triph-D1-27(black line). The spectra were recorded at 25 °C, in 120 mM $KClO_4$, pH 6, 600 MHz.*

Next, the thermal melting profile of RNAUU was recorded. Similarly to D1-27, also for this construct two melting temperatures could be identified (Appendix 2, Figure A 2.8). Interestingly, Tm_1 of RNAUU was much lower than the one of D1-27 ($\Delta Tm = 20.4 \pm 3.1$ °C) while Tm_2 was very similar (Table 4.3). This suggests that the first part of the construct is highly destabilized, which also justifies the absence of the imino proton resonances corresponding to this part of the construct (Figure 4.24, red line). Changes of Tm_1 and almost unaffected Tm_2 were also reported for our isolated platinated RNA species (Paragraph 4.4), even if ΔTm_1 was not as pronounced as it was found for RNAUU (Table 4.2).

Table 4.3: Summary of the melting temperatures for the deph-D1-27, Pt-deph- D1-27 and RNAUU constructs. The given Tm values are the average of at least five measurements. The errors of the melting temperatures correspond to standard deviation. The errors of the ΔTm were estimated using the standard error propagation calculations[18].

RNA construct	Tm_1 (°C)	ΔTm_1 (°C)	Tm_2 (°C)	ΔTm_2 (°C)
Deph-D1-27_pH 6.5	52.2 ± 2.1	-	74.2 ± 3.0	-
Pt-deph-D1-27_pH 6.5	44.8 ± 2.5	7.4 ± 3.3[a]	77.8 ± 1.0	3.6 ± 3.2[a]
Pt-triph-D1-27_pH 5	31.8 ± 2.3	20.4 ± 3.1[b]	76.4 ± 1.0	2.2 ± 3.2[b]

[a] The values refer to the difference between melting temperatures of D1-27 and platinated D1-27. [b] The values refer to the difference between melting temperatures of deph-D1-27 and RNAUU.

Lastly, the CD spectrum of RNAUU shows the characteristic pattern for an A-form RNA, but compared to the corresponding spectrum of deph-D1-27 few differences were found (Figure 4.25, black and blue line). Bathochromic shift of the band at 260 nm and reduced intensity of the band at 210 nm were observed. The changes at 260 nm can be attributed to changes of the helical parts of the RNA, while the changes of the 210 nm band may be connected with changes at the loop regions[23–25]. The destabilization of the first part of RNAUU due to replacement of the G-C with U-A base-pairs may be responsible for the bathochromic shift of the band at 260 nm , while the changes at 210 nm may reflect changes of the internal loop (the terminal loop is expected not to be affected based on the value of Tm_2 (Table 4.3). The bathochromic shift of the band at 260 nm was a characteristic observed in all Pt(II)-RNA adducts studied here showing that platinum(II) binding affects the base-pairing while only slight changes were observed for the band at 210 nm (Figure 4.25, red line) suggesting that the internal loop is not significantly affected upon platination.

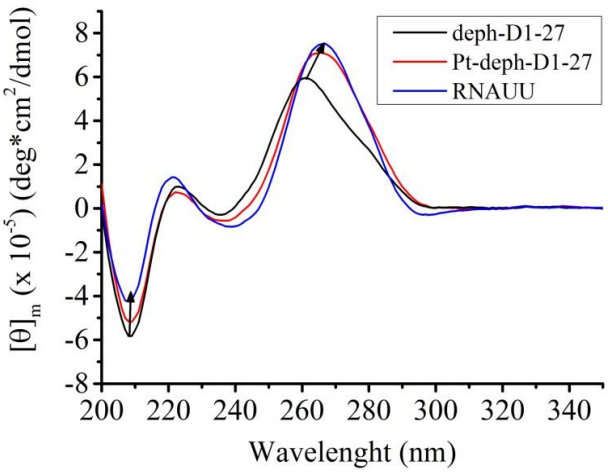

Figure 4.25: *Comparison of the CD spectra of deph-D1-27 (black), RNAUU (blue line) and Pt-deph-D1-27 (red line). C_{RNA} /$C_{Pt\text{-}RNA}$ = 1.3 μM, in 120 mM $KClO_4$, pH 6.5.*

Summing up, the RNAUU construct was used as a model RNA in order to investigate the effect of platination at the G1-G2 site. The two U-A base-pairs that were used instead of the more stable G-C ones could mimic the modification induced upon platination considering that the platinum(II) binding to nucleobases induces RNA destabilization. The characterization of RNAUU showed that the latter has a very similar behaviour as the Pt(II)-RNA adducts. The imino proton resonance profile of both species was almost identical suggesting the presence of similar structural modifications (Figure 4.24, red and blue line). Additionally, in both cases the first melting temperature was mostly affected, even if in the case of RNAUU a much larger ΔTm_1 was found (Table 4.3), suggesting stronger destabilization in this case. From the comparison of the CD spectra, a bathochromic shift of the band at 260 nm was seen for both the species, while only RNAUU showed significant change of the intensity of the band at 210 nm, indicating that the internal loop was probably affected. This is in line with the large ΔTm_1 found for RNAUU and suggests that in the case of the platinated RNA species the destabilization induced upon platination was not as pronounced as for the RNAUU species to influence the internal loop structure. Therefore, this comparison further supports the platination at the G1-G2 site and additionally suggests that the degree of changes upon platination is similar to some extent to the one induced by substituting the first two G-C base pairs with less stable U-A base-pairs.

4.11 Conclusions

The characterization of the Pt-RNA adducts migrating in the upper band was performed using various methods. Platinated adducts obtained using homogeneous Pt-deph-RNA as starting material were mainly characterized. However, very similar behaviour was observed for the Pt-triph-RNA adducts, thus suggesting the same platination pattern for the upper band species in the two cases. Each technique used provided us with an information about the binding of oxaliPt to the RNA. The thermal melting studies showed that the platination affects significantly only the first part the RNA construct, because only Tm_1 changed upon platination. Therefore, platination in this area was suggested. The observed reduction of Tm_1 compared to the unreacted RNA indicates destabilization of the RNA construct upon platinum(II) binding, thus suggesting intrastrand cross-link. Information about the binding sites could not be provided from this method. The CD spectra of the unreacted and platinated RNA showed that the platination did not change the overall RNA conformation, and the little changes observed are likely due to local perturbations caused by the presence of the platinum(II) moiety. More specifically the bathochromic shift of the band at 260 nm can be connected to intrastrand platinum(II) binding to RNA. The first indication about a possible platination site came from the enzymatic digestion / HPLC treatment of the non-platinated and platinated RNA species. The platinated RNA species have an extra peak in the HPLC chromatogram and from the comparison of the relative peak areas a loss of two guanines was postulated. The new peak has the same retention time as the Pt-GG species, which was formed upon platination of the GpG dinucleotide, thus suggesting platination at a GG site. Combining

the information collected so far, it seemed that two adjacent guanines were platinated, which should be located in the first part of the construct. The only two guanines fulfilling these criteria are G1 and G2. Further characterization, like ^{32}P-5′- and ^{32}P-3′-end radiolabelling techniques were employed in order to get information about the platination site. The ^{32}P-5′-end labelling approach showed that G23, which is located in the first part of the construct, is not directly platinated. However, no information on the first two nucleotides could be obtained with this technique. Therefore, we moved to ^{32}P-3′-end labelling, which showed changes of the intensity of the gel bands corresponding to G1 and G2 upon platination. This suggests platination at G1-G2, in agreement with the previous findings. At the end, ^{1}H-NMR spectra were recorded on isolated samples, and comparison of the imino proton resonances before and after platination was performed. The guanine imino proton resonances mostly affected by platination correspond to G1 and G2. Interestingly, the imino proton resonances of the sample isolated from the upper band are very similar to the ones of the RNAUU construct, confirming destabilization at the 5'-end in the presence of platinum(II), thus further supporting G1-G2 platination. Further confirmation that platination occurs at G1-G2 site came from the [^{1}H,^{13}C]-HSQC experiment performed on an isolated platinated sample, which suggests direct platination at these two guanines.

Summing up, upon interaction of oxaliPt with D1-27 under the experimental conditions used for this study, despite the presence of many possible platinum(II) binding sites, strong preference for platination at G1-G2 was observed, leading to monoplatinated RNA species with decreased gel mobility. The GG site of DNA is the most common platinum(II) binding site for platinum(II) anticancer complexes[59] and strong preference for this motif has been reported also for RNA platination with cisplatin[38]. Our data revealed that oxaliplatin also showed a strong preference for the most accessible GG site (G1-G2) which is in line with the currently reported finding on RNA platination.

4.12 Analysis and characterization of the platinated RNA species isolated from the lower band

As described in chapter 2, dephosphorylated RNA was used in order to have a homogeneous starting material (Paragraph 2.9). Interestingly, the number of bands on the gel increased from two to three when deph-RNA was used. More specifically a new faster migrating band appeared, which, from the MALDI-MS analysis, was found to contain a mixture of monoplatinated and diplatinated RNA, like the upper band, with the difference that the relative intensity of the diplatinated RNA species was higher (Chapter 2, Paragraph 2.9, Figure 2.45). Faster migrating bands upon platination of RNA were reported to contain cross-linked platinated RNA species[15]. Additionally, in our case, platination at different sites than G1-G2 (which was found for the species migrating in the upper band) could lead to more compact RNA conformation, resulting in the faster migrating band. To investigate the nature of the platinated

species responsible for this band, their characterization with CD, thermal melting studies and enzymatic digestion/ HPLC was performed. The analysis were carried out by using several different samples.

The thermal melting studies performed revealed that both melting temperatures were very similar to the untreated RNA (Table 4.4) while for the sample from the upper band the Tm_1 was significantly reduced. Similar melting temperatures to untreated RNA suggest that the changes induced upon platination did not affect RNA stability. This fact excludes the presence of platinum(II) cross-linked species, which would have stabilized the RNA construct resulting in increased melting temperatures.

Table 4.4: *Summary of the melting temperatures for deph- D1-27 as well as for its platinated adducts isolated from the upper and lower band. The given Tm values are the average of at least five measurements and are reported together with their standard deviation.*

RNA construct	Tm_1 (°C)	Tm_2 (°C)
Deph-D1-27_pH 6.5	52.2 ± 2.1	74.2 ± 3.0
Pt-deph RNA lower band_pH 6.5	52 ± 2.4	77.5 ± 1.6
Pt-deph RNA upper band_pH 6.5	44.8 ± 2.5	77.8 ± 1.0

The investigation of the nucleobases affected by platination using enzymatic digestion/HPLC was then performed. In the case of the platinated species isolated from the upper band, the analysis showed that the guanine content was reduced by two, and that a new peak appeared in the chromatogram, which had the same retention time as the independently prepared Pt-GpG species (Figure 4.11). In the case of the species isolated from the lower band, a new broader peak at the same retention time as before (26 min) appeared (Figure 4.26, right, lower panel) but the nucleobases affected differed from sample to sample. In some cases there was reduction by one G and one A, and in other cases there was reduction by one G and one U. That could indicate the formation of either GpA/ApG-Pt and GpU/UpG-Pt species or could correspond to a mixture of Pt-G / Pt-A and Pt-G / Pt-U monodentate platinum(II) species. Monodentate platination mode do not affect significantly the structure of the RNA (or DNA) and as such no significant changes of the melting temperature of the Pt(II)-RNA species are expected as well as no significant changes of their gel band mobility on a gel. Formation of these species could be in agreement with the results from the thermal melting study where Tm similar to the unreacted RNA were observed but is in contrary with the way that the band was migrating on the gel (faster migrating band). Given that the digestion studies indicated different nucleobases being affected compared to the upper band species, the fact that the peak corresponding to the platinum(II) containing moiety has the same retention time (26 min) in the two cases (upper and lower band) was somehow surprising. However, from a closer look of the new peak in the case of the lower band products (Figure 4.26, right, lower panel), it can be seen that the peak is broader than the one observed in the case of the upper band

products (Figure 4.26, right upper panel). This finding suggests that it consists of more than one species, whose nature is difficult to assess.

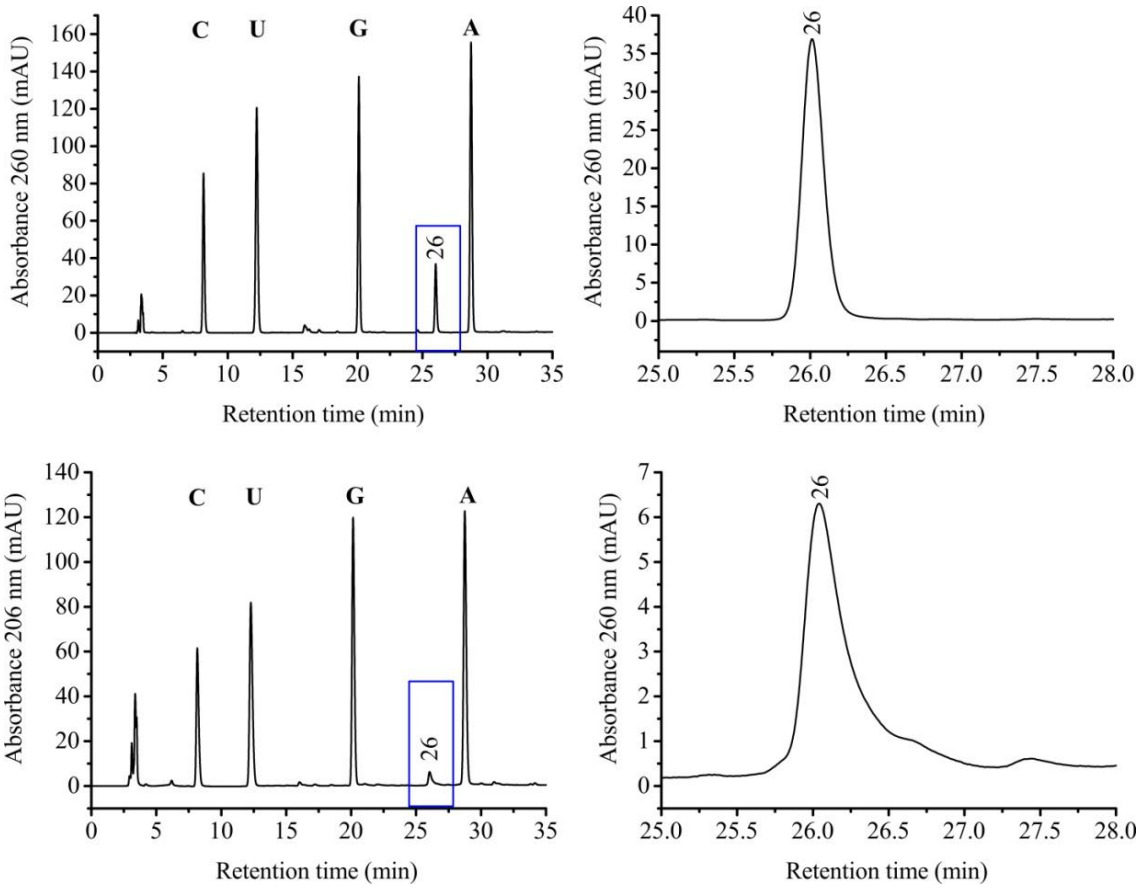

Figure 4.26: *Upper panel, left: HPLC chromatogram of the platinated RNA species isolated from the upper band, right: Zoom of the newly appeared peak at 26 min. Lower panel, left: HPLC chromatogram of the platinated RNA species isolated from the lower band, right: Zoom of the newly appeared peak at 26 min.*

With guanines and adenines being the most probable binding sites for oxaliPt[6], platination reactions of the dinucleotides GpG, GpA and ApG were performed[35] to investigate the nature of the composite peak observed in the case of the lower band species. Additional reactions were performed with 1:1:1 ratio of oxaliplatin and either AMP, GMP or a mixture of the two[35] (Appendix 2, Figure A 2.9). The platination of the dinucleotides led to the formation of platinated species, which eluted earlier compared to the peak at 26 min, excluding the possibility of having the formation of Pt-ApG and/ or Pt-GpA species (Appendix 2, Figure A 2.9). The reactions of oxaliPt with 2 eq of GMP and 1:1 GMP and AMP did not result in peaks which could have helped with the interpretation of the new peak from the lower band (at 26 min) with the peaks appearing having different retention time than 26 min (Appendix 2, Figure A 2.10). However, the reactions of oxaliPt with 2 eq of AMP was more informative. The main peak appeared in this latter case had retention time of 26.5 min, that is very similar to the new peak observed for the species isolated from the lower band. The presence of a mixture of Pt-GpG and A-Pt-A species

could be then responsible for the broad band observed (Figure 4.27). However, if only G and A were affected, we should have observed a loss of two guanosines and two adenosines, which was not the case. Therefore, with the current data, we can only conclude that the lower band contains multiple species platinated at different sites, which are not as homogeneous as the species isolated from the upper band.

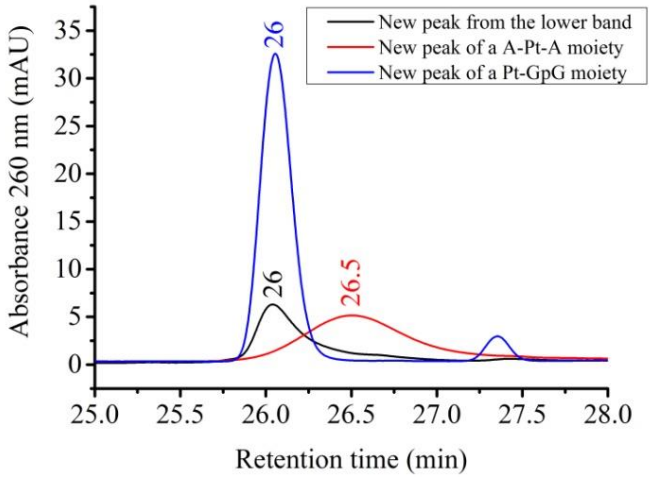

Figure 4.27: *HPLC chromatogram zoomed on the newly appeared peaks corresponding to Pt-GG moiety (blue line), to A-Pt-A moiety (red line) and to platinated RNA sample isolated from the lower gel band (black line). The mixture of Pt-GG and A-Pt-A moieties could be responsible for the tailing of the black line.*

The CD measurements of the platinated species isolated from the lower band revealed that, similarly to the species isolated from the upper band, the overall A-form conformation of the RNA was retained. Additionally, the bathochromic shift of the positive band at 260 nm was also observed, without though any change of the intensity. The only difference detected was the more pronounced reduction of intensity of the negative band at 210 nm suggesting further destabilization of the loops upon platination[21,22] in this case (Figure 4.28).

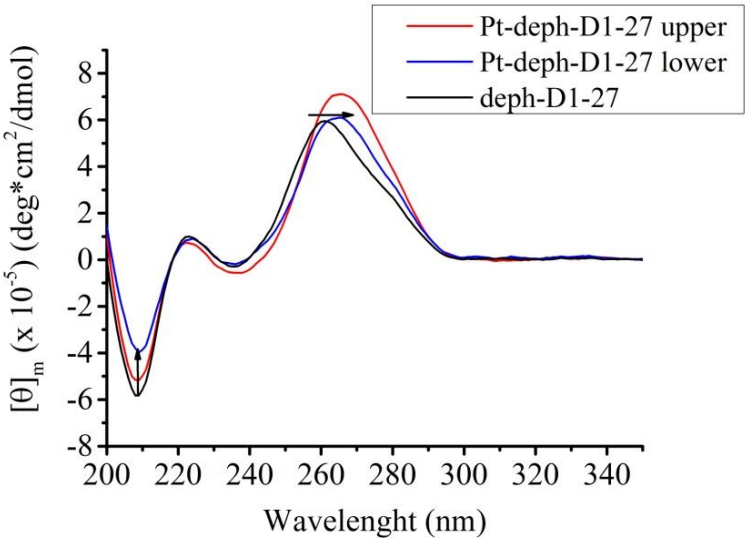

Figure 4.28: *Comparison of the CD spectra of deph-D1-27 (black) and the platinated deph-D1-27 isolated from the upper (red) and from the lower band (blue).* C_{RNA} */*$C_{Pt\text{-}RNA}$ *= 1.3 μM, in 120 mM* $KClO_4$*, pH 6.5.*

Summing up, the data collected on the platinated RNA species migrating in the lower band showed that their stability is similar to that of the untreated RNA, since similar thermal melting temperatures were observed (Table 4.4). This excluded the presence of platinum(II) cross-linked species, which was hypothesized due to the appearance of the faster migrating gel band. Indeed, if cross-linked species were present, stabilization of the construct was to be expected. Considering that the appearance of the faster migrating band was very reproducible, a possible scenario for the unexpected melting temperature observed was the transformation of the platinated RNA species upon isolation from the gel. The cross-linked RNA, which was initially formed, could be upon isolation transformed in a form which does not alter significantly the stability of the RNA[63]. Then, the CD signal of the platinated species isolated from the lower band suggested an overall similar conformation as the species isolated from the upper band, even if the negative band at 210 nm was more affected than before (Figure 4.28). Changes at the band at 210 nm is connected with changes at the loop regions, which could potentially explain the different mobility on the gel. The enzymatic digestion/ HPLC characterization clearly showed that different nucleobases were affected upon platination compared to the species isolated from the upper band. However, no precise information on the nature of the affected nucleotides were collected. The platinated RNAs migrating in the lower band represent secondary species considering that the main ones are platinated at the G1-G2 site. As such, they could be strongly influenced by slight changes of the experimental conditions. Additionally, the MALDI-MS spectra of the isolated species showed that they contained increased amount of diplatinated RNA compared to the species from the upper band making the interpretation of the results more difficult. Therefore, no clear conclusion could be drawn about the way that platinum(II) was bound to D1-27 in the case of the species isolated from the lower band.

In conclusion, even if different platinated species seem to be present in the lower migrating band as well as in the band containing unreacted RNA, they were not characterized because, in the first case they seem to be non-homogeneous, whereas in the second case it was not possible to separate them from unreacted RNA in our experimental conditions. For this reason, only the main homogeneous platinated species responsible for the slower migrating band was fully characterized, as extensively commented in this chapter.

4.13 References

1. *Encyclopedia of Life Sciences. Nucleic Acids: Thermal Stability and Denaturation* (John Wiley & Sons, Ltd, Chichester, UK, 2001).
2. Jean-Louis Mergny, Laurent Lacroix. Analysis of thermal melting curves. *Oligonucleotides* **13,** 515–537 (2003).
3. Laing, L. G. & Draper, D. E. Thermodynamics of RNA folding in a conserved ribosomal RNA domain. *J. Mol. Biol.* **237,** 560–576 (1994).
4. Serra, M. J. & Turner, D. H. Predicting thermodynamic properties of RNA. *Methods Enzymol.* **259,** 242–261 (1995).
5. Polonyi, C., Albertsson, I., Damian, M. S. & Elmroth, S. K. Comparison of cis- and oxaliplatin-induced destabilization of 15-mer DNA- and RNA duplexes by binding to centrally located GG- and GNG sequences. *Z. Anorg. Allg. Chem.* **639,** 1655–1660 (2013).
6. Snygg, A. S. & Elmroth, S. K. Expanding the chemical nature of siRNAs: oxaliplatin as metalation reagent. *Biochem. Biophys. Res. Commun.* **379,** 186–190 (2009).
7. Hagerlof, M., Papsai, P., Chow, C. S. & Elmroth, S. K. More pronounced salt dependence and higher reactivity for platination of the hairpin r(CGCGUUGUUCGCG) compared with d(CGCGTTGTTCGCG). *J. Biol. Inorg. Chem.* **11,** 974–990 (2006).
8. Coste, F., Malinge, J.-M., Serre, L., Leng, M., Zelwer, C., Shepard, W. & Roth, M. Crystal structure of a double-stranded DNA containing a cisplatin interstrand cross-link at 1.63 A resolution. Hydration at the platinated site. *Nucleic Acids Res.* **27,** 1837–1846 (1999).
9. Malinge, J.-M., Giraud-Panis, M.-J. & Leng, M. Interstrand cross-links of cisplatin induce striking distortions in DNA. *J. Inorg. Biochem.* **77,** 23–29 (1999).
10. Paquet, F., Perez, C., Leng, M., Lancelot, G. & Malinge, J.-M. NMR solution structure of a DNA decamer containing an interstrand cross-link of the antitumor drug cis-diamminedichloroplatinum (II). *J. Biomol. Struct. Dyn.* **14,** 67–77 (1996).
11. Ramachandran, S., Temple, B. R., Chaney, S. G. & Dokholyan, N. V. Structural basis for the sequence-dependent effects of platinum-DNA adducts. *Nucleic Acids Res.* **37,** 2434–2448 (2009).
12. Takahara, P. M., Rosenzweig, A. C., Frederick, C. A. & Lippard, S. J. Crystal structure of double-stranded DNA containing the major adduct of the anticancer drug cisplatin. *Nature* **377,** 649–652 (1995).
13. Todd, R. C. & Lippard, S. J. Structure of duplex DNA containing the cisplatin 1,2-$\{Pt(NH_3)_2\}^{2+}$-d(GpG) cross-link at 1.77 A resolution. *J. Inorg. Biochem.* **104,** 902–908 (2010).

14. van Boom, S. S., Yang, D., Reedijk, J., van der Marel, G. A. & Wang, A. H. Structural effect of intra-strand cisplatin-crosslink on palindromic DNA sequences. *J. Biomol. Struct. Dyn.* **13,** 989–998 (1996).

15. Hostetter, A. A., Chapman, E. G. & DeRose, V. J. Rapid cross-linking of an RNA internal loop by the anticancer drug cisplatin. *J. Am. Chem. Soc.* **131,** 9250–9257 (2009).

16. Lando, D. Y., Chang, C.-L., Fridman, A. S., Grigoryan, I. E., Galyuk, E. N., Hsueh, Y.-W. & Hu, C.-K. Comparative thermal and thermodynamic study of DNA chemically modified with antitumor drug cisplatin and its inactive analog transplatin. *J. Inorg. Biochem.* **137,** 85–93 (2014).

17. Lando, D. Y., Galyuk, E. N., Chang, C.-L. & Hu, C.-K. Temporal behavior of DNA thermal stability in the presence of platinum compounds. Role of monofunctional and bifunctional adducts. *J. Inorg. Biochem.* **117,** 164–170 (2012).

18. Bevington, P. R. & Robinson, D. K. Data reduction and error analysis for the physical sciences. 3rd ed. (McGraw-Hill, Boston, 2003).

19. Kypr, J., Kejnovska, I., Renciuk, D. & Vorlickova, M. Circular dichroism and conformational polymorphism of DNA. *Nucleic Acids Res.* **37,** 1713–1725 (2009).

20. Ranjbar, B. & Gill, P. Circular dichroism techniques: biomolecular and nanostructural analyses- a review. Biomolecular and Nanostructural Analyses- A Review. *Chem. Biol. Drug Des.* **74,** 101–120 (2009).

21. Stampfl, S., Lempradl, A., Koehler, G. & Schroeder, R. Monovalent ion dependence of neomycin B binding to an RNA aptamer characterized by spectroscopic methods. *Chembiochem* **8,** 1137–1145 (2007).

22. McPike, M. P. Footprinting, circular dichroism and UV melting studies on neomycin B binding to the packaging region of human immunodeficiency virus type-1 RNA. *Nucleic Acids Res.* **30,** 2825–2831 (2002).

23. Kruschel, D. & Sigel, R. K. Divalent metal ions promote the formation of the 5'-splice site recognition complex in a self-splicing group II intron. *J. Inorg. Biochem.* **102,** 2147–2154 (2008).

24. Bursova, V., Kasparkova, J., Hofr, C. & Brabec, V. Effects of monofunctional adducts of platinum(II) complexes on thermodynamic stability and energetics of DNA duplexes. *Biophys. J.* **88,** 1207–1214 (2005).

25. Macquet, J. & Butour, J. A circular dichroism study of DNA · Platinum complexes. *Eur. J. Biochem.* **83** (1978).

26. Reeder, F., Gonnet, F., Kozelka, J. & Chottard, J.-C. Reactions of the double-stranded oligonucleotide d(TTGGCCAA)$_2$ with cis-[Pt(NH$_3$)$_2$(H$_2$O)$_2$]$^{2+}$ and [Pt(NH$_3$)$_3$(H$_2$O)]$^{2+}$. *Chem. Eur. J.* **2,** 1068–1076 (1996).

27. Kjellström, J. & Elmroth, S. K. Similar rates for platination of hairpin loops and single-stranded DNA. *Dalton Trans.,* 2867–2871 (2003).

28. Meroueh, M., Kjellström, J., Mårtensson, K., Elmroth, S. K. & Chow, C. S. Reactions of platinum(II) complexes with a DNA hairpin, d(CGCGTTGTTCGCG):Structural characterization and kinetic studies. *Inorg. Chim. Acta* **297,** 145–155 (2000).

29. Baruah, H. & Bierbach, U. Biophysical characterization and molecular modeling of the coordinative-intercalative DNA monoadduct of a platinum-acridinylthiourea agent in a site-specifically modified dodecamer. *J. Biol. Inorg. Chem.* **9,** 335–344 (2004).

30. Shimelis, O. & Giese, R. W. Nuclease P1 digestion/high-performance liquid chromatography, a practical method for DNA quantitation. *J. Chromatogr. A* **1117,** 132–136 (2006).

31. Wietstock, S. M. DNA composition analysis by nuclease digestion and HPLC. *J. Chem. Educ.* **72,** 950 (1995).

32. Mowaka, S. & Linscheid, M. Separation and characterization of oxaliplatin dinucleotides from DNA using HPLC-ESI ion trap mass spectrometry. *Anal. Bioanal. Chem.* **392,** 819–830 (2008).

33. Giese, R. W., Shimelis, O. & Zhou, X. Scaled-down nuclease P1 for scaled-up DNA digestion. *Biotechniques* **34,** 908–909 (2003).

34. Ranogajec, A., Beluhan, S. & Smit, Z. Analysis of nucleosides and monophosphate nucleotides from mushrooms with reversed-phase HPLC. *J. Sep. Sci.* **33,** 1024–1033 (2010).

35. Zayed, A., Jones, G. D. D., Reid, H. J., Shoeib, T., Taylor, S. E., Thomas, A. L., Wood, J. P. & Sharp, B. L. Speciation of oxaliplatin adducts with DNA nucleotides. *Metallomics* **3,** 991–1000 (2011).

36. Aldag, J., Åse, S. S., Papsai, P. & Elmroth, S. K. C. Platination of full length tRNA^{Ala} and truncated versions of the acceptor stem and anticodon loop. *Dalton Trans.*, 5225 (2008).

37. Papsai, P., Aldag, J., Persson Tina, J. & Elmroth, S. K. Kinetic preference for interaction of cisplatin with the G–C-rich wobble basepair region in both tRNA^{Ala} and Mh^{Ala}. *Dalton Trans.,* 3515–3517 (2006).

38. Dedduwa-Mudalige, G. N. P. & Chow, C. S. Cisplatin targeting of bacterial ribosomal RNA hairpins. *Int. J. Mol. Sci.* **16,** 21392–21409 (2015).

39. Hedman, H. K., Kirpekar, F. & Elmroth, S. K. Platinum interference with siRNA non-seed regions fine-tunes silencing capacity. *J. Am. Chem. Soc.* **133,** 11977–11984 (2011).

40. Pluim, D., Maliepaard, M., van Waardenburg, R. C., Beijnen, J. H. & Schellens, J. H. ^{32}P-Postlabeling assay for the quantification of the major platinum-DNA adducts.

41. Chapman, E. G. & DeRose, V. J. Enzymatic processing of platinated RNAs. *J. Am. Chem. Soc.* **132,** 1946–1952 (2010).

42. Hilario, E. End labelling procedures. *Methods Mol. Biol.* **28,** 77–80 (2004).

43. Biondi, E. & Burke, D. H. RNA structural analysis by enzymatic digestion. *Methods Mol. Biol.* **1086,** 41–52 (2014).

44. Papsai, P., Snygg, A. S., Aldag, J. & Elmroth, S. K. Platination of full-length tRNA^{Ala} and truncated versions of the acceptor stem and anticodon loop. *Dalton Trans.*, 5225–5234 (2008).

45. Biondi, E. & Burke, D. H. *RNA structural analysis by enzymatic digestion* (2014).

46. Bartova, S., Alberti, E., Sigel, R. K. & Donghi, D. Metal ion binding to an RNA internal loop. *Inorg. Chim. Acta* **452,** 104–110 (2016).

47. Huang, Z. A simple method for 3'-labeling of RNA. *Nucleic Acids Res.* **24,** 4360–4361 (1996).

48. Figueroa, N., Keith, G., Leroy, J. L., Plateau, P., Roy, S. & Gueron, M. NMR study of slowly exchanging imino protons in yeast tRNA^{Asp}. *Proc. Natl. Acad. Sci. U. S. A.* **80,** 4330–4333 (1983).

49. Maria Pechlaner. PhD Thesis. University of Zurich, 2013.

50. Romaniuk, P. J., Hughes, D. W., Gregoire, R. J., Neilson, T. & Bell, R. A. Stabilizing effect of dangling bases on a short RNA double helix as determined by proton nuclear magnetic resonance spectroscopy. *J. Am. Chem. Soc.* **100,** 3971–3972 (1978).

51. Wu, Y., Bhattacharyya, D., King, C. L., Baskerville-Abraham, I., Huh, S.-H., Boysen, G., Swenberg, J. A., Temple, B. R., Campbell, S. L. & Chaney, S. G. Solution structures of a DNA dodecamer duplex with and without a cisplatin 1,2-d(GG) intrastrand cross-link: comparison with the same DNA duplex containing an oxaliplatin 1,2-d(GG) intrastrand cross-link. *Biochemistry* **46,** 6477–6487 (2007).

52. Bartova, S., Pechlaner, M., Donghi, D. & Sigel, R. K. Studying metal ion binding properties of a three-way junction RNA by heteronuclear NMR. *J. Biol. Inorg. Chem.* **21,** 319–328 (2016).

53. Vogtherr, M. & Limmer, S. NMR study on the impact of metal ion binding and deoxynucleotide substitution upon local structure and stability of a small ribozyme. *FEBS Lett.* **433,** 301–306 (1998).

54. Donghi, D., Pechlaner, M., Finazzo, C., Knobloch, B. & Sigel, R. K. The structural stabilization of the κ three-way junction by Mg(II) represents the first step in the folding of a group II intron. *Nucleic Acids Res.* **41,** 2489–2504 (2013).

55. Davis, J. H., Foster, T. R., Tonelli, M. & Butcher, S. E. Role of metal ions in the tetraloop-receptor complex as analyzed by NMR. *RNA* **13,** 76–86 (2007).

56. Fiore, J. L. & Nesbitt, D. J. An RNA folding motif: GNRA tetraloop-receptor interactions. *Q. Rev. Biophys.* **46,** 223–264 (2013).

57. Butcher, S. E., Dieckmann, T. & Feigon, J. Solution structure of a GAAA tetraloop receptor RNA. *EMBO J.* **16,** 7490–7499 (1997).

58. Lee, M.-K., Bottini, A., Kim, M., Bardaro, M. F., JR, Zhang, Z., Pellecchia, M., Choi, B.-S. & Varani, G. A novel small-molecule binds to the influenza A virus RNA promoter and inhibits viral replication. *Chem. Commun.* **50,** 368–370 (2014).

59. Alderden, R. A., Hall, M. D. & Hambley, T. W. The discovery and development of cisplatin. *J. Chem. Educ.* **83,** 728 (2006).

60. Hah, S.-S., Sumbad, R. A., de Vere White, Ralph W, Turteltaub, K. W. & Henderson, P. T. Characterization of oxaliplatin-DNA adduct formation in DNA and differentiation of cancer cell drug sensitivity at microdose concentrations. *Chem. Res. Toxicol.* **20,** 1745–1751 (2007).

61. Kozelka, J. Molecular origin of the sequence-dependent kinetics of reactions between cisplatin derivatives and DNA. *Inorg. Chim. Acta* **362,** 651–668 (2009).

62. Melnikov, S. V., Soll, D., Steitz, T. A. & Polikanov, Y. S. Insights into RNA binding by the anticancer drug cisplatin from the crystal structure of cisplatin-modified ribosome. *Nucleic Acids Res.* **44,** 4978–4987 (2016).

63. Pérez, C., Leng, M. & Malinge, J.-M. Rearrangement of interstrand cross-links into intrastrand cross-links in cis-diamminedichloroplatinum(II)-modified DNA. *Nucleic Acids Res.* **25,** 896–903 (1997).

5 Experimental

5.1 Preparation of RNA sample

5.1.1 General Procedure

5.1.1.1 Chemicals / Instrumentation

The DNA templates were obtained from Microsynth (Balgach, Switzerland) HPLC-purified. The nucleoside 5'-triphosphates (GTP, CTP, UTP) were purchased from Carl Roth GmbH (Karlsruhe, Germany) except for ATP, which was from GE Healthcare (Glattbrugg, Switzerland). Homemade T7 RNA polymerase was used for in-vitro RNA transcription[1]. All chemicals for the preparation of the RNA were at least puriss p.a. grade (or molecular biology grade) and obtained from Sigma-Aldrich (Buchs, Switzerland) or Merck (Zug, Switzerland). Denaturing polyacrylamide gels were prepared using AccuGel (40 % (w/v), 29:1 and 19:1 Acrylamide-Bisacrylamide) which was obtained from National Diagnostics (Hessle, UK). Ammonium persulfate (APS) was purchased from Carl Roth GmbH and Co (Karlsruhe, Germany). N,N,N,N tetramethylendiamine (TEMED), tris(hydroxymethyl)-aminomethane (TRIS), 4-(2-hydroxyethyl)piperazine-1-ethansulfonic acid (HEPES), ethylenediaminetetraacetic acid (EDTA), sodium chloride, potassium chloride, dithiothreitol (DTT), TritonTM X-100 were bought from Sigma-Aldrich (Buchs, Switzerland). 10x TBE buffer (0.89 M Tris Borate pH 8.3, 0.2 M Na_2EDTA) from National Diagnostics (Atlanta, USA) was used for the preparation of 1x TBE running buffer for electrophoresis. Homemade vertical gel electrophoresis apparatuses were used, equipped with power supplies from Thermo Fisher Scientific (Reinach, Switzerland) (EC 600 - 90; 4'000 V, 300 W, 300 mA maximum). Gels were visualized with a Bio-Vision system from Vilber (Eberhardzell, Germany). RNA was isolated via electroelution using the Elutrap System with BT1 and BT2 membranes (Whatman) and for RNA desalting and concentration ultrafiltration devices Vivaspin 2-mL with 3 kDa molecular weight cut off were purchased from Sartorius Stedim biotech (Aubagne, France). The Centrifuges Sorvall RC 6 Plus from Thermo Fischer Scientific (Reinach, Switzerland) with rotors SA-600, SH-3000 and SLA-3000, and Eppendorf 5804R with rotor A-4-44 were used. RNA samples were vacuum dried with a Concentrator 5301 from Eppendorf or a freeze dryer Alpha 2-4 LDplus from Christ (Osterode am Harz, Germany). The pH values of the RNA samples were determined using a Metrohm 605 pH-meter and a Minitrode glass electrode from Hamilton. UV/Vis measurements for RNA concentration were recorded on Cary 100 Bio and Cary 500 scan instruments from Varian, on a Lambda 25 UV spectrophotometer from PerkinElmer using a quartz cuvette of 10 mm path length, and on a Nanodrop 2000 from Thermo Scientific. In order to avoid RNA degradation and possible contamination of our samples all buffers, salt solutions and platination reactions were prepared in deionized RNAse-free water obtained from a TKA GenPure water purification system from TKA Wasseraufbereitungssysteme (Niederelbert, Germany). Deionized water was further purified by Millipore-filtration and autoclaved before use. All the solutions were filtered prior usage with 0.2 μm Filtropur syringe filters from Sarstedt AG

(Nümbrecht, Germany) or 0.22 µm Steritop bottle top filter units from Merck Millipore (Billerica, MA, USA).

5.1.1.2 Solutions / Buffers

15% denaturing gel solution (29:1) (7 M Urea, 1x TBE, 275 mL Acryl-Bisacryl)**:** 420 g Urea, 100 mL 10x TBE, 375 mL Acryl-Bisacryl 29:1, filled up with water until 1 L and filtrate with 0.22 µm Steritop™ bottle top filter.

15% denaturing gel solution (19:1) (7M Urea, 1x TBE, 275 mL Acryl-Bisacryl)**:** 420 g Urea, 100 mL 10x TBE, 375 mL Acryl-Bisacryl 19:1, filled up with water until 1 L and filtrate with 0.22 µm Steritop™ bottle top filter.

20% denaturing gel solution (29:1) (7 M Urea, 1x TBE, 250 mL Acryl-Bisacryl)**:** 420 g Urea, 100 mL 10x TBE, 500 mL Acryl-Bisacryl 29:1, filled up with water until 1 L and filtrate with 0.22 µm Steritop™ bottle top filter.

20% denaturing gel solution (19:1) (7 M Urea, 1x TBE, 250 mL Acryl-Bisacryl)**:** 420 g Urea, 100 mL 10x TBE, 500 mL Acryl-Bisacryl 19:1, filled up with water until 1 L and filtrate with 0.22 µm Steritop™ bottle top filter.

Transcription Buffer: 40 mM Tris-HCl (pH 7.5), 40 mM DTT, 2 mM spermidine, 0.01 % Triton X-100.

Denaturing Loading Buffer: 11.7 M urea, 40 mM Tris-HCl (pH 7.5), 0.1 % xylene cyanol (XC), 0.1 % bromphenol blue (BB), 230 mM sucrose, 0.8 mM EDTA pH 8.0.

Urea loading buffer for PAGE: 11.8 M Urea, 8.3 % sucrose, 42 mM Tris-HCl (pH 7.5), 0.8 mM EDTA (pH 8.0), 0.08 % (w/v) dye xylene cyanol (XC) and bromophenol blue (BB). Store at 4 °C.

TBE buffer for electrophoresis and electroelution (diluted to 1x from the 10x)**:** 0.89 M Tris-HCl (pH 8.3), 0.89 M boric acid, 0.002 M EDTA.

5.1.1.3 DNA Templates

The DNA templates used to transcribe the RNA samples (see below) contained 2'-methoxy groups on the two 5'-terminal guanosines, to avoid 3'-end inhomogeneity[2]. The 55 in the OT template sequences in the table below represents the modification inserted (e.g. a methoxy group).

RNA		DNA templates
D1-27	OT(met)	5′-55AACTTAGCTCCGAAGAGCATATTCCTATAGTGAGTCGTATTAATTTC-3′
	TS	5′-GAAATTAATACGACTCACTATAGGAATATGCTCTTCGGAGCTAAGTTCC-3′
D1-27_{GAAA}	OT(met)	5′-55AACTTAGCTCTTTCGAGCATATTCCTATAGTGAGTCGTATTAATTTC-3′
	TS	5′-GAAATTAATACGACTCACTATAGGAATATGCTCGAAAGAGCTAAGTTCC-3′
RNA 26	OT(met)	5′-55AACATGCTCCGAAGAGCATATTCCTATAGTGAGTCGTATTAATTTC-3′
	TS	5′-GAAATTAATACGACTCACTATAGGAATATGCTCTTCGGAGCATGTTCC-3′

5.1.1.4 RNA constructs

The following RNA constructs were transcribed:

1. D1-27: 5′-GGAAUAUGCUCUUCGGAGCUAAGUUCC-3′
2. D1-27_{GAAA}: 5′-GGAAUAUGCUCGAAAGAGCUAAGUUCC-3′
3. RNA 26: 5′-GGAAUAUGCUCUUCGGAGCAUGUUCC-3′

One more RNA construct was used for our study, which was bought form IBA (Goettingen, Germany), HPLC purified and was used without further purification.

4. RNAUU: 5′- UUAAUAUGCUCUUCGGAGCUAAGUUAA-3′

5.1.1.5 Experimental procedure

In the following, a general procedure for RNA preparation, isolation and purification is described.

All the RNA samples were synthesized by *in vitro* transcription with T7 polymerase from double-stranded DNA[1,3]. In order to achieve higher transcription yield, the concentration of DNA templates, $MgCl_2$, NTPs and T7 polymerase had to be optimized. For the 27nt-long RNA constructs (D1-27 and D1-27_{GAAA}) the following transcription conditions were used: 0.5 μM DNA template, 30 mM $MgCl_2$, 5 mM of each NTP (ATP, CTP, GTP, and UTP), and 1x T7 polymerase (from 20x) and for the 26 nt-long construct (RNA 26) were: 1 μM DNA template, 10 mM $MgCl_2$, 5 mM of each NTP (ATP, CTP, GTP, and UTP), and 1x T7 polymerase (from 20x). It should be noted that the amount of T7 polymerase used depended on polymerase activity, and had to be optimized for each polymerase batch. It usually varied between 20 and 50 μL per 1 mL transcription solution. All the above mentioned were mixed in 1x transcription buffer and the reaction was proceeding for 4 h at 37 °C while shaking at 300 rpm. After transcription, the RNA samples were purified by PAGE (15%) and extracted from the gel by electroelution. This was followed by ethanol precipitation, performed by adding 3x sample volume of ice-cold ethanol and 1/20 parts sample volume of 5 M NaCl. Upon centrifugation (30 min at 9500 rpm and 4 °C) the isolated precipitated RNA pellet was dried in a Concentrator 5301 from Eppendorf, re-dissolved in water, and desalted by ultrafiltration in Vivaspin devices. The final concentration was determined by UV absorption at 260 nm (D1-27: $\varepsilon_{260\ nm}$ = 266.4 mM^{-1} cm^{-1}, RNA 26: $\varepsilon_{260\ nm}$ = 254 mM^{-1} cm^{-1}, D1-27_{GAAA}: $\varepsilon_{260\ nm}$ = 277.6 mM^{-1} cm^{-1}). All the RNA samples were lyophilized and kept at − 20 °C.

5.1.2 Preparation of D1-27 and D1-27 $_{GAAA}$

Further details on preparations of the two constructs are described below.

5.1.2.1 Transcription

All the reagents were mixed and aliquoted in a volume of 1 mL in Eppendorf tubes. Last was added the T7 polymerase and the transcription was carried out in a thermomixer at 37 °C, 300 rpm for 4 h. After an hour, precipitation of magnesium pyrophosphate was visible. When the transcription was finished the Eppendorf tubes were centrifuged (10 min, 10000 rpm, 25 °C) and the supernatant was collected in Falcon tubes. Next step is the ethanol precipitation. 5 M sodium chloride (NaCl), 1/20 parts of the total volume, and 3x of the total volume 100 % ethanol (EtOH) were added to the solution. The samples were stored either for 1 h at − 80 °C or overnight at − 20 °C. Afterwards the Falcon tubes were centrifuged (30 min, 9500 rpm, 4 °C). The supernatant was collected and the RNA pellet was vacuum dried for 15 min at 30 °C in an Eppendorf concentrator. The dried RNA pellets were dissolved in ddH_2O in order to be further purified by polyacrylamide gel electrophoresis (PAGE).

5.1.2.2 RNA purification by 15% denaturing PAGE

The denaturing polyacrylamide gel solutions were prepared in advance, stored at 4 °C and protected against the light with aluminium foil. While being covered with aluminium foil, the beaker was transferred to a heating plate where was stirring for 1 h at 50 °C. Once the solution was clear, it was filtered through a membrane filter (Stericup, 0.22 μm) and stored at 4 °C.

For 5 mL transcription of D1-27, two gel plates were used. The glass plates (45 x 30 cm with 1.5 mm spacers) were assembled first and then the solution was prepared. For each gel 200 mL of gel solution were needed. This volume was transferred in a beaker and TEMED (100 μL) and APS (10 %, 1000 μL) were added and mixed. The gel solution was transferred with a 50 mL syringe into the assembled glass plates and the combs to create the pockets for sample loading were added at the end. The gel solution was allowed to polymerize for half an hour. Once it was ready, the combs for the pockets were removed and the gel plates were positioned to the vertical electrophoresis apparatus and pre-ran for 30 min at 20 W per plate. 500 μL of urea loading buffer were added to the RNA samples in water (usually 1 mL total volume). The loading buffer contains dyes (bromophenol blue and xylene cyanol) that serve as markers. This solution was loaded into the gel pockets and the gel was run for either 5 - 6 h at 25 - 40 W per plate, or overnight at 4 W per plate, with 1x TBE as running buffer. Images of the gels were recorded with BioVision 3026, under UV light. The RNA bands were excised from the gel, covered with cling film and stored at − 20 °C until electroelution.

5.1.2.3 RNA collection with electroelution

Electroelution was performed in order to collect the RNA from the gel. The gel pieces were transferred to the electroelution chambers, which were positioned into the electroelution apparatus. The whole apparatus was filled with 1x TBE and electric current was applied (200 V). Every hour

1 mL of solution was removed from the chambers and put into a Falcon tube, on ice. The procedure was repeated for 4-5 times. The gel pieces were checked with UV-shadowing to confirm that all RNA was extracted from the gel. Electroelution was followed by ethanol precipitation. In the Falcon tubes containing the RNA sample 3x sample volume of ice-cold ethanol and 1/20 sample volume of 5 M NaCl were added (final volume 10 - 12 mL). The falcons were kept for 1 h at − 80 °C and centrifuged for 30 min (9500 rpm, 4 °C). The supernatant was collected and the RNA pellet was vacuum dried. The concentration before desalting was determined by UV absorption at 260 nm (D1-27: $\varepsilon_{260\ nm}$ = 266.4 $mM^{-1}\ cm^{-1}$, D1-27_{GAAA}: $\varepsilon_{260\ nm}$ = 277.6 $mM^{-1}\ cm^{-1}$).

5.1.2.4 RNA desalting and concentration

Once the sample was isolated, desalting by ultrafiltration in Vivaspin devices took place both to desalt and concentrate it. The Vivaspin devices were first activated by washing twice with 70% EtOH and autoclaved ddH_2O. Afterwards the RNA sample was loaded and it was washed twice with 1 M $NaClO_4$ and ten times with autoclaved ddH_2O. The centrifugation was performed at 20 °C, 5000 rpm, long enough for the volume to be reduced from 2 mL to 200 μL. Each cycle lasted 15 - 30 min according to how concentrated the sample was. After collection of the sample the final concentration was determined by UV absorption at 260 nm (D1-27: $\varepsilon_{260\ nm}$ = 266.4 $mM^{-1}\ cm^{-1}$, D1-27_{GAAA}: $\varepsilon_{260\ nm}$ = 277.6 $mM^{-1}\ cm^{-1}$). All the RNA samples were lyophilized and kept at − 20 °C.

The yield for these two constructs was 150 - 300 nmol per 5 mL transcription.

5.1.3 Preparation of RNA 26

5.1.3.1 Transcription

The conditions mentioned above for the transcription of the 27nt-long constructs had to be modified for the 26nt-long one (RNA 26) in order to increase the yield. A colleague PhD student, Elena Alberti, performed the optimization. The following conditions were found to be the best: 1 μM DNA template, 10 mM $MgCl_2$, 5 mM of each NTP (ATP, CTP, GTP, and UTP), and 1x T7 polymerase (from 20x). After transcription, the RNA was purified by 15% PAGE, isolated by electroelution, desalted and concentrated by vivaspin, following the same procedures as mentioned above. The yield was 50 - 70 nmol per 5 mL transcription.

5.1.4 Large scale RNA dephosphorylation

Dephosphorylated RNA was used in order to have a homogeneous starting material for platination reactions (Chapter 2 Paragraph 2.9). In order to have enough material to work with, large scale dephosphorylation was performed. The dephosphorylation could take place either on a purified RNA sample or immediately after RNA transcription. In the second case, the RNA pellet was dissolved in ddH_2O and desalted with a NAP-10 column. Skipping this step led to reduced dephosphorylation efficiency. Because of reduced yield following the second way, the majority of the RNA samples were dephosphorylated upon purification.

The RNA samples were dephosphorylated with CIAP (Alkaline Phosphatase, Calf Intestinal), using the following procedure. In five 12 mL Falcons tubes 10x CIAP buffer, 10 mM Tris-HCl pH 8, RNA samples and CIAP were added. Each Falcon tube contained 100 µL RNA sample (100 - 400 nmol), 1 mL 10x CIAP buffer, 200 µL from 1 U/µL CIAP and was filled with ddH_2O until 10 mL. The five tubes were incubated at 37 °C for 15 min and then at 56 °C for other 15 min. Further 150 µL from 1 U/µL CIAP was added in each Falcon tube and the same incubation as mentioned before was repeated. 1 M EDTA (10 µL) was added to each tube in order to stop the reaction. The content from all the Falcon tubes was combined and transferred to two 50 mL Falcon tubes, and lyophilized overnight. Purification (15 % denaturing gel), isolation (electroelution) and desalting (Vivaspin) of the dephosphorylated RNA samples took place following the same procedures described above. To check the efficiency of the dephosphorylation, the RNA samples were analyzed with MALDI-MS and ^{31}P-NMR experiments were also recorded (Chapter 2, Paragraph 2.9, Figure 2.43).

5.2 Platination agents

This study was mostly dedicated to cisplatin and oxaliplatin as platination agents (Chapter 2 and 4). However, the behaviour of carboplatin, kiteplatin and [Pt(DACH)Cl_2] in comparison with the previous two was also briefly investigated (Chapter 3).

5.2.1 Chemicals / Instrumentation

All chemicals were bought at the highest purity grades (puriss p.a. or molecular biology grade), and synthesis were carried out with standard glassware. The Microbalance XS3DU was from Mettler Toledo (Greifensee, Switzerland). IR spectra were recorder with a FTIR Spectrometer (Perkin–Elmer, Switzerland) equipped with a Specac Golden GateTM ATR (attenuated total reflection) accessory. For the Flame Atomic Absorption Spectrometry a Varian AA240FS (Agilent Technologies, USA), using an UltraAA platinum lamp was used. The software was the SpectrAA. ^{1}H-NMR spectra were recorded on a Bruker DRX 500 MHz spectrometer using a cryo BBO probe using 3-(trimethylsilyl)-1-propanesulfonic acid sodium salt (TSP, $\delta = 0.0$ ppm) as reference and on a Bruker AV-400 (400 MHz) (Bruker Biospin AG, Fällanden, Switzerland) at the NMR facility of the University of Zurich. $K_2[PtCl_4]$, cis-diamminedichloridoplatinum(II) (cisplatin), [(1R,2R)-cyclohexane-1,2-diamine](ethanedioato-O,O')platinum(II) (oxaliplatin) and cis-diammine(cyclobutane-1,1-dicarboxylate-O,O')platinum(II) (carboplatin) were bought from Sigma Aldrich (Buchs, Switzerland) and used as received or activated before usage (see below). The complex [$PtCl_2$(cis-1,4-DACH)] (kiteplatin) was kindly provided by Prof. James Hoeschele (University of Michigan, Chemistry Department, USA) and Prof. Nicola Margiotta (University of Bari, Department of Chemistry, Italy). The complexes dichloro(1R,2R-diaminocyclohexane)platinum(II) [Pt(DACH)Cl_2] was synthesized based on literature procedures[4].

According to the needs, the complexes cisplatin, kiteplatin and [Pt(DACH)Cl_2] were activated following standard procedures (Paragraph 5.2.4).

5.2.2 Synthesis of (1R,2R)-diaminocyclohexane dichloroplatinum(II) [Pt(DACH)Cl_2]

Equimolar amounts of $K_2[PtCl_4]$ (189.2 mg, 0.455 mmol) and $C_6H_{10}(NH_2)_2$ (52 mg, 0.455 mmol) were dissolved in 1 mL and 400 µL of ddH_2O, respectively (Figure 5.1). The colourless $C_6H_{10}(NH_2)_2$ solution was added dropwise to the red $K_2[PtCl_4]$ solution under stirring, at room temperature, forming yellow precipitation. The reaction mixture was kept in the fridge for 1 h to complete the precipitation. The solid was separated from the supernatant, suspended in cold-water and transferred to a glass tube. The suspension was centrifuged, and the supernatant separated from the solid. The solid was further washed three times with cold water. The yellow precipitate was left in the glass tube overnight under the hood to air dry. Alternatively, the sample was transferred into an Eppendorf tube and lyophilized for a few hours. Yield: 52 mg, 30.8 %.

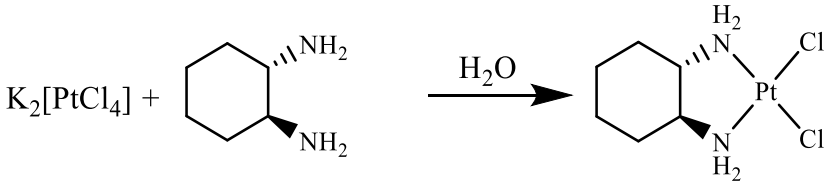

Figure 5.1: *Reaction scheme for the synthesis of [Pt(DACH)Cl_2]*

5.2.3 Characterization of [Pt(DACH)Cl_2]

Elemental analysis

Expected: C: 18.96 %, N: 7.37 %, H: 3.71 %

Measured: C: 18.79 %, N: 7.31 %, H: 3.72 %

IR (solid) [cm^{-1}]: 3274m, 3184m, 3102w, 2933w, 2920s, 2866m, 1566m, 754m. The IR spectrum is shown in Appendix 3. (Figure A 3.1, lower panel)

^{1}H-NMR (in DMSO, 500 MHz): 5.55 (m, NH_2); 5.05 (m, NH_2); 3.38 (H_2O); 2.65 (DMSO); 2.05 (s, C_6H_{10}); 1.95 (m, C_6H_{10}); 1.45 (m, C_6H_{10}); 1.20 (m, C_6H_{10}); 1.00 (m, C_6H_{10}). The NMR spectrum is shown in Appendix 3. (Figure A 3.3)

^{1}H-NMR (in 90% H_2O: 10% D_2O, 500 MHz): 1.1 (m, 2H); 1.3 (m, 2H); 1.5 (m, 2H); 2 (m, 2H); 2.3 (m, 2H); 4.7 (H_2O); 5.7 (s, NH_2). The NMR spectrum is shown in Appendix 3. (Figure A 3.4, blue line)

ESI-MS: m/z expected: 380; m/z measured: 386.1 [Pt(DACH)Cl_2].

IR and 1D-^{1}H-NMR spectra of the starting material 1,2-diaminocyclohexan (DACH) were also collected:

IR (liquid) [cm^{-1}]: 3360 w, 3279 w, 3177 w, 2920 s, 2853 m, 1595 m, 766 m. The IR spectrum is shown in Appendix 3. (Figure A 3.1, upper panel)

^{1}H-NMR (in DMSO, 500MHz): 0.95-1.09 (m, 2H); 1.12-1.24 (m, 2H); 1.57-1.67 (m, 2H); 1.70-1.80 (m, 2H); 2.06-2.16 (m, 2H); 2.56 (DMSO), 3.6 (H_2O). The NMR spectrum is shown in Appendix 3. (Figure A 3.2)

5.2.4 Activation of the platinum(II) compounds

Activation of the platinum(II) complexes is the hydrolysis of the Pt-Cl bonds to form Pt-water bonds. The activation can lead to either mono- or diaquo derivatives (Figure 5.2). These aqua derivatives are formed also in the cellular environment and this step is considered crucial for the further interactions of platinum(II) complexes with their cellular targets[5]. Cisplatin, [Pt(DACH)Cl_2] and kitePt were activated following the same procedure. 0.9 or 1.9 eq of 0.1 M $AgNO_3$ were added to the solution containing the platinum(II) complexes in order to form the mono- or diaquo platinum(II) complexes (Figure 5.2). The reaction mixture was incubated for 3.5 h at 37 °C in the dark. In the meanwhile, white precipitation of AgCl was formed. The reaction mixture was centrifuged (10 min, 9000 rpm, 25 °C) and the supernatant was collected. The platinum content of each sample was measured by F-AAS. The concentration of the platinum(II) complexes solutions varied between 0.6 and 1 mM. The [Pt(DACH)Cl_2] complex was activated in two different ways. In the first procedure, $AgNO_3$ was added to a clear solution of the complex. Complete dissolution of the complex in water was achieved by heating the solution at 37 °C for one hour, before addition of $AgNO_3$. In the second procedure, $AgNO_3$ was added to a suspension of the complex. Addition of $AgNO_3$ facilitates complete dissolution of [Pt(DACH)Cl_2]. Data from AAS confirm that both the procedures lead to the same results. However, ^{1}H-NMR spectra recorded on the samples prepared using the first procedures show extra peaks, probably due to degradation of the platinum(II) complex taking place during the heating step (Appendix 3, Figure A 3.5). For this reason, the second procedure was followed. The platinum(II) complex solutions were stored at − 20 °C.

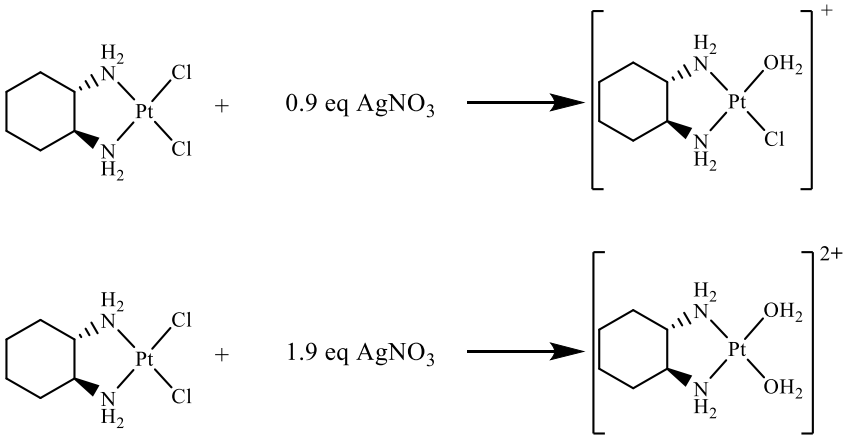

Figure 5.2: *Activation reactions for the formation of the monoaquated and diaquated [Pt(DACH)Cl_2] complexes. Activation of cisPt and kitePt took place under the same experimental conditions.*

5.2.5 NMR characterization of the $[Pt(DACH)Cl(H_2O)]^+$ complex

1D-^{1}H-NMR (in 90% H_2O:10%D_2O): 1.1 (m, 2H); 1.3 (m, 2H); 1.5(m, 2H); 2 (m, 2H); 2.3 (m, 2H); 4.7 (H_2O); 5.7 (s, NH_2). The NMR spectrum is shown in Appendix 3. (Figure A 3.4 red line)

5.3 Flame Atomic Absorption Spectrometry (F-AAS)

This technique was used to determine the concentration of the platinum(II) complexes. Standard solutions were prepared for 2 ppm (50 μL), 5 ppm (125 μL), 10 ppm (250 μL), 15 ppm (375 μL) and 20 ppm (500 μL) from 1000 ppm Pt stock solution, with final volume 25 mL, in order to build the calibration curve. 0.5 M $LaCl_3$ was prepared by dissolving 3.73 g of $LaCl_3$ in water. 3.6 mL (1 %) of 0.5 M $LaCl_3$ solution was added to all the samples and the standard solutions, which were then diluted with ddH_2O to 25 mL. All solutions were filtered before use. As baseline water solution with 1 % 0.5 M $LaCl_3$ was used. The $LaCl_3$ is used in F-AAS measurements in order to reduce the chemical interferences which could result in incomplete atomization of the sample. For the sample preparation a specific amount of the platinum(II) complex (0.4 - 0.6 mg) was weighted and dissolved in water. A 1% $LaCl_3$ solution was added to this sample, which was then filled with water until 5 mL in a volumetric flask. In the case of the activated platinum(II) complexes their solution was diluted with ddH_2O in a 5 mL volumetric flask with their final concentration to vary between 0.1 - 0.2 mM. The measurements were performed on a Varian AA240FS, using an UltraAA platinum lamp. The software used was the SpectrAA.

5.4 Platination reactions

5.4.1 Chemicals / Instrumentation

RNA samples for platination were prepared and purified as described above. Platinated samples were isolated using gels and electroelution in a similar way. They were desalted either by Vivaspin (see above) or by using NAP-10 columns (GE Healthcare, UK) depending on their amount.

5.4.2 Solutions / Buffers

60 mM $KClO_4$ - 10 μM EDTA: 40 μL from 150 mM $KClO_4$ and 100 μL of 10 mM EDTA were mixed and dissolved in water, in a final volume of 100 mL, and filtered with 0.22 μm filter.

1 M KCl: 7.4 g KCl was dissolved in water to a final volume of 100 mL; the resulting solution was then filtered with 0.22 μm filter.

150 mM $KClO_4$: 207.7 mg $KClO_4$ were dissolved in water to a final volume of 10 mL; the resulting solution was then filtered with 0.22 μm filter.

Na(I) MOPS: 1 mM MOPS + 5 M NaOH until pH 7.40. Final sodium(I) concentration is 1 mM.

5.4.3 Experimental procedure

For all the platination reactions, the following procedure was followed. The RNA sample was dissolved in ddH_2O and its concentration was determined via UV/Vis spectroscopy. The platinum agents were dissolved in water also, and their concentration was determined via F-AAS. The appropriate volumes of RNA and platinum agent were transferred into an Eppendorf tube. The reaction solutions and additional water were added, and the reaction mixture was placed in a thermomixer at 25 ° - 50° C (see below) for 15 h to 5 days. The RNA platination conditions differ for different platination agents, and had to be optimized. This was done for oxaliplatin and cisplatin (Chapter 2, Paragraph 2.3 - 2.5). Optimization of reaction buffer, time, temperature, salt concentration, RNA and platinum concentration took place. Different reaction solutions were used, namely MOPS buffer, plain water, and solutions containing different concentration of $KClO_4$ or KCl. The tested temperature were 25 °C, 37 °C and 50 °C and the reaction time varied from 15 h to 5 days. The RNA concentration tested was 0.1 - 0.5 mM and 1 - 10 eq of platinum(II) complexes were added. The final reaction volume was usually between 10 µL and 20 µL. The platinated samples were analysed by PAGE in denaturing conditions, and the reaction conditions were optimized until clear separation between the band corresponding to platinated and unreacted RNA was achieved on the gels. Gel percentage, temperature and running time were also subjected to optimization. Pictures of the gels were taken using UV shadowing. The gel bands were excised from the gel and recovered either with crush and soak or with electroelution. The samples were desalted with NAP-10 columns or with Vivaspin.

Detailed description of the optimization of the platination conditions for cisplatin and oxaliplatin reacting with D1-27 is provided in Chapter 2.

5.4.4 Separation / purification of the platinated RNA with PAGE

Separation between platinated and unreacted RNA samples was achieved by using denaturing PAGE. The platinated species due to higher molecular weight and different overall charge migrate slower on the gel compared to pure RNA. In order to increase the separation of the bands, gel percentage of the, temperature and running time were modified. The higher gel percentage the more intact the gel net becomes and therefore the better the separation is. The gel percentage used were 15 %, 18 % and 20 %. Additionally, to further improve the gel resolution 19:1 acrylamide - bis acrylamide gel solution was used instead of 29:1 (Chapter 2, Figure 2.44). The temperatures tested were room temperature and 4 °C (fridge). By running the gel in the fridge, the speed was lower and the separation was better. Lastly, by increasing the time that a gel run, the separation could be improved. For that reason, the running time was increased from 6 h to overnight and finally to 2 days. Another way to increase the running time was to use longer gel plates. Finally, the best conditions which allowed the maximum separation of the platinated from the unreacted RNA were: 20 % denaturing gel solution (19:1), using 45 cm long gel plates, running in the fridge for 2 days.

Both analytical and preparative gels were used. In the analytical gels small amounts of sample (0.5 -1 nmol) were loaded and the gels were used mostly for the optimization of the platination conditions. On the contrary, the preparative gels were used in order to isolate enough sample for the characterization (20 - 100 nmols). For the analytical gels 3 mm spacers were used and for the preparative gels the 1.5 mm ones. Gel preparation, sample loading and running and RNA isolation, purification and recovery were performed as described above (Paragraph 5.1.2.2).

5.4.5 Collection of the RNA samples with electroelution or crush and soak

The RNA samples were collected from the gel pieces by either electroelution or crush and soak technique. The first was the method of choice for samples isolated from preparative gels, while gel pieces isolated from analytical gels were processed with crush and soak. Electroelution and crush and soak were performed as described in paragraphs 5.1.2.3 and 5.10.2.

5.4.6 Desalting and concentration of the RNA samples (Vivaspin, NAP-10 columns)

The samples were desalted via Vivaspin or NAP-10 columns according to their amount. Consequently, all samples used for NMR studies (20 - 30 nmols) were desalted with Vivaspin. On the contrary, samples used for all the other studies were often desalted using NAP-10 columns (0.5 - 10 nmols). An advantage of using the Visaspin is that the Tris, coming from the previous used buffers, could be effectively removed. A disadvantage of the Vivaspin was that the recovery of the sample was maximum 60 - 70 % while with NAP-10 columns could be up to 85 - 95 %. Vivaspin desalting was performed as described above (Paragraph 5.1.2.4)

5.5 High performance liquid chromatography (HPLC)

5.5.1 Chemicals / Instrumentation

All chemicals were bought in the highest commercial grades and used without further purification. HPLC solvents (methanol, acetonitrile, triethylamine) were obtained in HPLC grade from Sigma Aldrich (Buchs, Switzerland). Deionised water was purified by Millipore-filtration and was always autoclaved before use. All buffers were filtered through 0.2 µm filters from Sarstedt AG (Nümbrecht, Germany). The P1 nuclease, ammonium acetate, sodium acetate and zinc chloride were purchased from Sigma Aldrich (Buchs, Switzerland) and the Thermosensitive Alkaline Phosphatase (TSAP) from Promega (Dübendorf, Switzerland). The Microbalance XS3DU was from Mettler Toledo and was used for the preparation of the standard nucleoside solutions (Greifensee, Switzerland). The analytical HPLC analyses were performed on a Dionex Ultimate 3000 HPLC system equipped with a Diode Array Detector (DAD) using the software Chromeleon 7.1. An analytical X-Bridge C18 RP column (3.5µm, 4.6 x 150 mm) from Waters (Baden-Dättwil, Switzerland) was used for the isolation, purification and quantification of the platinated RNA samples as well as for the enzymatic digestion of the unreacted

and platinated RNA samples. In addition to the chosen column, the performances of the following columns were investigated in order to find the appropriate stationary phase: Reverse Phase C18 Ultraphere(R) (5 µm, 80Å, 4.6 x 250 mm) from Beckman & Coulter (Fullerton, USA), reverse phase cross-linked poly(styrene-co-divinylbenzene) polymer PRP(R)-h1 (5 µm, 100 Å, 4.6 x 250 mm) from Hamilton (Bonaduz AG, Switzerland) and reverse phase Nucleodur C18 Gravity column (5 µM, 4 x 250 mm) from Macherey-Nagel (Switzerland).

5.5.2 Buffers

Standard nucleoside solutions: Guanosine (ε_{253nm} = 13700 $M^{-1}cm^{-1}$), 0.7 mg in 1 mL; Adenosine (ε_{260nm} = 15400 M^{-1} cm^{-1}), 1 mg in 1 mL; Uridine (ε_{260nm} = 10000 M^{-1} cm^{-1}), 1.3 mg in 1 mL; Cytidine: (ε_{270nm} = 9000 M^{-1} cm^{-1}), 1.19 mg in 1 mL.

P1 nuclease buffer: 30 mM NaOAc pH 5.2 and 250 µM $ZnCl_2$.

TEAA buffer for HPLC analysis: 0.1 M TEA, pH = 7.0 adjusted with acetic acid, 0.5 % Acetonitrile.

Ammonium acetate buffer for HPLC analysis: 0.04 M NH_4OAc, pH = 6.5 adjusted with acetic acid.

Ammonium acetate buffer for HPLC analysis: 0.02 M NH_4OAc, pH = 6.0 adjusted with acetic acid.

5.5.3 HPLC methods

Different methods were tested to find the best separation conditions. The methods 6 and 7 were chosen for the evaluation of the RNA samples as well as for the purification and quantification of the Pt(II)-RNA adducts (see Chapter 2, Paragraph 2.8.1). In the following, details of all the methods investigated are listed.

Method 1: Column: RP cross-linked poly(styrene-co-divinylbenzene) polymer PRP®–h1 column (5 µm, 4.6 x 250 mm) from Hamilton; Wavelength: 260 nm; Flow rate: 1 mL / min; Buffer A: 23 mM TEAA, pH = 6.9; Buffer B: Acetonitrile; Gradient: 2 min equilibration 0 % B, 0 - 8 min 0 % B, 8 - 22 min 0 - 18.5 % B, 22 - 23 min 18.5 - 100 % B, 23 - 24 min 100 - 100 % B, 24 - 24.5 min 100 - 0 % B, 24.5 - 27.0 min 0 % B.

Method 2: Column: Waters X-Bridge C18 (3.5 µm, 4.6 x 150 mm); Wavelength: 260 nm; Flow rate: 1 mL / min; Buffer A: 23 mM TEAA, pH = 6.9; Buffer B: Acetonitrile; Gradient: 2 min equilibration 0% B, 0 - 4 min 2 -2 % B, 4 - 18 min 2 - 35 % B, 18 - 25 min 35 - 50 % B, 25 - 28 min 50 % B, 28 - 35min 50 - 90 % B, 35 - 40 min 90 % B, 40 - 42 min 90 - 2 % B, 42 - 45 min 2 % B.

Method 3: Column: Waters X-Bridge C18 (3.5 µm, 4.6 x 150 mm); Wavelength: 260 nm; Flow rate: 1 mL / min; Buffer A: 100 mM TEAA, pH = 6.9; Buffer B: Acetonitrile; Gradient: 2 min equilibration 2% B, 0 - 4 min 2 -2 % B, 4 - 9 min 2 - 35 % B, 9 - 12 min 35 - 25 % B, 12 - 15 min 25- 35 % B, 15- 17 min 35 - 2 % B, 17 - 19 min 2- 0 % B.

Method 4: Column: Waters X-Bridge C18 (3.5 μm, 4.6 x 150 mm); Wavelength: 260 nm; Flow rate: 1 mL / min; Buffer A: 100 mM TEAA, pH = 6.9; Buffer B: Acetonitrile; Gradient: 2 min equilibration 2% B, 0 - 4 min 2 % B, 4 - 40 min 2 - 35 % B, 40 - 43 min 35 % B, 43 - 45 min 35- 2 % B, 45- 50 min 2% B.

Method 5: Column: Waters X-Bridge C18 (3.5 μm, 4.6 x 150 mm); Wavelength: 260 nm; Flow rate: 1 mL / min; Buffer A: 100 mM TEAA, pH = 6.9; Buffer B: Acetonitrile; Gradient: 5 min equilibration 2% B, 0 - 4 min 2 -2 % B, 4 - 60 min 2 - 30 % B, 60 min 30 - 30 % B, 60 - 68 min 30- 2 % B, 68- 70 min 2% B.

Method 6: Column: Waters X-Bridge C18 (3.5 μm, 4.6 x 150 mm); Wavelength: 260 nm; Flow rate: 1 mL / min; Buffer A: 100 mM TEAA and 0.5 % acetonitrile, pH = 6.9; Buffer B: Acetonitrile; Gradient: 5 min equilibration 2% B, 0 - 10 min 2 -10 % B, 10 - 10.5 min 10 - 40 % B, 10.5 - 17 min 40 % B, 17 - 19 min 40- 2 % B, 19- 20 min 2% B.

Method 7: Column: Waters X-Bridge C18 (3.5 μm, 4.6 x 150 mm); Wavelength: 260 nm; Flow rate: 1 mL / min; Buffer A: 100 mM TEAA and 0.5 % acetonitrile, pH = 7.0; Buffer B: Acetonitrile; Gradient: 5 min equilibration 2 % B, 0 - 10 min 2 - 8 % B, 10 - 15 min 8 - 9.2 % B, 15 - 18 min 9.2 - 9.2 % B, 18 - 25 min 9.2 - 9.4 % B, 25 min 9.4 - 30 % B, 25 - 27 min 30 % B, 27 - 30 min 30 - 2% B

Method 8: Column: Waters X-Bridge C18 (3.5 μm, 4.6 x 150 mm); Wavelength: 260 nm; Flow rate: 0.5 mL / min; Buffer A: 40 mM $NH_4CH_3CO_2$, pH = 6.5; Buffer B: Methanol; Gradient: 15 min equilibration 100 - 0 % B, 0 - 5 min 0 % B, 5 - 33 min 0 - 16.8 % B, 33 - 35 min 16.8 - 100 % B, 35 - 38 min 100 % B.

Method 9: Column: Waters X-Bridge C18 (3.5 μm, 4.6 x 150 mm); Wavelength: 260 nm; Flow rate: 0.5 mL / min; Buffer A: 40 mM $NH_4CH_3CO_2$, pH = 6.5; Buffer B: Methanol; Gradient: 15 min equilibration 100 - 0 % B, 0 - 5 min 0 % B, 5 - 55 min 0 - 30 % B, 55 - 65 min 30 - 100 % B, 65 - 68 min 100 % B.

5.5.4 Experimental procedure

5.5.4.1 Preparation of RNA and platinated RNA samples for HPLC analysis

0.2 - 0.4 nmol of RNA and platinated RNA samples were diluted in water to final volume of 20 μL. 15 μL were injected in the HPLC machine, corresponding to 0.15 - 0.3 nmol of sample. The RNA samples were separated on a X-Bridge C18 RP column (3.5 μm, 4.6 x 150 mm). The mobile phase components were A: 100 mM TEAA and 0.5 % acetonitrile, pH 7.0; B: Acetonitrile. Methods 2, 6 and 7 were used for analysis and purification of the RNA and Pt(II)-RNA samples as well as to directly follow platination reactions (Chapter 2, Paragraph 2.8). All the chromatograms were recorded at 25° C.

5.5.4.2 Enzymatic digestion and analysis of unreacted and platinated RNA samples with HPLC

Nuclease P1 is a zinc-dependent endonuclease that cleaves single stranded DNA and RNA to yield nucleoside 5′-phosphates and 5′-phosphooligonucleotides[6]. Samples containing 0.2 nmol of unreacted and platinated RNA were digested with 2.3 μL (1 U/μL) P1 nuclease and buffer containing 30 mM NaOAc pH 5.2 and 250 μM $ZnCl_2$, in a final volume of 20 μL for 15 min at 37 °C. The digested nucleotides were dephosphorylated with 4 μL (4 U/μL) of thermosensitive alkaline phosphatase (TSAP) for 30 min at 37 °C. The TSAP was irreversibly inactivated by heating at 74 °C for 15 min. The solution was then ready for immediate analysis by HPLC. The injection volume was 15 μL. The nucleosides were separated on a X-Bridge C18 RP column (3.5 μm, 4.6 x 150 mm). All the chromatograms were recorded at 25 °C. Methods 8 and 9 were used for the separation (mobile phase components: A: 40 mM NH_4OAc, pH 6.5 and B: Methanol). Nucleoside standards were used to determine the retention time of the four nucleosides. The standards were prepared by dissolving the pure nucleosides in water and calculating their concentration via UV/Vis. The chromatograms of the digested platinated RNAs were evaluated based on the differences of the relative peak area with respect to unreacted RNA samples. Appearance of new peaks was also observed (Chapter 4, Paragraph 4.6). Relative peak areas were measured directly using the software of the HPLC machine (Chromeleon 7.1). All the HPLC chromatogram pictures were prepared with OriginPro 9.1G.

5.6 Circular dicroism (CD) measurements

5.6.1 Chemicals / Instrumentation

$KClO_4$ was bought from Merck (Zug, Switzerland). CD measurements were carried out on a Jasco J-810 spectropolarimeter from Jasco (Easton, MD, USA) equipped with a peltier thermostat, with continuous flow of N_2 with a rate of 5 L / min at room temperature. Data evaluation was done using the supplied software, Spectra Manager and Spectra Analysis. All the CD spectra pictures were prepared with OriginPro 9.1G.

5.6.2 Experimental procedure

CD Spectra were recorded at 25 °C on a Jasco J-810 spectrometer using a 1 cm path length quartz cuvette with volume capacity of 1 mL (Hellma Analytics, Germany). The RNA concentration was in the range 1.1 - 1.5 μM and the pH was 5 - 6.5. The final salt concentration in the samples was 120 mM $KClO_4$, obtained using a 400 mM $KClO_4$ starting solution. Continuous scans were performed between 200 and 350 nm with scanning speed of 50 nm / min, data pitch of 1 nm, response of 0.5 s, and band width of 1 nm. Ten scans were averaged, the blank was subtracted from each spectrum, and data were zero-corrected at 350 nm. Each measurement was repeated twice. In the graphs, circular dichroism is represented as molar ellipticity [θ] using the following equation:

$$[\theta]\ (\mathrm{deg.cm^2.dmol^{-1}}) = \theta\ (\mathrm{mdeg}) / (10 \times c \times l)$$

where: [θ] is Molar ellipticity, θ is Ellipticity, c is the Molar concentration of the sample in mole / L and *l* is the cuvette pathlength in cm. Using molar ellipticity the plotted data are concentration independent[7].

5.7 UV thermal melting experiments

5.7.1 Chemicals / Instrumentation

UV-thermal melting measurements were performed on Cary 100 UV/Vis, Lambda 25 and 850 UV/Vis (PerkinElmer, Schwerzenbach, Switzerland) spectrophotometers. The cuvettes used for these measurements were 1 cm path-length quartz cuvettes with total volume capacity of 1 mL and were purchased from Hellma (Müllheim, Germany) or Starna (Hainault, UK).

5.7.2 Experimental procedure

Thermal melting studies were conducted for the unreacted and platinated RNA samples using a concentration of 1.1 - 1.5 µM at pH 5.0 and pH 6.5 in water with 120 mM $KClO_4$ on Lambda 25 and 850 UV/Vis spectrophotometers (PerkinElmer) equipped with a temperature control unit. The experiments were performed recording the absorption at 260 nm during heating and cooling of the sample. All the samples were covered with paraffin oil to avoid sample evaporation and furthermore the cuvettes were closed with their caps. The heating and cooling cycles were performed at a rate of 1 °C / min for a temperature range of 25 °C to 90 °C with starting and returning temperature of 25 °C. The heating and cooling cycles were repeated three to four times and the melting temperatures were obtained by calculating the first derivative of each melting curve[8]. The values of each Tm was averaged and the errors correspond to standard deviation. All the pictures for the thermal melting studies were prepared with OriginPro 9.1G.

5.8 MALDI-MS measurements

Matrix-assisted laser desorption ionization mass spectrometry (MALDI-MS) spectra were recorded at the Functional Genomics Center Zurich (FGCZ) by Dr. Serge Chaesnov. More details on mass measurements are provided and discussed in Chapter 2, Paragraph 2.7. Selected mass spectra are given in the Appendix 1. All the mass spectrum pictures were prepared with OriginPro 9.1G.

5.9 NMR experiments

5.9.1 Chemicals / Instrumentation

RNA samples for NMR studies were prepared by transcription using natural abundance nucleotides. The Pt(II)-RNA samples were purified by denaturing gels, isolated with electroelution and desalted via Vivaspin as described above. ^{1}H-NMR spectra were recorded on deph- and triph-D1-27, and their corresponding platinated species. ^{31}P-NMR spectra were recorded to confirm successful dephosphorylation (Chapter 2, Paragraph 2.9). The samples were dissolved either in D_2O (Armar Chemicals, Switzerland) or in H_2O / D_2O (90:10) using deionized, millipore-filtered water, in the presence of 120 mM KCl or $KClO_4$, based on the requirements of each experiment. The time evolution NMR experiments were performed in the presences of 120 mM KCl, while all the other experiments in 120 mM $KClO_4$. The RNA concentration was checked via UV/Vis and varied from 0.1 to 0.4 mM while the platinum(II) concentration was usually 5x the RNA concentration in the time evolution experiments. The pH was between 6.5 and 7.0 and it was adjusted with addition of KOH, KOD, HCl or DCl, according to the needs. For all NMR measurements, 5 mm Shigemi® tubes were used. 4,4-dimethyl-4-silapentane-1-sulfonic acid (DSS) (Bruker Biospin AG, Fällanden, Switzerland) was used as an external direct reference for ^{1}H resonances and indirect reference for ^{13}C resonances[9]. ^{31}P spectra were referenced to external 85% H_3PO_4. NMR spectra were recorded on a Bruker Avance 700 MHz spectrometer with a 5 mm CRYO TXI inverse triple-resonance probe-head with z-gradient coil, on a Bruker Avance 600 MHz spectrometer with a 5 mm CRYO TCI inverse triple-resonance probe head with z-gradient coil, and on a Bruker DRX 500 MHz spectrometer using a cryo BBO probe at the NMR facility of the University of Zurich. The software used for processing the data and preparing the 1D NMR pictures was TopSpin 3.0 or TopSpin 3.2. (Bruker Biospin AG, Switzerland) and all assignments were made in Sparky (http://www.cgl.uscf.edu/home/sparky/). The 2D NMR pictures were prepared using CorelDraw X3 and MestReNova version 10.0 (Mestrelab Research S.L.)

5.9.2 Experimental procedure

Time evolution NMR experiments were used to study RNA platination by following the changes induced by the platinum binding in the imino proton region. Imino proton resonances are visible when there are stable hydrogen bonds between the bases[10]. Therefore, changes affecting the imino resonances, like chemical shift and / or intensity, are indicative of structural modifications. The platination reactions were performed using 0.1 mM RNA, 5 eq of platination agent, 120 mM KCl, and were allowed to proceed for 1 day at 25 °C in the NMR tube. These are the conditions that were found to favour a clear separated upper band on the gel, containing the platinated species, in the case of oxaliplatin (Chapter 2, Paragraph 2.4.4). First, ^{1}H-NMR spectra were recorded before the addition of the platination agent. After addition, ^{1}H-NMR spectra were recorded every 1 h for 24 h. Time evolution NMR experiments were recorded for D1-27, deph-D1-27, D1-27$_{GAAA}$ and RNA 26 using oxaliplatin as platination agents.

In the case of D1-27, different amounts (1-20 equiv) as well as different kind of platination agents (monoaquated cisPt and monoaquated kitePt) were also used (Chapter 3, Paragraphs 3.5 - 3.7). To evaluate the changes, the percentage of the intensity of the imino proton resonances was plotted over time.

^{1}H-NMR spectra in the range 4 - 25 °C were also recorded on platinated samples isolated from the various bands on the gel (Chapter 4, Paragraph 4.8). Moreover, a [^{1}H,^{13}C]-HSQC spectrum on the aromatic region (C8 and C2 of purines, C6 of pyrimidines) and a [^{1}H,^{1}H]-NOESY spectrum were recorded on a natural abundance platinated sample isolated from the upper band of a gel corresponding to a platination reaction performed on triph-D1-27 (Chapter 4, Paragraph 4.8, Appendix 2, Figures A 2.6 - A 2.7).

5.10 ^{32}P 5′- and 3′-end labelling of RNA

5.10.1 Chemicals / Instrumentation - Solutions / Buffers

5.10.1.1 Chemicals / Instrumentation

The general procedures to prepare, isolate and purify RNA samples and to prepare and run gels are the same as commented above. For radioactive labelling [γ-^{32}P]-ATP (150 mCi / mL, 6000 Ci / mmol) and [α-^{32}P]-dCTP (6000 Ci / mmol, 20 mCi / mL) from PerkinElmer were used. For measuring the concentration of the labelled RNA, scintillation counts were performed on a scintillation counter 22000CA Liquid Scintillation Analyzer from Canberra Packard. RNase T1 1000 U/µL and Nuclease S1 100 U/µL were obtained from Termo Scientific (Reinach, Switzerland). T4 polynucleotide kinase 10 U/µL, thermosensitive alkaline phosphatase (TSAP) 1 U/µL and alkaline phosphatase calf intestinal (CIAP) 1 U/µL were bought from Promega (Dübendorf, Switzerland). The concentration of the labelled RNA was measured by scintillation counting. The overall RNA concentration was determined spectroscopically using a Picodrop CUBE (Labgene, Switzerland) from the absorbance at 260 nm in order to determine the labelling efficiency The gels were dried on WhatmannTM Chromatography paper from GE Healthcare (Little Chalfont, UK) on gel driers from Uniequip (Planegg, Germany) or Biometra (Goettingen, Germany). For visualization of the labelled RNA bands screening was performed using Storage Phosphor Screens from GE Healthcare. Phosphoimaging was performed with a Typhoon scanner FLA 9000 from GE Healthcare.

5.10.1.2 Solutions / Buffers

15% denaturing gel solution (29:1) (7 M Urea, 1x TBE, 375 mL Acryl-Bisacryl)**:** 420 g Urea, 100 mL 10 x TBE, 375 mL Acryl-Bisacryl 29:1, filled up with water until 1 L and filtrate with 0.22 µm Steritop™ bottle top filter.

15% denaturing gel solution (19:1) (7 M Urea, 1x TBE, 375 mL Acryl-Bisacryl)**:** 420 g Urea, 100 mL 10x TBE, 375 mL Acryl-Bisacryl 19:1, filled up with water until 1 L and filtrate with 0.22 µm Steritop™ bottle top filter.

20% denaturing gel solution (29:1) (7 M Urea, 1x TBE, 250 mL Acryl-Bisacryl)**:** 420 g Urea, 100 mL 10x TBE, 500 mL Acryl-Bisacryl 29:1, filled up with water until 1 L and filtrate with 0.22 µm Steritop™ bottle top filter.

20% denaturing gel solution (19:1) (7 M Urea, 1x TBE, 250 mL Acryl-Bisacryl)**:** 420 g Urea, 100 mL 10 x TBE, 500 mL Acryl-Bisacryl 19:1, filled up with water until 1 L and filtrate with 0.22 µm Steritop™ bottle top filter.

Formamide loading buffer: 82 % (v/v) formamide, 0.16 % (w / v) xylene cynol (XC), 0.16 % (w/v) bromophenol blue (BB), 10 mM EDTA (pH 8.0 at 20 °C).

Urea loading buffer for PAGE: 11.8 M Urea, 8.3 % sucrose, 42 mM Tris-HCl (pH 7.5), 0.8 mM EDTA (pH 8.0), 0.08 % (w/v) dye xylene cyanol (XC) and bromophenol blue (BB).

TBE buffer for electrophoresis and electroelution (diluted to 1x from the 10x): 0.89 M Tris-HCl (pH 8.3), 0.89 M boric acid, 0.002 M EDTA.

10x Sodium carbonate (Na_2CO_3) solution: 0.5 M Na_2CO_3 (pH 9.0 at 23 °C), 10 mM EDTA (pH 8.0 at 20 °C).

10x Sodium citrate buffer: 0.25 M trisodium citrate (pH 5.0 at 23 °C). Adjust the pH by addition of concentrated HCl.

5x Reaction buffer (S1): 200 mM sodium acetate (pH 4.5), 1.5 M NaCl, 10 mM $ZnSO_4$.

2x Quenching solution (colourless gel loading solution): 82 % (v/v) Formamide and 10 mM EDTA (pH 8.0).

ME Buffer: 10 mM MOPS (pH 6.0), 1 µM EDTA.

5.10.2 5'-end radiolabelling of D1-27

D1-27 was transcribed from double stranded DNAs and carried a 5'-triphosphate. This needs to be removed before 5'-end labelling. Dephosphorylation of 120 pmol RNA in a final volume of 50 µL took place with Thermosensitive Shrimp Alkaline Phosphatase (TSAP). 4 µL of the TSAP (1 U/µL) were added to the RNA sample, followed by incubation at 37 °C for 30 min with 300 rpm shaking. The RNA was subsequently purified by phenol-chloroform extraction and dissolved in 16 µL of ME buffer. Dephosphorylated RNA (240 pmol) was dissolved in 28 µL of ME buffer and mixed with 3 µL of ^{32}P-γ-ATP (3000 Ci / mmol), 4 µL of T4 polynucleotide kinase (PNK, 10 U/µL) and 4 µL of PNK buffer

(10x). The reaction mixture was incubated at 37 °C for 30 min without mixing. Afterwards an equal amount of formamide loading buffer was added to the mixture. The 5′-labelled RNA was purified by denaturing PAGE (15% w/v). The RNA in the gel was visualised by phosphoimaging and the RNA bands were excised from the gel. The RNA gel band was placed into a small Eppendorf tube with a hole, which was placed in a bigger Eppendorf tube, in order to be crushed into smaller pieces by centrifugation at 9500 rpm at room temperature for 2 min. 500 μL of crush and soak buffer were added to each Eppendorf tube. The samples were soaked in the buffer at 4 °C for 5 - 8 hours vortexing every 30 min, or overnight, with comparable recovery efficiency. Afterwards the samples werecentrifugedat9500 rpm and at 4° C for 3 min and the supernatant was collected. The RNA in the supernatant was precipitated adding 3 volumes of ice cold absolute ethanol and keeping the sample at – 20 °C overnight or at – 80 °C for 1 hour. After ethanol precipitation the samples were centrifuged at 9500 rpm and at 4 °C for 40 min and the pellets were dried in a Speed Vac evaporator and dissolved in 20 -80 μL of water. The concentration of the labelled RNA was measured by scintillation counting. The overall RNA concentration was determined spectroscopically from the absorbance at 260 nm in order to determine the labelling efficiency. Upon optimization of the labelling reaction conditions (concentration of the reactants and incubation time) the labelling efficiency increased from 0.01 to 10 %. The radiolabelled RNA samples were stored at − 20 °C.

5.10.3 3′-end radiolabelling of D1-27

In this case, D1-27 was 3′-end labelled with α-^{32}P-dCTP using the Szostak (splint) method[11]. The length of the DNA oligo splint (DNA 16, 21, 23), its concentration (1 μM - 50 μM) as well as the reaction time (5 min - 2 h) were optimized (Chapter 4, Paragraph 4.7.4). The optimal procedure was the following: Five samples of 25 pmols with final volume of 5 μL each were mixed with 0.5 μL 10x annealing buffer, 2 μL DNA 16 (3′-CCTCGATTCAAGGGCC-5′) oligo splint (10 μM) and 2.5 μL water. The samples were heated to 95 °C for 30 sec and then cooled down to 59 °C with 0.3 °C / min. Afterwards they were kept in ice for 15 min. The five samples were combined and to the annealing mixture 5 μL Klenow buffer (1x), 10 μL α-^{32}P-dCTP (20 μCi / μL), 3.3 μL Klenow enzyme (10 U/μL) and water to final volume of 50 μL were added. The reaction mixture was incubated at 37 °C for 1 h. Afterwards an equal amount of formamide loading buffer was added to the mixture. The 3′-labelled RNA was purified and isolated using the same procedure as described above for the 5′-end labelled RNA.

Oligo DNA splints used for 3′end labelling

During the optimization of the labelling procedure three DNA constructs were tested but the best labelling efficiency was achieved using the DNA 16.

DNA 23: 5′-CCGGGAACTTACGTCCGAAGAGC-3′

DNA 21: 5′-CCGAACTTAGCTCCGAAGAGC-3′

DNA 16: 5′-GCGGGAACTTAGCTCC-3′

5.10.4 Preparation of radiolabelled platinated D1-27

For the preparation of labelled platinated RNA the experimental procedure followed is exactly the same as when unlabelled platinated RNA is prepared. The only difference is that both labelled and unlabelled RNA are used. More specifically the platination reactions of D1-27 with oxaliplatin were performed using the optimal conditions found for oxaliplatin (0.1 mM un labelled RNA, 5 eq of oxaliplatin, incubation for 1 day at 25 ℃ in 120 mM KCl) but also 1 - 2 nM of end radiolabelled D1-27 was added in the platination reaction mixture.

5.10.5 Alkaline hydrolysis and enzymatic digestions of the radiolabelled RNA samples

Both unreacted and platinated ^{32}P-end labelled RNAs were subjected to alkaline hydrolysis and enzymatic digestions. For all samples four lanes were loaded: control, partial hydrolysis ladder lane (OH^-), RNase T1 lane (T1) and S1 nuclease lane (S1). Equal amount of ^{32}P-end labelled RNA and final volume of 10 μL were used in all cases. The final concentration of the labelled RNA was 0.1 nM. 25 % denaturing gels were used and they were run at room temperature for 4 - 6 h.

Control lane: The control is crucial in order to check the extent of degradation of the RNA sample. Ideally this lane should contain only one band corresponding to the full-length RNA. In this case, all cleavage products seen in the other lanes are real and can be considered for further evaluation. For the preparation, ^{32}P-end labelled RNA is diluted in water and equal volume of formamide buffer is added. The sample is stored in liquid nitrogen until loaded on the gel.

Partial alkaline hydrolysis ladder lane: ^{32}P-end labelled RNA in water was mixed with 8 μL of 0.5 M Na_2CO_3 and 8 μL of ddH_2O. The mixture was gently mixed by pipetting and incubated for 10 min at 90 °C. Equal volume of formamide buffer was added. The sample was stored in liquid nitrogen until loaded on the gel.

RNase T1 ladder lane: RNase T1 was used to digest the ^{32}P-end labelled RNAs. RNase T1 cleaves single-stranded RNA after guanosine residues on their 3'-end and therefore digestion of 3' or 5' labelled RNA with this enzyme leads to a ladder of G residues. ^{32}P-end labelled RNA in water was mixed with 6 μL colourless gel loading buffer, 1 μL citrate buffer and 2 μL T1 (20 U/μl). The mixture was gently mixed by pipetting and incubated for 20 min at 55 °C. Equal volume of formamide buffer was added. The sample was stored in liquid nitrogen until loaded on the gel.

S1 nuclease ladder lane: The S1 nuclease is known to cleave single-stranded region caused by, e.g., mismatches or loops. This enzyme was used to identify loop regions and/or structural changes induced by platination on the labelled samples. ^{32}P-end labelled RNA in water was mixed with 2 μL reaction buffer (5x), 4.1 μL $ZnSO_4$, 0.8 μL S1 (0.8 U/μL) and 2.1 μL water. The mixture was gently mixed by pipetting and incubated for 20 min at 25 °C. Equal volume of formamide buffer was added. The sample was stored in liquid nitrogen until loaded into the gel.

5.11 Plasmid binding studies

The plasmid binding studies were performed during a short-term scientific mission (STSM) funded by the COST Action CM1105 which was performed in the laboratory of Prof. Sofi K. C. Elmroth in Lund, Sweden. For this study the pUC19 plasmid (2686 bp) (pUC18 plasmid, purified by use of a midi-prep kit from Sigma– Aldrich) was used and the platination agents investigated were the monoaquated complexes of cisPt, kitePt, and [Pt(DACH)Cl_2].

5.11.1 Buffers

200 mM Na_2HPO_4 / NaH_2PO_4 (NaPi) buffer pH 5.8: Mixing 23 mL of 200 mM NaH_2PO_4 solution with 2 mL of 200 mM Na_2HPO_4 solution.

200 mM K_2HPO_4 / KH_2PO_4 (KPi) buffer pH 5.8: Mixing 23 mL of 200 mM KH_2PO_4 solution with 2 mL of 200 mM K_2HPO_4 solution.

Loading dye with NaCl: 1.1 M urea, TBE, 33 % (v/v) formamide, 0.025 % (w/v) bromophenol blue, 0.025 % (w/v) xylene cyanol, 500 mM NaCl.

5.11.2 Experimental procedure

The ratio between DNA plasmid concentration (C_{DNA}) and the concentration of the platinum(II) complexes (C_{Pt}) ($r_f = C_{Pt}/C_{DNA}$) used for the binding study varied between 0 and 0.5. All platination reaction experiments were performed in 200 mM Na_2HPO_4 / NaH_2PO_4 (NaPi) and K_2HPO_4 / KH_2PO_4 (KPi) buffer pH 5.8, incubating at 37 °C for 1 day. The reactions were quenched by addition of 5 µL loading dye with NaCl. The platination reactions were analyzed on 2% agarose-TAE gel containing 0.6 µg / mL ethidium bromide (EB) using 1x Tris-Acetic acid-EDTA (TAE) as running buffer. The gels were run for 1.5 h at 70 V. The gel images were visualized by UV light and a photo was taken using a MP-4 Polaroid camera and analyzed by DiMAGE Capture A2.

5.12 References

1. Gallo, S., Furler, M. & Sigel, Roland K. O. *In vitro* transcription and purification of RNAs of different size. *CHIMIA* **59,** 812–816 (2005).
2. Kao, C., Rudisser, S. & Zheng, M. A simple and efficient method to transcribe RNAs with reduced 3' heterogeneity. *Methods* **23,** 201–205 (2001).
3. Donghi, D. & Sigel, Roland K. O. Metal ion-RNA interactions studied via multinuclear NMR. *Methods Mol. Biol.* **848,** 253–273 (2012).
4. Kidani, Y., Inagaki, K., Iigo, M., Hoshi, A. & Kuretani, K. Antitumor activity of 1,2-diaminocyclohexaneplatinum complexes against Sarcoma-180 ascites form. *J. Med. Chem.* **21,** 1315–1318 (1978).
5. Lau, J. K.-C. & Ensing, B. Hydrolysis of cisplatin--a first-principles metadynamics study. *Phys. Chem. Chem. Phys.* **12,** 10348–10355 (2010).
6. Giese, R. W., Shimelis, O. & Zhou, X. Scaled-down nuclease P1 for scaled-up DNA digestion. *Biotechniques* **34,** 908–909 (2003).
7. Berova, N., Nakanishi, K. & Woody, R. *Circular dichroism. Principles and applications.* 2nd ed. (Wiley-VCH, New York, 2000).
8. Jean-Louis Mergny, Laurent Lacroix. Analysis of thermal melting curves. *Oligonucleotides* **13,** 515–537 (2003).
9. Markley, J. L., Bax, A., Arata, Y., Hilbers, C. W., Kaptein, R., Sykes, B. D., Wright, P. E. & Wüthrich, K. Recommendations for the presentation of NMR structures of proteins and nucleic acids. IUPAC-IUBMB-IUPAB inter-union task group on the standardization of data bases of protein and nucleic acid structures determined by NMR spectroscopy. *J. Biomol. NMR* **12,** 1–23 (1998).
10. Figueroa, N., Keith, G., Leroy, J. L., Plateau, P., Roy, S. & Gueron, M. NMR study of slowly exchanging imino protons in yeast $tRNA^{Asp}$. *Proc. Natl. Acad. Sci. U. S. A.* **80,** 4330–4333 (1983).
11. Huang, Z. A simple method for 3'-labeling of RNA. *Nucleic Acids Res.* **24,** 4360–4361 (1996).

6 Summary

The nucleic acids, DNA and RNA, are chemically very similar, but, since DNA is considered the source of all the vital information for life, it was the one that was mostly studied as potential drug target. However, studies of the past decades revealed new classes of biologically relevant non-coding RNAs, which are involved in crucial biological functions, like regulation of transcription and translation, control of gene expression and catalysis of protein synthesis. The multiple biologically important roles of RNA together with the great variety of new classes of functional non-coding RNAs found, have promoted RNA to an important potential drug target. The variety of RNA roles is to a great extent connected with its peculiar structure. More specifically RNA molecules can adopt a wide range of alternative conformations, which vary from local (e.g. bulged nucleotides) to drastic rearrangements of its secondary structure and tertiary folding. Due to the negative charge of its backbone, metal ions are crucial for correct RNA folding and are eventually involved in catalysis. Formation of complex three-dimensional RNA structures create binding pockets, which could be specifically targeted by metal ions. Targeting these complex structures with small molecules could interfere with RNA function. Considering this, the development of small molecules for RNA targeting has received a lot of attention.

Cisplatin, oxaliplatin and carboplatin are the three platinum(II) complexes which are used in clinics worldwide (Figure 6.1). Despite their success, their severe side effects and tumour resistances are limiting their usage. Platinum(II) anticancer drugs in general are thought to exert their anticancer activity mainly upon covalent binding to nuclear DNA. However, numerous studies showed that cisplatin toxicity could result also from various sources including interactions with proteins, lipids, peptides and RNA. For this purpose research has been dedicated on the one hand to the development of new platinum(II) complexes which could have better performance, on the other hand to the in-depth understanding of their mechanism of action, performing studies on their interaction with biological targets other than DNA. Toward this direction, besides platinum(II)-DNA studies, the interaction between platinum(II)-protein have also received a lot of attention but much less studied are the platinum(II)-RNA interactions.

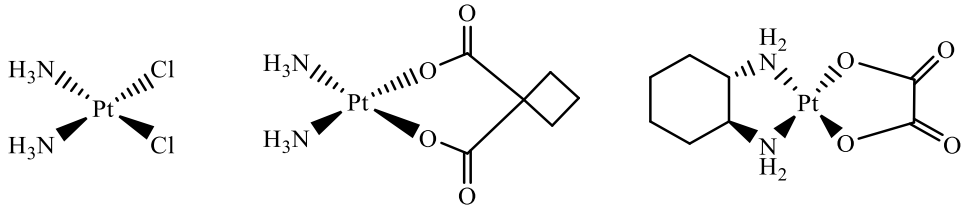

Figure 6.1: *Platinum(II) drugs which are in clinical use worldwide: Left: cisplatin; middle: carboplatin: right: oxaliplatin.*

Recent reports revealed that platinum accumulated in total 4- to 20-fold more in total cellular RNA than in genomic DNA and that important RNA-based activities like transcription, splicing and translation are inhibited upon administration of cisplatin. Studies on RNA duplexes, hairpin models as well as more

structured RNAs revealed that a common characteristic of all the Pt(II)-RNA adducts is the binding of platinum(II) in non-Watson-Crick base paired regions and its high selectivity towards the GG sites **(Chapter 1)**.

In this thesis we mainly investigated the interaction of oxaliplatin (Figure 6.1, right) with a model RNA construct (D1-27) (Figure 6.2) and characterized its isolated monoplatinated RNA adducts using various biochemical and spectroscopic techniques. D1-27 represents a good RNA model for many reasons: 1) it contains biologically relevant RNA structural motifs (internal and terminal loops) and various guanines and adenines which represent potential platinum(II) binding sites, allowing to study possible sequence and structure preferences of platinum binding, 2) its NMR characterization in solution is known making easier the NMR investigation of its platinated adducts and 3) NMR studies on its interaction with metal ions have been recently reported, giving us information about the regions which are available for metal-ion binding. Additionally to D1-27, few other RNA constructs were employed in this study, mostly to evaluate the influence of the various structural elements of D1-27 in its interaction with oxaliplatin (Figure 6.2).

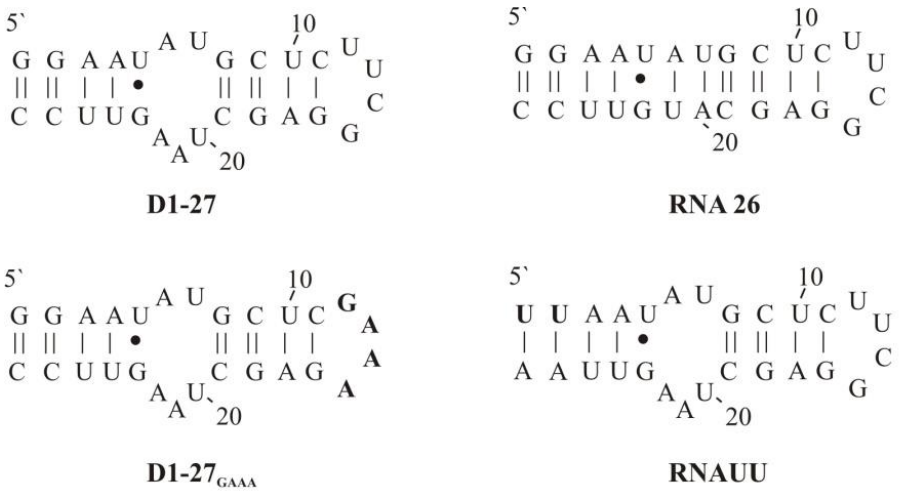

Figure 6.2: *The secondary structures of all RNAs used in this study. Starting from the main construct D1-27 other three D1-27 analogues were used. RNA 26 does not contain the internal loop, D1-27$_{GAAA}$ has a -GAAA- tetraloop instead of a -UUCG- and the RNAUU has two U-A base-pairs instead of 2 G-C base-pairs.*

In the first part of **Chapter 2** are discussed the reasons why this study was conducted using oxaliplatin as platination agent. Upon platination a slower migrating band (upper) was formed and, from MALDI-MS characterization, it was found that it contained a mixture of monoplatinated and diplatinated RNA, with the first being the major species (Figure 6.3, red frame). The lower band (Figure 6.3, green frame) contained mostly unreacted RNA but also monoplatinated and diplatinated RNA

species as its MALDI-MS revealed. However, due to its heterogeneity, the sample isolated from the lower band was not used for further characterization. Considering the sample isolated from the upper band, since no separation between the two species was achieved using denaturing PAGE, the use of HPLC was attempted. Despite the optimization, the retention time of the mono- and diplatinated RNA were very close, and no successful separation was obtained. Next, the use of HPLC for the isolation and purification of the platinated RNAs instead of dPAGE was attempted, with the platination mixture being directly injected in the HPLC machine after the end of the reaction. However, no advantage with respect to dPAGE separation was obtained, and all the samples were then purified and isolated using denaturing gels. Unfortunately, isolation of pure monoplatinated RNA was not possible, likely because of the heterogeneity of the reaction mixture. However, HPLC could be used to quantify the diplatinated species (12 %). The heterogeneity observed could be the result of the use of RNA samples with triphosphate and diphosphate groups at the 5′-end, which led to the formation of platinated RNA species with different number of phosphate groups. In order to have a homogeneous starting material, D1-27 was dephosphorylated before being used for platination.

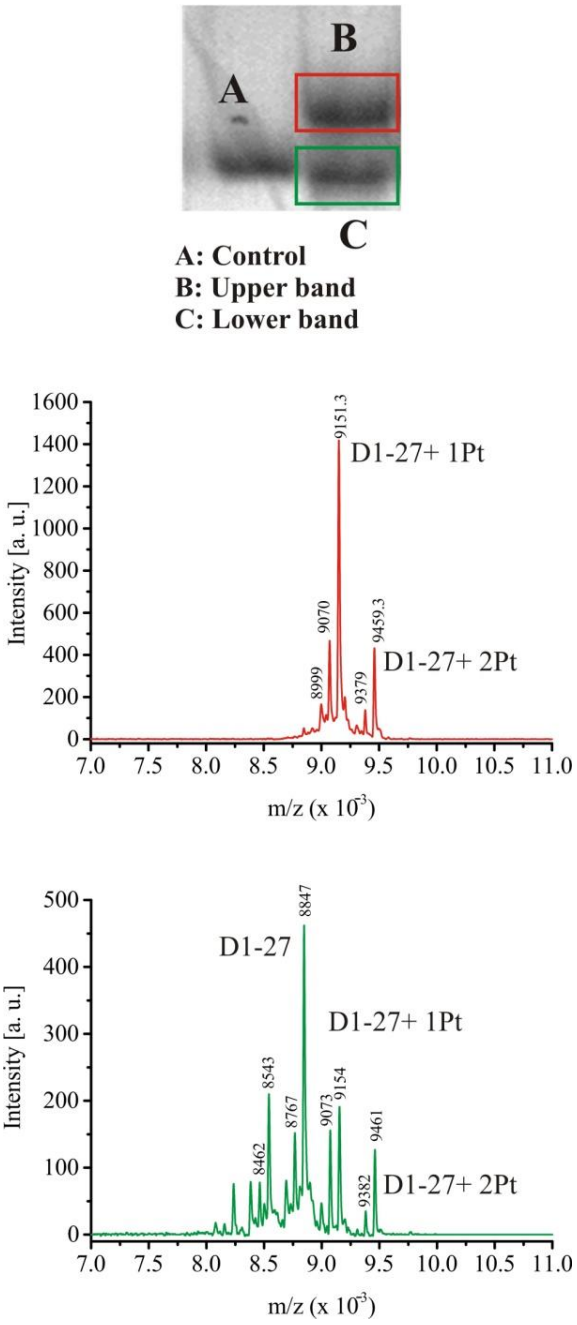

Figure 6.3: *20 % denaturing PAGE for the platination reaction of D1-27 with oxaliPt (0.25 mM RNA incubated with 5 eq of oxaliPt at 25 °C for 1 day in the presence of 120 mM KCl). The gel was run at 4 °C. Characteristic mass spectra of the samples isolated from the upper and lower band are depicted.*

The platination of deph-D1-27 resulted in a gel with three bands instead of the two always observed when triphosphate-D1-27 (triph-D1-27) was used (Figure 6.4). In addition to the slower migrating band observed also in the previous case (upper), a new faster migrating band (lower), which consisted of monoplatinated and diplatinated RNA, appeared. By using deph-RNA the chromatogram of the platinated RNA species isolated from the upper band was improved and two main peaks were observed

corresponding to monoplatinated and diplatinated RNA. Now, contrary to what previously observed, isolation of a more homogeneous platinated sample seems to be possible, but further optimization is required if the method is to be used to obtain large amount of homogeneous sample. However, since the monoplatinated species in the sample isolated from the upper band always accounted for around 90 % of the total sample, we proceeded with further characterization of these isolated platinated RNA species (see below).

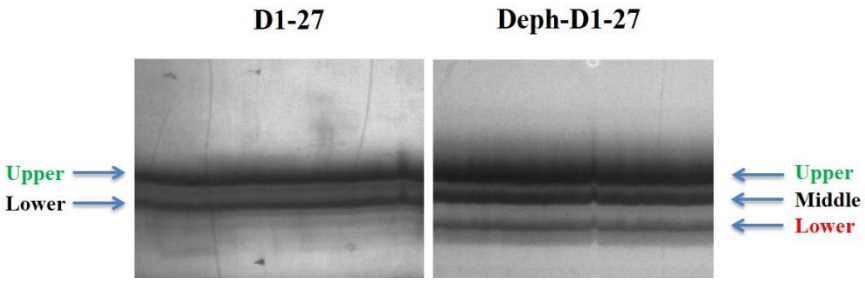

Figure 6.4: *20 % denaturing PAGE for the platination reaction of triph-D1-27 (left) and deph-D1-27 (right) with oxaliPt. In the same colours are indicated the bands that had similar MS spectra. The gel was run at 4 °C.*

Chapter 3 is mainly devoted to the time evolution NMR experiments as a quick way to follow and evaluate platination reactions. These NMR experiments together with denaturing PAGE, were utilized in order to compare the behaviour of different platination agents, namely oxaliplatin, cisplatin and kiteplatin, towards D1-27. Information about the platination reaction rates of all three platinum(II) complexes were also collected from DNA unwinding experiments. The most important results obtained from these experiments are summarized in Table 6.1. For the platination of D1-27 with oxaliPt the influence of the terminal tetraloop (D1-27$_{GAAA}$), the presence of the internal loop (RNA 26) and the role of the 5′-end phosphate group (deph-D1-27) on the platinum(II) binding sites were investigated. From this study it was concluded that there is no interaction at the terminal -UUCG- tetraloop and a very possible target is the G1-G2 site. Contrarily, the variations observed at G8 could be linked to structural changes induced upon platination at, for example, G1-G2, which may affect G8 because of the presence of the internal loop. The removal of the triphosphate group (deph-D1-27) led to similar conclusions, with the difference that the reaction at the G1-G2 site was not as fast as before. Lastly, the replacement of the -UUCG- tetraloop for the -GAAA- one made the terminal loop region more prone to platinum binding.

Even if changes in the imino proton resonances allow collecting important information on platination reactions, this approach cannot be used alone for the evaluation of direct platinum binding sites, because the imino proton resonances are influenced by many different experimental factors and are very sensitive to local structural changes (see behaviour of G8).

A first evaluation of the different platinum binding preferences and reaction kinetics of monoaquated cisPt and monoaquated kitePt [(Pt(cis-1.4DACH)Cl (H_2O)]$^+$ compared to oxaliPt was performed with the combination of time evolution NMR experiments and PAGE analysis under the same platination reaction conditions (Table 6.1). CisPt was found to be the agent, which was binding faster and less specific to RNA and oxaliPt was the one with good specificity and good reaction kinetics. KitePt exhibited an average behaviour between the other two, because it seemed to be more specific than cisPt but less than oxaliPt. Indeed, in addition to G1-G2 platination, another site seems to be platinated, in line with the results obtained from the MALDI-MS spectrum of its isolated platinated species, which show that the diplatinated species is the major one. However, further experiments are required to identify the second platination site. Plasmid binding assays confirmed the above-mentioned behaviour. In the end the kinetics and the role of K(I) and Cl^- in the platination reactions of all three platinum(II) complexes was investigated using PAGE analysis. Furthermore, time evolution NMR experiments were employed to follow the platination reaction of monoaquated cisPt in the presence and absence of K(I) and Cl^-, which further supported its high reactivity and reduced specificity.

Table 6.1: *Summary of the results obtained from the experiments commented in chapter 3. Time evolution ^{1}H-NMR experiments and denaturing PAGE assays were performed under the same experimental conditions.*

		D1-27	
Method	Oxaliplatin	Kiteplatin	Cisplatin
Time evolution ^{1}H-NMR experiments	G1-G2	G1-G2 & a second platination site	non-specific interaction
Plasmid binding assays	Coalescent point at r_f=0.5	Coalescent point at r_f=0.5 but the smeary band appeared earlier than oxaliPt = faster than oxaliPt	Coalescent point at r_f=0.15 Faster compared to the other two complexes
PAGE	Two bands Upper: mainly monoplatinated species	Two bands Upper: mainly diplatinated species	Extended smeary band

Chapter 4 is dedicated to the characterization of the platinated species, which were isolated from the upper band of denaturing gels run on reaction mixtures performed with both triph- and deph-D1-27. In all cases, the main species contained in the samples is monoplatinated RNA (88 %), even if a small percentage of diplatinated RNA (12 %) is present. The characterization of the Pt-RNA adducts migrating in the upper band was performed using various methods. Platinated adducts obtained using homogeneous Pt-deph-RNA as starting material were mainly characterized. However, very similar behaviour was observed for the Pt-triph-RNA adducts, thus suggesting the same platination pattern for the upper band species in the two cases. Each technique used provided us with an information about the binding of oxaliPt to the RNA construct. The thermal melting studies (Figure 6.5, A) showed that the platination affects significantly only the first part the RNA construct, because only Tm_1 changed upon platination. Therefore, platination in this area was suggested. The reduction of Tm_1 compared to the unreacted RNA indicates destabilization of the RNA construct upon platinum binding, thus suggesting intrastrand cross-link. No information about the binding sites could be provided from this method. The CD spectra of the unreacted and platinated RNA showed that the platination did not change the overall RNA conformation, and the little changes observed are likely due to local perturbations caused by the presence of the

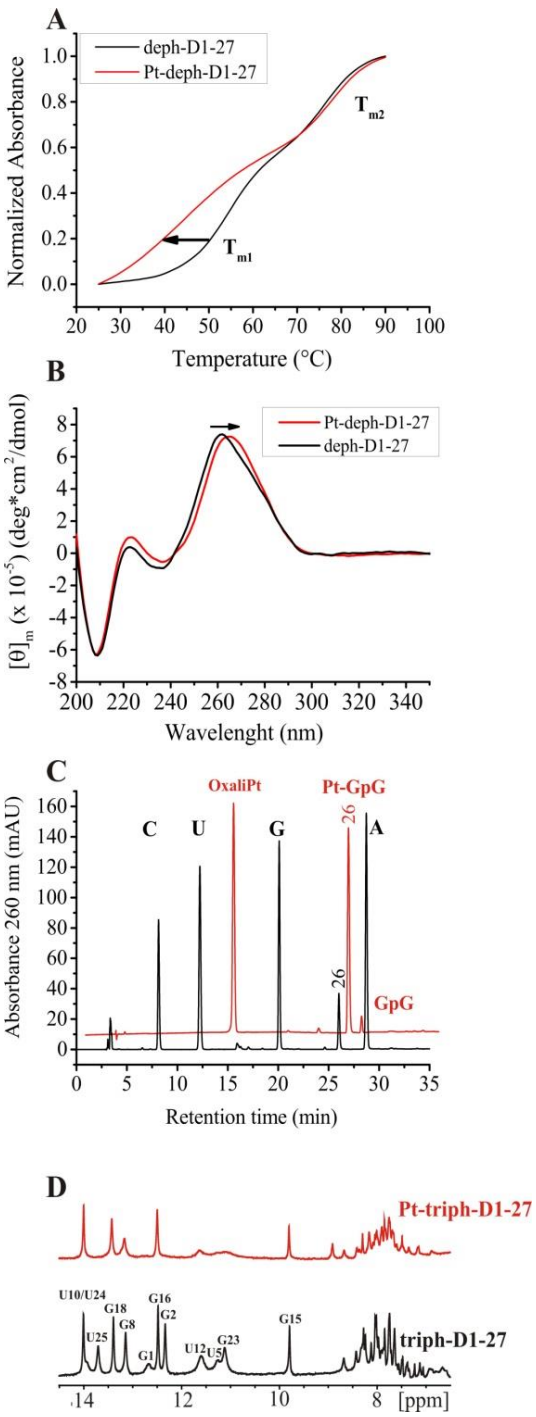

Figure 6.5: *Summary of the most important methods used for the characterization of the Pt-RNA sample isolated from the upper band. A: Indicative thermal melting profiles for deph-D1-27 (black) and Pt-deph-D1-27 (red). B: Comparison of the CD spectra of D1-27 (black) and Pt-D1-27 (red). C: HPLC chromatograms of the digestion of Pt-deph-D1-27, which led to the appearance of a new peak (black) and of the reaction of the GpG dinucleotide with oxaliPt (red). The chromatogram in red is shifted to facilitate comparison. D: ^{1}H-NMR spectra (aromatic and imino proton regions) of the D1-27 (black) and Pt- D1-27 sample isolated from the upper band (red line).*

platinum moiety (Figure 6.5, B). More specifically the bathochromic shift of the band at 260 nm can be connected to intrastrand platinum binding to RNA. The enzymatic digestion / HPLC treatment of the non-platinated and platinated RNA species gave us the first indication about a possible platination site (Figure 6.5, C). The platinated RNA species have an extra peak in the HPLC chromatogram and from the comparison of the relative peak areas a loss of two guanines was estimated. The new peak has the same retention time as the Pt-GpG species, which was formed upon platination of the GpG dinucleotide, thus suggesting platination at a GG site. From the combination of the collected information so far, it seemed that two adjacent guanines were platinated, which should be located in the first part of the construct. The only two guanines fulfilling these criteria are G1 and G2. Further characterization, like ^{32}P-5′- and ^{32}P-3′-end radiolabelling techniques were employed in order to get information about the platination site. Partial alkaline hydrolysis and enzymatic digestions on platinated ^{32}P-5′-end labelled samples showed that G23, which is located in the first part of the construct, is not directly platinated. However, no information on the first two nucleotides could be obtained with this technique. Therefore, we used ^{32}P-3′-end labelled samples. In this case, we observed changes of the intensity of the gel bands corresponding to G1 and G2 upon platination. This suggests platination at G1-G2, in agreement with the previous findings. At the end, ^{1}H-NMR spectra were recorded on isolated samples, and comparison of the imino proton resonances before and after platination was performed (Figure 6.5, D). The guanine imino proton resonances mostly affected by platination correspond to G1 and G2. Interestingly, the imino proton resonances of the isolated upper band are very similar to the ones of the RNAUU construct (Figure 6.2), confirming destabilization at the 5'-end in the presence of platinum(II), likely due to G1-G2 platination. Also, a [^{1}H,^{13}C]-HSQC experiment performed on an isolated platinated sample further supports direct platination at G1 and G2. Finally, in order to investigate the nature of the species responsible for the faster migrating band (lower) observed when dephosphorylated RNA is used as starting material in the platination reactions, (Figure 6.4) a preliminary characterization was performed, consisting of CD, thermal melting studies and enzymatic digestion/ HPLC. The platinated RNAs migrating in the lower band represent secondary species considering that the main ones are platinated at the G1-G2 site. MALDI-MS spectra of the sample isolated from this band showed that there is an increased amount of diplatinated RNA compared to the species isolated from the upper band. Moreover, enzymatic digestion / HPLC analysis were not consistent, since the results vary as different samples were used and a mixture of differently platinated species was found to be formed. Due to their heterogeneity as well as to the presence of increased amount of diplatinated species, no clear conclusion could be drawn about the way that platinum was bound to D1-27 in these minor species.

Summing up, upon interaction of oxaliplatin with D1-27 under the experimental conditions used for this study, despite the presence of many possible platinum(II) binding sites, strong preference for platination at G1-G2 was observed, leading to monoplatinated RNA species with decreased gel mobility. The GG site of DNA is the most common platinum binding site for platinum(II) anticancer

drugs[47] and strong preference for this motif has been reported also for RNA platination with cisplatin. Our data revealed that oxaliplatin also showed a strong preference for the most accessible GG site (G1-G2) which is in line with the currently reported finding on RNA platination.

Despite their widespread use, platinum(II) anticancer drugs have severe side effects as well as some tumours display intrinsic or acquired resistance towards them. Moreover, despite their importance, there is still lack of comprehensive understanding of their complex biological activity, including how intracellular molecules are targeted by them. An approach to eliminate their side effects is trying to develop a better understanding of their mechanism of action, which may be achieved by in-depth studies on their interaction with biomolecules other than DNA. RNA may represent a good platinum(II) drug target, considering its importance and involvement in crucial cellular functions. Along this line, early studies revealed that platinum(II) drugs can inhibit important RNA-based activities which are crucial for the survival of the cell. Considering this we performed a detailed study on the interaction of oxaliplatin with an RNA model (D1-27) from which we aimed at investigating the possible platinum binding sites. An accurate knowledge on platinum binding sites in RNA molecules does not only provide a way for predicting modification sites in other biologically relevant RNA molecules but also helps towards the better understanding of the versatile nature of platinum(II) drugs anticancer activity. All these could lead to the design of new less toxic and more effective platinum(II) drugs and/ or to novel therapies towards cancer treatment.

7 Zusammenfassung

Die Nukleinsäuren DNS und RNS sind sich chemisch gesehen sehr ähnlich. Da die DNS der Träger der Erbinformation in allen lebenden Organismen ist, wurde jedoch hauptsächlich nur sie als potentielles Zielmolekül für Medikamente wahrgenommen und untersucht. In den vergangenen Jahrzehnten haben aber zahlreiche Studien gezeigt, dass nichtkodierende RNS in vielen essentiellen biologischen Prozessen involviert ist, wie z.B. Kontrolle der Genexpression durch die Regulierung von Transkription und Translation oder als Katalysator in der Proteinbiosynthese. Bis heute werden stetig neue Klassen nichtkodierender RNS mit neuen Funktionen gefunden, wodurch die RNS als potentielles Ziel für Medikamente immer mehr in den Fokus rückt. Dass die RNS so eine grosse Vielfalt von Aufgaben übernehmen kann, ist hauptsächlich auf ihre einzigartige Struktur zurückzuführen. Die einzelsträngigen RNS Moleküle können sich in verschiedene komplexe Strukturen falten, die neben den typischen doppelsträngigen Bereichen, die auch in DNS zu finden sind, viele Alternativkonformationen aufweisen. Strukturvariationen in der RNS-Struktur reichen von kleinen lokalen Unterschieden (z.B. Wölbung formende Nukleotide) bis hin zu verschiedenen Sekundärstrukturen und tertiären Faltungen. Die Metallionen sind für die korrekte Faltung und somit auch für die Funktion von RNS entscheidend. Metallionen schirmen zum einen die negativen Ladungen des Phosphatrückgrats voneinander ab, können aber auch spezifisch in Strukturmotive der RNS binden und so zum Beispiel eine bestimmte Faltung stabilisieren oder auch direkt in der Katalyse von Ribozymen (katalytisch aktive RNS) mitwirken. Das zunehmende Interesse gezielt Funktionen von RNS Molekülen zu beeinflussen, hat in den letzten Jahren die Entwicklung und Synthese kleiner RNS-bindender Moleküle stark vorangetrieben.

Die drei Platin(II)-Komplexe Cisplatin, Oxaliplatin und Carboplatin werden heutzutage weltweit als Krebsmedikamente in Kliniken verwendet (Abbildung 7.1). Trotz ihres Erfolges, ist ihr Einsatz mit schwerwiegenden Nebenwirkungen verbunden und durch Tumorresistenzen begrenzt. Es wird angenommen, dass ihre Wirkungsweise gegen den Krebs hauptsächlich auf eine kovalente Anbindung an die nukleare DNS beruht. Zahlreiche Studien mit Cisplatin haben jedoch ebenfalls gezeigt, dass die toxische Wirkung auch andere Gründe haben kann, einschliesslich der Wechselwirkungen mit Proteinen, Fettsäuren, Peptiden und RNS.Die Forschung hat sich deshalb einerseits der Entwicklung neuer Platin(II)-Komplexe verschrieben, mit dem Ziel die Nebenwirkungen zu begrenzen und das Problem der Resistenzen zu lösen. Auf der anderen Seite wird seit Jahren der genaue Wirkungsmechanismus nicht nur mit DNS, sondern auch mit anderen Biomolekülen untersucht. In diesem Zusammenhang hat vor allem die Interaktion zwischen Platin(II) und Proteinen viel Beachtung gefunden, wohingegen die Platin(II)-Interaktion mit RNS viel weniger studiert wurde.

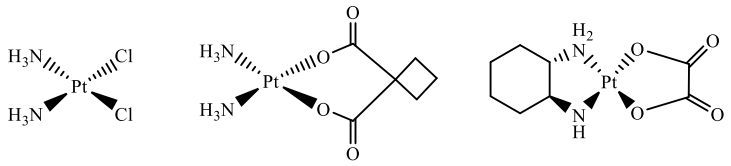

Abbildung 7.1: *Platin(II)-Medikamente, die weltweit klinisch verwendet werden: Links: Cisplatin; Mitte: Carboplatin; Rechts: Oxaliplatin.*

Aktuelle Studien belegen, dass Platin(II)-Komplexe sich 4 bis 20 mal mehr in zellulärer RNS als in genomischer DNS ansammeln, und dass wichtige RNS-basierte Prozesse wie Transkription, Spleissen und Translation durch die Verabreichung von Cisplatin unterbunden werden. Studien mit RNS-Doppelhelixen, RNS-Haarnadelstrukturen und anderen RNS-Strukturen zeigen, dass alle Pt(II)-Komplexe besonders gern an Stellen ohne Watson-Crick-Basenpaarung und an GG-reiche RNS-Regionen binden. **(Chapter 1)**.

In dieser Dissertation wurde die Wechselwirkung der drei verschiedenen Pt(II)-Komplexen Oxaliplatin, Cisplatin und Kiteplatin mit einem modellhaften RNS-Konstrukt (D1-27) (Abbildung 7.2) untersucht. Oxaliplatin ist dabei der Fokus dieser Arbeit, da nur mit diesem Komplex monoplatinierte RNS-Addukte isoliert werden konnten, die anschliessend mit Hilfe

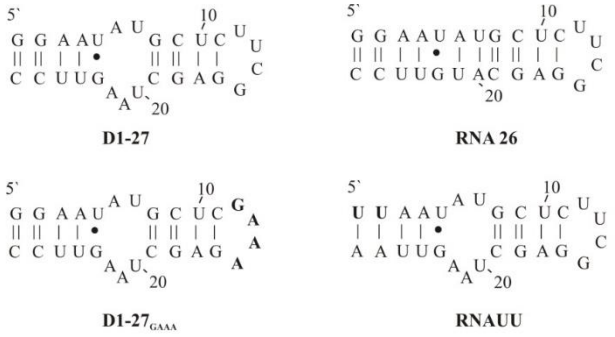

Abbildung 7.2: *Die Sekundärstrukturen aller in dieser Studie verwendeten RNS-Konstrukte. Ausgehend vom Hauptkonstrukt D1-27 wurden drei weitere D1-27-Analoga verwendet. RNS 26 enthält keine interne Schleife, D1-27$_{GAAA}$ hat eine -GAAA- anstelle einer -UUCG- Tetraschleife und das RNAUU hat zwei U-A Basenpaare anstelle zweier G-C Basenpaare.*

von diversen biochemischen und spektroskopischen Techniken charakterisiert wurden. Die D1-27 RNA ist aus folgenden Gründen ein gut geeignetes RNS-Modell: 1. Es enthält biologisch relevante RNS-Sekundärstrukturen (interne und terminale Schleifen, sogenannte loops) und mehrere aufeinanderfolgende Guanine und Adenine, die potentielle Liganden für die Platin(II)-Bindungen darstellen. Dadurch können mögliche Struktur- und Sequenzpräferenzen der Platinierung gut untersucht werden. 2. Die NMR-Struktur von RNS D1-27 in Lösung ist bekannt, was die NMR-Charakterisierung seiner platinierten Addukte sehr erleichtert. 3. NMR-Studien, die die Wechselwirkung von D1-27 mit Metallionen analysiert haben, wurden kürzlich veröffentlicht. Die dort gefundenen und beschriebenen Metallionenbindungsstellen sind auch potentielle Bindungsstellen für die Platin(II)-Komplexe. Um den Einfluss der einzelnen Strukturelemente in D1-27 auf die Wechselwirkung mit Oxaliplatin zu

analysieren, wurden zusätzlich zu D1-27 noch drei weitere RNS-Konstrukte verwendet (Abbildung 7.2).

Im ersten Teil des zweiten Kapitels **(Chapter 2)** werden die Resultate gezeigt und erläutert, die erklären warum hauptsächlich Oxaliplatin als Platinierungswirkstoff in unsere Studie verwendet wurde. Denaturierende Polyacrylamid-Gelelektrophorese (dPAGE) nach der Platinierungsreaktion von D1-27 RNS mit Oxaliplatin ergab zwei Banden, **B** und **C** (Abbildung 7.3 oben rechts). Mittels MALDI-Massenspektrometrie (MALDI-MS) wurde festgestellt, dass die langsamer laufende Bande **B** eine Mischung aus mono- und di-platinierter RNS war, mit der monoplatinierte Spezie als Hauptprodukt (roter Rahmen, rotes MS Spektrum). Die untere Bande **C** (grüner Rahmen, grünes MS Spektrum) enthielt hauptsächlich unreagierte RNS, aber wie das MALDI-MS Spektrum zeigt, zu einem kleinen Anteil auch mono- und di-platinierte RNS. Aufgrund ihrer Heterogenität wurde die untere Bande nicht für eine weitere Charakterisierung verwendet. Mit Hilfe von Hochleistungsflüssigkeits-chromatographie (HPLC)

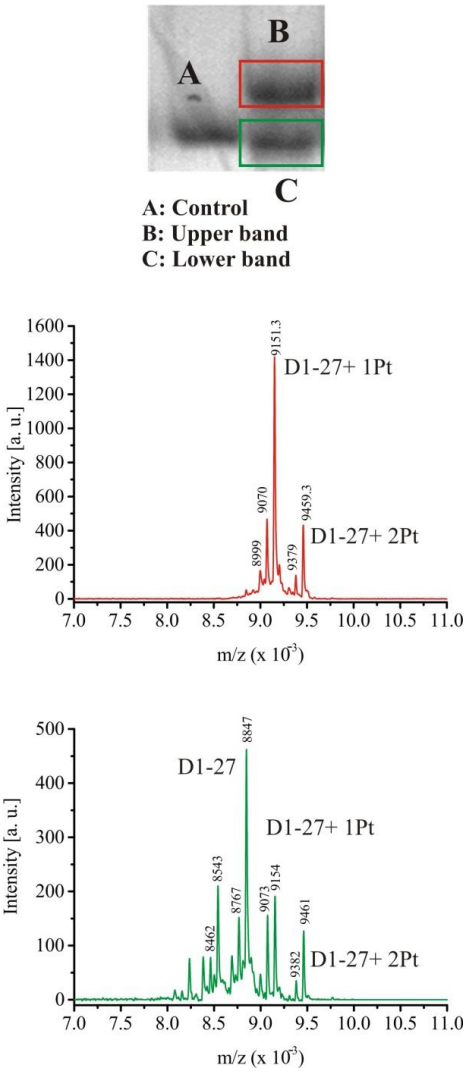

Abbildung 7.3: *20 % denaturierendes PAGE für die Platinierungs-reaktion von D1-27 mit oxaliPt (0.25 mM RNS inkubiert mit 5 eq oxaliPt bei 25 °C für 1 Tag in Gegenwart von 120 mM KCl). Das Gel lief bei 4 °C. Die charakteristischen Massenspektren der oberen (rot) und der unteren Bande (grün) sind dargestellt.*

haben wir versucht die mono- und di-platinierten Spezien der Bande **B** voneinander zu trennen. Trotz Optimierung der Trennungsbedingungen waren die Retentionszeiten der mono- und di-platinierten RNS zu ähnlich, um die beiden Spezien erfolgreich separieren zu können. Es wurde daher versucht das Reaktionsgemisch direkt nach der Platinierung mit Hilfe der HPLC aufzutrennen, aber auch das ohne Erfolg. Da gegenüber der dPAGE-Trennung kein Vorteil erzielt werden konnte, wurden alle RNS-Proben nach erfolgter Platinierung weiterhin mit denaturierenden Gelen aufgereinigt und isoliert. Die Isolation einer reinen monoplatinierter RNS war leider nicht möglich, wahrscheinlich aufgrund der Heterogenität des Reaktionsgemisches. Nichtsdestotrotz konnte mittels HPLC die diplatinierte Spezie quantifiziert werden (12 %). Die direkte Verwendung transkribierter RNS könnte der Grund für die beobachtete Heterogenität der Proben sein, da diese sowohl Tri-, Di- also auch Monophosphatgruppen am 5′-Ende

tragen können. Um mit einem homogenen Ausgangsmaterial zu starten, wurde D1-27 vor der Platinierung dephosphoryliert. Die Platinierung von deph-D1-27 resultierte in einem Gel mit drei Banden anstatt der zwei Banden die für D1-27 beobachtet wurden (Abbildung 7.4). Zusätzlich zu den langsamer laufenden Banden B (upper) und C (middle), die auch bei der nicht dephosphorylierten Probe beobachtet wurden, erschien noch eine neue, schneller laufende Bande (lower), die mono- und di-platinierter RNS enthielt. Das Chromatogramm der oberen Bande von deph-D1-27 zeigte nun neu Hauptfraktionen, welche der mono- und di-platinierten RNS entsprechen. Im Gegensatz zu den nicht dephosphorylierten Proben, scheint nun die Isolation einer homogeneren platinierten Probe möglich. Es sind dennoch weitere Optimierungsschritte notwendig, um mit dieser Methode eine grössere Menge an homogener platinierter RNA zu isolieren. Da aber 90 % der oberen Bande der monoplatinierten Form entsprach, fuhren wir ohne eine weitere Aufreinigung mit der Charakterisierung fort (siehe unten).

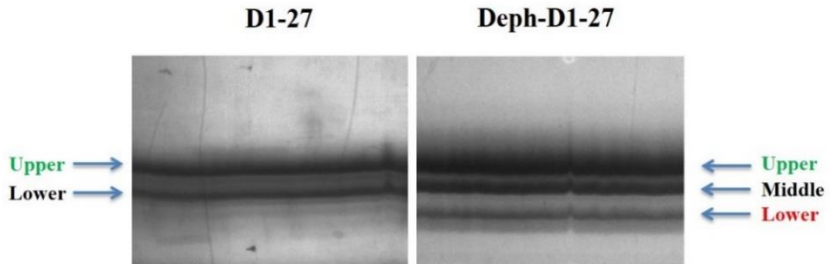

Abbildung 7.4: *20 % denaturierendes PAGE für die Platinierungsreaktion von D1-27 (links) und deph-D1-27 (rechts) mit oxaliPt. Die Banden mit ähnlichen MS-Spektra sind mit gleicher Farbe markiert. Das Gel lief bei 4 °C.*

In Kapitel 3 **(Chapter 3)** werden hauptsächlich die Ergebnisse der NMR-Zeitentwicklungsexperimente, eine Methode mit der die Platinierungsreaktionen schnell und einfach qualitativ verfolgt und ausgewertet werden können, beschrieben und diskutiert. Diese Ergebnisse zusammen mit den der denaturierenden PAGE Experimente wurden verwendet um das Verhalten der drei verschiedenen Platinierungsstoffe, namentlich Oxaliplatin, Cisplatin und Kiteplatin, gegenüber D1-27 zu vergleichen. Platinierungsreaktionsraten aller drei Platin(II)-Komplexe wurden zusätzlich aus DNS-Entwindungsexperimenten abgeschätzt. Die wichtigsten Resultate dieser Experimente sind in Tabelle 7.1 zusammengefasst. Die Platinierung von D1-27 mit oxaliPt wurde hinsichtlich des Einflusses der terminalen Tetraschleife (D1-27$_{GAAA}$), der Gegenwart einer internen Schleife (RNS 26) und der Rolle der Phosphatgruppe am 5′-Ende (deph-D1-27) auf die Platin(II)-Bindungsstellen untersucht. Aus dieser Studie wurde geschlossen, dass es mit Oxaliplatin keine Wechselwirkung an der terminalen -UUCG- Tetraschleife gibt und dass G1-G2 eine sehr wahrscheinliche Bindungsstelle ist. Im Gegensatz dazu wurden die beobachtete Variationen am G8 nicht einer direkten Platinierung sondern einer Strukturänderung zugeordnet. Vermutlich wird durch die Platinierung von G1-G2 die Struktur der internen Schleife verändert und so auch die Umgebung von G8 beeinflusst. Das Entfernen der Triphosphatgruppe (deph-D1-27) liess ähnliche Schlüsse zu, mit dem Unterschied, dass die Reaktion

an der G1-G2-Stelle nicht so schnell ablief wie zuvor. Zu guter Letzt machte das Ersetzen der -UUCG- durch die -GAAA- Tetraschleife die Region der terminalen Schleife empfänglicher für Platinbindungen.Auch wenn die Änderungen der Imino-Protonen-Resonanzen wichtige Rückschlüsse auf die Platinierungsreaktionen erlauben, kann dieser Methode nicht eigenständig für die Bestimmung der Platinbindungsstellen verwendet werden, da die Imino-Protonen-Resonanzen sehr stark auch von anderen experimentellen Bedingungen abhängig sind (wie z.B. Temperatur, pH, etc.).

Die Platinbindungspräferenzen und Reaktionskinetiken von monohydratisierten cisPt und monohydratisierten kitePt wurde mit der von oxaliPt, durch Kombination von NMR-Zeitentwicklungsexperimenten und PAGE-Analyse unter gleichen Platinierungsreaktionsbedingungen, verglichen (Tabelle 7.1). CisPt reagierte am schnellsten und am unspezifischsten mit D1-27, während oxaliPt recht spezifisch aber viel langsamer an D1-27 bindet. Das Verhalten von KitePt liegt zwischen dem von cisPt und oxaliPt, es ist spezifischer als cisPt aber unspezifischer als oxaliPt. Die Reslutate des MALDI-MS-Spektrum weisen auf eine diplatinierte Spezie als Hauptprodukt hin und lassen so eine zusätzliche Platinierungsstelle zu G1-G2 vermuten. Um die zweite Platinierungsstelle genau zu identifizieren sind aber noch weitere Experimente nötig. Das generell gefundene Verhalten der Komplexe wurde zusätzlich durch Plasmidbindungsuntersuchungen bestätigt. Weiterhin wurde die Kinetik und die Rolle von K(I) und Cl^- in den Platinierungsreaktionen aller drei Platin(II)-Komplexe mit Hilfe der PAGE-Analyse untersucht und im Fall von monohydratisierten cisPt NMR-Zeitentwicklungsexperimentein An- und Abwesenheit von K(I) und Cl^- durchgeführt, die zusätzlich die schnelle unspezifische Reaktion von cisPt bestätigten.

Tabelle 7.1: *Zusammenfassung der Resultate aus Kapitel 3. ^{1}H-NMR-Zeitentwicklungsexperimente und denaturierende PAGE-Untersuchungen wurden unter den gleichen Experimentalbedingungen durchgeführt.*

		D1-27	
Methode	Oxaliplatin	Kiteplatin	Cisplatin
^{1}H-NMR Zeitentwicklungs-experimente	Platinierung von G1-G2	Platinierung von G1-G2 & eine zweite Platinierungsstelle	Unspezifische Wechselwirkung
Plasmidbindungs-untersuchungen	Koaleszenzpunkt bei r_f=0.5	Koaleszenzpunkt bei r_f=0.5, aber die schmierige Bande erschien früher als bei oxaliPt → Reaktion ist schneller als bei oxaliPt	Koaleszenzpunkt bei r_f=0.15 schnellste Reaktionsrate
PAGE	Zwei Banden Oberes: hauptsächlich monoplatinierte Formen	Zwei Banden Oberes: hauptsächlich diplatinierte Formen	Erweiterte schmierige Bande

In Kapitel 4 **(Chapter 4)** werden die platinierten Addukte, die aus der oberen Bande der denaturierenden Gele von deph- und D1-27 RNS mit oxaliPt extrahiert wurden, mit verschiedenen spektroskopischen Methoden und Verdauungsexperimenten charakterisiert. Sowohl für die deph-D1-27 als auch für D1-27 wurde vorwiegend monoplatinierte RNS (88 %) mit einem kleinen Anteil diplatinierter RNS (12 %) gefunden. Die Pt-RNS-Addukte aus den oberen Banden der beiden D1-27 Spezien weisen ein sehr ähnliches Verhalten auf, was auf ein identisches Platinierungsschema hindeutet. Thermische UV-Schmelzstudien (Abbildung 7.5, A) zeigten, dass durch die Platinierung nur Tm_1, der Schmelzpunkt, welcher der Helix G1-U5 und G23-C27 zugeschrieben wird, signifikant von der Platinierungsreaktion beeinflusst wird. Die starke Destabilisierung (ΔTm= 7.4 °C) lässt eine *Intrastrang* Platinierung in diesem Bereich vermuten. Ein Vergleich der CD-Spektren der RNS vor und nach der Platinierungsreaktion zeigte, dass die Platinierung keinen sichtbaren Einfluss auf die RNS-Struktur hatte und die kleinen Unterschiede vermutlich auf minimalen lokalen Variation beruhen, verursacht durch die Anbindung der Platingruppe (Abbildung 7.5, B). Genauer gesagt, die bathochrome Verschiebung der Bande bei 260 nm kann auf eine Intrastrang-Platinbindung an RNS zurück geführt werden.

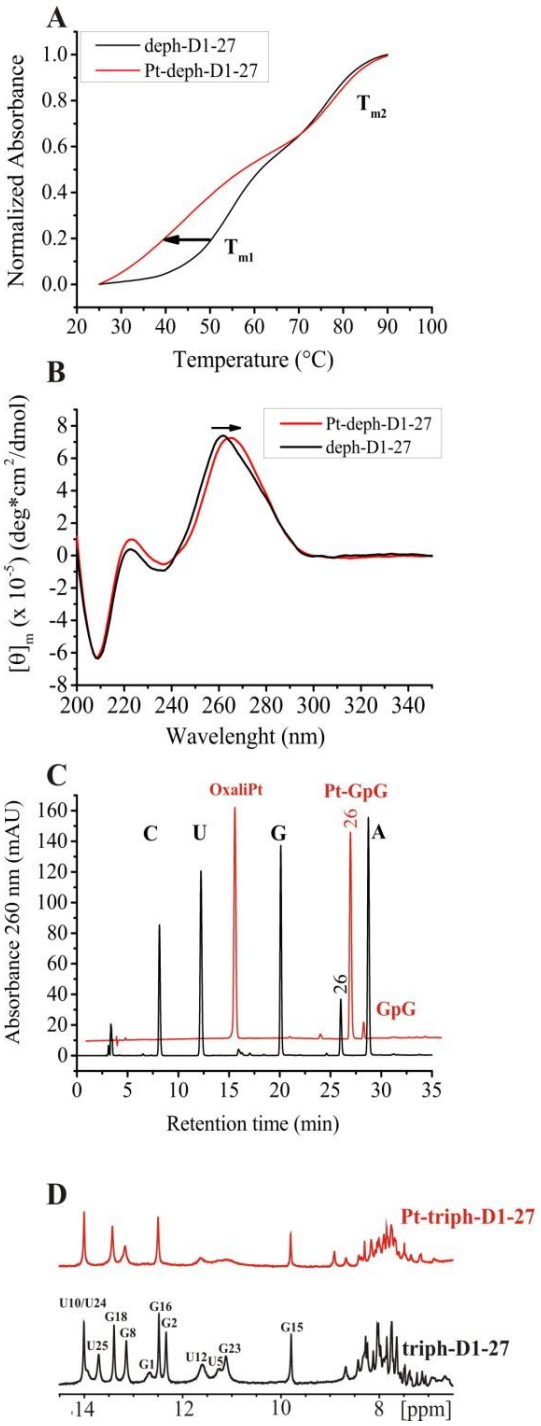

Abbildung 7.5: *Zusammenfassung der wichtigsten genutzten Methoden, um die aus dem oberen Band extrahierte Pt-RNS-Probe zu charakterisieren. A: Indikative thermische Schmelzprofile des deph-D1-27 (schwarz) und Pt-deph-D1-27 (rot). B: Vergleich der CD-Spektren von D1-27 (schwarz) und Pt-D1-27 (rot). C: HPLC-Chromatogramme der Verdauung von Pt-deph-D1-27 mit Nuclease P1, welche zum Erscheinen eines neuen Signals führte (schwarz), und der Reaktion des GpG-Dinukleotids mit oxaliPt (rot). Das rote Chromatogramm wurde verschoben, um ihren Vergleich zu erleichtern. D: ^{1}H-NMR-Spektra (aromatische und Imino-Protonen-Regionen), der D1-27 (schwarz) und der Pt- D1-27-Probe, die aus dem oberen Band extrahiert wurde (rote Linie).*

Das HPLC-Chromatogramm nach enzymatischer Verdauung der unreagierten und der platinierten RNS ergab das erste Indiz einer möglichen Platinierungsstelle (Abbildung 7.5, C). Die platinierten RNS-Arten hat zusätzlich zu den vier Signalen der einzelnen Nukleoside noch ein zusätzliches Signal. Der Vergleich der relativen Flächen der Signale ergab ein Verlust von zwei Guaninen und das neue Signal hat die gleiche Retentionszeit wie ein Pt-GpG, welches bei der Platinierung vom Dinukleotid GpG entsteht. Somit weist alles auf die Platinierung zwei benachbarter Guanine im Helixteil G1-U5 und G23-C27 von D1-27 hin. Die einzigen zwei Guanine, die diese Kriterien erfüllen, sind G1 und G2. Um die Platinierungsstelle weiter zu charakterisieren, wurde D1-27 am 5′- bzw. 3′-Ende mit ^{32}P radiomarkiert sowie anschliessend alkalisch und enzymatisch verdaut. Gelauswertungen der ^{32}P-5′-Ende-markierten und verdauten Proben zeigten, dass G23, welches im ersten Teil des Konstrukts vorkommt, nicht direkt platiniert wird. Allerdings konnten mit diesem Verfahren keine Informationen über die zwei Nukleotide G1 und G2 erhalten werden. Mit Hilfe der ^{32}P-3′-Ende-markierten Proben konnten wir aber zeigen, dass die Intensitäten der Gelbanden von G1 und G2 durch die Platinierung stark beeinflusst werden und somit in Übereinstimmung mit den vorherigen Ergebnisse eine Platinierung von G1-G2 zeigen. Zusätzlich wurde mittels ^{1}H-NMR-Spektroskopie die Imino-Protonen-Resonanzen der extrahierten platinierten Probe mit denen der unplatinierten Probe verglichen (Abbildung 7.5, D). Die Imino-Protonen-Resonanzen von G1 und G2 sind in der platinierten Probe nicht mehr sichtbar. Interessanterweise sieht das Spektrum der extrahierten platinierten Bande dem des RNAUU-Konstrukts sehr ähnlich (Abbildung 6.2), was wiederum für eine Destabilisierung am 5′-Ende durch Platinierung von G1-G2 spricht. Wie vorher erwähnt, ergab die Platinierungsreaktionen der dephosphorylierten RNS nicht nur die Banden B und C sondern zusätzlich auch noch eine schneller laufende Bande (Abbildung 7.4, lower). Auch diese Bande wurde aus dem Gel extrahiert und mittels CD Spektroskopie, thermische UV-Schmelzstudien und enzymatischer Verdauung / HPLC charakterisiert. Die platinierte RNS der unteren Bande enthielt eine zweite Form einer monoplatinierten RNA, angesichts dessen, dass die primären an der G1-G2-Stelle platiniert werden. MALDI-MS-Spektren dieser Bande zeigten, im Vergleich zur langsamer laufenden Bande B, einen grösseren Anteil an diplatinierter RNS. Leider waren die enzymatische Verdauung und HPLC-Analyse nicht konsistent. Da die Messungen mit verschiedenen Proben durchgeführt wurden, bildeten sich wahrscheinlich ein Mix aus unterschiedlich platinierter RNA. Aufgrund dieser Probenheterogenität sowie dem Vorkommen einer höheren Menge an diplatinierter RNA, konnten keine Schlussfolgerungen gezogen werden, auf welchem Weg Platin noch an D1-27 binden kann.

Unsere Studie hat gezeigt, dass die Wechselwirkung zwischen Oxaliplatin und D1-27, trotz der Gegenwart mehrer möglicher Platinierungsstellen, eine starke Präferenz für die Platinierung von G1-G2 zeigt. Die gebildete monoplatinierte RNS-Form konnte im Gel aufgrund ihrer verringerten Gelmobilität identifiziert und analysiert werden. In DNS ist das GG-Motiv die häufigste Bindungsstelle für Platin(II)-Antikrebsmedikamente und auch bei der RNS-Platinierung mit Cisplatin wurde sie als

präferierte Sequenz identifiziert. Unsere Resultate zeigen, dass auch Oxaliplatin eine starke Präferenz für GG-Motive (G1-G2) hat, was mit den bekannten Erkenntnissen über RNS-Platinierung übereinstimmt.

Trotz grosser Verbreitung von Platin(II)-Komplexe als Antikrebsmedikamente, ist die Anwendung meist mit schweren Nebenwirkungen verbunden und etliche Tumore weisen intrinsische oder akquirierte Resistenzen auf. Obwohl diese Medikamente teilweise seit Jahrzehnten im Einsatz sind, ist ihre komplexe Wirkungsweise z.B Wechselwirkung mit den verschiedensten intrazellulären Molekülen, noch nicht vollständig verstanden. Ein Ansatz zur Eliminierung ihrer Nebenwirkungen ist ein besseres Verständnis des Wirkungsmechanismuses durch eingehende Studien, die nicht nur die Wechselwirkung mit DNS sondern auch mit anderen Biomolekülen wie Proteine und RNS zum Ziel haben. Gerade RNS könnte ein gutes Platin(II)-Zielmolekül darstellen, da es zum einem dem DNS Molekül gleicht und zum anderen in vielen wichtigen Zellfunktionen involviert ist. Frühere Studien haben bereits gezeigt, dass Platinmedikamente wichtige RNS-basierte Aktivitäten blockieren können, die für das Überleben der Zelle ausschlaggebend sind. Basierend auf diesen Kenntnissen, führten wir eine detaillierte Studie durch in der die Wechselwirkung zwischen Oxaliplatin und einer Modell-RNS (D1-27) im Mittelpunkt stand, um mögliche Platinanbindungsstellen zu lokalisieren. Die Bestimmung und genaue Untersuchung von Platinbindungsstellen in RNS-Molekülen eröffnet nicht nur die Möglichkeit, Platinierungsstellen in anderen biologisch relevanten RNS-Molekülen vorherzusagen, sondern verbessert auch das allgemeine Verständnis des komplexen Antikrebswirkungsmechanismus von Platin(II)-Medikamenten. Diese Ergebnisse sind von grosser Bedeutung um neue, weniger giftige und effektivere Platin(II)-Medikamente herzustellen und/ oder neuartigen Krebsbehandlungsmethoden zu entwickeln.

8 Appendices

Appendix 1 - Chapter 2

In appendix 1 the MALDI-MS spectra of untreated and platinated RNA samples as well as a HPLC chromatogram are reported. They all refer to experiments described in chapter 2 and are related mostly to the optimization of the platination reaction conditions for cisplatin and oxaliplatin.

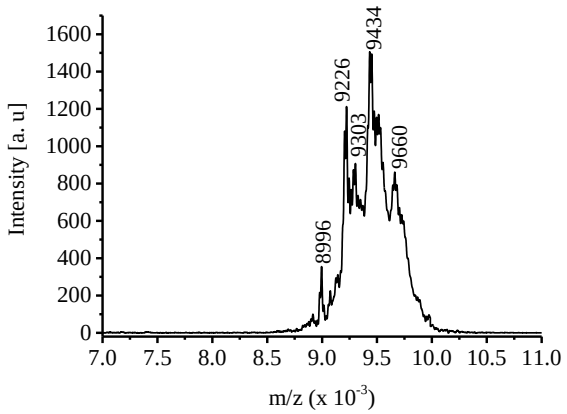

RNA species	Predicted mass (m/z)	Experimental mass (m/z)
Monoplatinated D1-27 – {HPO_3}	8997	8996
Diplatinated D1-27 – {HPO_3}	9226	9226
Diplatinated D1-27	9306	9303
Triplatinated D1-27 – {HPO_3}	9438	9434
Tetraplatinated D1-27 – {HPO_3}	9650	9660

Figure A 1.1: *MALDI-MS spectrum of the platinated RNA species isolated from the upper bands of the gels corresponding to platination performed using 4 eq and 5 eq of monoaquated cisPt.*

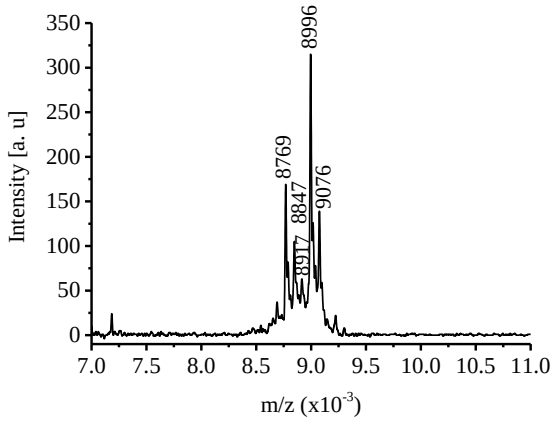

RNA species	Predicted mass (m/z)	Experimental mass (m/z)
D1-27– {HPO_3}	8768	8769
D1-27	8848	8847
Monoplatinated D1-27 – 2{HPO_3}	8917	8917
Monoplatinated D1-27 – {HPO_3}	8997	8996
Monoplatinated D1-27	9076	9076

Figure A 1.2: *MALDI-MS spectrum of the platinated RNA species isolated from the upper bands of the gel corresponding to platination performed using 1 eq of monoaquated cisPt at 37 °C.*

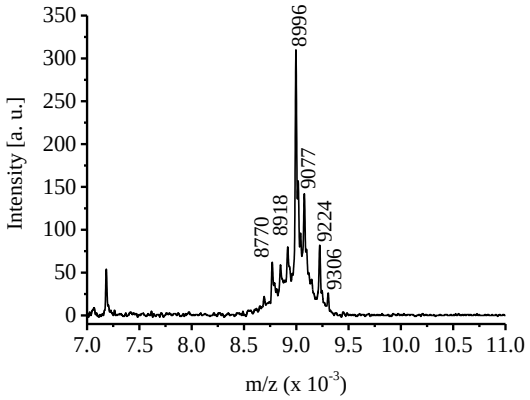

RNA species	Predicted mass (m/z)	Experimental mass (m/z)
D1-27– {HPO_3}	8768	8770
Monoplatinated D1-27 – 2{HPO_3}	8917	8918
Monoplatinated D1-27 – {HPO_3}	8997	8996
Monoplatinated D1-27	9076	9077
Diplatinated D1-27 – {HPO_3}	9226	9224
Diplatinated D1-27	9306	9306

Figure A 1.3: *MALDI-MS spectrum of the platinated RNA species isolated from the upper bands of the gel corresponding to platination performed using 1 eq of monoaquated cisPt at 50 °C.*

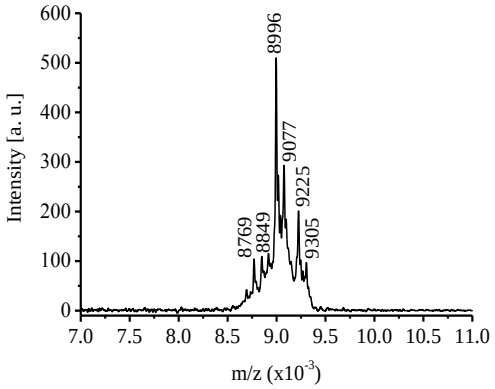

RNA species	Predicted mass (m/z)	Experimental mass (m/z)
D1-27 – {HPO_3}	8768	8769
D1-27	8848	8849
Monoplatinated D1-27 – {HPO_3}	8997	8996
Monoplatinated D1-27	9076	9077
Diplatinated D1-27 – {HPO_3}	9226	9225
Diplatinated D1-27	9306	9305

Figure A 1.4: *MALDI-MS spectrum of the platinated RNA species isolated from the upper bands of the gel corresponding to platination performed using 2 eq of monoaquated cisPt at 37 °C.*

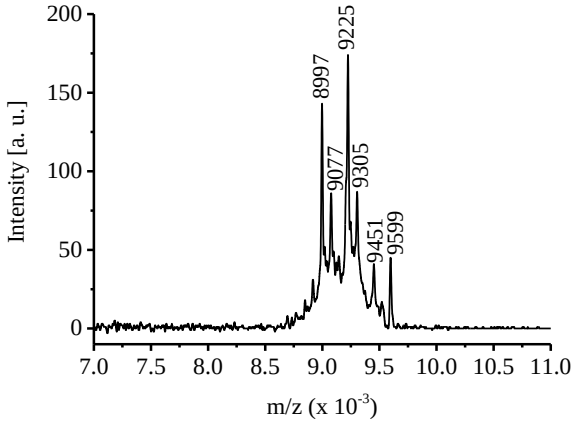

RNA species	Predicted mass (m/z)	Experimental mass (m/z)
Monoplatinated D1-27 – {HPO_3}	8997	8997
Monoplatinated D1-27	9076	9077
Diplatinated D1-27 – {HPO_3}	9226	9225
Diplatinated D1-27	9306	9305
Triplatinated D1-27 – {HPO_3}	9438	9451
Tetraplatinated D1-27 – 2{HPO_3}	9570	9599

Figure A 1.5: *MALDI-MS spectrum of the platinated RNA species isolated from the upper bands of the gel corresponding to platination performed using 2 eq of monoaquated cisPt at 50 °C.*

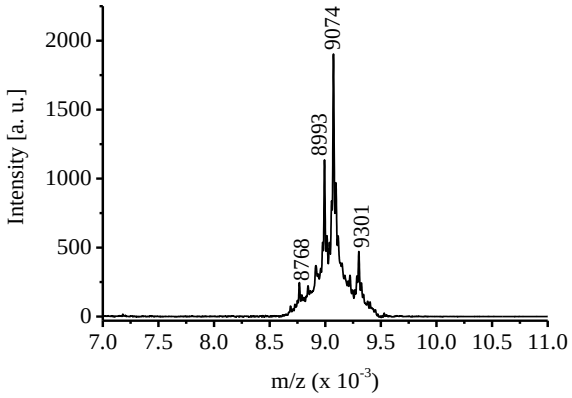

RNA species	Predicted mass (m/z)	Experimental mass (m/z)
D1-27 – {HPO_3}	8768	8768
Monoplatinated D1-27 – {HPO_3}	8997	8993
Monoplatinated D1-27	9076	9074
Diplatinated D1-27	9306	9301

Figure A 1.6: *MALDI-MS spectrum of the platinated RNA species isolated from the "faster migrating" upper band of the gel corresponding to platination performed using 0.5 mM RNA and 1 eq of monoaquated cisPt.*

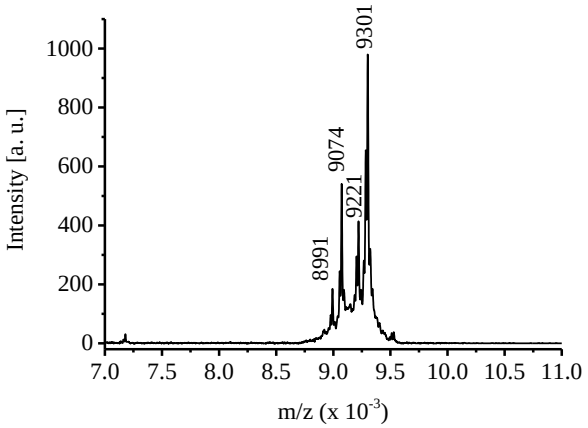

RNA species	Predicted mass (m/z)	Experimental mass (m/z)
Monoplatinated D1-27 – {HPO_3}	8997	8991
Monoplatinated D1-27	9076	9074
Diplatinated D1-27 – 2{HPO_3}	9226	9221
Diplatinated D1-27	9306	9301

Figure A 1.7: *MALDI-MS spectrum of the platinated RNA species isolated from the slower migrating upper band of the gel corresponding to platination performed using 0.5 mM RNA and 1 eq of monoaquated cisPt.*

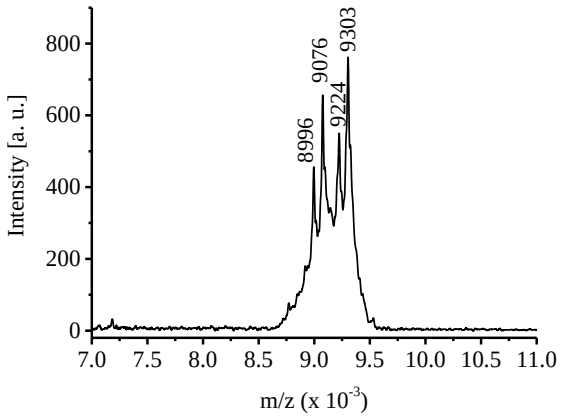

RNA species	Predicted mass (m/z)	Experimental mass (m/z)
Monoplatinated D1-27 – {HPO_3}	8997	8996
Monoplatinated D1-27	9076	9076
Diplatinated D1-27 – 2{HPO_3}	9226	9224
Diplatinated D1-27	9306	9303

Figure A 1.8: *MALDI-MS spectrum of the platinated RNA species isolated from the upper bands of the gel corresponding to platination with monoaquated cisPt for 4 days.*

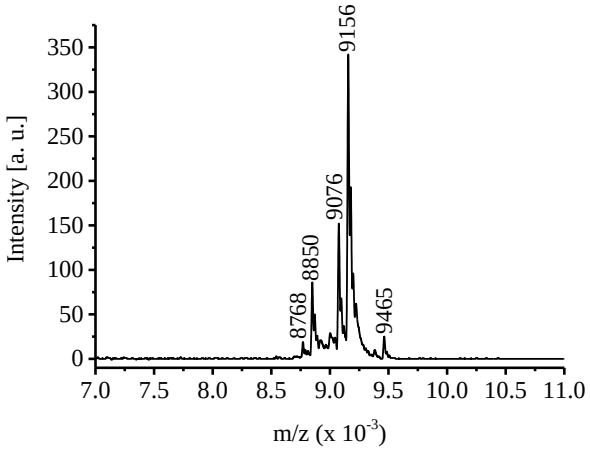

RNA species	Predicted mass (m/z)	Experimental mass (m/z)
D1-27 – {HPO_3}	8768	8768
D1-27	8848	8850
Monoplatinated D1-27 – {HPO_3}	9077	9076
Monoplatinated D1-27	9157	9156
Diplatinated D1-27	9466	9465

Figure A 1.9: *MALDI-MS spectrum of the platinated RNA species isolated from the upper band of a gel corresponding to platination performed using 5 eq of oxaliPt, incubating for 2 days, at 25 °C.*

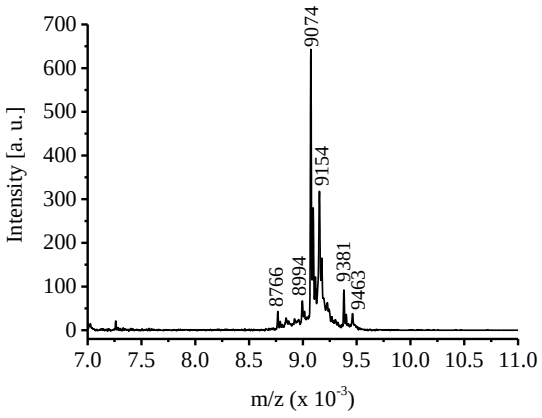

RNA	Predicted mass (m/z)	Experimental mass (m/z)
D1-27 – {HPO_3}	8768	8766
Monoplatinated D1-27 – 2{HPO_3}	8997	8994
Monoplatinated D1-27 – 1{HPO_3}	9077	9074
Monoplatinated D1-27	9157	9154
Diplatinated D1-27 – 1{HPO_3}	9386	9381
Diplatinated D1-27	9466	9463

Figure A 1.10: *MALDI-MS spectrum of the platinated RNA species isolated from the upper band of the gel corresponding to platination performed using 5 eq of oxaliPt, incubating for 16 h, at 37 °C.*

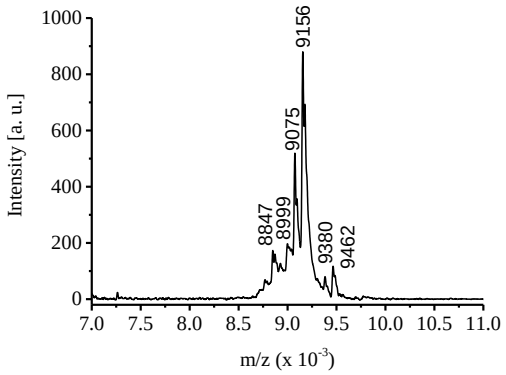

RNA species	Predicted mass (m/z)	Experimental mass (m/z)
D1-27	8848	8847
Monoplatinated D1-27 – 2{HPO_3}	8998	8999
Monoplatinated D1-27 – 1{HPO_3}	9077	9075
Monoplatinated D1-27	9157	9156
Diplatinated D1-27 – 1{HPO_3}	9387	9380
Diplatinated D1-27	9466	9462

Figure A 1.11: *MALDI-MS spectrum of the platinated RNA species isolated from the upper band of the gel corresponding to platination performed using 5 eq of oxaliPt and 0.25 mM of RNA for 1 day at 25 °C.*

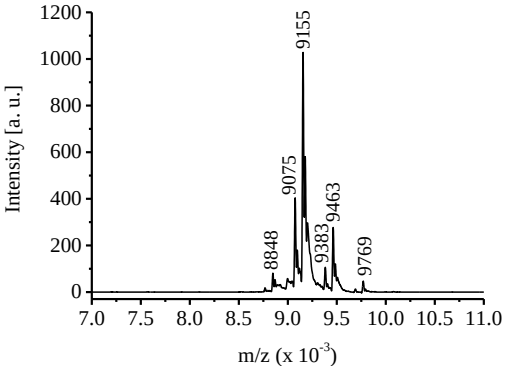

RNA species	Predicted mass (m/z)	Experimental mass (m/z)
D1-27	8848	8848
Monoplatinated D1-27 – 1{HPO_3}	9077	9075
Monoplatinated D1-27	9157	9155
Diplatinated D1-27 – 1{HPO_3}	9386	9383
Diplatinated D1-27	9466	9463
Triplatinated D1-27	9775	9769

Figure A 1.12: *MALDI-MS spectrum of the platinated RNA species isolated from the upper bands of the gel corresponding to platination performed using 5 eq of oxaliPt incubating for 2 days at 25 °C in the presence of 120 mM $KClO_4$.*

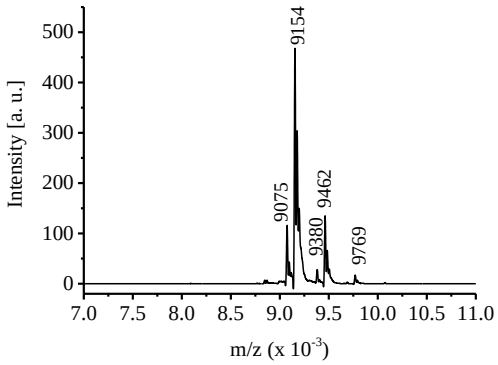

RNA species	Predicted mass (m/z)	Experimental mass (m/z)
Monoplatinated D1-27 – 1{HPO_3}	9077	9075
Monoplatinated D1-27	9157	9154
Diplatinated D1-27 – 1{HPO_3}	9386	9380
Diplatinated D1-27	9466	9462
Triplatinated D1-27	9775	9769

Figure A 1.13: *MALDI-MS spectrum of the platinated RNA species isolated from the upper bands of the gel corresponding to platination performed using 10 eq of oxaliPt incubating for 1 day at 25 °C in the presence of 120 mM $KClO_4$.*

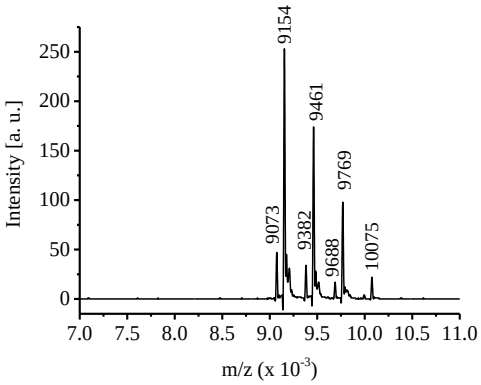

RNA species	Predicted mass (m/z)	Experimental mass (m/z)
Monoplatinated D1-27 – 1{HPO_3}	9077	9073
Monoplatinated D1-27	9157	9154
Diplatinated D1-27 – 1{HPO_3}	9386	9382
Diplatinated D1-27	9466	9461
Triplatinated D1-27– 1{HPO_3}	9695	9688
Triplatinated D1-27	9775	9769
Tetraplatinated D1-27	10084	10075

Figure A 1.14: *MALDI-MS spectrum of the platinated RNA species isolated from the upper bands of the gel corresponding to platination performed using 10 eq of oxaliPt incubating for 2 days at 25 °C in the presence of 120 mM $KClO_4$.*

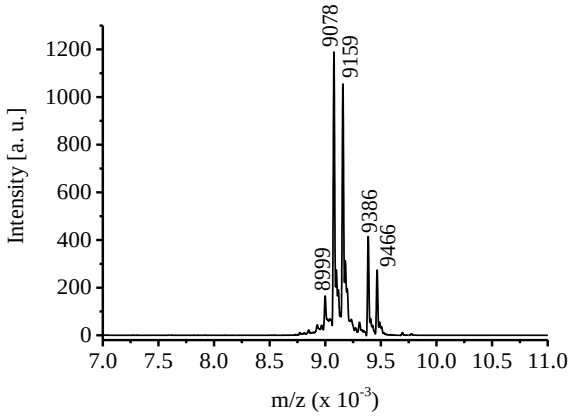

RNA species	Predicted mass (m/z)	Experimental mass (m/z)
Monoplatinated D1-27 – 2{HPO_3}	8997	8999
Monoplatinated D1-27 – 1{HPO_3}	9077	9078
Monoplatinated D1-27	9157	9159
Diplatinated D1-27 – 1{HPO_3}$_3$	9386	9386
Diplatinated D1-27	9466	9466

Figure A 1.15: *MALDI-MS spectrum of the platinated RNA species isolated from the upper band (in water) in the blue frame in Figure 2.20.*

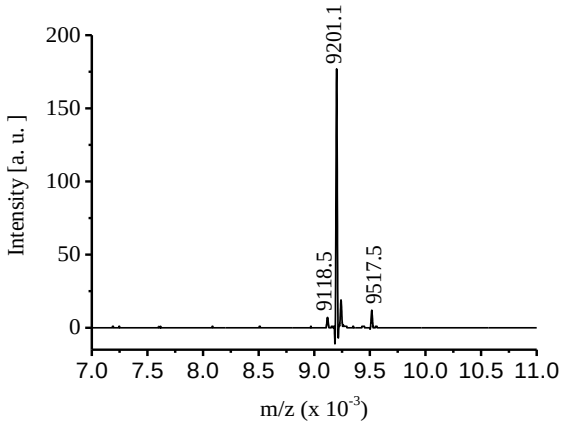

RNA species	Predicted mass (m/z)	Experimental mass (m/z) *
Monoplatinated D1-27 – 1{HPO_3}	9077	9118
Monoplatinated D1-27	9157	9201
Diplatinated D1-27	9466	9517

Figure A 1.16: *MALDI-MS spectrum of the platinated RNA species isolated from the upper bands of the gel corresponding to platination performed in the presence of 80 mM KCl.*

*There was an acetonitrile moiety corresponding to +41 in the experimental mass

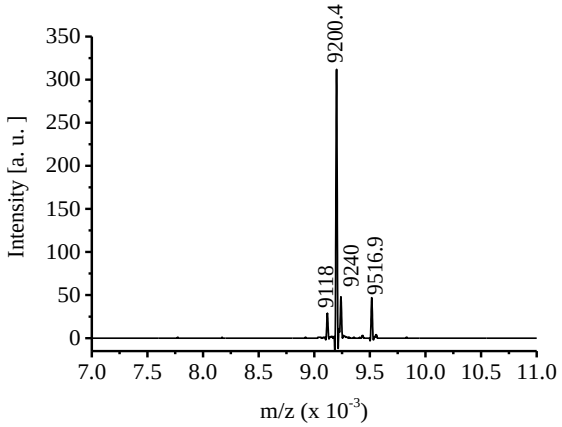

RNA species	Predicted mass (m/z)	Experimental mass (m/z)*
Monoplatinated D1-27 – 1{HPO_3}	9077	9118
Monoplatinated D1-27	9157	9200
Diplatinated D1-27	9466	9517

Figure A 1.17: *MALDI-MS spectrum of the platinated RNA species isolated from the upper bands of the gel corresponding to platination performed in the presence of 120 mM KCl.*

*There was an acetonitrile moiety corresponding to +41 in the experimental mass

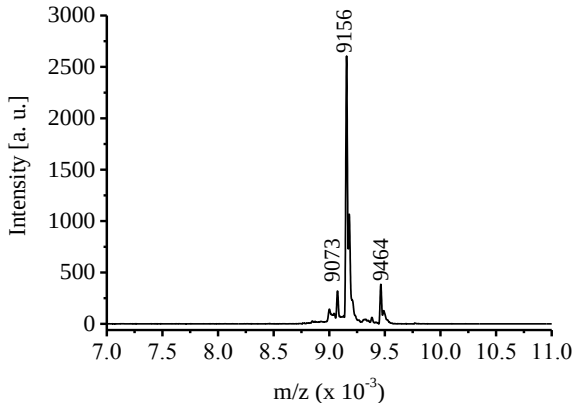

RNA species	Predicted mass (m/z)	Experimental mass (m/z)
Monoplatinated D1-27 – 1{HPO_3}	9077	9073
Monoplatinated D1-27	9157	9156
Diplatinated D1-27	9466	9464

Figure A 1.18: *MALDI-MS spectrum of the platinated RNA species isolated from the upper bands of the gel corresponding to platination performed in the presence of 200 mM KCl.*

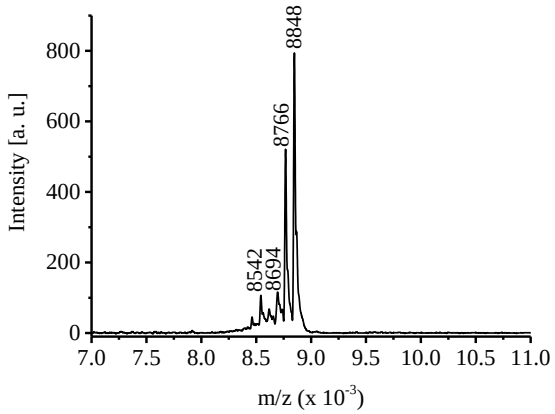

RNA species	Predicted mass (m/z)	Experimental mass (m/z)
D1-27 – CMP	8543	8542
D1-27 – 2{HPO_3}	8688	8694
D1-27 – 1{HPO_3}	8768	8766
D1-27	8848	8848

Figure A 1.19: *MALDI-MS spectrum for the RNA sample used as control in the gel in Figure 2.26 (blue frame).*

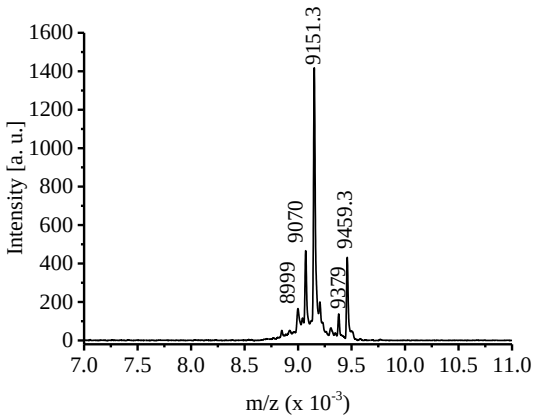

RNA species	Predicted mass (m/z)	Experimental mass (m/z)
Monoplatinated D1-27 – 2{HPO_3}	8998	8999
Monoplatinated D1-27 – 1{HPO_3}	9077	9070
Monoplatinated D1-27	9157	9151
Diplatinated D1-27 – 1{HPO_3}	9387	9379
Diplatinated D1-27	9466	9459

Figure A 1.20: *MALDI-MS spectrum for the platinated RNA species isolated from the upper band of the gel in Figure 2.26 (red frame).*

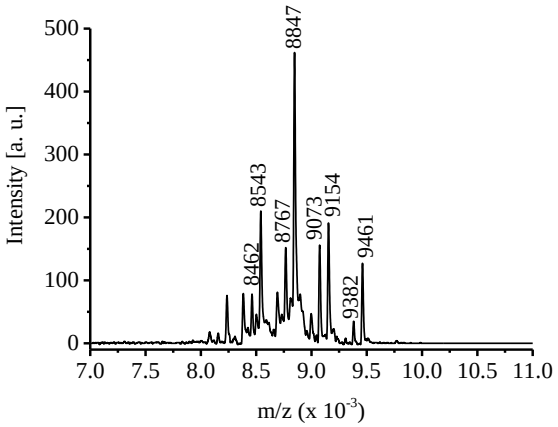

RNA species	Predicted mass (m/z)	Experimental mass (m/z)
D1-27 - 1CMP – 1{HPO_3}	8463	8462
D1-27 – 1CMP	8453	8543
D1-27 – 1{HPO_3}	8768	8767
D1-27	8848	8847
Monoplatinated D1-27 – 1{HPO_3}	9077	9073
Monoplatinated D1-27	9157	9154
Diplatinated D1-27 – 1{HPO_3}	9387	9382
Diplatinated D1-27	9466	9461

Figure A 1.21: *MALDI-MS spectrum for the platinated RNA species isolated from the lower band of the gel in Figure 2.26 (green frame).*

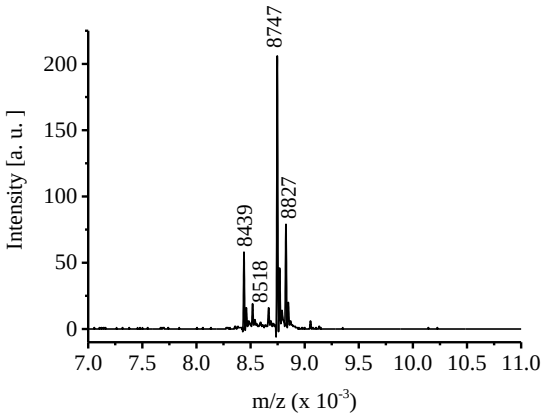

RNA species	Predicted mass (m/z)	Experimental mass (m/z)
RNA 26 – 1{HPO_3}	8439	8439
RNA 26	8519	8518
Monoplatinated RNA 26 – 1{HPO_3}	8748	8747
Monoplatinated RNA 26	8827	8827

Figure A 1.22: *MALDI-MS spectrum for the platinated RNA species resulting from the platination of RNA 26 with oxaliPt.*

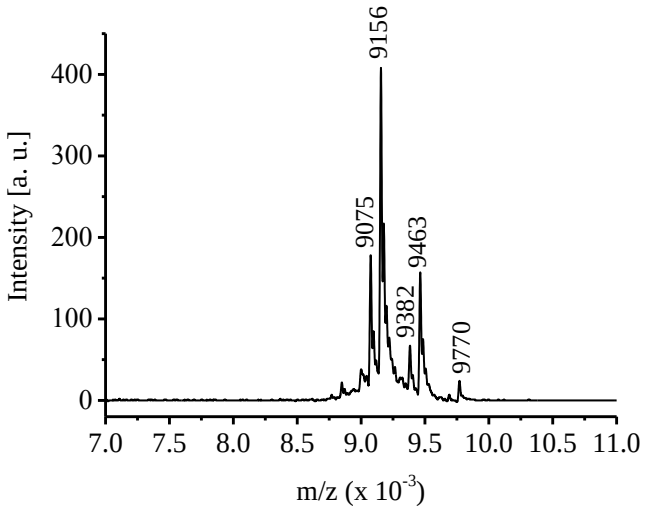

RNA species	Predicted mass (m/z)	Experimental mass (m/z)
Monoplatinated D1-27 – 1{HPO_3}	9077	9075
Monoplatinated D1-27	9157	9156
Diplatinated D1-27 – 1{HPO_3}	9387	9382
Diplatinated D1-27	9466	9463
Triplatinated D1-27	9775	9770

Figure A 1.23: *MALDI-MS spectrum for the platinated RNA species isolated from the upper band resulting from the reaction of 10 eq of oxaliPt with D1-27 for 2 days (diplatinated RNA).*

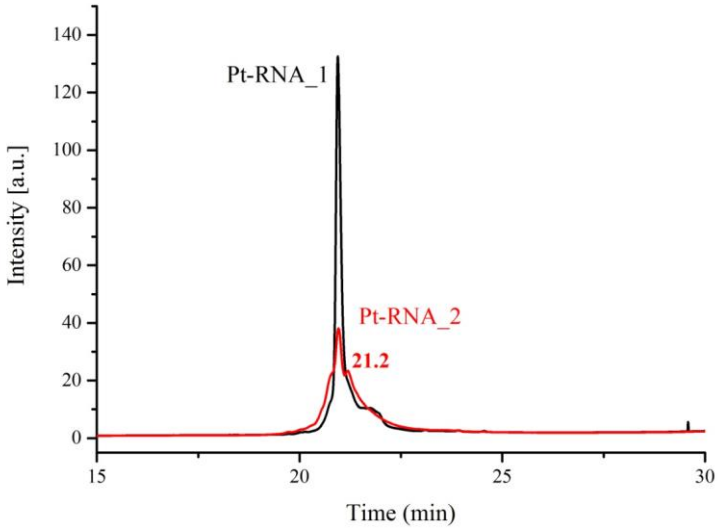

Figure A 1.24: *Chromatograms corresponding to platinated RNA with the monoplatinated adducts as main species (black line) and of platinated RNA with increased amount of diplatinated RNA (peak at 21.2 min) (red line).*

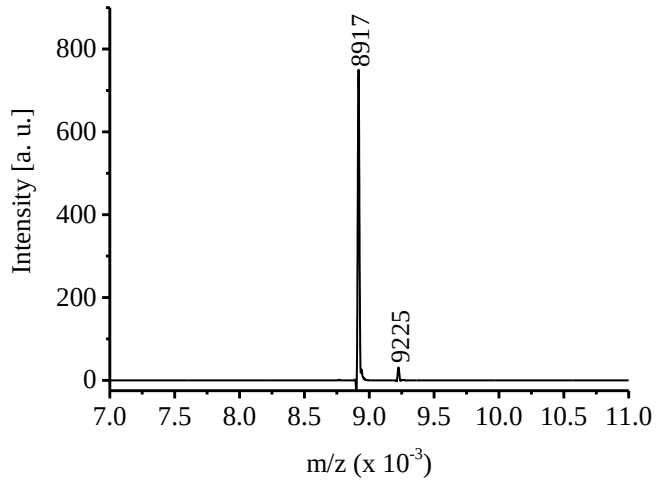

RNA species	Predicted mass (m/z)	Experimental mass (m/z)
Monoplatinated D1-27 – 3{HPO_3}	8917	8917
Diplatinated D1-27 – 3{HPO_3}	9227	9225

Figure A 1.25: *MALDI-MS spectrum for the platinated RNA species isolated from the upper band of the gel corresponding to platination of deph-D1-27 with oxaliPt (Figure 2.45, green line).*

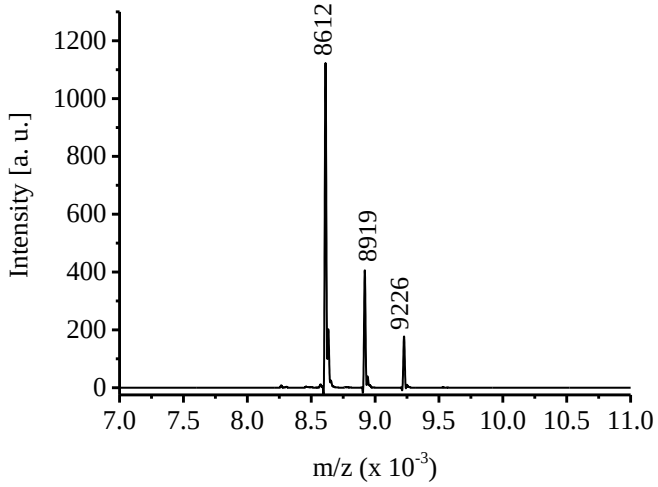

RNA species	Predicted mass (m/z)	Experimental mass (m/z)
D1-27 – 3{HPO_3}	8608	8612
Monoplatinated D1-27 – 3{HPO_3}	8917	8919
Diplatinated D1-27 – 3{HPO_3}	9227	9226

Figure A 1.26: *MALDI-MS spectrum for the platinated RNA species isolated from the middle band of the gel corresponding to platination of deph-D1-27 with oxaliPt (Figure 2.45, black line).*

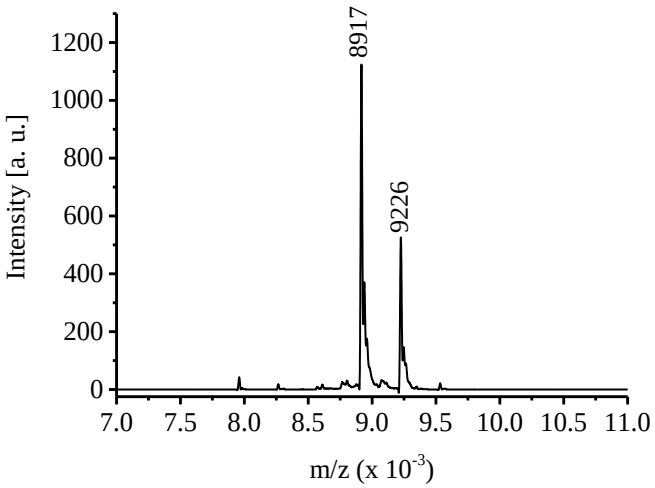

RNA species	Predicted mass (m/z)	Experimental mass (m/z)
Monoplatinated D1-27 – 3{HPO_3}	8917	8917
Diplatinated D1-27 – 3{HPO_3}	9227	9226

Figure A 1.27: *MALDI-MS spectrum for the platinated RNA species isolated from the lower band of the gel corresponding to platination of deph-D1-27 with oxaliPt (Figure 2.45, red line).*

Appendix 2 – Chapters 3 - 4

In appendix 2 additional NMR spectra, CD spectra of untreated and platinated RNA samples as well as HPLC chromatograms are reported. They all refer to experiments described in chapters 3 and 4.

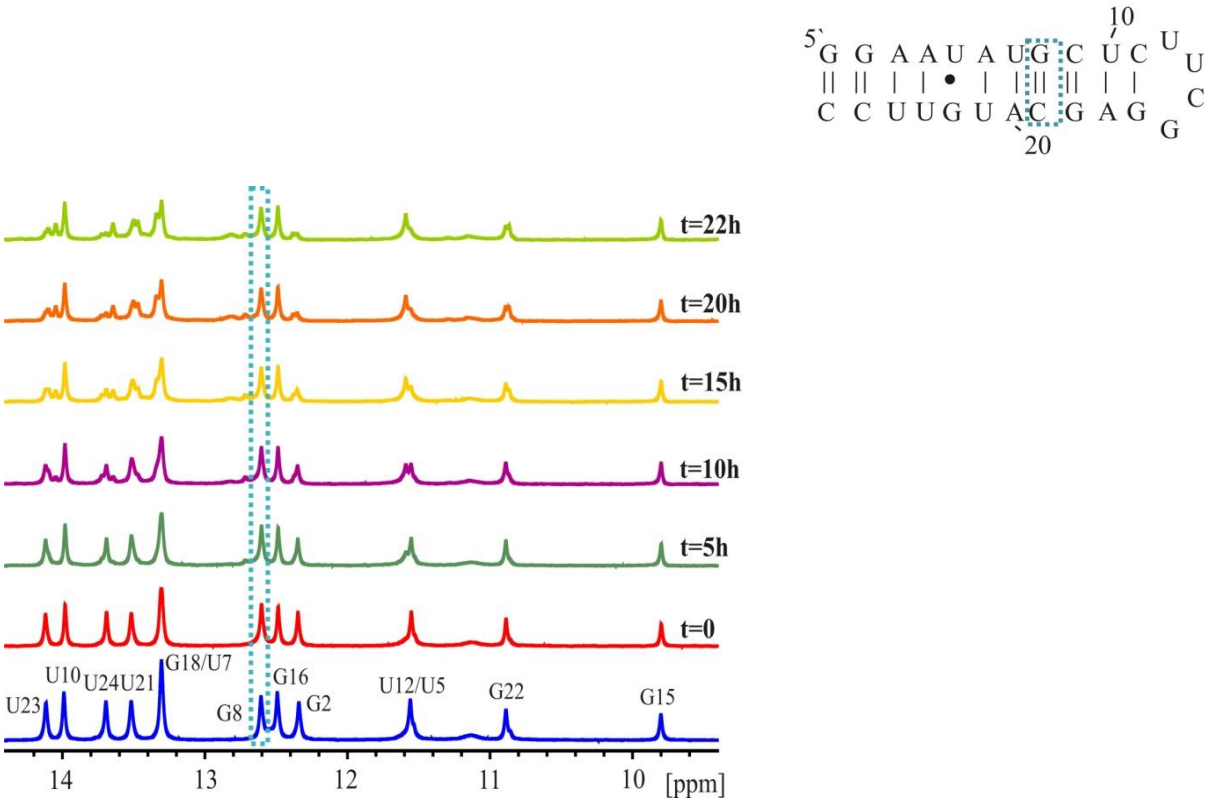

Figure A 2.1: *Time evolution NMR experiment for the platination of deph-RNA 26 with oxaliPt (left), Right Top: Secondary structure of RNA 26. (5 eq. of oxaliPt, 0.1 mM deph-RNA 26, 25 °C, 120 mM KCl, pH 6, 600 MHz)*

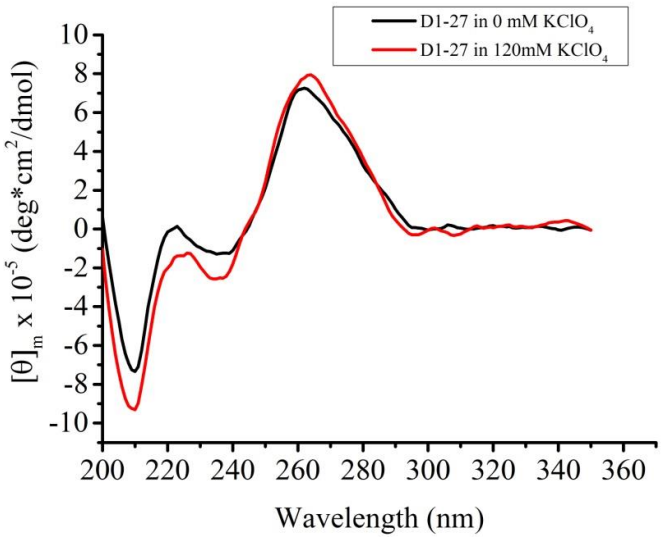

Figure A 2.2: *Comparison of the CD spectra of triph-D1-27 in the presence of 0 mM (black) and 120 mM (red) $KClO_4$. C_{RNA} = 1.3 µM, pH 6.5.*

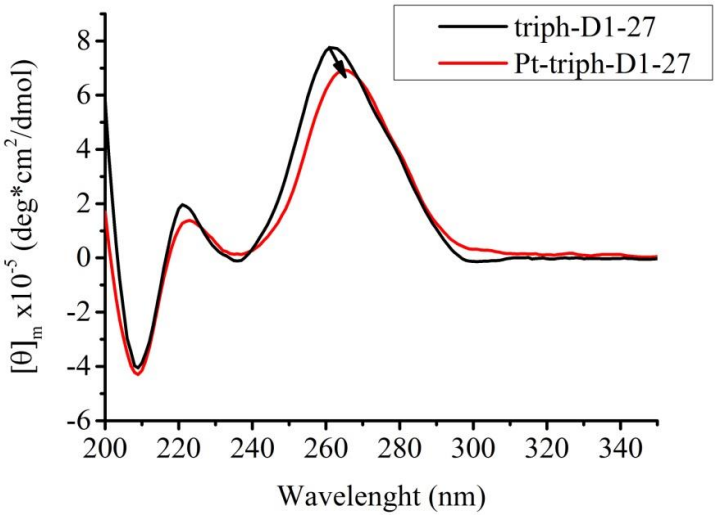

Figure A 2.3: *Comparison of the CD spectra of triph-D1-27 (black) and the platinated triph-D1-27 (red).* C_{RNA} *and* $C_{Pt\text{-}RNA}$ *= 1.3 μM, in 120 mM* $KClO_4$*, pH 6.5.*

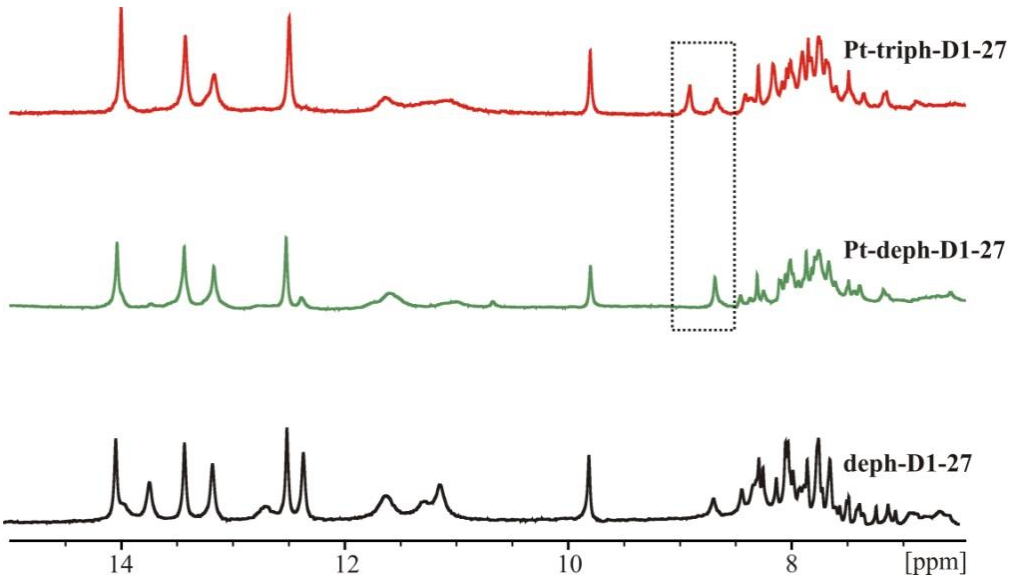

Figure A 2.4: *Comparison of* ^{1}*H-NMR spectra (aromatic and imino proton regions) of the untreated deph-D1-27 (black line), Pt-deph-D1-27 sample (green line) and Pt-triph-D1-27 sample (red line). In the black dotted frame is indicated the down-field shifted peak corresponding to H8 of the platinated guanosines. The spectra were recorded in 90%* H_2O*:10%* D_2O *at 25 °C on 600 MHz.*

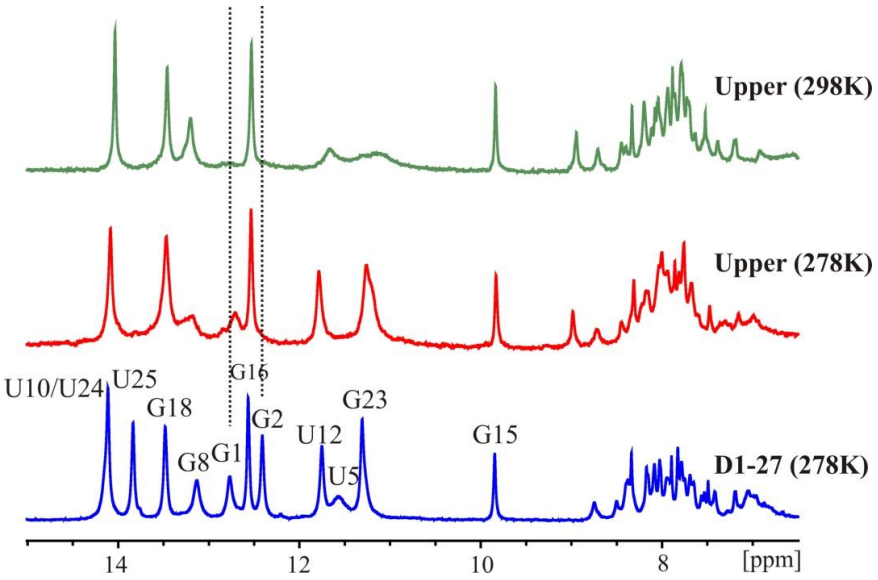

Figure A 2.5: *^{1}H-NMR spectra (aromatic and imino proton regions), including imino proton assignment, of the untreated D1-27 (blue line), Pt-triph-D1-27 sample isolated from the upper band (red line) and recorded at 4 °C and Pt-triph-D1-27 sample isolated from the upper band (green line) and recorded at 25 °C. The spectra were recorded in 120 mM $KClO_4$, pH 6, 600 MHz. The spectrum in green line corresponds to the one shown in Figure 4.22 (red line).*

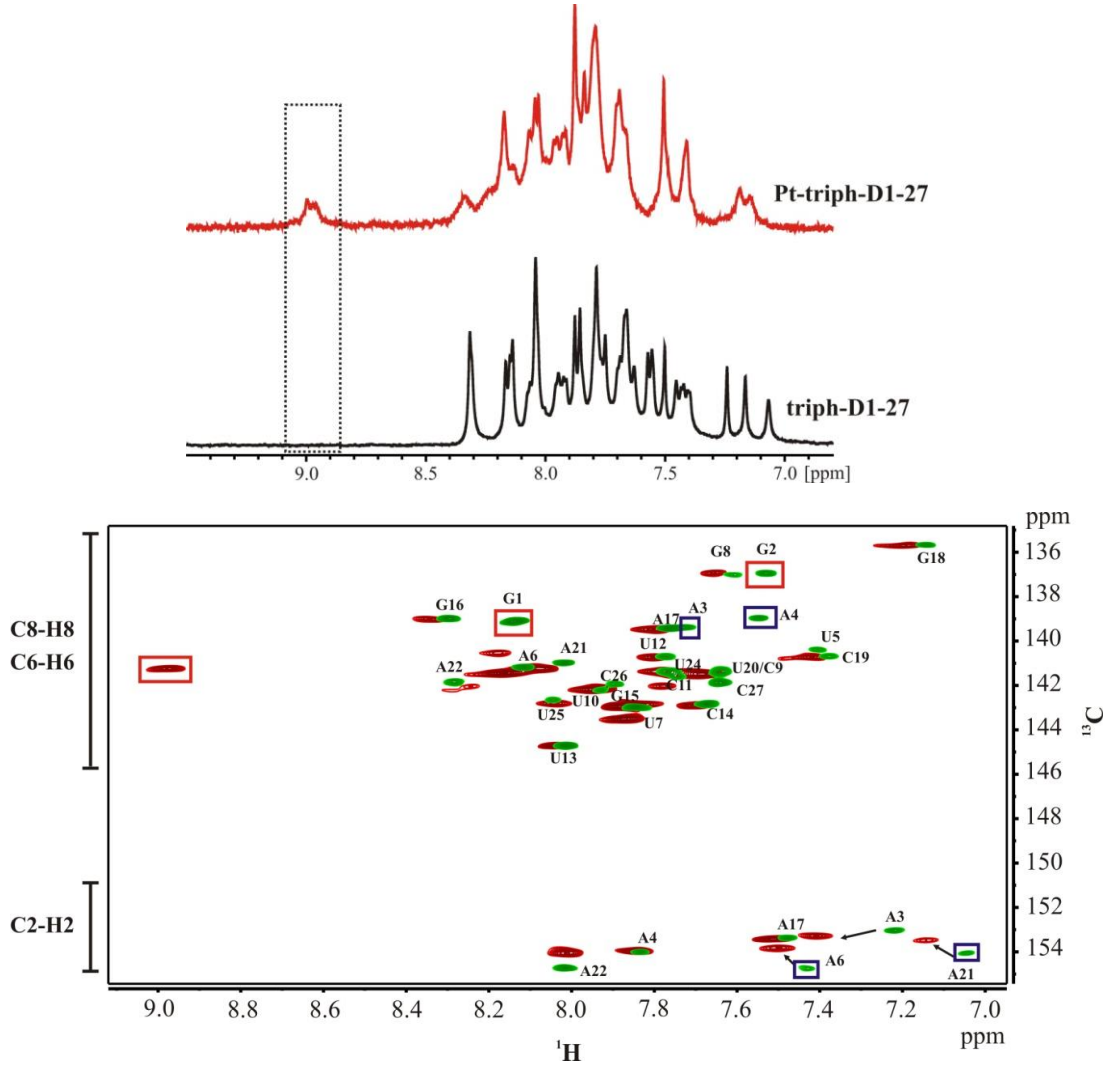

Figure A 2.6*: Upper panel: Comparison of [1]H-NMR spectra (aromatic region) of the untreated triph-D1-27 (black line) and of the Pt-triph-D1-27 sample (red line). In the black dotted frame are indicated the down-field shifted peak(s) corresponding to H8 of the platinated guanosines. The spectra were recorded in 100 % D_2O at 25 °C on 600 MHz. Lower panel: Overlay of the aromatic region (C8-H8 and C2-H2 of purines and C6-H6 of pyrimidines) of [[1]H,[13]C]-HSQC spectra recorded on unreacted (green) and platinated (red) D1-27. The platinated sample was isolated from the upper band of a platination reaction performed using triph-D1-27. (0.69 mM RNA, 120 mM $KClO_4$, pD 6.9, 4 °C, 700 MHz for the unreacted RNA; 0.2 mM RNA, 120 mM $KClO_4$, pD 7,* 25 °C*, 600 MHz for the platinated sample).The labels refer to non-platinated D1-27. The cross-peak G23C8-H8 is very weak, and it is not visible at the contour level used in this Figure. Chemical shifts for both the species are reported in Table A 2.1.*

Red boxes indicate guanine cross-peaks, which significantly shift upon platination, while the blue boxes indicate cross-peaks of other residues that also move upon platination. In the less crowded C2-H2 regions, arrows have been added to better visualize the shift of the cross-peaks. The Figure has been prepared with MestReNova version 10.0 (Mestrelab Research S.L.) and CorelDRAWX3.

Table A 2 1: *^{1}H and ^{13}C chemical shifts of guanine (C8H8), adenine (C8H8 and C2H2) as well as uracil and cytosine (C6H6) resonances of unreacted and platinated D1-27. The platinated sample was isolated from the upper band of a platination reaction performed using triph-D1-27. The following sample conditions were used: 0.69 mM RNA, 120 mM $KClO_4$, pD 6.9, 25 °C, 700 MHz for the unreacted RNA; 0.2 mM RNA, 120 mM $KClO_4$, pD 7, 25 °C, 600 MHz for the platinated sample. Chemical shift differences (Δδ) between platinated and unreacted sample are indicated in the last column.*

[a] C8 and C6 resonances of A4 and C26 significantly shift; however their assignment is unclear because they seem to overlap with other signals; w = weak; n.v. = not visible.

Residue	Atom	D1-27 δ [ppm]	Platinated D1-27 δ [ppm]	Δδ [ppm]
G1	**C8**	139.11	141.29	2.18
	H8	8.14	9.00	0.86
G2	**C8**	136.95	141.23	4.28
	H8	7.53	8.97	1.44
A3	**C2**	153.04	153.29	0.25
	H2	7.22	7.41	0.19
	C8	139.40	140.56	1.16
	H8	7.72	8.18	0.46
A4	**C2**	154.01	153.96	–0.05
	H2	7.83	7.85	0.02
	C8	138.95	141.36[a]	2.41
	H8	7.55	8.14	0.59
U5	**C6**	140.39	140.78	0.39
	H6	7.40	7.48	0.08
A6	**C2**	154.75	153.83	–0.92
	H2	7.43	7.50	0.07
	C8	141.18	141.45	0.27
	H8	8.12	8.17	0.05
U7	**C6**	142.98	142.85	–0.13
	H6	7.85	7.83	–0.02
G8	**C8**	137.02	136.95	–0.07
	H8	7.61	7.66	0.05
C9	**C6**	141.38	141.51	0.13
	H6	7.64	7.68	0.04
U10	**C6**	142.22	142.16	–0.06
	H6	7.93	7.94	0.01
C11	**C6**	141.40	141.38	–0.02
	H6	7.76	7.79	0.03
U12	**C6**	140.71	140.79	0.08
	H6	7.77	7.81	0.04
U13	**C6**	144.71	144.72	0.01

	H6	8.01	8.04	0.03
C14	**C6**	142.83	142.90	0.07
	H6	7.67	7.70	0.03
G15	**C8**	142.98	142.99	0.01
	H8	7.85	7.85	0.00
G16	**C8**	138.99	139.00	0.01
	H8	8.29	8.34	0.05
A17	**C2**	153.37	153.41	0.04
	H2	7.48	7.52	0.04
	C8	139.43	139.48	0.05
	H8	7.76	7.81	0.05
G18	**C8**	135.67	135.69	0.02
	H8	7.14	7.19	0.05
C19	**C6**	140.71	140.73	0.02
	H6	7.38	7.42	0.04
U20	**C6**	141.38	141.52	0.14
	H6	7.64	7.70	0.06
A21	**C2**	154.05	153.46	–0.59
	H2	7.05	7.15	0.10
	C8	140.98	141.24	0.26
	H8	8.02	8.08	0.06
A22	**C2**	154.73	154.06	–0.67
	H2	8.11	8.01	–0.10
	C8	141.84	142.04	0.20
	H8	8.28	8.24	–0.04
G23	**G8**	138.18w	n.v.	-
	H8	7.92	7.95	0.03
U24	**C6**	141.59	142.04	0.45
	H6	7.75	7.78	0.03
U25	**C6**	142.65	142.81	0.16
	H6	8.04	8.05	0.01
C26	**C6**	141.94	142.07[a]	0.13
	H6	7.89	7.94	0.05
C27	**C6**	141.88	143.52	1.64
	H6	7.64	7.87	0.23

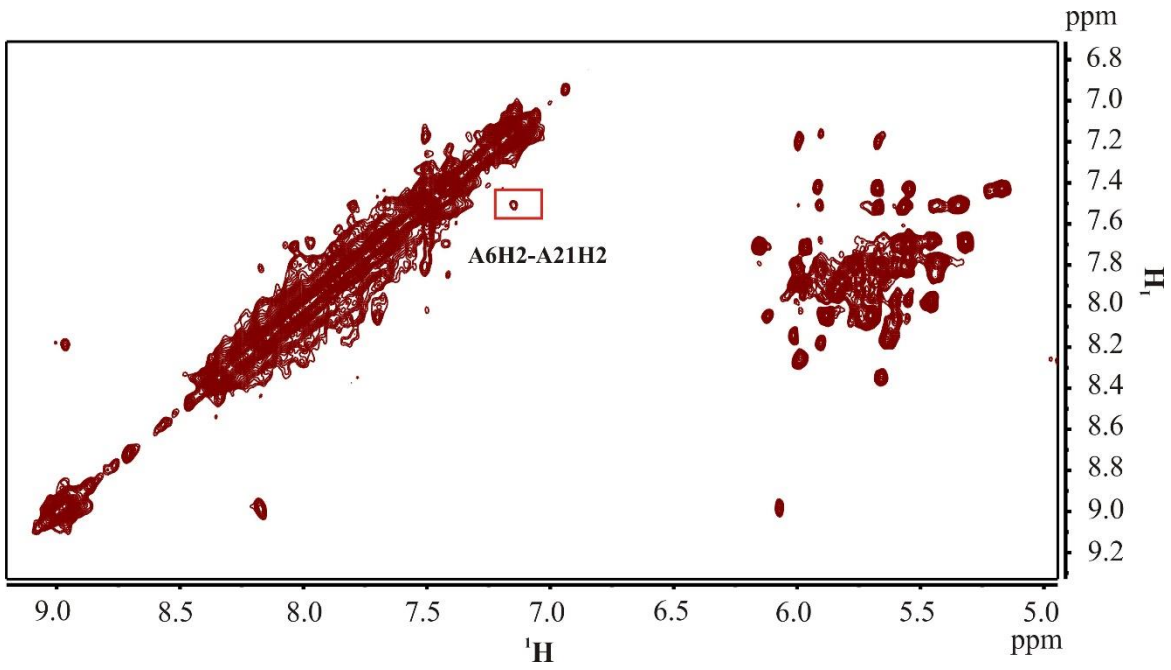

Figure A 2.7: *Zoom of a [^{1}H,^{1}H]-NOESY spectrum (sequential walk and aromatic staking regions) recorded on a platinated sample isolated from the upper band of a platination reaction performed using triph-D1-27 (0.2 mM RNA, 120 mM $KClO_4$, pD 7, 25 °C, 600 MHz). The box indicates the cross-peak between A6H2 and A21H2, which suggests that the adenine stacking in the internal loop is not completely broken upon platination. The Figure has been prepared with MestReNova version 10.0 (Mestrelab Research S.L.) and CorelDRAWX3.*

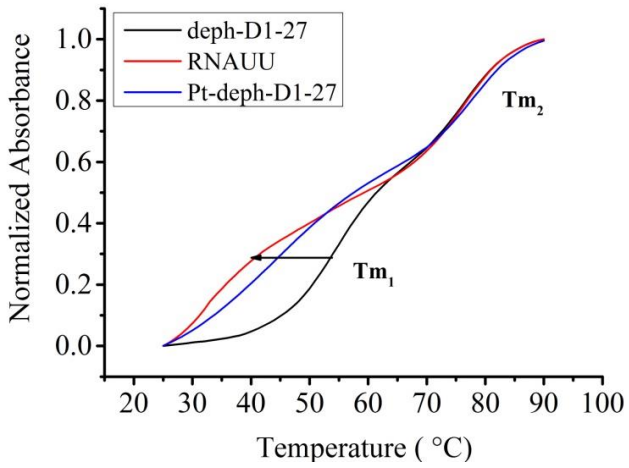

Figure A 2.8: *Indicative thermal melting profiles for unreacted deph-D1-27 (black line), platinated deph-D1-27 (blue line) and RNAUU (red line). They were monitored at 260 nm, data collected from 20 °C to 90 °C at a rate of 1 °C / min. C_{RNA} = 1.3 μM, 120 mM $KClO_4$, pH 6.5.*

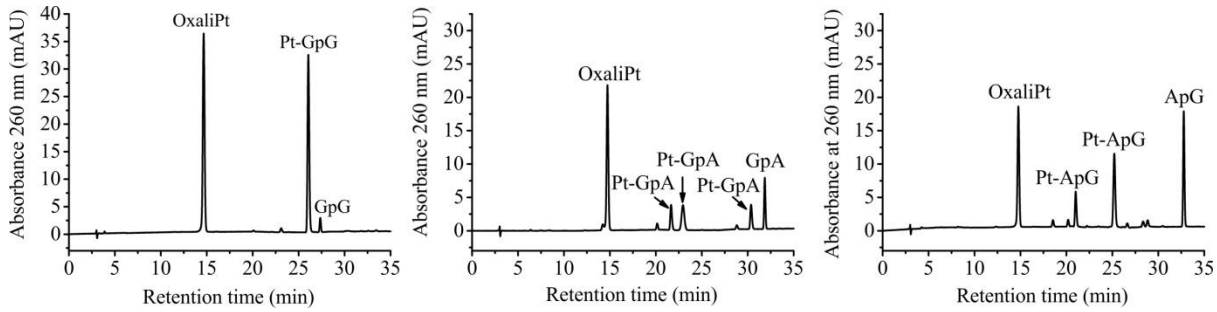

Figure A 2.9: *HPLC chromatograms of the reactions of GpG dinucleotide (left), GpA dinucleotide (middle) and ApG dinucleotide (right) with oxaliplatin. After 1 day of interaction, new peak(s) appeared corresponding to platinated dinucleotides. Experimental conditions:* $C_{dinucleotide}$*=0.2 mM,* C_{Pt}*= 2 mM, at 37 °C, in dd*H_2O*.*

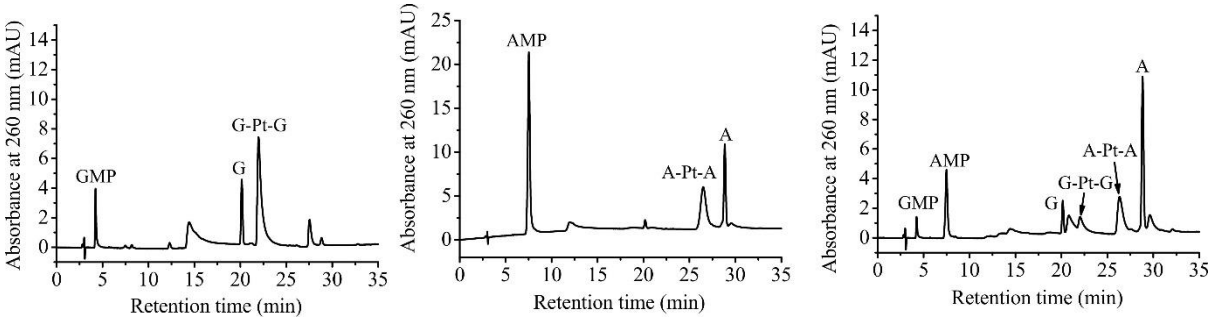

Figure A 2.10: *HPLC chromatograms of the reactions of GMP and AMP with oxaliplatin in 2 GMP:1 oxaliPt (left), 2 AMP:1 oxaliPt (middle) and 1 GMP:1 AMP:1 OxaliPt (right) ratio. The attribution of the peaks corresponding to GMP, AMP, A (adenosine) and G (guanosine) were performed upon injection of their standard solutions. On the left and middle chromatograms the new main peaks appeared were attributed to the platinated nucleotides based on literature data (see ref 35 in chapter 4) and the peaks of the chromatogram on the right was performed upon comparison with the other two. Experimental conditions:* $C_{dinucleotide}$*=0.5 mM,* C_{Pt}*= 5 mM, incubation for 5 days at 37 °C, in dd*H_2O*.*

Appendix 3 - Chapter 5

In appendix 3 IR and ^{1}H-NMR spectra of DACH, [Pt(DACH)Cl_2], [Pt(DACH)Cl(H_2O)]$^{+}$ and [Pt(DACH)(H_2O)$_2$]$^{2+}$ are reported. They all refer to experiments described in chapter 5.

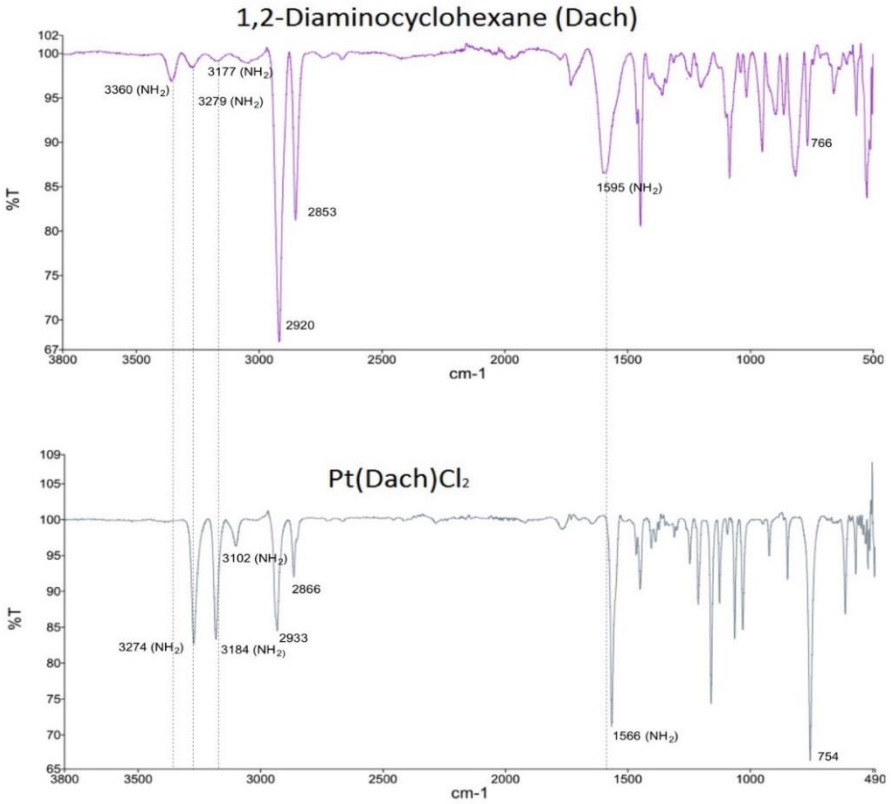

Figure A 3.1: *IR spectra of DACH (upper panel) and [Pt(DACH)Cl$_2$] (lower panel).*

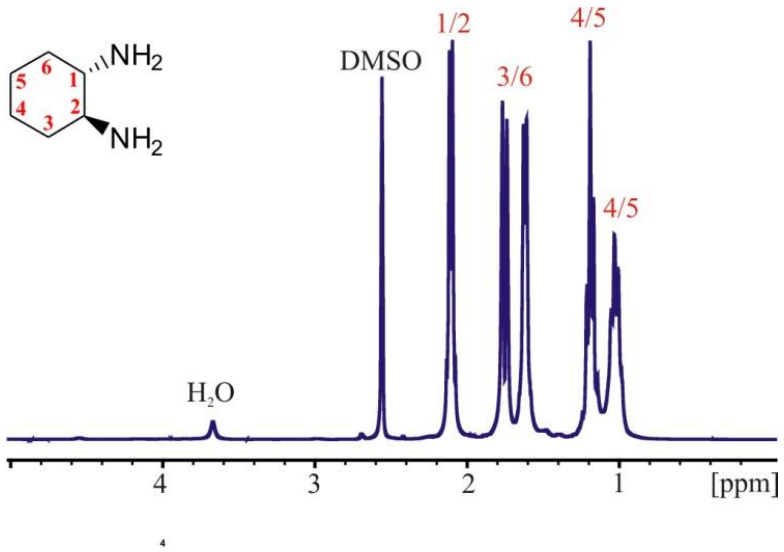

Figure A 3.2: *^{1}H-NMR spectrum of DACH in DMSO at 25 °C recorded on 500 MHz, including proton attributions.*

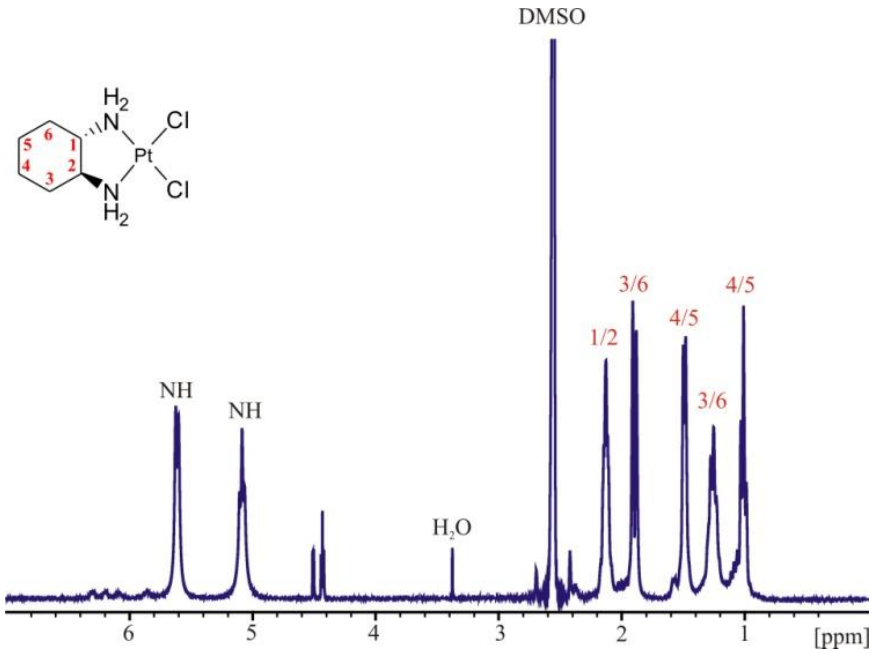

Figure A 3.3: *^{1}H-NMR spectrum of [Pt(DACH)Cl$_2$] in DMSO at 25 °C recorded on 500 MHz, including proton attributions.*

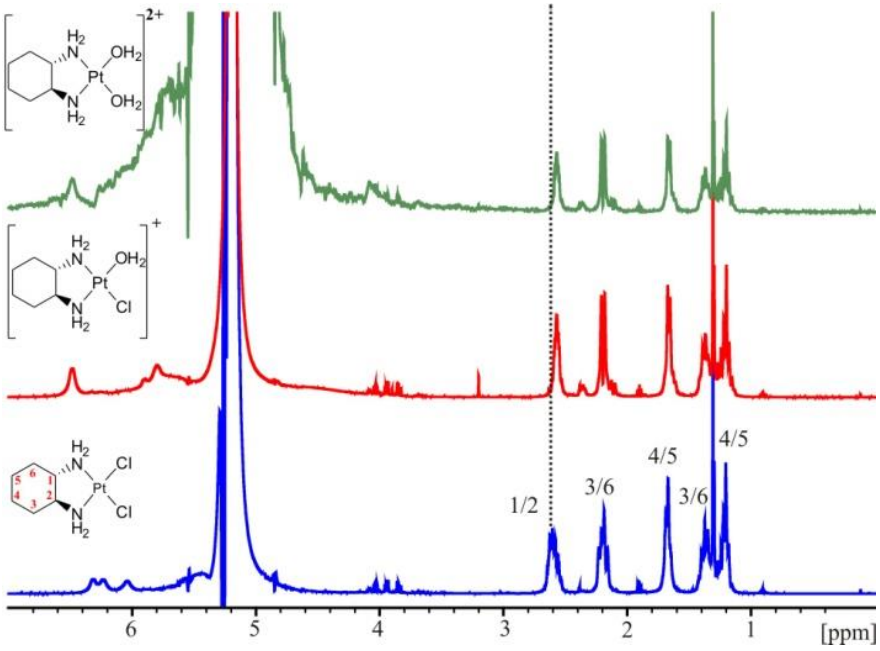

Figure A 3.4: *^{1}H-NMR spectra of [Pt(DACH)Cl$_2$] (blue line), [Pt(DACH)(H$_2$O)Cl] (red line) and [Pt(DACH)(H$_2$O)$_2$] (green line) in 90 % H$_2$O / 10 % D$_2$O at 25 °C recorded on 500 MHz, including proton attribution.*

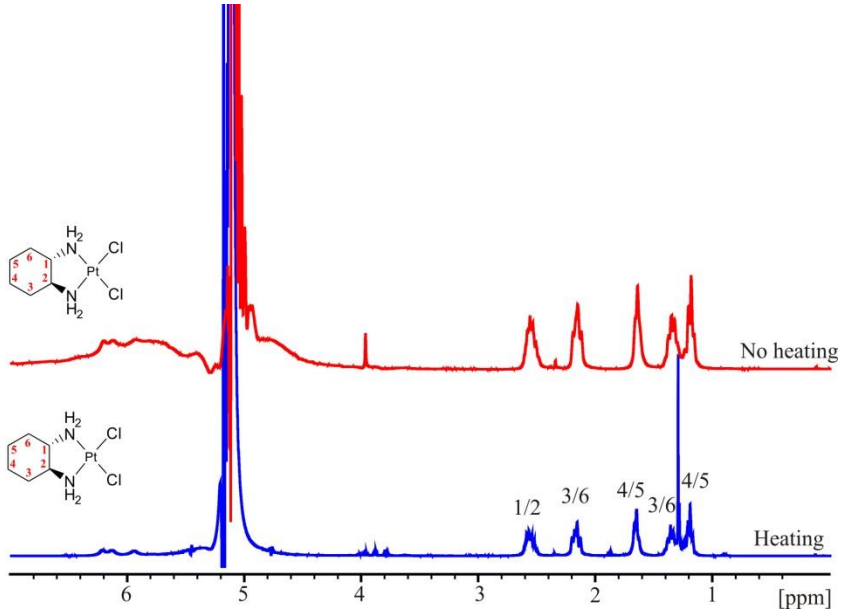

Figure A 3.5: *^{1}H-NMR spectra of [Pt(DACH)Cl$_2$] dissolved in 90 % H$_2$O / 10 % D$_2$O with (blue line) and without heating (red line) the sample, respectively. Interestingly, the spectrum recorded on the sample that was previously heated at 40 °C for 20 - 30 min shows a few additional peaks, which may be due to degradation products formed upon heating (25 °C, 500 MHz).*

Appendix 4 - STSM report

Kinetic studies of platinum(II) complexes binding to RNA

11.10.15 - 15.11.15

Applicant Details

Marianthi Zampakou

Group Dr. Daniela Donghi., Prof. Roland K.O. Sigel, WG2

Department of Chemistry, University of Zurich

Winterthurerstrasse 190, CH-8057 Zurich, Switzerland

Host Institution

Prof. Sofi K.C. Elmroth, WG2

Department of Biochemistry and Structural Biology

Lund University, P.O. Box 124, SE-22100, Lund, Sweden

1. Purpose of the STSM

The aim of my 5 weeks stay in the group of Prof. Sofi Elmorth in Lund was to monitor the kinetics of two different platinum(II) complexes namely (cis-1,2- DACH)dichloridoplatinum ([Pt(DACH)Cl_2]) and (cis-1,4- DACH)dichloridoplatinum (kiteplatin) with different RNA constructs and compare their behaviour with literature data on cisplatin previously reported from Elmroth's group.

2. Description of the work and the main results

2.1: UV measurements

I followed the kinetics of the reaction between the monoaquo form of [Pt(DACH)Cl_2] ([Pt(DACH)(H_2O)Cl]$^+$) and the two RNA constructs depicted in Figure 1, by measuring the change in absorbance at 260 nm at 38 °C for 24 hours. The reaction was followed in potassium phosphate buffer, K_2HPO_4/KH_2PO_4 pH 5.7 (KPi) and sodium phosphate buffer Na_2HPO_4 / NaH_2PO_4 pH 5.7 (NaPi) and four different platinum concentrations were used (7.5 μM, 15 μM, 30 μM, 45 μM). Preliminary experiments with both RNA constructs (Picture 1) in the two different phosphate buffers gave results difficult to interpret. The shape of the curve indicates that there is more than one event taking place during the reactions and in all cases the curve does not reach a plateau, suggesting that the reaction is not finished. In a try to understand this behaviour, several experiments were performed, including blank experiments to investigate the stability of our platinum complexes in phosphate buffer. Unfortunately, the UV machine did not work properly and we had several problems. Consequently, the measurements with [Pt(DACH)(H_2O)Cl]$^+$ could not be repeated neither the experiments with monoaquo kiteplatin could be run. Prof. Sofi K. C. Elmroth has ordered a new UV machine and all the kinetic measurements will be repeated in the future, to understand from where this unusual behaviour comes from.

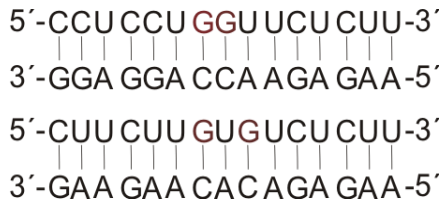

Picture 104: *Secondary structure for RNA1(GG) and RNA2(GNG).*

2.2: Fluorescence measurements

Taking into consideration that I could not finish the initially planned project we decided to start another one based on a different method that Elmorth's group has developed in order to follow kinetics. In this case we studies the kinetics of the RNA platination by using RNA1 (duplex that contains GG platination site) modified with a fluorescence label at the 5´-end (6-FAM) and a quencher at the 3´-end. The melting of the two strands induced by platination results in an increase of fluorescence. With a real time PCR (rt-PCR) we could monitor the desired product at any point during the platination reaction by measuring fluorescence over time. The following samples were prepared: RNA1 in Na / KPi buffer for four

different platinum concentration (7.5 μM, 15 μM, 30 μM, 45 μM). Both monoaquated [Pt(DACH)Cl_2] and monoaquated kiteplatin were used. All measurements were conducted in triplicates.

The addition of platinum to RNA solution results to kinetic traces that can be described by single-exponential function. Under pseudo-first order conditions with [C_{Pt}] >> [RNA], the observed rate constant (k_{obs}) which was obtained by a fit of a single-exponential function to the experimentally obtained ΔE-values (E= emission) should be linearly dependent on platinum concentration [C_{Pt}][2,3]. For that reason, the observed rate constants were plotted as a function of added C_{Pt} and a linear dependence was observed. From the slope of the plot of the k_{obs} *vs* C_{Pt} the apparent second-order rate constant ($k_{2,app}$) was directly obtained. The data shows that both complexes have slower reactivity compared to cisplatin with k_{2app} ca. 2.8 $M^{-1}s^{-1}$ while for cisplatin[2] k_{2app} is 7.72 $M^{-1}s^{-1}$. The monoaquated [Pt(DACH)Cl_2] behaves the same in both phosphate buffers, while the monoaquated kiteplatin has higher reactivity in KPi buffer (k_{2app} 4.26 $M^{-1}s^{-1}$ in KPi, 2.89 $M^{-1}s^{-1}$ in NaPi). Similar behaviour had reported for the monoaquated cisplatin[3] (Table 1).

Experimental details: C_{RNA}= 3 μM (1.5 μM per strand), C_{Pt} = 7.5 - 45 μM, in 122 mM KPi / NaPi buffer, pH 5.7, V_f = 40 μL, 37 °C for 600 min.

Table 1: *Summary of the reaction rate constants (k_{obs} and k_{2app}) for the RNA1.*

	k_{obs} x10^4 (s^{-1})				
C_{Pt}	**7.5 μM**	**15 μM**	**30 μM**	**45 μM**	**k_{2}app (M^{-1} s^{-1})**
[Pt(DACH)Cl_2] Na^+	0.78±0.14	1.11±0.02	1.73±0.05	1.67±0.03	2.49±0.84
[Pt(DACH)Cl_2] K^+	1.07±0.01	1.09±0.02	1.45±0.03	2.11±0.03	2.82±0.53
Kiteplatin Na^+	0.79±0.12	0.77±0.14	-	1.79±0.04	2.89±0.59
Kiteplatin K^+	0.61±0.08	0.83±0.12	-	2.17±0.05	4.26±0.27
Cisplatin Na^+	0.54	1.60	2.70	3.50	7.72±0.45
Cisplatin K^+	1.3 ± 0.3	2.2 ± 0.3	3.8 ± 0.3	4.7 ± 0.2	9.2±0.6

2.3: Plasmid binding studies

Given that the UV measurements for the study of the kinetics of the platination reaction were not conclusive, we decided to start another small side project. This was based on a previous study published from the Elmroth group[4]. Utilizing the ability of the platinum (II) anticancer drugs as DNA unwinding agents we studied the DNA binding affinity of the monoaquated complexes of cisplatin, kiteplatin and

[Pt(DACH)Cl_2] with the negatively supercoiled pUC18 plasmid. Additionally, we compared their behaviour in two different phosphate buffers (NaPi, KPi). Upon platination supercoiled and relaxed forms can be visualized by agarose gel electrophoresis. By increasing the amount of platinum complexes bound to DNA it could be detected the appearance of a slower migrating supercoiled plasmid band. The point at which the supercoiled and relaxed forms coincide is called coalescence point. For these studies we used the conditions that were previously reported from the Elmroth's group[4]. The ratio of nucleotide concentration (C_{DNA}) and concentration of platinum compounds (C_{Pt}) (r_f=C_{Pt}/C_{DNA}) was varied from 0 to 0.5. Each platinum complex have its coalescence point at the same r_f in NaPi and KPi buffer meaning that they exhibit similar behaviour in both buffers. Cisplatin is the one that reacts the fastest, as expected, having the coalescence point much earlier compared to the other two complexes. Amongst the other two kiteplatin is faster considering that we have the appearance of the slower migrating supercoiled band earlier (picture 2).

Experimental conditions: 2 % agarose gel, 70 V for 1.5 h, incubation for 24 h, 37 °C with r_f varying from 0 to 0.5, 200 mM Na_2HPO_4 / NaH_2PO_4, 200mM K_2HPO_4 / KH_2PO_4, pH 5.8, [pUC18] = 0.03 µM

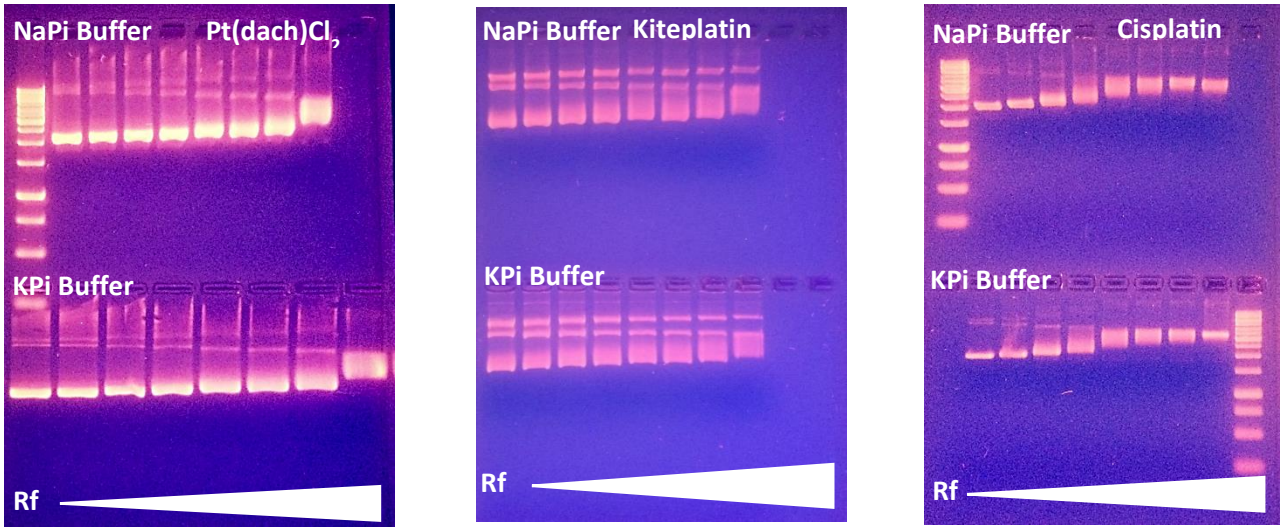

Picture 2: *Gel mobility shift assay of platinum complex with supercoiled and relaxed forms of the pUC18 plasmid.*

2.4: References

1.S. Verstraete, O. Heudi, A. Cailleux, P. Allain, Journal of Inorganic Biochemistry, 2001, 84, 129
2.C. Polonyi, A. Alshiekh, L A. Sarsam, M. Clausén ,S.K.C.Elmroth, Dalton Trans., 2014, 43, 11941
3.A. Alshiekh, M. Clausén , S.K.C.Elmroth, Dalton Trans., 2015, 44, 12623
4. M.S. Damian, H.K. Hedman, S.K.C. Elmroth, U. Diederichsen, Eur. J. Org. Chem. 2010, 6161

3. Conclusion and outlook

Due to technical problems, we were not able to perform the kinetic measurements. Preliminary experiments on the interaction of $[Pt(DACH)(H_2O)Cl]^+$ with the RNA1 and RNA2 were not conclusive and fully understood. The measurements will be performed once the new UV machine will arrive. The fluorescence measurements took place as an alternative way to follow the kinetics of the platination reactions. The monoaquated $[Pt(DACH)Cl_2]$ and monoaquated kiteplatin were used. Both complexes exhibit lower reactivity compared to cisplatin. Kiteplatin is reacting faster in KPi buffer, behaviour that is in accordance with was is reported to the literature for the cisplatin. From the plasmid binding studies we conclude that monoaquated cisplatin binds faster than the monoaquated $[Pt(DACH)Cl_2]$ and monoaquated kiteplatin. From the comparison of the last two, we can conclude that monoaquated kiteplatin reacts faster considering that we have the appearance of the slower migrating supercoiled band earlier.

4. Personal feedback

The opportunity of working for few weeks in another lab abroad has been very useful. From the scientific point of view, the discussions with the members of Elmroth's group were very helpful. Despite the technical problems that we enfaced during my stay, we were able to find alternatives and continue. The alternatives that we tried gave me the opportunity to learn new techniques. Additionally, the discussions with Prof. Sofi K. C. Elmroth were very advantageous for the continuation of my project in Zurich.

9 Curriculum Vitae

PERSONAL DATA

Name	ZAMPAKOU
First Name	MARIANTHI
Date of birth	01.08.1987
Nationality	Greek

EDUCATION

2003–2005 Secondary school, Unified Lyceum of N. Zichni, Serres, Greece

2005–2010 Bachelor in Biochemistry / Biotechnology – Food Chemistry. Aristotle University of Thessaloniki, Greece, Research Dissertation: *"Overexpression and purification of the A1 domain of the VON WILLEBRAND factor",* Supervisor: Prof. Theodora Choli-Papadopoulou

2010–2012 Master in Inorganic Chemistry. Aristotle University of Thessaloniki, Greece, Research Dissertation: *"Synthesis, characterization and biological evaluation of manganese complexes with non-steroidal drugs as ligand",* Supervisor: Prof. Psomas George

2012–2016 Doctoral studies in Chemistry, Department of Chemistry, University of Zurich, Switzerland. Research Dissertation: *"Interaction of Platinum(II) anticancer drugs with RNA",* Supervisor: Dr. Daniela Donghi, (Responsible Faculty Member Prof. Dr. Roland K.O. Sigel). Member of the graduate school of Chemical and Molecular Sciences Zürich

PRACTICAL EXPERIENCE AND TEACHING

2011-2012 Tutor at the laboratory courses of General Inorganic Chemistry and Inorganic Chemistry II at the Laboratory of Inorganic Chemistry at the Aristotle University of Thessaloniki

2013 Teaching assistant in the Inorganic Chemistry laboratory course (ACPII) at the department of Chemistry at the University of Zurich

2014 Teaching assistant in the Inorganic Chemistry laboratory course (ACPII) at the department of Chemistry at the University of Zurich

2015 Teaching assistant in the Inorganic Chemistry laboratory course (ACPII) at the department of Chemistry at the University of Zurich

2015 Teaching assistant (short-term project) in the Inorganic Chemistry laboratory course (ACPI) at the department of Chemistry at the University of Zurich

COURSES AND AWARDS

2014 Course from the CMSZH graduate school: Communication Skills for Leaders,

Metrohm, Zofingen, Switzerland

2015 Course from the CMSZH graduate school: Leadership Skills, Mettler Toledo, Greifensee, Switzerland

2015 Course from the CMSZH graduate school: Management Skills, Sigma-Aldrich, Buchs, Switzerland

2015 SCNAT/SCS/SSFEC Chemistry Travel Award

CONFERENCES-SCHOOLS/POSTER PRESENTATION

07.2013 Marianthi Zampakou and Daniela Donghi, "Interaction of Platinum compounds with RNA", 16th International Conference on Biological Inorganic Chemistry, Grenoble, France

09.2013 Marianthi Zampakou and Daniela Donghi, "Exploring the Interaction of Platinum Drugs with RNA", 1st International Symposium on Functional Metal Complexes that Bind to Biomolecules (2nd Whole Action Meeting of the COST action CM1105), Barcelona, Spain

09.2013 Marianthi Zampakou and Daniela Donghi, "Interaction of platinum anticancer drugs and RNA", Swiss Chemical Society Fall meeting 2013, Lausanne, Switzerland

10.2013 Marianthi Zampakou and Daniela Donghi, "Interaction of platinum anticancer drugs with RNA", 8th Annual Dorothy Crowfoot Hodgkin Symposium and the Hofmann Award Lecture, Zurich, Switzerland

01.2014 Marianthi Zampakou and Daniela Donghi, "RNA and platinum (II) anticancer drugs", Swiss RNA Workshop 2014, Bern, Switzerland

08.2014 Marianthi Zampakou and Daniela Donghi, "Purification and isolation of platinated RNA", 12th European Biological Inorganic Chemistry Conference, 2014, Zurich, Switzerland

09.2014 Marianthi Zampakou and Daniela Donghi, "Purification and isolation of RNA-platinum adducts", Chemistry of Metals in biological Systems, Summer school, 2014, Louvain-la-Neuve, Belgium

06.2015 Marianthi Zampakou and Daniela Donghi, "Interaction of Oxaliplatin and RNA: Investigation of the Platinum Binding Sites", 13th International Symposium on Applied Bioinorganic Chemistry ISABC 13, 2015,Galway, Ireland

09.2015 Marianthi Zampakou and Daniela Donghi, "Interaction of Oxaliplatin and RNA: Investigation of the Platinum Binding Sites", SCS Fall Meeting 2015, 2015, Lausanne, Switzerland

10.2015 Short-Term Scientific Mission from COST Action CM1105: 5 weeks stay in the group of Prof. Sofi Elmorth in Lund. Project: "Kinetic studies of platinum(II) complexes binding to RNA"

CONFERENCES/ORAL PRESENTATION

08.2014 Marianthi Zampakou and Daniela Donghi, "Influence of Oxaliplatin on RNA structure", COST CM1105, 2014, Zurich, Switzerland

PUBLICATIONS

- E. Koumousi, M. Zampakou, C. Raptopoulou, V. Psycharis, C. Beavers, S. Teat, G. Psomas T. Stamatatos, Inorganic Chemistry, 2012, 51, 7699-7710

- M. Zampakou, M. Akrivou, E. Adreadou, C. Raptopoulou, V. Psycharis, A. Pantazaki, G. Psomas, Journal of Inorganic Biochemistry, 2013, 121, 88-99
- M. Zampakou, N. Rizek, V. Tagoulis, A. Papadopoulos, F. Perdih, I. Turel, G. Psomas, Inorganic Chemistry, 2014, 53, 2040-2052
- M. Zampakou, S. Balala, F. Perdih, S. Kalogiannis, I. Turel, G. Psomas, RSC Advances, 2015, 5, 11861-11872
- M. Zampakou, V. Tangoulis, C.P. Raptopoulou, V. Psycharis, A.N. Papadopoulos, G. Psomas, Eur. J. Inorg. Chem., 2015, 2285–2294
- E. Alberti, M. Zampakou, D. Donghi, J. Inorg. Biochem., 2016, 163, 278-291